Dr. rer. nat. K. Rurack

Steady-State and Time-Resolved Spectroscopy of Ion-Sensitive Fluorescent Probes

Forschungsbericht 235

Berlin 2009

Impressum

Forschungsbericht 235:
Steady-State and Time-Resolved Spectroscopy of Ion-Sensitive Fluorescent Probes

2009

Herausgeber:
BAM Bundesanstalt für Materialforschung und -prüfung
Unter den Eichen 87
12205 Berlin
Postanschrift: 12200 Berlin
Telefon +49 30 8104-0
Telefax +49 30 8112029
E-Mail: info@bam.de
Internet: www.bam.de

Layout: BAM-Arbeitsgruppe Z.64

ISSN 0938-5533
ISBN 3-89701-362-2

Zusammenfassung

Im Mittelpunkt der vorliegenden Arbeit stehen Untersuchungen des spektroskopischen und komplexometrischen Verhaltens verschiedener Ionen-sensitiver Fluoreszenzsonden. Drei der vier Sondentypen folgen dabei einem herkömmlichen Prinzip zur Signalerzeugung und entsprechen in ihrem molekularen Aufbau einem *fluoreszierenden Liganden* ($BP(OH)_2$) bzw. sogenannten *intrinsischen* Ladungstransfer-(ICT)-Fluoreszenzsonden (Donor-Akzeptor-substituierte Chalkone) und Elektronentransfer-(ET)-Fluoreszenzsonden (substituierte Triaryl-Δ^2-pyrazoline). Die beiden letzten Systeme sind modular konzipiert, so dass signalgebender Fluorophor und komplexierender Rezeptor gezielt modellierbar sind. Im Fall der ICT-Sonden sind beide Einheiten elektronisch konjugiert, bei den ET-Sonden sind sie dagegen elektronisch weitgehend entkoppelt und das Signal wird durch Beeinflussung eines weitreichenden Elektronentransferprozesses generiert. Die Sonde vierten Typs, ein Bordipyrromethenderivat (BDP), ist ebenfalls modular aufgebaut. Bei ihr sind Fluorophor und Rezeptor aber nur durch den stark vorverdrillten Aufbau des Moleküls „virtuell" entkoppelt. Neben diesem Einsatz eines alternativen Mechanismus zur Signalerzeugung standen vor allem die Steuerung der Selektivität durch gezielte Modifikation des Rezeptors sowie mögliche Verbesserungen der fluorometrischen Metallionenanalytik hinsichtlich Nachweisselektivität und -sensitivität durch Aufnahme zeitaufgelöster Fluoreszenzspektren (TRES) im Vordergrund der Untersuchungen.

Unter Zuhilfenahme einer Reihe von Modellsubstanzen, NMR spektroskopischer Messmethoden und quantenchemischer Rechnungen wurden ausserdem allgemeine Erkenntnisse über das lichtinduzierte Verhalten der einzelnen Farbstoffklassen gewonnen.

Der fluoreszierende Ligand $BP(OH)_2$ zeigt, analog seiner Mutterverbindung 2,2'-Bipyridyl, komplexierungsinduzierte Änderungen in seinem Absorptions- und Fluoreszenzverhalten bei Anwesenheit von Übergangs- und Schwermetallionen. Während paramagnetische Ionen wie Cu^{II} oder Ni^{II} (und auch Hg^{II}) zur statischen Fluoreszenzlöschung führen, bilden die diamagnetischen Ionen Zn^{II} und Cd^{II} stark fluoreszierende Komplexe mit einer ionenspezifischen Fluoreszenzlebensdauer im ns-Zeitbereich. Beide Komplexe sind im angeregten Zustand stabil, was sich u. a. in einer, gegenüber dem freien Liganden stark herabgesetzten Geschwindigkeitskonstante für strahlungslose Desaktivierungsprozesse manifestiert. Die Absorptions- und Emissionsspektren der Komplexe überlappen stark und eine Unterscheidung mittels statischer Spektroskopie ist in beiden Fällen nur sehr begrenzt möglich. Die Trennung beider Komponenten gelingt allerdings unter Einsatz der zeitaufgelösten Fluoreszenzspektroskopie und an mehreren synthetischen Zn^{II}/Cd^{II}-haltigen Proben konnte beispielhaft der Gewinn an Selektivität durch Aufnahme der TRES mit anschliessender global-analytischer Auswertung gezeigt werden.

Die intrinsischen Fluoreszenzsonden des Chalkontyps tragen den Kationen-selektiven Rezeptor im Donorteil des Moleküls und zeigen bei Komplexierung durch Schwächung des Donors eine starke Abnahme des intramolekularen Ladungstransferprozesses. Im unkomplexierten Zustand erfolgt Fluoreszenz, je nach molekularem Aufbau und Polarität des Lösungsmittels, aus einem polaren direkt angeregten (E*) oder unter Einfachbindungsverdrillung und Reaktion im angeregten Zustand besetzten, hochpolaren Ladungstransferzustand (A*). Als konkurrierende Prozesse spielen dabei mögliche Besetzungen eines nicht fluoreszierenden, polaren (K*) bzw. schwach polaren (P*) Übergangszustandes eine Rolle. Desweiteren ist in diesem Farbstoffsystem die Möglichkeit der Fluoreszenzlöschung durch benachbarte, tiefliegende $n\pi^*$ Zustände (in unpolaren Lösungsmitteln) sowie durch verstärkte interne Konversion aufgrund des geringen energetischen Abstandes von Grund- und angeregtem Zustand (in hochpolaren Lösungsmitteln) gegeben. Bei Kationenkomplexierung in polaren Lösungsmitteln wird vor allem, wie oben angedeutet, der Donor abgeschwächt, und es kommt zu einer moderaten Fluoreszenzverstärkung. Neben der erhöhten Fluoreszenzquantenausbeute resultiert der Effekt in Ionen-spezifischen Fluoreszenzlebensdauern der Komplexe. Durch den Austausch eines Stickstoff-Sauerstoff- gegen einen Stickstoff-Schwefel-Makrozyklus im Rezeptorteil des Systems konnte die Ionenselektivität von den Alkali- und Erdalkalimetallionen zu den thiophilen Metallionen Ag^{I} und Hg^{II} umgeleitet werden, wobei insbesondere die Fluoreszenzverstärkung in Gegenwart des herkömmlich als Fluoreszenzlöscher bekannten Hg^{II}-Ions analytisch wertvoll ist.

Die ET-Sonden des Triaryl-Δ^2-pyrazolin-Typs zeigen gegenüber den ICT-Sonden nur geringe spektrale Effekte, die Ionen-induzierte Fluoreszenzverstärkung ist dagegen wesentlich grösser. Durch den gezielten Einsatz der unterschiedlichen Rezeptoren lassen sich hier ebenfalls die Selektivitäten steuern. In vergleichenden Untersuchungen konnten für die 5-*p*-*N,N*-Dialkylanilino-3-benzthiazol-1-phenyl-Δ^2-pyrazoline die intramolekularen Prozesse charakterisiert werden, die Fluoreszenzlöschung im unkomplexierten und ein „Anschalten" der Fluoreszenz im gebundenen Zustand bewirken. In diesen Molekülen findet der intramolekulare Ladungstransfer im Hauptchromophor im sub-ps Bereich statt und wird in hochpolaren Lösungsmitteln durch einen Elektronentransferprozess auf der ps-Zeitskala vom weitgehend elektronisch entkoppelten Rezeptor zum Akzeptorteil des Hauptchromophors gelöscht.

Die „virtuelle" Entkopplung von Fluorophor und Rezeptor im BDP-Derivat ermöglicht schliesslich die Erzeugung von sehr grossen Fluoreszenzverstärkungssignalen bei Komplexierung. In diesen stark vorverdrillten Donor-Akzeptor-Biarylen geht der direkt angeregte emittierende Zustand (LE) in polaren Lösungsmitteln in einen hochpolaren, verdrillten radikalionischen Ladungstransferzustand (CT) über. Emission aus letzterem ist stark verboten und erfolgt, je nach Lösungsmittelpolarität, (weit) rotverschoben zur Fluoreszenz des LE, so dass schon in mittelpolaren Lösungsmitteln eine weithin getrennte, duale Fluoreszenz zu beobachten ist. In hochpolaren Lösungsmitteln sind beide Fluoreszenzen nahezu vollständig gelöscht. Metallionenkomplexierung führt zur Unterbrechung des CT-Prozesses und somit zu einem „Anschalten" der LE-Emission mit Fluoreszenzverstärkungsfaktoren > 1000. Dieser Prozess ist dabei so sensitiv, dass für die meisten Kationenkomplexe zwei spektral sehr stark überlappend absorbierende und emittierende Komplexkonformere anhand ihrer Fluoreszenzlebensddauer unterschieden werden können.

Summary

The present work is focused on the study of the spectroscopic and complexometric behavior of different ion-sensitive fluorescent probes. Three of the four types of probes studied follow a conventional principle of signal generation and their molecular constitution corresponds to either a *fluorescent ligand* ($BP(OH)_2$), so-called *intrinsic* charge transfer (ICT) fluorescent probes (donor-acceptor-substituted chalcones), or *electron transfer* (ET) fluorescent probes (substituted triaryl-Δ^2-pyrazolines). The latter two systems are designed in a modular way and thus, both the signal generating fluorophore and the complexing receptor can be carefully tuned. Whereas in the case of the ICT probes both units are electronically conjugated, these moieties are more or less electronically decoupled in the ET probes and signal generation is based on the modification of a long range electron transfer process. The fourth type of probe investigated, a boron dipyrromethene derivative (BDP), is also designed in a modular way. But here, due to the highly pretwisted constitution of the molecule, fluorophore and receptor are only "virtually" decoupled. Besides employing this alternative mechanism of signal generation, control of the selectivity by carefully directed receptor design and improvement of the selectivity and sensitivity of fluorometric metal ion analysis by recording time resolved emission spectra (TRES) were the main aims of these investigations.

Furthermore, with the aid of various model compounds, NMR spectroscopy as well as quantum chemical calculations, a fundamental understanding of the photophysical behavior of the different classes of dyes was obtained.

In accordance with its parent compound 2,2'-bipyridyl, the fluorescent ligand $BP(OH)_2$ shows complexation induced changes of its absorption and emission behavior in the presence of heavy and transition metal ions. Whereas paramagnetic ions such as Cu^{II} or Ni^{II} (and also Hg^{II}) lead to static fluorescence quenching, the diamagnetic ions Zn^{II} and Cd^{II} form strongly fluorescent complexes with ion specific fluorescence lifetimes in the ns time range. Both complexes are stable in the excited state which is manifested by a strongly reduced rate constant of non radiative deactivation compared to that of the free ligand. Both the absorption and emission spectra of the complexes largely overlap and a discrimination with steady-state fluorometry is very limited. Nevertheless, with time resolved fluorometry a separation of both components is possible and for a series of synthetic Zn^{II}/Cd^{II} containing samples this gain in selectivity by global analysis of the time resolved emission spectra (TRES) could be demonstrated.

The intrinsic fluorescent probes of chalcone type contain a cation selective receptor in the donor part of the molecule and show a strong decrease of the intramolecular charge transfer process due to complexation induced weakening of the donor. Depending on molecular probe design and solvent polarity, the fluorescence of the uncomplexed molecule occurs either from a polar directly exicted (E*) or a highly polar charge transfer state (A*) which is populated via an excited state reaction involving single bond twisting. Here, competing processes include population of a non emissive polar (K*) or weakly polar (P*) transient state. Furthermore, the fluorescence of these dyes can be quenched by energetically close lying $n\pi^*$ states (in apolar solvents) or by enhanced internal conversion due to the decreasing energy gap between ground and excited state (in highly polar solvents). As mentioned above, the donor strength is reduced upon cation complexation in polar solvents and a moderate fluorescence enhancement occurs. Besides increased fluorescence quantum yields, this effect results in ion specific fluorescence lifetimes of the complexes. Upon exchanging the aza oxa for an aza thia macrocycle in the receptor part of the system, the cation selectivity could be tuned from alkali and alkaline earth metal ions to the thiophilic metal ions Ag^{I} and Hg^{II}. Here, especially the fluorescence enhancement in the presence of the well-known quencher Hg^{II} is analytically valuable.

Upon cation binding the ET probes of the triaryl-Δ^2-pyrazoline type show very small spectral shifts but much larger fluorescence enhancement compared to the ICT probes. Again, by problem specific use of different receptors, the selectivities can be controlled. Based on a detailed investigation, for the 5-*p*-*N,N*-dialkylanilino-3-benzthiazol-1-phenyl-Δ^2-pyrazolines, the intramolecular processes which lead to fluorescence quencing in the unbound state and "switching on" of the fluorescence in the complexed state could be identified. For these molecules, the intramolecular charge transfer in the basic chromophore occurs in the sub ps time range and is quenched by an electron transfer process from the largely electronically decoupled receptor to the acceptor part of the basic chromophore on the ps time scale in highly polar solvents.

"Virtually" decoupling fluorophore and receptor in the BDP derivative finally makes it possible to yield extremely high complexation induced fluorescence enhancement signals. For these highly pretwisted donor acceptor biaryls, the directly excited emissive state (LE) forms a highly polar, twisted charge separated charge transfer state (CT) in polar solvents. Emission of the latter is strongly forbidden and, depending on solvent polarity, is largely red shifted compared to the LE fluorescence. Thus, a largely separated dual fluorescence is already observed in solvents of medium polarity and in highly polar solvents both fluorescence bands are nearly completely quenched. Metal ion complexation blocks off the CT process and leads to a "switching on" of the LE emission yielding fluorescence enhancement factors > 1000. This process is so sensitive that for most of the cation complexes studied, two emissive complex conformers with strongly overlapping absorption and emission spectra occur which could be distinguished by their fluorescence lifetimes.

Inhalt

Seite

1 Introduction

1.1 Fluorometric Metal Ion Analysis

1.1.1 Background and Motivation

The detection and quantification of metals, especially metal ions, is of great importance in any kind of chemical, biological, and environmental analysis. Alkali and alkaline-earth metals as well as transition and heavy metals affect biotic and abiotic systems in many different ways. Depending on the abiotic environment and/or the biological species of interest, the physiological, ecological, and toxicological effects of a metal are usually strongly structure-specific, i. e., they depend on the species. Furthermore, the partitioning of metals in a certain environment or biota is governed by different acid-base affinities, kinetics, spatial (e. g., membranes) and temporal distribution [1].

Metals can be divided into three main groups according to their biological effectiveness, which are (i) essential (trace) elements, (ii) sub-toxic contaminants, and (iii) acute toxics. Taking a closer look at a list of both essential (Na, K, Mg, Ca, Cr, Mn, Fe, Co, Ni, Cu, Zn, Mo) and hazardous elements (Cr, Cu, Zn, Ag, Cd, Ni, Sn, Hg, Tl, Pb, Bi) [1], the fine line which exists for many heavy and transition metals between these stages, is apparent (solid curve in *Fig. 1*). In ionic form, metals such as Zn or Cu are often essentially involved in biochemical reactions on a trace level (< 1 µM), i. e., catalysis, transport, and biosynthesis. However, at higher concentrations, accumulation of these ions in an organism can lead to unhealthy interactions in biochemical redox processes (Cu^{II} oxidizes thiol groups), inhibition of enzyme activity (Ag^{I} inhibits glutathione peroxidase)[i], or induction of allergic reactions (Ni^{II}) [2]. Furthermore, there are some heavy metal ions such as Cd^{II} and Hg^{II} which are toxic for most living organisms even at extremely low concentrations (dotted curve in *Fig. 1*). The chronic toxic potential of these two metal ions includes, e. g., nephrotoxicity due to accumulation of these ions in the kidneys [2] and potential carcinogenic, cocarcinogenic, and mutagenic action (Cd^{II} salts) [3]. Additionally, a lot of heavy and transition metal ions affect the toxicity of organic xenobiotics through interaction with metabolizing enzymes or interaction at the protein synthesis (e. g., Zn^{II} increases tumor incidence by methylbenzyl-nitrosamine) [3]. On the other hand, most alkali and alkaline-earth metal ions are important for vital biological processes, e. g., the control of ion-pumping activity by Ca^{II} or Sr^{II} [4] or the regulatory influence of free Mg^{II} concentration on the function of cardiac muscle cells [5].

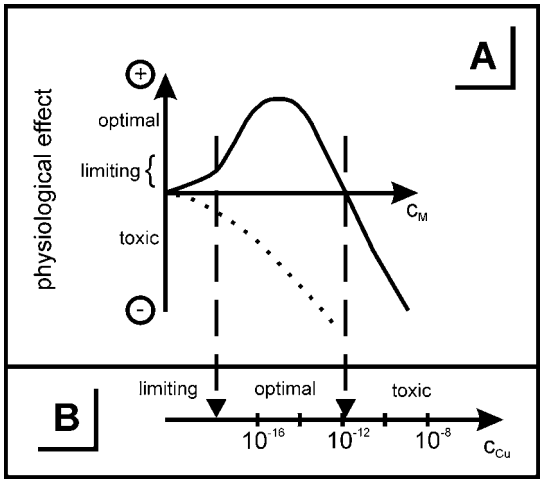

Fig. 1
*Physiological effects of metals as a function of their concentration. General case **A**: solid curve denotes an essential element, dotted curve a not needed element. The axis in **B** examplifies the reactive concentration range for the effect of Cu on algae (adapted from ref. [1]).*

Due to many industrial production processes, increasing traffic volume, intensive agriculture, and (hazardous) waste disposal, the anthropologically disposed light and heavy metals are a major source of contamination in the environment and metal cycles on a local and global basis have been considerably modified by human activity. Judged by the atmospheric interference factor[ii], which reflects the importance of the anthropogenic flux of a metal, Cu, Zn, Ag, Sb, Sn, Hg, Pb are the most potentially hazardous metals on the global scale [1]. And whereas most alkali and alkaline-earth metal ions are involved in biological processes on a physiological concentration scale (µM-mM level), these heavy and transition metal ions unfold their biogenic potential already in the sub-micromolar concentration range.

In terms of environmental mobility and bioavailability, metal ions, and especially heavy metal ions that are dissolved in water, are amongst the most dangerous contaminants. Dissolved metal ions are easily transported in aquifers, taken up by plants or aquatic organisms, and most of them often interfere with any kind of dissolved organic or inorganic matter in water. Abiotic interactions may change the solubility, the valence state and charge, as well as the chemical ligands or chelation of a metal ion, which all influence its bioavailability *(Fig. 2)* [1, 3]. Remobilization of metal ions from the soil or sediment is possible by changes in pH, redox conditions (not

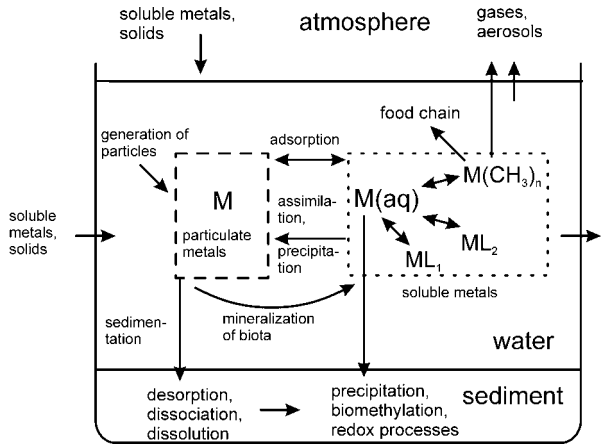

Fig. 2
Influence of adsorption, settling particles, complexation, and organic ligands on free metal ion concentration in aquatic ecosystems (schematic representation, based on ref. [1])

i) Glutathione peroxidase is a radical scavenger for any kind of oxygen radicals generated in the organism by biochemical redox processes.

ii) atmospheric interference factor for a certain metal = [total anthropogenic emission/(continental + volcanic fluxes)] x 100.

only for the commonly known redoxlabile ions like Fe and Mn, but also for Zn, Cd, and Ni), and salt concentration [6]. Moreover, the interactions with dissolved organic matter are numerous [7]. Although complexes of humic substances with metal ions possess a generally higher stability than metal complexes with inorganic ligands [8], humic substances act as ion exchangers depending on various complex stability equilibria. Here, the most important metal ions are Cu^{II} and Fe^{III}. Furthermore, chelators from industrial waste waters such as EDTA[iii] and NTA can act as ion mobilizers. The resulting complexes then may enhance the uptake of Cd^{II}, Cu^{II}, or Hg^{II} [3, 9]. Another important source of metal contamination is biodegredation due to microbial reaction that can lead to remobilization of metals from the humic acid reservoir [10] and humic acids can alleviate the toxic effect of those metals present at higher concentrations [11].

The actual mobility of metal ions in any kind of aquifer is mostly pH-controlled. At a pH of 4.2-6.6, Cd^{II}, Ni^{II}, and Zn^{II} are relatively mobile, but at pH values between 6.7 and 8.8, Zn^{II} is only moderately and Ni^{II} only slowly mobile; Cu^{II} and Pb^{II} are slowly mobile throughout the pH range 4.2-8.8 [12]. Soil-solution interactions and metal distribution based on adsorption, cation exchange reactions, complexation and diffusion as well as multireaction equilibria are often involved in this field of ion mobility. Generally, the transition metal ions can be divided into three groups of different mobility, the mainly free (or hydrated) cations (Co, Mn, Cd), the intermediately complexed (Zn, Ni), and the mainly complexed cations (Cu, Pb, Fe) [12].

Because the transport into a cell is slow in comparison to the preequilibration processes in solution, the uptake of metal ions by the cell predominantly depends on the free metal ion concentration in the surrounding medium (*Fig. 2*) [1]. For example, the free Cu^{II} ion activity or concentration is very important for organisms and indeed, algae growth in seawater as well as rivers and lakes is mainly regulated by free Cu^{II} (part B in *Fig. 1*) [1]. In this case, the total amount of Cu is of no ecotoxicological and analytical value because Cu^{I} mostly does not induce effects Cu^{II} induces and the complexed or adsorbed amount of Cu^{II} is biologically inactive. Furthermore, having in mind the complexometric behavior of Cu^{II} and Zn^{II}, the competition of these ions for organic ligands in limnic ecosystems is obvious. Thus, for ecotoxicological reasons, the determination of free Cu^{II} and Zn^{II} ions is more desirable than the quantification of the total Cu and Zn concentrations [13]. The same holds true for another prominent pair of metal ions, Zn^{II} and Cd^{II}. Because of their similar electronic nature, they compete in biological uptake and transport processes and often contribute to either biological health or disease. When Zn^{II} competes successfully with Cd^{II}, it can inhibit harmful reactions of Cd^{II} (e. g., the induction of tumors). Other relevant competing metal pairs are Cd^{II} and Ca^{II} (impaired Ca^{II} absorption by Cd^{II} leads to Ca^{II} depletion from bones) and Pb^{II} and Ca^{II} (direct competition in neuro-chemistry (synaptosomal Ca^{II} transport)) [3]. Additionally, the detection of the physiologically important free metal ion concentrations of alkali and alkaline-earth metals in biological samples has received much attention in biochemical analysis and especially in clinical diagnostics.

iii) ethylenediaminetetraacetic acid and nitrilotriacetic acid, mainly from detergents

The importance of this context is also reflected by the rapidly growing field of risk assessment, standard setting, health standards, guidelines, and legislative regulations. Most of these guidelines and regulations are based upon exposure effect/response relationships manifested in exposure limits (international: OELs, ADIs; national: TLVs, MACs, MPCs)[iv] and monitoring programs (environmental monitoring, e. g., in water or soil; biological monitoring, e. g., in plants or organisms; biological effect monitoring BEM) [14]. During the past 5-10 years, the ongoing reevaluation of, for instance, OELs shows that many of these regulations inadequately consider metal speciation and the increasing incongruity between BEM and OELs stresses the need for chemical speciation[v] [6, 14, 17].

1.1.2 Possibilities and Applications

The difficulties analytical chemists encounter when trying to determine exactly the actual amount of a given species in a sample of biological importance are obvious and the “major enemy” in water analysis was described by *Turekian* in 1977 as “the great particle conspiracy (that) is active from land to sea to dominate the behavior of the dissolved species” (*Turekian*, cited in ref. [1]). Therefore, when dealing with the sensitive detection of single species, separately or simultaneously, one has to be aware of all the other “chemical aggregate states” of the same element, i. e., ions in various oxidation states or organometallic compounds, which could be dissolved, complexed, or adsorbed, and which often interfere in chemical analysis.

Before giving a short survey of the analytical possibilities in metal ion analysis, some important characteristics of the liquid matrices, which may (strongly) interfere with a particular analytical method, will be briefly discussed.

In seawater, only alkali metal ions are mostly hydrated while even 50 % of Ca^{II} and Mg^{II} are present as sulfate and carbonate ion pairs [18]. The partitioning is very different under fresh water conditions (pH 8.0) where metal ions predominantly occur as free aquo ions (group I) or complexed ions (group II),

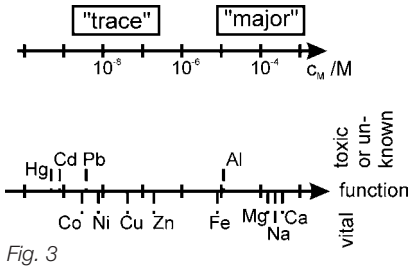

Fig. 3
Concentration ranges of “trace” and “major” metals (upper part) and total concentrations (average values) of metals in natural fresh waters (adapted from ref. [1]).

iv) OELs – occupational exposure limits by WHO and EEC; ADIs – acceptable daily intake values by WHO and FAO; TLVs – threshold limit values in the U.S.A.; MACs – maximal allowable concentrations in Germany; MPCs – maximal permissible concentrations in Russia.

v) In some countries, speciation programs have already been established, e. g., the Swiss MELIMEX (metal limnological experiment) from the late 1970ies, probing the ecological consequences of heavy metal loadings on the limnic ecosystem [15] or the more general German ESB (environmental specimen banking) program (starting in 1985), a systematic collection, characterization, and storage of representative environmental samples from marine, limnic, and terrestrial ecosystems. In the latter case, AAS, ICP-MS, ASV, and NAA are the main techniques involved, but the development of the analytical procedures is still on the way [16].

Table 1
Occurrence of metal ions under fresh water conditions (pH 8.0), explanation see text (table adapted from ref. [20]).

Group	Metal	Major Species	$c_{M^{n+}} / c_M^{tot}$
I	Li, Na, K	Li^I, Na^I, K^I	1.00
	Ba	Ba^{II}	0.95
	Mg, Ca, Sr	Mg^{II}, Ca^{II}, Sr^{II}	0.94
II	Ag	Ag^I, AgCl	0.6
	Cd	Cd^{II}, $CdCO_3$	0.5
	Ni, Zn	Ni^{II}, $NiCO_3$, Zn^{II}, $ZnCO_3$	0.4
	Cu	$CuCO_3$, $Cu(OH)_2$	0.01
	Pb	$PbCO_3$	5×10^{-3}
	Hg	$Hg(OH)_2$	1×10^{-10}

the latter reflecting the Irving-Williams series *(Table 1)* [19, 20]. Here, the total amount of Pb lies in the concentration range of 10-50 ng l^{-1}/400 ng l^{-1} (in natural/polluted water) and is bound to particles, whereas Cd is nearly totally dissolved and available in its free ionic form in the typical concentration ranges of 5-20 ng l^{-1}/15-75 ng l^{-1} and for Cu, 1 % of the 50-200 ng l^{-1}/2000 ng l^{-1} are directly accessible as free ions [18]. Regarding in situ analysis, the electrolytic range under investigation with an ionic strength of 10^{-2} M (fresh water) and of 0.7 M (seawater) can be of major importance [18].

In natural surface water reservoirs, a lot of oxidizing and reducing agents as well as natural sensitizers and quenchers are present; and sunlight wavelengths below 325 nm produce 10^{19} solvated electrons per liter per hour (0.026 M reducing power l^{-1} h^{-1}). The typical pH range in lakes is 5.0-9.0, in oceans 7.6-8.4, depending on both, the amount of dissolved gases and temperature [21].

When dealing with remote sensing of metal ions in biotic samples (e. g., body tissues or fluids), the picture gets a lot more complicated. Most of all, the high electrolytic concentration, high molar absorptivity, and autofluorescence of many amino acids and proteins are responsible for even more viscious matrix effects. Details will not be given here and the following discussion of analytical techniques, possibilities, problems, and developments will focus on water analysis, but the reader should keep in mind that the situation is nearly always more complicated in biological matrices.

The analytical techniques known for the determination of metal ions can be divided into three groups, (i) "hot" methods (e. g., F/GFAAS or ICP-AES/MS), (ii) "cold" methods (e. g., HPLC (IEC), ASV, ISE, T/XRF), both mostly after sampling and sample preparation, and (iii) "*in situ*" techniques (e. g., ISE, ASV, fluorometry employing waveguide fluorosensors). Whereas "hot" methods usually yield only the total metal concentration, most of the "cold" methods suffer from contamination during sampling, which is one of the most severe and most frequent sources of error and one of the most crucial steps, as well as from contamination during sample preparation (e. g., membrane filtration) [22]. Many of these laboratory-based analytical techniques are handicapped by disruptive preparation techniques which may alter the chemical speciation of metals or lead to a loss of analyte before analysis, e. g., freezing, lyophilization, changes in pH, light-catalyzed reactions, reaction with the sample container [6]. Another problem of the rapid analysis of metal ions down to the trace level is preconcentration (e. g., with different chelators or column techniques). Here, detection power and vulnerability due to matrix interferences are often limiting factors.

This leaves only few analytical techniques which are suitable for the on-line and *in situ* monitoring of the free metal ion concentration, i. e., ISE, ASV, and fluorometry. However, in the case of most heavy and transition metals, the ion-specific electrode is not sensitive enough to permit the measurement of free metal ion activity and even for the most convenient method today, ASV, strong interferences are observed for electrochemically labile complexes, e. g., carbonates [10, 18]. In any case, special attention has to be focussed on soluble complex formers, e. g., humic and fulvic acids, which tie up metal ions.[vi]

The third analytical technique suitable for *in situ* determination or remote sensing of metal ions in solution, is fluorometry, especially in combintaion with fiber optics and sensors equipped with metal ion-sensitive fluorescent probes.[vii] These so-called "optrodes" can be directly inserted into a liquid sample and produce a quantitative fluorescence signal with high spatial resolution in real time and without the need of sophisticated and expensive instrumentation [26]. Although most metal ions of interest are non-fluorescent, their fluorometric detection is possible with the aid of fluorescent ligands or specially tailored fluorescent probes (see below). Fluorescence spectroscopy is a very sensitive method (down to single molecule detection) and could be employed for highly selective meas-urements as well as for screening purposes (depending on the fluorescent probe used). With the choice of an appropriate receptor (of the probe), complexation could be quick and reversible resulting in an analytically favorable fast system response. "Zero"-background measurements are possible with NIR-fluorescent probes and, depending on the design principle of the fluorescent probe, cation-induced changes in intensities, ratios of intensities (internally calibrated "2-band systems") and/or fluorescence lifetimes could be measured. Additionally, fluorometry is a non-destructive method and with the aid of lasers as excitation sources, only small sample volumes are required. Furthermore, limiting factors often encountered in the simultaneous determination of ions in liquid solutions with steady-state fluorometry can be improved employing time-resolved fluorometry. Time-resolved recording of fluorescence spectra enables not only the simultaneous determination of spectrally very similar analytes having different fluorescence decay times but additionally allows for the temporal discrimination of scattered light and background fluorescence. Moreover, the detection of a certain fluorescence lifetime at a given wavelength contains two independent analyte-specific informations.

---

vi) Examples for the interaction and bioavailability of free Cu^{II} and Zn^{II} and their effect on a limnic ecosystem are given in ref. [23], the speciation of Hg is for example reviewed in ref. [24], and a review of instrumental techniques for the determination of heavy metal-humic substance complexes and interactions was published in ref. [25].

vii) Note that optrodes can be utilized for UV/Vis/NIR spectrophotometric sensing as well.

The main problems encountered in fluorometric metal ion analysis are the relatively small dynamic range (i. e., compared to electrochemical methods), the influence of the matrix and quenchers, the tedious "desktop-design" of fluorescent probes (especially in terms of predictability of spectral data, fluorescence quantum yields, and lifetimes of the different complexes), the photochemical stability, and the water solubility of the fluorescent probes.

Concerning matrix interferences, humic substances are the most prominent intruders due to their absorption up to 650 nm (maximum at 260-300 nm with the molar absorptivity decreasing with increasing wavelength) and their (pH-dependent) fluorescence in the 450-540 nm region (with flat maxima and low fluorescence quantum yields) [27]. Furthermore, some of the metal-humic acid complexes are fluorescent [28].[viii, ix]

With respect to the "cold" analytical methods discussed before, most of the advantages of fluorescence measurements described can be utilized for analyte detection in combination with one of those methods, namely HPLC. Lasers are the ideal excitation sources for the small sample volumes in LC capillaries. The sensitivity of ion exchange chromatography can be enhanced by measuring laser-induced fluorescence [31]. Moreover, besides retention time and emission wavelength, the time-resolved recording of fluorescence contains a third and independent analyte-specific parameter.

1.2 Spectroscopic Behavior of Metal Ion Complexes

According to their fluorometric behavior, metal ions can be divided into two groups, (i) certain luminescent rare-earth and (ii) non-fluorescent main group and transition metal ions. The latter group, the ions of interest here, can be further divided into two groups concerning their "passive" fluorometric, or more generally speaking, spectroscopic behavior: (i) diamagnetic ions with a closed d subshell (main group metal ions, Zn^{II}, Cd^{II}, and Hg^{II}) and (ii) paramagnetic ions with an open d shell (transition metal ions such as Cu^{II}, Ni^{II}, or Fe^{II}) [32].

The diamagnetic ions usually form fluorescent complexes with fluorescent or non-fluorescent ligands, where the metal ion does not largely influence the $\pi\rightarrow\pi^*$ transitions of the organic fluorophore. Thus, the emission spectra of the free and complexed fluorophore are often very similar. In contrast, complexes of a certain fluorophore with various M^{n+} could differ in their fluorescence quantum yields and lifetimes. For these complexes, normally the fluorescence decay time decreases with increasing atomic number (Z) of the complexed ion, mostly due to enhanced spin-orbit coupling (heavy atom effect) [33]. The spin-orbit coupling constant ζ shows a Z^4 dependence and is itself proportional to the intersystem crossing rate ($k_{isc} \propto \zeta n,l^2$; n, l-quantum numbers). But especially this effect of complex formation on the fluorescence lifetime of a particular probe can be of analytical value since it allows for the discrimination between various metal ions in mixtures employing time-resolved fluorometry without prior separation [34-37].

Whereas diamagnetic metal ions do not absorb in the UV/Vis range of the spectrum,[x] paramagnetic ions with unfilled subshells may exhibit absorption bands in this spectral region due to metal ion centered d-d transitions [38]. These metal-centered and spin-allowed (but formally forbidden) d-d transitions possess only weak oscillator strength but are often lower lying in energy than the $\pi\rightarrow\pi^*$ transitions of the ligand. Thus, in complexes with a lowest spin-allowed transition of such a nature, non-radiative deactivation most successfully competes with emission and leads to the well-known fluorescence quenching in these complexes.

Depending on the relative energy level position of the orbitals involved, absorption of a photon in complexes with paramagnetic metal ions may also lead to promotion of an electron from a metal-centered to a ligand-centered orbital or vice versa (MLCT, metal-to-ligand charge transfer; LMCT, ligand-to-metal charge transfer) [39]. Furthermore, state mixing (with π-type d_{xz} and d_{yz} atom orbitals of the metal ion) is often observed for these complexes which opens another pathway to enhanced spin-orbit coupling resulting in fluorescence quenching [39, 40]. Increasing rate constants of spin-forbidden intersystem crossing transitions ($S_1\rightarrow T_n^*$) as well as spin-forbidden radiative processes ($T_1^*\rightarrow S_0$ phosphorescence) or energy transfer are often observed [41]. Another fact that has to be considered in fluorometeric analysis of paramagnetic metal ions is the heavy atom effect. As discussed for diamagnetic ions, this effect reinforces the trends already described for paramagnetic ions and non-radiative deactivation processes tend to be favored over fluorescence.

Chelates with paramagnetic central ions that are easily reducible or oxidizable such as $Ru(bipy)_3^{2+}$ often show MLCT and/or LMCT luminescence [32]. For these complexes, the absorption spectrum is often a linear combination of ligand centered $\pi\rightarrow\pi^*$ and MLCT transitions[xi] and luminescence is assigned to long-lived processes [32a]. However, the picture simplifies for most analytically relevant paramagnetic ions, e. g., Cu^{II}, Ni^{II}, or Co^{II}, which normally do not show any MLCT or LMCT luminescence. But accordingly, these analytically advantageous properties are inapplicable for the transition metal ions studied in this thesis.

1.3 Fluorescent Probes

The term "fluorescent probes", with respect to metal ion sensing, combines organic sensor molecules which can interact with a metal ion either "actively" or "passively". In this case, "actively" means that a probe molecule actually forms a complex with the metal ion (already in the ground state), whereas "passive interaction" stands for any kind of excited-state photophysical reaction between a metal ion and a probe molecule. Fluorescent probes of the first type contain metalophile coordination sites and the complexation-induced photophysical effects are often observed in both, the ground

viii) The study of the interaction and complexation of Cu^{II} with humic and fulvic acids by means of fluorescence spectroscopy (e. g., Stern-Volmer analysis of fluorescence quenching data and titrations) was described in detail by *Esteves da Silva, Lombardi,* and *Butler* [29].

ix) For a more general introduction to fluorometric (metal ion) analysis in biological and biochemical samples, the reader is referred to ref. [30].

x) The spin-allowed, metal-localized transitions are normally much higher in energy than any $S_0\rightarrow S_1^*$ transitions localized on an organic ligand.

xi) The weak d-d transitions are mostly hidden by the transitions with higher oscillator strength.

and the excited state. Thus, e. g., in these probes, any quenching of the emission (e. g., with paramagnetic ions) can be described as static quenching. On the other hand, for the second group of fluorescent sensor molecules, all the processes providing the analytical signal (mostly luminescence quenching) are diffusion controlled, e. g., dynamic quenching is observed. As this work only deals with "active" fluorescent probes, which is by far the dominant group of sensing molecules, "passive" probes are not considered any further.[xii]

1.3.1 Classification

Based on the spectroscopic behavior of metal ions, the procedures for fluorometric determination of these non-fluorescent analytes often entail complexation of the metal ion with an organic bi- or multidentate ligand (chelating ligands, podands), yielding a fluorescent complex. In other cases, metal ion-induced quenching of the fluorescence of an organic sensor molecule is utilized to transduce the analytical signal.[xiii] As indicated in Ch. 1.2, the possibilities in fluorometry with well-known organic ligands as ion sensors are partly very limited, mainly with respect to the lack of spectral differences in both absorption and emission. Additionally, a lot of these ligands are not very ion-selective. Thus, besides the search for new *fluorescent ligands*, the design of fluorescent probes showing larger complexation-induced spectral shifts, higher selectivity, and stronger ion-induced fluorescence enhancement became of growing interest [44]. The synthetic possibilities of carefully directed control and alteration of these properties shifted research activities from fluorescent ligands to fluorescent probes built in a modular way, i. e., chromophore and receptor unit can be altered separately and specifically. Within this framework of modular probes, three main design principles have been developed during the past 20 years.[xiv] Two of them involve cation-induced modifications of intramolecular electron or charge transfer processes and these probes are commonly labeled *intrinsic* and *(P)ET fluorescent probes*, depending on the electronic conjugation of receptor and fluorophore subunit.[xv] The sensing principle of the third type of probe is based on cation-controlled excimer or *exciplex formation*. All the sensor approaches and their signalling mechanisms will be introduced in the following chapter.

xii) For analytical applications of "passive" fluorescent probes, see ref. [42].

xiii) The topic of fluorometric metal ion analysis is reviewed every two years in *Analytical Chemistry*, in subsections of the general reviews on the use of fluorometry in chemical analysis [43].

xiv) Besides these "classic" fluorescent probes a large number of other probes and reagents is employed in this field of analytics. The reader is referred to the follwing review articles for further details on, e. g., calixarenes [45], transition metal complexes as probes [46], and specific compounds used in optrodes [47]. A general review covering most of the field of fluorescent sensors and switches has only appeared recently [48].

xv) To avoid any confusion, the term *(P)ET fluorescent probe* is used instead of the term *conjugate fluorescent probe* [49, 50]. Within the latter nomenclature, *intrinsic* probes are not seen as being "modular" but as being a subgroup of fluorescent ligands. Only probes with a fluorophore-spacer-receptor design are modular, i. e., they exist of receptor and fluorophore in a *conjugate* arrangement. *Conjugate* in this sense means the exact opposite of direct electronic conjugation.

1.3.2 Design Principles

1.3.2.1 Fluorescent Ligands

Organic molecules acting as bi- or multidentate ligands for metal ions could either be fluorescent in both the uncomplexed and complexed state or they are virtually non-fluorescent as free probe and form fluorescent metal ion complexes. Having the spectroscopic behavior of metal ions given above (Ch. 1.2) in mind, this accounts only for the detection of diamagnetic ions. Paramagnetic metal ions usually lead to static fluorescence quenching, i. e., the stable complexes formed in the ground state are excited and deactivation of the S_1 state is predominantly non-radiative. Thus, fluorescence quenching studies are mostly performed when fluorescent ligands are employed to probe paramagnetic ions [51, 52].

In the free ligand, the non- (n-) and the π-bonding orbitals are occupied and both, $n\rightarrow\pi^*$ and $\pi\rightarrow\pi^*$ transitions are possible in absorption. Upon complexation to diamagnetic ions, i. e., coordination to a heterocyclic nitrogen atom, the n-bonding orbitals are lowered in energy and thus the $n\rightarrow\pi^*$ transitions are raised in energy. Accordingly, the main absorption bands of these complexes originate from ligand centered $\pi\rightarrow\pi^*$ transitions, which are mainly unperturbed by metal ion complexation and show similar energies of absorption and oscillator strengths as the free ligand. Additionally, the lowest excited singlet state in these complexes is expected to have $\pi\pi^*$ nature. The possibilities for metal ion detection due to spectral separation of a mixture of various emitting complexes of a certain probe are mostly poor and today, only selective fluorescent ligands, applications in LC or in combination with time-resolved fluorometry play a role in analytical chemistry. However, numerous applications of fluorescent chelates of organic ligands have been described in the literature over the past 130 years,[xvi] ranging from simple extraction experiments via pre- or post-column derivatization procedures in chromatography to *in situ* sensing with fiber optics and immobilized probe molecules [51, 52, 55].

1.3.2.2 Modular Intrinsic Fluorescent Probes

The development of specifically designed fluorescent probes started at the interface of photophysical and supramolecular chemistry. On the one side, the discovery of crown ethers and related compounds [56, 57] opened up new possibilities for improved selectivity in metal ion recognition and on the other side, the specific tuning of chromo- and fluorophores in fields of advanced dye applications (e. g., laser dyes) lead to the combination of crown ether-derived receptors with certain fluorophores yielding so-called fluoroionophores [58]. Especially the rapidly expanding area of crown ether research made the development of receptors for alkali and alkaline-earth metal ions possible, ions, for which a lack of selective or sensitive fluorescent ligands existed. To meet the interfering matrix effects and to provide sensors which could be excited and detected in the visible range of the spectrum, donor-acceptor-substituted aromatic or heteroaromatic fluorophores showing intense intramolecular charge transfer

xvi) In 1867, *Goppelsröder* proposed the first analytical application of an organic ligand in fluorometric metal ion analysis, i. e., the determination of Al^{III} with Morin [53]. And still today, new fluorescent ligands are developed [54], although the main research interest is shifted towards modular fluorescent probes.

absorption and emission bands ≥ 400 nm were mainly chosen for the fluoroionophore design. Thus, the first fluoroionophores developed for alkali and alkaline-earth metal ions contained a tetra- or pentaoxa monoaza or benzo crown ether, where the nitrogen atom or the phenyl ring of the crown was part of the fluorophore, i. e., served as donor moiety [58]. Accordingly, the sensing principle of intrinsic fluorescent probes is based on cation-induced perturbation of the ICT reaction leading to both shifts in absorption and emission (see *Fig. 4A*) [59, 60]. Upon complexation of an ion, the electron densities in the molecule are changed resulting in a reduction of the donating ability of the receptor moiety. Depending on the fluorophore chosen, effects of complexation on the fluorescence quantum yield and lifetime are also observed (both, enhancement and quenching), but mostly the intensity effects are less pronounced than the corresponding spectral changes.

1.3.2.3 Modular (P)ET – (Photoinduced) Electron Transfer – Fluorescent Probes

In contrast to the directly coupled fluorophore and receptor of intrinsic probes, a short alkyl spacer (typically one or two methylene groups) resides between these two functional parts of the molecule in the ideal (P)ET probe [61, 62]. Thus, the forces that could be active in these electronically decoupled systems must be of long-range nature such as electron transfer. In an ideal system, the spectral properties of the free probe molecule directly resemble those of the fluorophore but due to the energy level of the HOMO of the receptor, a fast electron transfer quenches the emission from the fluorophore *(Fig. 4B)*. Accordingly, in an ideal electronically decoupled system, complexation of a cation to the receptor part of the molecule does not change the energetic position of the fluorophore-based HOMO and LUMO, respectively. However, the energy levels of the receptor are drastically altered and the redox potential is increased leading to a lowering of the energy of the receptor's HOMO. This lowering of the energy of the receptor's HOMO prevents or slows down the light-induced electron transfer process being responsible for the quenching of the fluorophore emission in the uncomplexed probe. Correspondingly, absorption of a photon by the complex results in fluorescence, i. e., the emission of the probe is "switched on" due to the blocking of this fluorescence deactivation pathway *(Fig. 4B)*. The analytically valuable signals which could be derived from such a (P)ET system,

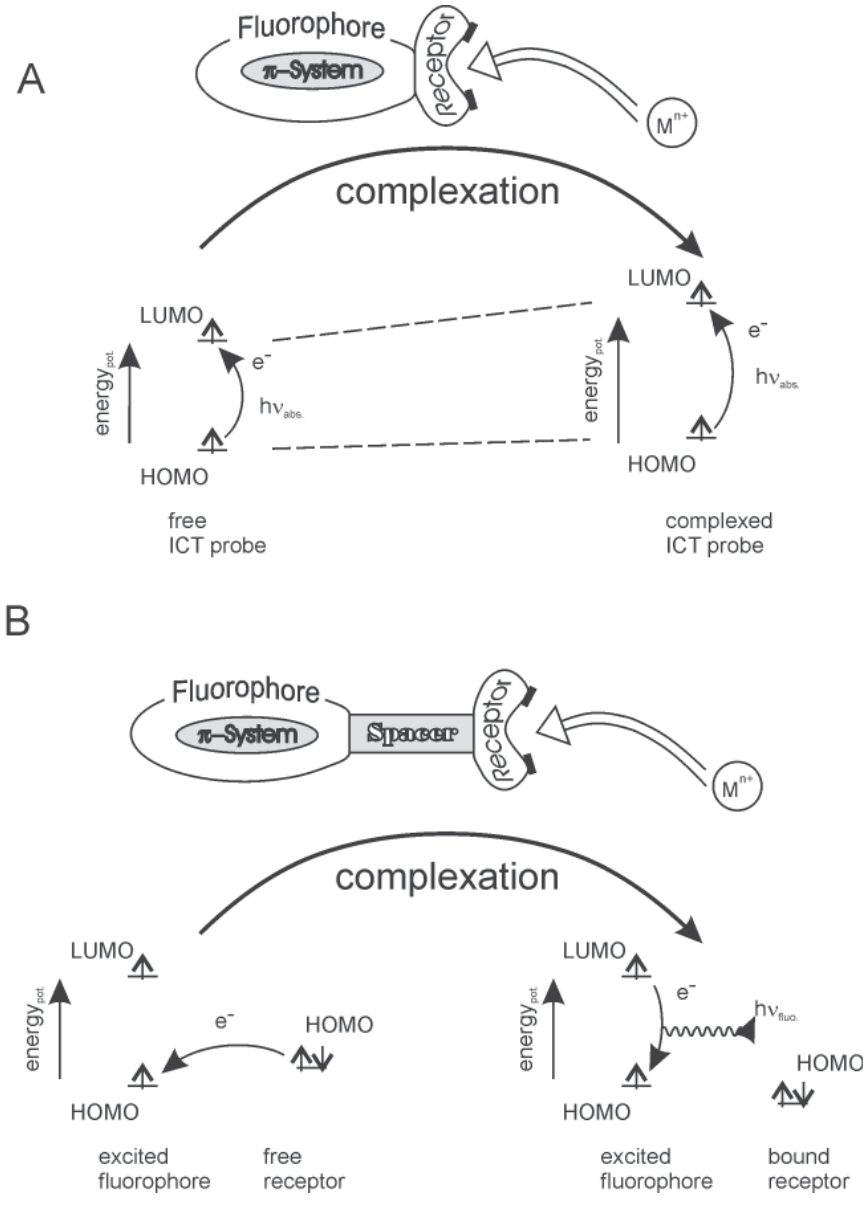

Fig. 4
Schematic description of the two main classes of modular fluorescent probes. ***A*** *- intrinsic probe,* ***B*** *- ideal (P)ET probe; explanation see text.*

are drastic changes in fluorescence intensity and lifetime. In contrast to intrinsic probes, fluorescence enhancement factors (FEF) of 30 to 300 are observed for (P)ET probes, but on the other hand, complexes of a particular (P)ET probe with different metal ions cannot be spectrally separated [61, 63].

However, when (weak) electronic interactions occur in these spacer-bridged probes, the picture in *Fig. 4B* is not valid anymore since the MOs are not strictly localized on either fluorophore or receptor. Especially when the fluorophore itself shows (strong) ICT characteristics and the quenching ET is only a second, competing intramolecular charge/electron transfer process, the term "PET" is misleading. Thus, the formally decoupled fluorophore-spacer-receptor probes are referred to as ET probes in the following chapters.

1.3.2.4 Modular Fluorescent Probes Based on Exciplex or Excimer Formation

The last class of fluorescent probes which will be discussed only briefly in this introduction, are fluorescent probes based on exciplex or excimer formation. Many of these probes contain two (or more) fluorophores of the same type which are integrated in or attached to a crown ether [64] or calixarene body [65] and are able to form fluorescent excimers (or exciplexes, if two different fluorophores are involved). In the uncomplexed state, the flexibility of the crown moieties leads to no particular spatial arrangement of the two fluorophores and the fluorescence spectrum is dominated by monomer emission from both fluorophores. Upon complexation, coordination of one or two metal ions to the crown ether's heteroatoms leads to a strong reduction of the conformational flexibility and to a prearrangement of the two fluorophores (e. g., at a certain distance and orientation that is required for energy transfer). This results in a strong enhancement of excimer emission and a corresponding decrease in monomer emission. The mechanism of the second group of these probes is mainly based on nitrogen-aryl interaction and accordingly, these probes consist of an aromatic fluorophore and a nitrogen containing crown ether or cryptand receptor [66]. Most of the systems described in the literature so far are anthracenophanes [64b, 67] and exciplex probes containing the aromatic hydrocarbons naphthalene [64d], anthracene [66a-c], and pyrene [68] and an amine donor. Among others, (differently substituted) bicoumarines [69], thiophenes [65b, 70], or pyridine substituted [65d] probes are found.

1.3.3 The Story so far

The Story so far will comprise some examples of modular fluorescent probes including intrinsic as well as ET probes, historic as well as recent developments, comments on chromophore as well as receptor diversity, and will give some instrumental information.

Starting with intrinsic probes, about two decades ago, *Vögtle* et al. published their pioneering work on chromo- and fluoroionophores [58, 71] and nearly fifteen years ago, this class of reagents was introduced to analytical chemistry, mainly biochemical analysis, on an applicationary level [72-75]. By the end of the 1980ies, first publications dealing with the complexation-induced mechanisms governing the photophysical behavior of these ICT probes were published [76, 77a, 78]. Since then, a lot of research groups have developed new intrinsic fluorescent probes with a great variety of spectral properties. Besides the commercially available probes based mostly on substituted benzofuranes [72a, c, d, 79, 80] and rhodamine-related structures [81-83], chromophoric systems such as heterocyclic styrene analogues [76, 84, 85], coumarins [74, 86 [xvii], 87-89], merocyanines [77], acridinium derivatives [78], various functionalized styryl and cyanine dyes [90-95], donor-acceptor-substituted stilbenes [96], squaraine dyes [97-99], as well as a lot of other chromophores [73, 100-106] have been utilized for the design of such modular probes.

Research in the field of modular fluorophore-spacer-receptor probes started *ca.* 20 years ago as well. *Sousa* et al. incorporated naphthalene units in polyether chains [49, 107] and until today, polyaromatic hydrocarbon fluorophores play a major role in (P)ET probe design. Most widely used is the fluorophore anthracene [108-113]. Heterocyclic fluorophores include pyrazoline derivatives [85a, 108e, 114-116] substituted coumarins [117, 118], and various other dyes [105a, 119].

In contrast to the great variety of fluorophores, only a considerably small number of different receptors has been employed so far. About at least half of the modular fluorescent probes described until today carry one of the well-known A15C5[xviii] or B15C5 [90a, c-f, 102, 104c, 108b, h] receptors and a lot of the remaining reagents are equipped with the related crown ether derivatives A12C4 [89c, 97b, 102, 103a, 119d], A18C6,[xix] B18C6 [89b, 101, 108b, 119c], $A_2$18C6 [86b, c, 87, 104b, 105b, 108d, 117, 118, 119a], $A_2$15C5 [105b, 114b, 117], or their cryptand analogues [74, 88, 89a, d, 108d, 112]. Some of the more "exotic" receptors comprise the sulfur containing $BT_2$18C6 [90d], $T_4$14C4 [110e, f], and $A_2T_2$14C4 [120], open chain polyethers with chromophoric endgroups [69a, 121], or a polyether with an incorporated chromophore where the heteroatoms of the chromophore take part in coordination as "pseudo"-macrocyclic donor atoms [104d]. Moreover, polyaza crown ether analogues and open chain polyamines are used in various ET probes [109, 110a-e, g, 113c, 119e]. For the great majority of intrinsic probes equipped with crowns and cryptands, the nitrogen atom of the aza crown (or the phenyl ring of the benzo crown) represents the donor part of the probe[xx]. The same principle is used in the second (and only other) group of wide-spread receptors, derivatives of the open chain chelating agents EGTA or BAPTA [72a, 79b, 80-83, 98c, 108e, g, 114a].

Despite their unique complexation properties and their large number of derivatives and functionalized analogues described

xvii) The coumarin derivatives investigated by Valeur et al. are no intrinsic probes in the strict sense, since the crown ether moiety and the coumarin chromophore are not directly coupled but linked by a methylene spacer. However, the working principle and observed behavior is an "intrinsic one" because incorporation of a cation in the crown leads to electrostatic interactions with the adjacent carbonyl groups of the coumarin and induces a change in acceptor strength.

xviii) see refs 72c, 76-78, 79a, 84, 85, 86a, b, d, 89e, 90e, 91, 92, 93b, c, 94-96, 97a, 99, 102, 103, 104e, 105, 106, 108a, 116, 118, 119b

xix) see refs 73, 93a, 98b, c, 102, 104a, 105b, 108a, c, 111, 113a, 118, 119a

xx) Only recently, *Lapouyade* et al. developed stilbene-related ICT probes with a donor-donor configuration. Whereas one donor is a dimethylamino group, the other one is an aza crown. Upon metal ion binding, this second donor is turned into an acceptor and a bathochromic shift is observed in the optical spectra [96d].

and synthesized so far, this lack of control of the specifity of a given probe via its receptor is remarkable. Since their discovery [56], a vast quantity of crown ethers and crytands with ring sizes ranging from 3 to > 20, donor atoms ranging from nitrogen to selenium, and functionalization with many different side arms or subsituents have been described [122, 123]. Even more variations are possible and were (partly) realized with bi- or polycyclic cryptands [57, 124].

The lack in receptor variety is partly understandable, because in the beginning of fluoroionophore research, the predominant aim was the development of probes for alkali and alkaline-earth metal ions relevant in medical and biological chemistry[xxi]. However, the rapidly growing interest in environmental sensing of heavy and transition metal ions over the past 15 years did not lead to further diversity on the receptor side of the probes synthesized lately. Accordingly, the number of fluoroionophores for alkali and alkaline-earth metal ions is still large compared to that for heavy and transition metal ions, especially in the field of intrinsic probes [69a, 78b, 80, 82a, 86c, 90d, 104a, 105b, 126]. Here, the concept of modular ET probes seems to be more promising for the development of probes for heavy and transition metal ions[xxii], [109, 110a-e, g, 112, 113c, 119d, e].

However, the main problem in fluorometric heavy and transition metal ion determination resides with most of the probes developed so far, showing complexation-induced non-specific fluorescence quenching due to heavy atom effect or paramagnetism [128]. Even a lot of other sensing concepts realized lately were not very successful in solving this disadvantage[xxiii]. Only very few examples of fluorescent probes undergoing fluorescence enhancement upon coordination to these well-known quenchers have been reported [105, 112, 135].

Devoting the attention once more to the instrumental and analytical side of metal ion determination with fluoroionophores, the considerably small number of publications dealing with the time-resolved emission behavior of the probes and their complexes is apparent[xxiv]. As already mentioned above, employing TRES with lasers as excitation sources should lead to improved sensitivity and selectivity in the case of modular fluorescent probes as well.

1.4 The Scope of this Thesis

In this thesis, four different types of fluorescent probes for metal ions are investigated and compared. Besides the description of the photophysical properties and complexation behavior of each system, the attention is especially directed towards new possibilities in ion discrimination by both the choice of a specific receptor and application of time-resolved fluorometry. Furthermore, a new design principle for fluorescent probes showing extremely high fluorescence enhancement factors is presented.

The fluorescent ligand 2,2‘-bipyridyl-3,3‘-diol is introduced for the determination of heavy and transition metal ions and its potential in ion sensing via a two-dimensional approach, the wavelength- and time-resolved emission matrix, is described.

In order to get more insight into fluorescence enhancement or quenching processes observed for ICT fluorescent probes, donor-acceptor-substituted chalcones are investigated. Within this part of the work, both the influence of the acceptor on the photophysical properties of a particular chromophoric system and the influence of the receptor on ion recognition are examined.

The applicability of new receptors for improved cation selectivity and fluorescence enhancement generation is a major question adressed by the investigation of the triaryl-Δ^2-pyrazoline-based ET probes. Besides the well-known A15C5 receptor, its thia analogue has been chosen as a binding unit.

In an attempt to design highly efficient fluorescent probes, a combined, “quasi-CT/ET” approach is realized and the “virtual” or “zero”-spacer, highly pretwisted *b*oron *dip*yrromethene probe BDP-A15C5 is photophysically and complexometrically studied.

Finally, a comparison of the fluorescent probes is given, the different design principles serving as a background.

---

xxi) For examples on fluorescent probe applications in ion detection in recent medical chemistry research, see ref. [125].

xxii) During the past few years, another class of fluorescent probes, which is neither a (simple) ligand nor an intrinsic or ET probe, attracted some attention, i. e., spiro compounds [127]. They are photoswitchable between the open and closed (spiro) form and often the open form binds transition metal ions which in turn leads to changes in both absorption and emission.

xxiii) Fluorescent polymers on thiourea-basis [129], metal-chelating lipid membranes [130], newly designed Schiff base ligands [131], and functionalized podands [132], enzymatic sensors [133], or functionalized cyclodextrins [134].

xxiv) see refs 49, 76, 77a, b, d, 79, 81, 84, 85, 86b, d, 90a, 92, 96a, d, 97, 103, 104d, 105, 106, 107, 116, 119b, e

2 Experimental

2.1 Synthesis of Fluorescent Probes

2.1.1 2,2'-Bipyridyl-3,3'-diol ($BP(OH)_2$)

Most of the steady-state experiments dealing with the investigation of the fluorescent ligand $BP(OH)_2$ were performed with material provided by Prof. *Langhals*, University of Munich, the synthesis being described in ref. [136]. Time-resolved fluorescence and NMR experiments were carried out with $BP(OH)_2$ purchased from Aldrich. Whereas the former was not purified additionally, the latter was recrystallized from light petroleum and checked for purity by HPLC. Both charges showed identical spectroscopical behavior.

2.1.2 Chalcone Derivatives

The different donor- and/or acceptor-substituted chalcones were synthesized by the group of Prof. *Tolmachev* and Dr. *Bricks*, Academy of Sciences of the Ukraine in Kiev. Most of the synthetic details are already published and described in refs [85] and [137]. In general, the synthetic route consists of reaction of the fluorophore precursor 2-acetyl-X (X = benzothiazole, phenyl, etc.) with the corresponding 4-substituted benzaldehyde derivative [71c, 76, 85, 137b, c]. The 4-unsubstituted and 4-dimethylamino-substituted benzaldehyde precursors are commercially available and in the case of the A15C5 derivatives it was obtained from commercially available Ph-A15C5 via Vilsmeier reaction. For the synthesis of the $AT_4$15C5 derivatives, a similar strategy was employed, i. e., the preparation of the sulfur analogue 4-(*N*-$AT_4$15C5)-benzaldehyde in a first step followed by its condensation with 2-acetyl-X [137b, 138]. The synthesis of the bridged chalcones is described in [139].

2.1.3 Triaryl-Δ^2-Pyrazoline Derivatives

The triaryl-Δ^2-pyrazoline derivatives were synthesized by the group of Prof. *Tolmachev* and Dr. *Bricks* as well. Most of the synthetic details are described in refs [85] and [116]. In principle, the pyrazolines were obtained by refluxing the corresponding chalcone in ethanol with phenylhydrazine in the presence of acetic acid [85, 116].

2.1.4 Boron Dipyrromethene Derivatives

The boron dipyrromethene derivatives were synthesized by the group of Prof. *Daub*, University of Regensburg. Most of the synthetic details are described in refs [106] and [140]. Principally, the BDP dyes were obtained by reacting 2,4-dimethylpyrrole first with the corresponding benzaldehyde and then with dichlorodicyanobenzoquinone followed by addition of $BF_3 \cdot Et_2O$ [106].

All the chemical structures were confirmed by elemental analysis, ^{1}H-NMR, ^{13}C-NMR, and IR spectroscopy as well as mass spectrometry. For the chalcones and Δ^2-pyrazolines, synthesized by the Kiev group and characterized in Berlin (at BAM), purity was checked by reversed phase HPLC (HPLC set up from Merck-Hitachi; typical separation conditions: RP18 column, acetonitrile/water = 75/25 as eluent) employing UV detection (UV detector from Knaur; fixed wavelength and/or diode array detection). NMR spectra were obtained with a 500 MHz NMR spectrometer Varian $Unity_{plus}$ 500. IR spectra were measured with a Bruker FTIR-Spectrometer IFS66v. Mass spectra were recorded on a Finnigan MAT 95 spectrometer with an ESI-II/APCI-Source for electrospray ionization and the base peaks $[M+Na]^+$ were determined.

2.2 Metal Salts

All the analytical complexation studies in aqueous solutions were carried out with metal sulfates and nitrates from Aldrich and Merck of the highest purity commercially available. For the investigations in organic solvents (acetonitrile, methanol, ethanol) the corresponding perchlorates were purchased from ALFA, Aldrich, and Arcos. Alkali and alkaline-earth metal salts were dried in a vacuum oven at 140 °C and additionally/or 200 °C yielding $Me^{I}ClO_4$ and $Me^{II}(ClO_4)_2$. Heavy and transition metal perchlorates were dried to a definite water content employing different procedures described in ref. [141]. For example, in a typical procedure, $Hg^{II}(ClO_4)_2$ was dried at 75 °C for 12 h yielding $Hg^{II}(ClO_4)_2 \times 3H_2O$ and the dihydrate of zinc perchlorate was obtained by drying the raw product at 100 °C i. vac. for 12 h. Stock solutions were kept in an evacuated desiccator (P_2O_5) and stored in the dark at 4 °C.

2.3 Solvents and Buffers

Bidistilled water (pH 6.4) was provided by the Laboratory for Trace Elemental Analysis, BAM, Berlin, and the organic solvents used were of UV-spectroscopic grade and purchased from Merck, Fluka, or Aldrich. For the temperature-dependent photophysical experiments, the organic solvents were dried additionally [142].

Buffer salts for the adjustment of certain pH values of aqueous solutions as well as buffer salts employed in the analytical experiments in organic solvents were of analytical grade and purchased from Aldrich and Merck. For pH control, glycine/sodium chloride (tunable pH range < 3.4), citric acid/sodium hydroxide (tunable pH range < 6.4), potassium dihydrogenphosphate/disodium hydrogenphosphate (tunable pH range 5.4-8.0), soda/hydrochloric acid (tunable pH range 10.1-11.4), and borax/hydrochloric acid or sodium hydroxide (tunable pH range 9.4-11.0) buffers were used. The ionic strength of the organic solutions was kept constant with 0.1 M solutions of tetraethylammonium perchlorate in the corresponding solvent.

All the solvents and buffer solutions were checked for fluorescent impurities prior to use. Concentrated perchloric acid (70 %, Suprapur, Merck) was used for protonation reactions in acetonitrile solutions, concentrated hydrochloric acid (30 %, Suprapur, Merck), and sodium hydroxide monohydrate (Suprapur, Merck) were used for protonation/deprotonation reactions in aqueous solutions. All the organic stock solutions were kept under nitrogen and stored in the dark at 4 °C.

All the complexometric experiments reported here for fluorescent probes carrying crown ether receptors were carried out in acetonitrile, the solvent showing the complexation-

induced changes best. Due to the relatively high complex stability constants of the crown ethers and main group metal ions in acetonitrile, full complexation is more easily achieved in this solvent than in alcohols or water (i. e., in acetonitrile the smallest excess of metal cation is required to yield full complexation). Upon reaction between a metal ion and a crown ether, the solvent molecules in the primary solvation sphere of the cation have to be replaced (at least partly) by the ligand's donor heteroatoms. For the hard main group metal ions, this process is most favored in acetonitrile since this "soft" [143] solvent (only one nitrogen donor atom) has the weakest solvation ability compared to the "hard" solvents such as alcohols or water.

2.4 Basic Experimental Conditions

2.4.1 Sample Preparation

Most of the photophysical and all the analytical experiments were carried out in air-saturated solutions. In a typical complexation experiment, the solutions were pipetted in the following order: (i) V_L µl diluted stock solution of the fluorescent probe, (ii) V_{solv} µl of the solvent or buffer solution, and (iii) V_M µl diluted stock solution of the metal salt, acid, or any other solution (Appendix B). The solutions were stirred for 1 to 2 minutes and measured usually within 5 to 10 minutes after mixing. Except where otherwise noted, complexation was finished immediately after addition of the solution containing the metal salt and no slow reaction kinetics were observed in any experiment.

In experiments carried out in aqueous solution for pH-sensitive reactions (e. g., some titrations of $BP(OH)_2$), adequate buffers were employed. Typically, a phosphate buffer of pH 7.6 was used to keep the solutions at constant ionic strength.

2.4.2 Titration Experiments

In the case, where only results of absorption measurements were analyzed for a certain quantity, a typical UV/Vis-spectrophotometric titration was carried out in a 50 mm absorption cell by addition of small amounts of the titrant solution. When dealing with colored (paramagnetic) metal salt solutions the spectra were additionally corrected. For a combined spectrophotometric/fluorometric or for a solely fluorometric titration, 10 mm quartz cells were employed and for each titration step, a new solution was prepared. For more experimental details, see Appendix B.

2.5 Steady-State Spectroscopy

2.5.1 Absorption

Absorption spectra were recorded on a Carl Zeiss Specord M400/M500 absorption spectrometer and, only for the temperature-dependent absorption experiments, a Bruins Instruments Omega 10 spectrophotometer was employed. Quartz absorption cells of 10 and 50 mm optical pathlengths were usually used.

2.5.2 Fluorescence

Steady-state emission spectra were recorded on a Perkin Elmer LS50B and a Spectronics Instruments 8100 spectrofluorometer. For the fluorescence experiments, only dilute solutions with an optical density (o. d.) below 0.01 at the excitation wavelength (o. d. < 0.04 at the absorption maximum) were used.

For a typical analytical experiment with the LS50B fluorometer, excitation and emission wavelengths were selected by monochromators with 2.5 nm (excitation) and 7.5 nm (emission) spectral bandwidth and the spectra were scanned at a speed of 100 nm min^{-1}. A typical emission spectrum recorded with the 8100 fluorometer (equipped with additive double monochromators) was obtained with excitation and emission monochromators set at 2/8/2 nm (excitation) and 4/8/4 nm (emission) spectral bandwidth and a scan speed of 100 nm min^{-1}.

Whereas no polarizers were employed for the LS50B measurements, the emission polarizer was set at 54.7° for a typical emission experiment with the 8100 fluoro-meter. For the fluorescence excitation experiments, excitation polarizers were set at 0° (8100 fluorometer). All the fluorescence measurements were performed with a 90° setup and all the fluorescence spectra presented here are corrected for the spectral response of the detection system (calibrated quartz halogen lamp placed inside an integrating sphere; Gigahertz-Optik) and for the spectral irradiance of the excitation channel (calibrated silicon diode mounted at a sphere port; Gigahertz-Optik).

2.5.2.1 Determination of Fluorescence Quantum Yields

For the determination of the relative fluorescence quantum yields (ϕ_f), the optical densities of the dilute solutions at the excitation wavelengths were determined with a 100 mm absorption cell and were adjusted to an optical density of 0.1 ± 0.001. These solutions were transferred to a 10 mm quartz cell and the fluorescence measurements were performed either with the setup described above or, for highly fluorescent molecules with a small Stokes shift, the solution with the adjusted absorption was transferred to a 1 mm absorption cell and the fluorescence measurements were performed with a front face setup at an angle of 53° (minimum reflexion at maximum fluorescence signal). 2-Aminopyridine in 0.1 *N* H_2SO_4 (ϕ_f = 0.66 ± 0.05)[xxv] [144a], quinine sulfate in 1 *N* H_2SO_4 (ϕ_f = 0.55 ± 0.03) [144a, 146], coumarin 1 in ethanol (ϕ_f = 0.5) [147], fluorescein 27 in 0.1 *N* NaOH (ϕ_f = 0.90 ± 0.03) [148], DCM in methanol (ϕ_f = 0.43 ± 0.08) [149], and rhodamine 101 in ethanol (ϕ_f = 1.00 ± 0.02) [145a, b] were used as fluorescence standards in the recommended wavelength regions. The fluorescence quantum yields were calculated from several independent measurements (usually *N* = 4 or 6) and the calculated uncertainties of measurement are ± 5 % (for $\phi_f > 0.2$), ± 10 % (for $0.2 > \phi_f > 0.02$), ± 20 % (for $0.02 > \phi_f > 5 \times 10\text{-}3$), and ± 30 % (for $5 \times 10\text{-}3 > \phi_f$), respectively.

xxv) The data for 2-aminopyridine reported in the literature are divergent, but 0.66 seems to be the most reliable one. *Velapoldi* corrected his earlier published value of 0.42 [144b] and *Eaton* reports a close value of 0.6 [145a]. However, *Chen* published a value of 0.73 [145c].

2.6 Time-Resolved Fluorometry

Time-resolved fluorescence measurements were either performed with a laser impulse fluorometer with ps time resolution (ps-LIF) [37] or with synchrotron radiation from the Berlin Storage Ring for Synchrotron Radiation (BESSY) [36, 150]. Both setups are described in more detail in the following subsections.

In all the cases, fluorescence was collected at right angles. With both instruments, the fluorescence decay curves were recorded with a time-correlated single photon counting setup (TCSPC) [37, 150] and typical count rates were in the order of 1-4 x 10^3 counts s^{-1}. For all the fluorescence measurements, emission polarizers were set at 54.7°.

Temporal calibration of the experimental setups for the time-resolved measurements was checked with pinacyanol in ethanol (τ_f = 13 ± 1 ps) [151], rose bengal in methanol (τ_f = 0.50 ± 0.02 ns) [145a, b], POPOP in ethanol (τ_f = 1.35 ± 0.20 ns) [144c], and fluorescein 27 in 0.1 *N* NaOH (τ_f = 4.50 ± 0.03 ns) [144c].

2.6.1 ps Laser Impulse Fluorometer

The block diagram of the ps-LIF is shown in *Fig. 5*. Excitation source is a regenerative mode-locked Ti:Sapphire laser (Spectra Physics Model 3950) pumped with the 8 (to 11) W all-lines output of a cw argon ion laser (Spectra Physics Model 2040E-15S) providing pulses with 1.4 ps duration at a repetition rate of 82 MHz. For the measurement of decay times in the ns time domain, the repetition rate was reduced to 4 MHz by synchronized pulse selection (Spectra Physics Model 3980). Second harmonic generation was obtained in a 10 mm LBO crystal. Depending on the required excitation wavelength, the second harmonic was used directly or the sum frequency of the ground wave and the second harmonic was generated in a 10 mm BBO crystal (MHG system: Spectra Physics Model 3981-3). The laser beam was attenuated using a double prism attenuator from LTB and typical excitation energies were in the nW to µW range (average laser power). The excitation energies were checked and adjusted with a calibrated Si diode (Model 221 with 100:1 attenuator 2550, Graseby) and an optometer (Model S370, Graseby).

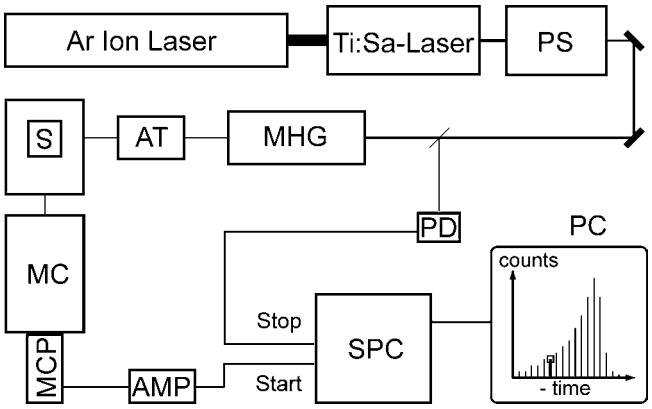

Fig. 5
Block diagram for time-resolved measurements with the ps-LIF: pulse selector (PS), multi harmonic generation (MHG), attenuator (AT), sample (S), monochromator (MC), micro channel plate photomultiplier tube (MCP), amplifier (AMP), photodiode (PD), single photon counting setup (SPC), personal computer (PC); description see text.

In a typical experiment, the pulse peak power was 3 x 10^{-3} W (5 x 10^{-2} W) in the 82 MHz (4 MHz) mode. For example, concerning a typical measurement at 470 nm the sample was excited with ca. 10^5 photons per pulse.

The emission wavelengths were selected with a subtractive double monochromator (AMKO Model 01-002S) and a typical bandwidth of 8 nm.

Due to repetitive laser pulsing with a definite temporal spacing, for TCSPC detection, an emitted photon detected by the MCP and passed through a CFD provides the "start" signal of the TAC (for abbreviations see Appendix A). The event is stopped by an excitation pulse registered by the PD and passed through a CFD (and a delay line). After A/D conversion the signals are stored in a MCA (micro channel analyzer, PC slot card). The temporal response of the system was typically 35 ps (optimum: 25 ps) and for a single decay, typically data were accumulated up to 10 000 counts in the peak channel (CPC).

The fluorescence lifetime profiles were recorded with time divisions of 5.2 ps $channel^{-1}$ (82 and 4 MHz version), 13.1 ps $channel^{-1}$ (82 MHz version), and 52.6 ps $channel^{-1}$ (4 MHz version) yielding the corresponding experimental accuracies of ± 3 ps, ± 8 ps, and ± 0.04 ns, respectively. For the estimation of the color shift (wavelength-dependent temporal response of the detection system) between the instrumental response function and the actual fluorescence decay, the fluorescence of coumarin 1 (in ethanol), fluorescein 27 (in 0.1 *N* NaOH), and DCM (in ethanol) were quenched by saturation with potassium iodide and their decay profiles were recorded at the corresponding emission wavelengths.

2.6.2 BESSY

The pulsed excitation source BESSY allowed for a temporal resolution of ca. 100 ps (single-bunch mode; 4.8 MHz) and the excitation wavelength of the synchrotron radiation was selected with a monochromator with 4 nm spectral bandwidth. The emission monochromator was usually set at a spectral bandwidth of 8 nm. The fluorescence decay curves were recorded with a time division of 55.5 ps chn^{-1} and an experimental accuracy of ± 0.04 ns. With this excitation source, decays were typically accumulated up to 5 000 CPC.

2.7 Temperature-Dependent Measurements

The temperature-dependent measurements were performed with a continuous flow He cryostat CF 1204 from Oxford Instruments. Liquid helium was pumped from a storage container via a transfer tube (GFS 300, Oxford Instruments) and flow control (VC 30, Oxford Instruments) by a gas flow pump (GF 2, Oxford Instruments) through the cryostat. The temperature was externally controlled by heating and flow adjustment with the temperature controller ITC 4 from Oxford Instruments. The temperature in the sample rod was monitored via the temperature-dependent resistance of a sensor which was calibrated with a Peltier element. When a constant current is applied, the voltage and thus the resistance measured is proportional to temperature.

Method of Cooling. The temperature was gradually decreased in steps of 15 or 20 degrees (at > 170 K) with

equilibration times of 20 min at every point of measurement. Then the sample was immediately chilled (with liquid He to T = 10 or 30 K), equilibrated for 40 min, and heated up in steps of 20 K (equilibration time of 20 min) to 170 K.

2.8 Mathematical Treatment of Spectroscopic Data

2.8.1 Steady-State Spectra

Spectral band shape fitting of absorption and emission spectra was usually done with the non-linear curve fitting routine implemented in the software package Origin (Vers. 3 to 5, Microcal, Inc.) based on gaussian or lognormal fitting procedures.

For the analytical measurements, the spectra of mixtures were analyzed with the software packages AproMax and ParaMax (Dr. *Stahl*/BAM) based on a linear singular value decomposition algorithm to give the single spectral contours of the species. A typical data record analyzed consisted of 500 points for a single steady-state spectrum.

2.8.2 Fluorescence Decay Data

Analysis of fluorescence decay data was made on a PC using the software packages DecaMax (Dr. *Stahl*/ BAM), Globals Unlimited V2.2 (Laboratory for Fluorescence Dynamics, University of Illinois), IBH Decay Analysis Software V4-4.2 (IBH Consultants Ltd.), SP (Dr. *Klock*/Technical University Berlin), and FLA 900 (Edinburgh Analytical Instruments). For the global analysis of fluorescence decays recorded at different emission wavelengths, the Globals Unlimited and IBH DAS software packages were employed. The data record analyzed typically consisted of 4000 data points at maximum for the single decay, respectively.

The goodness of the fit of the single decays, as judged by reduced chi-squared (χ_R^2), the autocorrelation function *C(j)* of the residuals, and the Durbin-Watson parameter *(DW)*, was always acceptable yielding values of $\chi_R^2 < 1.2$ and $DW > 1.8$. Within the global analysis of the decays recorded at different emission wavelengths, the decay times of the species are linked while the program varies the preexponential factors and time constants until changes in the error surface (χ^2 surface) are minimal, i. e., convergence is reached. The fitting results are judged for every single decay (local χ_R^2) and for all the decays (global χ_R^2). Except as otherwise indicated, the errors for all the meas- urements presented here were below global $\chi_R^2 = 1.2$.

2.8.3 Complexometric Titrations

The complex stability constants reported here were determined from absorption ($BP(OH)_2$), fluorescence (Δ^2-pyrazolines and BDPs) or from measurements of both spectra (D-A-chalcones), in some cases for Li^I and Ca^{II} also conductometrically [77a,152]. The important equations are included in Appendix B.

2.9 NMR Spectroscopy

One- and two-dimensional NMR spectra - COSY (90°) and $^1H/^{13}C$-HECTOR - were measured using a Bruker spectrometer DMX 400 (5 mm tube, CD_3CN, deuterium lock). In all the cases, the solvent employed was deuterated acetonitrile.

2.10 Conductometry

For some cations, the complex stability constants were also determined conductometrically with a LF 537 conductometer from WTW with a calibrated LTA1 conductivity cell (WTW) with a cell constant of 0.993 cm^{-1} at a constant temperature of 25 ± 0.1°C. In a typical conductometric experiment, 20 ml of a 2 x 10^{-4} M metal ion perchlorate solution were placed in a specially designed cell in a thermostated water bath HME 1 (Peter Huber Kältemaschinenbau GmbH) equipped with a magnetic stirrer and aliquots of a 4 x 10^{-3} M solution of the ligand containing 2 x 10^{-4} M metal ion were added thus keeping the overall ionic strength constant. The specific conductivity of the mixture was measured and the complex stability constants were calculated as described in the literature assuming a 1:1 stoichiometry of the complexes formed [152].

2.10.1 Comparison of logK_s Obtained by Optical Spectroscopy and Conductometry

As follows from *Table 23*, p. 64, the complex stability constants obtained by absorption and fluorescence spectroscopy are in good agreement with those obtained conductometrically. The optical determination of complex stability constants is based on the occurrence of chelation-induced spectral changes, i. e., for the ICT systems described in Ch. 4.5 on the interaction between the nitrogen atom of the crown ether receptor and the cation. The conductometric determination of complex stability constants is based on a decrease in ion mobility upon complex formation and is thus independent of the coordination sites of the receptor involved in cation chelation. Furthermore, a good agreement between the optically and conductometrically obtained complex stability constants support any considerations on well-defined complex stoichiometries.

2.11 Quantum Chemical Calculations

Theoretical results presented in this work were mainly calculated with HyperChem V4.0 and 4.5, Hypercube, Inc. and partly with Ampac V5.0, Semichem, Inc.. Geometry optimizations were performed employing the semi-empirical AM1 method (gradient < 0.01) [153]. Rotational energy barriers were calculated by iterative twisting of the certain bond(s) of interest. The energies of the corresponding perpendicular structures were found by optimizing the geometry with the exception of a single fixed dihedral angle of 90°. Transition energies were calculated on the basis of the corresponding ground state geometries and 1SCF calculations with a CI of 8 by the methods AM1 and ZINDO/S [154].

2.12 A Word on LODs

Concerning possible applications of a fluorescent probe, sensitivity (i. e., the limit of detection or LOD) is a major criterion for its analytical value. Keeping in mind the two major fields of application mentioned in Ch. 1.1.2, i.e., *in situ* sens-

ing employing fiber optics and detection in HPLC, especially in the case of *in situ* analysis, where preconcentration of the analyte is avoided in order to detect the actual concentration in solution, this point is of high importance.

For fluorometric metal ion analysis employing fluorescent probes, the LOD is governed by the S/N ratio of the instrument and method employed and by the change in signal provided by a certain pair of probe and analyte. Accordingly, for a given experimental setup (steady-state or time-resolved and a certain excitation intensity) the LOD is proportional to the fluorescence enhancement induced by complexation, the $\log K_S$ of the complex formed, and the spectral and/or temporal (i. e., fluorescence lifetime) differences in absorption and/or emission of free and complexed probe.

In order to compare steady-state and time-resolved fluorometry, the LOD of a reference compound (cresyl violet) was determined with the ps-LIF and the LS50B spectrofluorometer. As will be seen in subsequent sections of this work, cresyl violet with both absorption and emission band well within the visible range of the spectrum and a fluorescence quantum yield of 0.54 [145a] is in many respects comparable to the complexes investigated in this work (Some of the probes are even stable (modified) laser dyes allowing for relatively high excitation intensities.). For the determination of the LOD of cresyl violet in methanol, conventional methanol of spectroscopic grade was used and the experiments were carried out under normal laboratory conditions. When counting single photons, the desired total experiment time, the autofluorescence of the solvent employed (or medium of interest), and the fluorescence quantum yield of the analyte are the limiting factors. Thus, for cresyl violet a LOD of 10^{-15} M was realized with the ps-LIF setup at BAM in a total experiment time of 20 min [155]. The LOD obtained with the Perkin Elmer LS50B fluorometer was ca. three orders of magnitude higher than that obtained with the ps-LIF with the electronic noise (S/N ratio) of the fluorometer being the limiting factor. However, a steady-state fluorometer equipped with, e. g., a laser as excitation source and a photon counting detection system can yield comparable LODs.

Analytically more relevant LODs for the probes and complexes studied have not been obtained since both instrumental setups (HPLC and fiber optics) could not be realized at BAM (or HUB) and were not accessible to the author within a reasonable expense.

In principle, for HPLC, fluorometry is the most sensitive detection method when detecting single molecules in capillaries with lasers as excitation sources. Provided the decay kinetics of the analyte under investigation are straightforward (mono-exponential decay), a burst of a few hundred photons is sufficient to detect the decaying species quantitatively (amplitudes) and qualitatively (lifetime) [156].

3 2,2‘-Bipyridyl-3,3‘-diol – a Fluorescent Ligand

3.1 Introductory Words

In the 1980ies, *Siemanowski* and *Witzel* as well as *Langhals* et al. reported on the interference of heavy metal impurities with the synthesis of 2,2‘-bipyridyl-3,3‘-diol, $BP(OH)_2$ *(Scheme 1)* [136, 157]. This fact, the well-known metal complexing ability of the parent compound 2,2‘-bipyridine (bipy) [158], and the characteristic photophysical properties of $BP(OH)_2$ [159a, b] suggested the applicability of this molecule as a fluorescent probe for heavy and transition metal ions and led to the studies presented in the following chapter.

After an introduction to $BP(OH)_2$ and its solvent-dependent photophysical properties, the complexation behavior and cation-induced photophysical effects are described and discussed. The mechanistic considerations given subsequently are mainly based on results obtained with steady-state and dynamic optical spectroscopy and additionally include ^{1}H-NMR data. Furthermore, a comparison between the complexation behavior and corresponding spectroscopic changes of the photophysical properties of the related compounds 2,2‘-bipyridine (bipy), 2,2‘-bipyridyl-3-ol (BPOH), and *o*-(2-pyridino)phenol (oPP, *Scheme 1*) is made in the subsections of this chapter. Finally, possible applications in metal ion analysis are elucidated and the potential of TRES in fluorometric metal ion determination is shown.

An important prerequisite for the understanding of the photophysical behavior of the title compound is the molecular structure of $BP(OH)_2$ (*Schemes 1* and *2*). Two strong internal hydrogen bonds between the pyridine nitrogen atoms and the hydroxyl groups are present in the molecule (at least in organic solvents). Accordingly, $BP(OH)_2$ is perfectly planar in the ground state (dienol form - DE, *Scheme 2*), which has been found by X-ray spectroscopy [159j] and is supported by quantum chemical calculations [160-162].

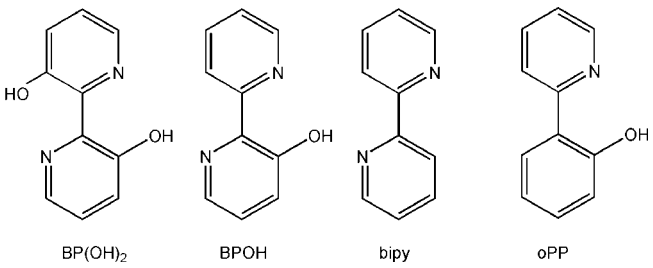

Scheme 1
Chemical Structures of $BP(OH)_2$, BPOH, bipy, and oPP.

3.2 Photophysics — Literature Review and Own Results

The spectroscopic behavior of $BP(OH)_2$ has been intensively studied both experimentally [35-37, 159, 163-167] and theoretically [160-162]. Whereas the high insensitivity to the influence of its environment in many organic solvents is well known, spectroscopic data on $BP(OH)_2$ in aqueous solutions are considerably sparse [35-37, 159 m, 165, 167]. In this work, mainly the behavior of $BP(OH)_2$ in aqueous solutions is studied and furthermore some results are obtained (and

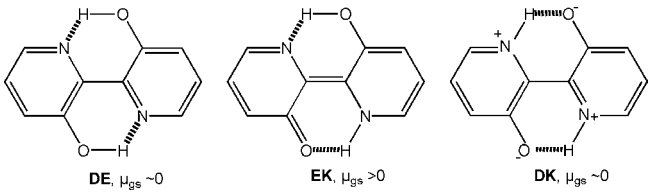

Scheme 2
Scheme of enol-keto tautomerism of BP(OH)2 , DE, EK, DK, and μ_{gs} denote the dienol, enol-keto, and "diketo" tautomers and the ground state dipole moment.

reproduced) in organic solvents (mostly polar a/protic). *Table 2* combines the spectroscopic data on $BP(OH)_2$ in organic solvents and aqueous solutions of different pH.

3.2.1 Photophysics in Apolar Solvents – the ESIPT Mechanism

In apolar organic solvents, the emissive state was characterized as an ESIPT (excited-state *i*ntramolecular *p*roton transfer) state which fluoresces with a quantum yield of ca. 0.3 and shows a largely Stokes-shifted emission spectrum (ca. 10000 cm^{-1}, *Table 2* and *Fig. 6A*) [159a, b, d, i, m, 166].

The position of both the absorption and the emission band lacks any pronounced solvent dependence and absorption and fluorescence excitation spectra match. The large Stokes shift suggests that the emitting species is different from the only stable species in the ground state, the dienol (DE) tautomer. But like DE, the emitting state, characterized as diketo (^{1}DK*) tautomer, has a vanishing dipole moment *(Scheme 2)* [159i, k, l, n]. For both species, the vanishing dipole moments were confirmed experimentally [159k, l]. Although the shape of the potential energy surface in the ground (and in the excited) state is still under discussion, no enol-keto (EK) and no diketo (DK; or better: no zwitterionic dienolate) tautomer could be yet detected experimentally [159i]. Recent quantum chemical calculations revealed that the potential energy surface in the ground state consists of three minima corresponding to the three tautomers but the (local) minima of EK and DK lie energetically much higher than the (global) minimum of DE [160, 161, 162a, b]. Therefore, the energetic barrier for proton transfer (PT) in the ground state is too high enabling no experimentally traceable population of EK and DK. In accordance, the back reaction (PT from DK via EK/or directly to DE) is described as being nearly barrierless [161a, 162a]. Concerning the excited state behavior of $BP(OH)_2$, emission from instantaneously formed ^{1}DE* has never been observed experimentally and even at 4.2 K, the steady-state emission spectrum resembles that at room temperature [159b]. Thus, the excited-state reaction to the ^{1}EK* and ^{1}DK* species seems to be barrierless and completed within ≤ 100 fs [163]. Employing fluorescence up-conversion, *Zhang* et al. were able to discriminate between a red-shifted ^{1}EK* emission at 17600 cm^{-1} (fluorescence lifetime τ_f = 10 ps in

Table 2
Spectroscopic data of $BP(OH)_2$ in selected organic solvents (upper section) and in aqueous solutions of different pH (middle section). The data published for aqueous solutions so far are shown in the lower section and stress the special attention which has to be paid to pH adjustment ($\tilde{\nu}$ (exc) - maximum of fluorescence excitation spectrum). The data given in the middle section correspond to the pH regions indicated by the pK_a values and are not strictly related to the main species (see text).

Main Species	Solvent	pK_a	$\tilde{\nu}$ (abs)	$\tilde{\nu}$ (exc)	$\tilde{\nu}$ (em)	$\Delta\tilde{\nu}$ (abs-em)
			10^3 cm^{-1}	10^3 cm^{-1}	10^3 cm^{-1}	10^3 cm^{-1}
$BP(OH)_2$	Hex	-	29.2	29.2	19.8	9.4
$BP(OH)_2$	CH	-	29.4 [a]	n.r.	19.4 [a]	10.0 [a]
$BP(OH)_2$	Et_2O	-	29.4 [b]	n.r.	19.6 [b]	9.8 [b]
$BP(OH)_2$	MeCN	-	29.4 [a,c]	29.4 [c]	19.7 [c], 19.4 [a]	9.7 [c], 10.0 [a]
$BP(OH)_2$	EtOH	-	29.4 [b,c]	29.4 [c]	20.7 [c], 20.8 [b]	8.7 [c], 8.6 [b]
$BP(OH)_2$	MeOH	-	29.2 [c]	29.2 [c]	20.8 [c]	8.4 [c]
$[HBP(OH)_2]^+$	H_2O		27.5 (24.8)	= abs.	21.0	6.5
		2.78 [d]				
$BP(OH)_2$	H_2O		28.8, 24.8 (23.2)	= abs.	21.5	7.3
$BP(OH)_2$	H_2O		28.8, 24.8 (23.2)	= abs., 27.5 [e]	21.3 (23.6)	7.5 (3.9) [e]
		9.73				
$[BP(OOH)]^-$	H_2O		30.4 (25.6)	29.8 [f]	20.0 (23.6)	10.4
		12.52				
$[BP(O)_2]^-$	H_2O		32.0	31.5 [f]	23.2 [f]	8.8
$BP(OH)_2$	H_2O	n.r.	27.4 [g]	n.r.	22.5 [g]	4.9 [g]
$BP(OH)_2$	H_2O	n.r.	29.3 (25.0, 23.2) [h]	n.r.	21.5 [h]	7.8 [h]
$BP(OH)_2$	H_2O	n.r.	28.1 (24.0, 22.5) [i]	n.r.	n.r.	-

[a] ref. [163a]; [b] ref. [166]; [c] this work; [d] pK1 ~ -0.1; [e] observed at 23600 cm^{-1}; [f] very broad; [g] ref. [159h]; [h] ref. [159m]; [i] ref. [165].

Table 2
continued

Main Species	Solvent	pK_a	ϕ_f	τ_f	k_f^{DK}	k_{nr}^{DK}
				ns	10^8 s^{-1}	10^8 s^{-1}
$BP(OH)_2$	Hex	-	0.30	3.1	0.97	2.2
$BP(OH)_2$	CH	-	0.31 [a]	3.2 [b]	0.97 [a,b]	2.1 [a,b]
$BP(OH)_2$	Et_2O	-	0.21 [c]	2.6 [c]	0.81 [c]	3.0 [c]
$BP(OH)_2$	MeCN	-	0.09 [d]	1.0 [d], 1.1 [b]	0.90 [d]	9.1 [d]
$BP(OH)_2$	EtOH	-	0.18 [d,e] 0.28 [c]	2.1 [d], 2.2 [c]	0.86 [d], 1.25 [c]	3.9 [d], 3.2 [c]
$BP(OH)_2$	MeOH	-	0.10 [d], 0.25 [c]	1.2 [d], 1.3 [c]	0.83 [d], 1.92 [c]	7.5 [d], 5.7 [c]
$[HBP(OH)_2]^+$	H_2O	2.78 [f]	0.07 - 0.05	~ 0.7	1.0 [g]	12.7 [g]
$BP(OH)_2$	H_2O		0.05 - 0.04	~ 0.6	0.90 [g]	18.0 [g]
$BP(OH)_2$	H_2O	9.73	0.04 - 0.025	~ 0.45 [h]	0.89 [g]	21.3 [g]
$[BP(OOH)]^-$	H_2O	12.52	0.025 - 0.005	~ 0.08 [h]	-	-
$[BP(O)_2]^-$	H_2O		< 0.005	n.d.	-	-
$BP(OH)_2$	H_2O	n.r.	0.08 [e]	1.0 [e]	0.80 [e]	9.2 [e]
$BP(OH)_2$	H_2O	n.r.	0.04 [i]	0.9 [i]	0.41 [i]	10.7 [i]
$BP(OH)_2$	H_2O	n.r.	n.r.	n.r.	-	-

[a] ref. [159d]; [b] ref. [163a]; [c] ref. [166]; [d] this work; [e] ref. [159h]; [f] pK1 ~ -0.1; [g] calculated for pH 1.2, 3.1, and 6.4 (<τf> ~ τf (main component) in the main emissionband); [h] see *Table 3*, p. 26 for more detailed information; [i] ref. [159m]

cyclohexane) and the normally observed, strong fluorescence from $^1DK^*$ emission at 19400 cm^{-1} (τ_f = 3.2 ns in cyclohexane; *Scheme 3*) [163a].

The fluorescence quantum yield ϕ_f of ca. 0.3 increases with decreasing temperature and reaches a maximum value of 0.7 at < 77 K [159b]. As possible mechanisms accounting for the non-radiative loss of energy of $^1DK^*$, solute-solvent interactions (especially in protic solvents), torsional motions of the two pyridyl rings or twisted intramolecular charge transfer (TICT) formation, the proximity effect (due to close lying nπ* states), and triplet population are discussed [159b, e, 162a, 166]. In the case of the latter, the population of $^3DE^*$ should play no role in the excited state because the primary ESIPT reaction is too fast [159e]. Furthermore, no $^3EK^*$ has been found either [159e].

Although no phosphorescence was observed, transient absorption signals of the $^3DK^*$ species were measured by Sepiol et al. in apolar solvents suggesting radiationless depopulation of $^3DK^*$ [159e, i]. The PT reaction cycle described by *Grabowska* et al., extended by the fluorescence up-conversion results, shows the exceptional PT behavior of $BP(OH)_2$ *(Scheme 3)*.

The importance of the internal hydrogen bonds in $BP(OH)_2$ is additionally stressed by the fact that all the "flexible" related compounds, BPOH, oPP (investigated here and in refs [159b, 166, 168], *Fig. 6*), and HPP (see Appendix D for chemical structure [169]) are only weakly fluorescent at best. On the other hand, all those compounds which are more or less "forced" to perform ESIPT due to their "forced planarity" are

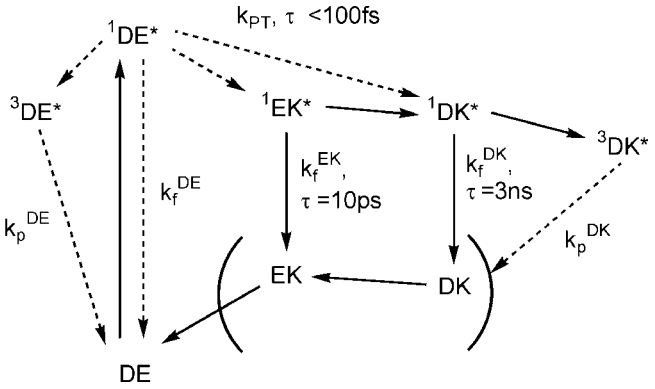

Scheme 3
Generalized scheme of the ESIPT reaction mechanism of $BP(OH)_2$. For clearness, only reactions and possible radiative deactivations are included. Arrows with solid lines denote processes which have been identified experimentally and arrows with broken lines correspond to processes not yet experimentally described. The time constants included were taken from ref. [163a] and describe the kinetics in apolar solvents. The backwards PT reaction in the ground state is put in brackets because the real mechanism is still under discussion [161a, 162a, 163a, b]. Energy barriers for the reactions are omitted as well.

at least moderately fluorescent, e. g., HBQ [165, 168a, 170] and HdihBQ [168a] (see Appendix D for chemical structure), supporting the generally accepted reaction scheme.

3.2.2 Photophysics in Polar Solvents

Upon going from apolar via polar aprotic to polar protic solvents, solute-solvent interactions are enhanced and result in an increase in radiationless deactivations of the excited singlet state(s) (for spectra see part A in *Fig. 6*). However, the spectral features are nearly unchanged *(Table 2)*.

3.2.3 pH-Dependent Photophysics in Aqueous Solutions

In water, the intramolecular hydrogen bonds are partially broken up and the planar stabilization is weakened resulting in a spectroscopically very different ground state behavior and reduced fluorescence quantum yield [35-37, 159 m, 165, 167]. The photophysical behavior as a function of pH is very complex owing to the four de/protonation sites *(Scheme 4)*, the enol-keto tautomerism, and solute-solvent interactions.

In part B of *Fig. 6*, the steady-state spectra of $BP(OH)_2$ in aqueous solutions of different pH are shown and the UV/Vis-spectrophotometric pH titration spectra are given in Appendix C.

3.2.3.1 Behavior at Acidic pH

At acidic pH (pH < 2) a mixture of positively charged species (no tautomers in the strict sense, *Scheme 4*) accounts for the broad absorption spectrum showing at least two subbands (broad maximum at 27500 cm^{-1} and a shoulder at 24800 cm^{-1}). The protonated species already present a "prearranged PT site" depending on the actual pH. Upon excitation, the hydroxyl oxygen atom becomes more acidic[xxvi] and deprotonation leads to formation of emissive $^1DK^*$ (for a reaction scheme see *Scheme 5* and the description given for BPOH on p. 28ff.). For every species in the first two rows in *Scheme 4*, such a "PT by deprotonation" can occur in the excited state resulting in the highest fluorescence quantum yield observed in aqueous solutions *(Table 2)*. Furthermore, at pH << 7, excitation at any wavelength between 320 and 450 nm (31 200 and 22 200 cm^{-1}) yields the same emission spectrum. A similar behavior is observed for the fluorescence excitation spectra, i. e., an emission wavelength-independent band shape. Correspondingly, at low pH, the fluorescence excitation spectrum always matches the absorption spectrum and therefore all the different ground state species should undergo a fast (pseudo and/or real) ESIPT reaction leading to fluorescent $^1DK^*$.

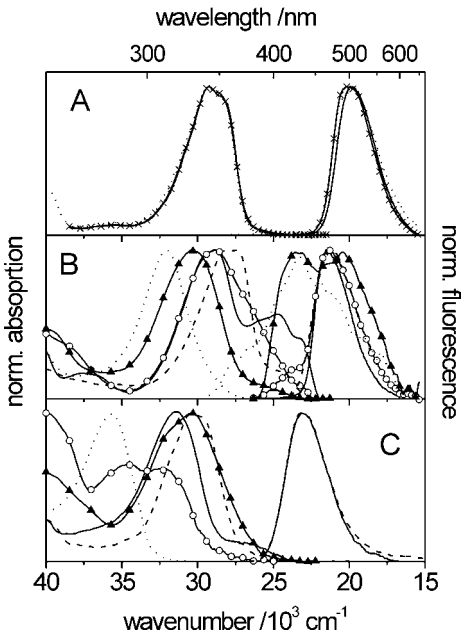

Fig. 6
*Normalized steady-state spectra of $BP(OH)_2$. **A** - organic solvents (hexane —, dichloromethane X, acetonitrile .....); **B** - aqueous solutions of different pH (pH 1.5 - -, pH 4.8 —, pH 8.7 o, pH 11.7▲, pH 13.1 .....); **C** - BPOH at different pH, bipy, and oPP in water (BPOH at pH 1.5 - -, BPOH at pH 6.5 —, BPOH at pH 11.5 ▲, bipy ....., oPP o). Bipy, oPP, and BPOH at pH 11.5 are non-fluorescent (c_L = 5 x 10^{-6} M; excitation at absorption maximum). In **B**, the emission spectra at pH 1.5 and 4.8 are superimposed.*

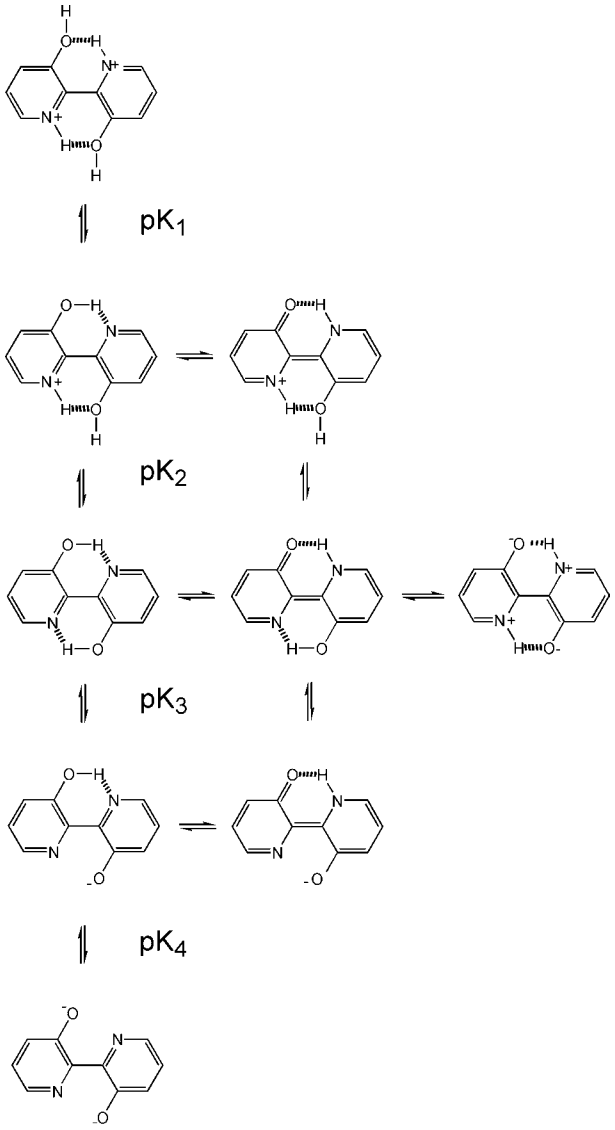

Scheme 4
Generalized scheme of possible protolytic (vertical) and PT (horizontal) equilibria of $BP(OH)_2$. Solute-solvent interactions are not included. The labels pK denote macroscopic equilibria and arrows indicate microscopic equilibria. A description of the procedure of the spectrophotometric determination of the "pK_a" values is given in Appendix C.

xxvi) The charge redistribution in the excited state has been well-documented by *Waluk* et al. [160].

This was experimentally confirmed by a comparative study of $BP(OH)_2$ and the corresponding "ground state diketo tautomer", DDB (see Appendix D for chemical structure), carried out by *Borowicz* et al. who found a very different ground state but a very similar excited-state behavior for both compounds [159 m]. Furthermore, the band positions of 28500 cm^{-1} (abs.) and 20700 cm^{-1} (em.) given by this group for DDB closely resemble those found here for protonated $BP(OH)_2$ and the fluorescence quantum yield (0.032) and lifetime (0.74 ns) are very similar as well (cf. *Table 2*) [159 m].

In the pH region < 7, the fluorescence quantum yield decreases moderately *(Table 2)*. A plot of ϕ_f as a function of pH is shown in *Fig. 7* and reveals the influence of pH via ground state conformation of the molecule upon the ESIPT process.

An analysis of the pH-dependent fluorescence lifetime of $BP(OH)_2$ as a function of excitation and emission wavelength yielded monoexponential decay behavior at pH < 4, consistent with steady-state spectroscopy. At pH > ca. 4, the decays could only be fitted to two exponentials but in neither case rise times were detected for any combination of excitation and emission wavelength. Selected pH-dependent time-resolved emission data of $BP(OH)_2$ are summarized in *Table 3*. As was mentioned for the pH dependence of the fluorescence quantum yield, the fluorescence lifetimes similarly decrease with increasing pH (0.73 ns at pH 1.2; 0.46 ns at pH 5.2 (main component)).

3.2.3.2 Behavior at Medium pH

A comparison of the absorption spectra of $BP(OH)_2$ shown in part B of *Fig. 6* with those displayed in part A (in organic solvents) suggests that at medium pH, the dominant tautomer is still DE. The absorption spectrum is very broad and composed of a few subbands.

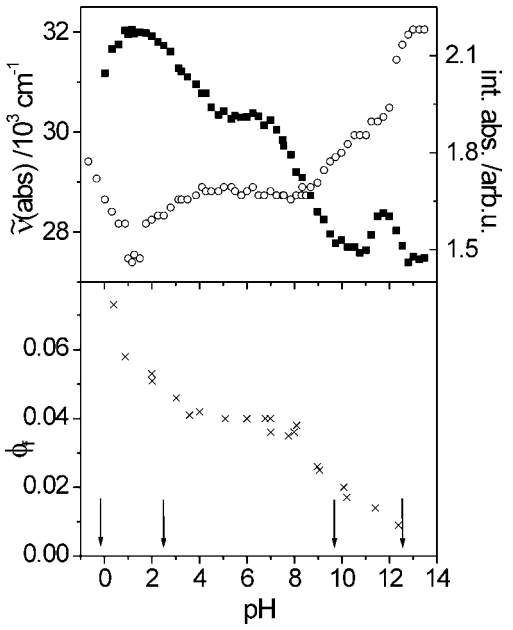

Fig. 7
Dependence of position (o) and integral (■) of the low energy absorption band (upper part) and of the fluorescence quantum yield (lower part) of $BP(OH)_2$ on pH. Arrows correspond to pK_a values (Table 2, p. 22).

Different enol-keto tautomers and solute-solvent interactions/complexes account for the shape of the overall absorption band (*Fig. 6* and *Scheme 4*) and quantum chemical calculations support this fact.[xxvii] The corresponding steady-state emission spectra are only slightly blue-shifted compared to the emission spectra in organic solvents and maintain their shape. The fluorescence quantum yield is constant over a wide pH range. However, time-resolved fluorometry reveals a more complicated emission behavior, observed in the steady-state fluorescence spectra only at higher pH. Even at a pH of 5.2, a slow decay component with a very low relative amplitude, being dependent on excitation and emission wavelength, is detected *(Table 3)*. The fluorescence lifetime of 2.8 ns given in *Table 3* corresponds to the best global fit of the 15 decays analyzed for this pH. From *Table 3*, the wavelength dependence of the slow decay component is obvious. Excitation at ca. 380 nm (26300 cm^{-1}) and detection at 440 nm (22700 cm^{-1}) yielded the largest a_{rel} for this component, 440 nm being the shortest detection wavelength employed. The lack of rise times suggests that two or more species are simultaneously excited and two excited transient species emit in different regions of the spectrum.

On the other hand, decays obtained for excitation at 425 nm (23500 cm^{-1}) could always be fitted to a single exponential with a decay time corresponding to the main component. Judging from the Stokes shift of such a species, i. e., ≥ 2000 cm^{-1}, possibly DK (or solvent-complexed DK) absorbs in this wavelength region but this could not be verified. How-

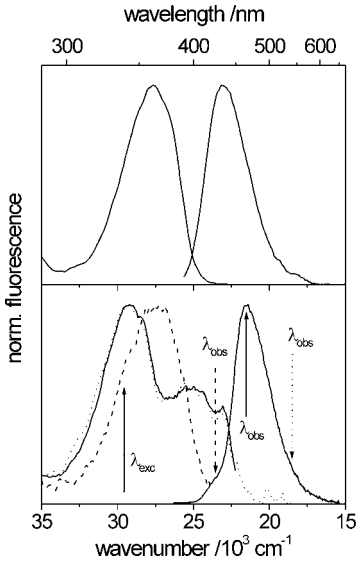

Fig. 8
Lower part: Steady-state fluorescence spectra of $BP(OH)_2$ at pH = 7.5. The emission spectrum was recorded for excitation at 337 nm, the observation wavelengths for the fluorescence excitation spectra are 430 nm (- -), 480 nm (—), and 550 nm (.....), respectively (c_L = 5 x 10^{-6} M). The absorption spectrum is very similar to ..... (Fig. 70, Appendix C). The corresponding fluorescence excitation and emission spectra of BPOH are included in the upper part for comparison.

xxvii) In contrast to polar organic solvents (DE is energetically favored), both tautomers (DE and DK) were found to be equally stable in aqueous solution (semi-empirical and ab *initio* calculations) [162c]. This stability should be due to solute-solvent complex formation of a $BP(OH)_2$ molecule with preferrably two water molecules [162c]. These authors did not report on EK but it is inferred here that this tautomer is sufficiently stabilized as well.

Table 3
Selected time-resolved emission data of BP(OH)2 in aqueous solutions of different pH. The results shown are the best global fits obtained for a set of 15 decays for each pH (global $\chi_R^2 < 1.3$). Data obtained with the TCSPC setup at BESSY.

pH	$\tilde{\nu}$ (exc)	$\tilde{\nu}$ (em)			$\tilde{\nu}$ (em)			$\tilde{\nu}$ (em)		
	10^3 cm^{-1}	22700 cm^{-1}			21500 cm^{-1}			19300 cm^{-1}		
		τ_1 /ns, a_{rel}	τ_2 /ns [a], a_{rel}	τ_3 /ns, a_{rel}	τ_1 /ns, a_{rel}	τ_2 /ns [a], a_{rel}	τ_3 /ns, a_{rel}	τ_1 /ns, a_{rel}	τ_2 /ns [a], a_{rel}	τ_3 /ns, a_{rel}
1.2	27.5	0.73, 1	-	-	0.73, 1	-	-	0.73, 1	-	-
	25.5	0.73, 1	-	-	0.73, 1	-	-	0.73, 1	-	-
3.1	27.5	0.56, 1	-	-	0.56, 1	-	-	0.56, 1	-	-
	25.5	0.56, 1	-	-	0.56, 1	-	-	0.56, 1	-	-
5.2	28.9	0.45, 0.995	2.8, 0.005	[b]	0.45, 0.999	2.8, 0.001	[b]	0.45, 0.999	2.8, 0.001	[b]
	26.0	0.45, 0.989	2.8, 0.011	[b]	0.45, 0.997	2.8, 0.003	[b]	0.45, 0.998	2.8, 0.002	[b]
	23.5	0.45, 1	2.8, 0	[b]	0.45, 1	2.8, 0	[b]	0.45, 1	2.8, 0	[b]
6.4	28.9	0.45, 0.993	4.8, 0.007	[b]	0.45, 0.998	4.8, 0.002	[b]	0.45, 1	4.8, 0	[b]
	26.0	0.45, 0.982	4.8, 0.018	[b]	0.45, 0.995	4.8, 0.005	[b]	0.45, 0.997	4.8, 0.003	[b]
	23.5	0.45, 1	4.8, 0	[b]	0.45, 1	4.8, 0	[b]	0.45, 1	4.8, 0	[b]
8.2	28.9	0.44, 0.983	5.6, 0.017	-	0.44, 0.996	5.6, 0.004	-	0.44, 0.998	5.6, 0.002	-
	26.5	0.44, 0.947	5.6, 0.053	-	0.44, 0.984	5.6, 0.016	-	0.44, 0.992	5.6, 0.008	-
9.2	28.9	0.44, 0.002	2.2, 0.001	0.07, 0.997	0.44, 0.610	2.2, 0.002	0.07, 0.388	0.44, 0.41	2.2, 0	0.07, 0.59
	26.5	n.d.	n.d.	n.d.	0.44, 0.988	2.2, 0.012	0.07, 0	n.d.	n.d.	n.d.
10.3	30.0	0.40, 0	2.8, 0	0.08, 1	0.40, 0.22	2.8, 0	0.08, 0.78	0.40, 0.16	2.8, 0	0.08, 0.84
	26.5	n.d.	n.d.	n.d.	0.40, 0.516	2.8, 0.032	0.08, 0.452	n.d.	n.d.	n.d.

[a] Due to partly very low a_{rel}, the uncertainty is < ± 1.5 ns when fitting the single decays. [b] Better global fits are obtained when adding a third, fast decay component (< 60 ps), but the resulting $<\tau_i>$ does not change largely. The tendency of a_{rel} of the third component is in both cases the same as the tendency of a_{rel} of τ_1.

ever, the lifetime of the main component shows a similar tendency as ϕ_f, i. e., no pH dependence in this pH region.

Taking another look at *Scheme 4* it is obvious that the species diversity at ambient and slightly higher pH can have its origin in varying amounts of mono-protonated, neutral, and mono-deprotonated forms as well as their possible tautomers, having different photophysical properties. At a certain pH, e. g., pH 7.2, all the species centered around pK_2, pK_3, and the corresponding microscopic equlibria in *Scheme 4* can be present in solution (and ground state solute-solvent complexes are not counted).

3.2.3.3 Behavior at Basic pH

Basicity changes the photophysical properties of $BP(OH)_2$ even more pronounced (*Figures 6* and *70*, p. 24 and Appendix C, and *Table 2*, p. 22). In absorption, the low-energy bands decrease in intensity with increasing pH and above pH ca. 10, the main band is blue-shifted as well. Correspondingly, in the emission spectrum the appearance of the hypsochromically shifted shoulder already observed in the time-resolved experiments at medium pH, is detectable at ca. 23600 cm^{-1}. Moreover, it depends on excitation wavelength and this behavior is reflected by the fluorescence excitation spectra. Recording a fluorescence excitation spectrum with the wavelength of the emission monochromator set in the high-energy shoulder yields a spectrum centered at 27500 cm^{-1}, whereas tuning the observation wavelength to 20000 cm^{-1} yields a fluorescence excitation spectrum resembling the absorption spectrum *(Fig. 8)*.

The hypsochromic shift of the main absorption band at pH > ca. 10 is accompanied by a further decrease in fluorescence quantum yield and lifetime (*Fig. 6*, p. 24, *Tables 2* and *3*, pp. 22, 26). This marked effect points to the involvement of a deprotonation step of a hydroxyl group (cf. pK_a values in *Table 2*, p. 22). A comparison of the absorption spectra recorded at pH 11.7 and 13.1 (part B in *Fig. 6*, p. 24) with those of the related compounds displayed in part C supports this explanation of the nature of the predominant species in solution. Between pH 10 and 12.5, the long-wavelength absorption band of $BP(OH)_2$ resembles very much the longest-wavelength absorption band of BPOH suggesting a dominant presence of the mono-deprotonated form. This is additionally stressed by the weaker emission of $BP(OH)_2$ at these pH values. The emission spectrum at pH 11.7 consists of at least two bands, the main band being shifted to lower energies. Keeping in mind the comparatively high fluorescence quantum yield of the $^1DK^*$ emission (ϕ_f = 0.04), the fluorescence quantum yield observed at pH ca. 12 (ϕ_f = 0.009) seems to originate partly from remaining $^1DK^*$ contributions. At pH > 12.5, the main absorption band is shifted to even higher energies accompanied by a further decrease in ϕ_f. The photophysical properties of $BP(OH)_2$ at such basic pH values point to a complete deprotonation of the molecule.

Again, a change in pH induces a change in fluorescence lifetime. Whereas at pH 8.2, decay times τ_f of 0.44 ns and 5.6 ns are observed, measurements at pH 10.3 yielded decay times of 0.08 ns, 0.40 ns, and 2.8 ns, respectively. However, the time-resolved measurements presented here could only underline the results obtained with steady-state spectroscopy. Due to the gap in excitation wavelengths from 330 to 370 nm of the ps-LIF, all the measurements were made with the setup at BESSY and here the temporal resolution of 55.5 ps $channel^{-1}$ was the limiting factor for a further investigation of the fast decay components.

3.2.3.4 Radiative and Non-Radiative Deactivation

It is obvious that k_f is only slightly affected by a change in solvent polarity and proticity (0.97 x 108 s^{-1} in cyclohexane, 0.9 x 10^8 s^{-1} in ethanol and acetonitrile, 1.0 x 10^8 s^{-1} at pH 1.2, 0.89 x 10^8 s^{-1} at pH 6.4). On the other hand, k_{nr} is increased by an order of magnitude on going from CH to neutral H_2O (2.1 x 10^8 s^{-1} in cyclohexane, 21.3 x 10^8 s^{-1} at pH 6.4). (The rate constants of radiative and non-radiative deactivation included in *Table 2*, p. 22 were estimated assuming that only one emissive species is predominantly present for $BP(OH)_2$ in aqueous solution and mainly contributes to the measured quantities ϕ_f and τ_f in the pH region between pH 1 and 6.5.) Distorted H-bonds, solute-solvent interactions, and enhanced torsional motions of the two pyridyl rings account for this behavior.

At this point, a short intermediate summary of the main findings and features of $BP(OH)_2$ in solution is given. In all the organic solvents, DE is the only stable tautomer in the ground state and populates the only emissive $^1DK^*$ tautomer in a fast ESIPT reaction. In acidic aqueous solution, protonated species are present. Their excitation is followed by deprotonation in the excited state leading to $^1DK^*$ formation as well. When going to medium pH, a second (minor) ground state species occurs which is not converted into $^1DK^*$ (and vice versa) in the excited state but emits at higher frequencies. Its possible nature will be discussed below. Basicity leads to a successive loss of the PT sites in the molecule and quenches fluorescence. Both fluorescence quantum yield and lifetimes (of the main species) decrease in the order of apolar > polar (organic solvents) > (aqueous solution of) acidic pH > medium pH > basic pH.

3.2.4 Comparison between $BP(OH)_2$ and Model Compounds

The photophysical behavior of BPOH, with only one possible ESIPT reaction site should, to some extent, be comparable to that of $BP(OH)_2$. Thus, a comparison between the photophysics of $BP(OH)_2$ and the solvent-dependent behavior of this model compound should provide additional information concerning the ground and excited-state behavior of $BP(OH)_2$ in aqueous solutions. *Table 4* combines some pH- and solvent-dependent photophysical data of BPOH. Other model compounds introduced already, i. e., oPP, HPP, and HBQ, are only briefly referred to.

3.2.4.1 BPOH in Aprotic Solvents

The spectroscopic properties of BPOH in organic solvents are included in *Table 4*.

In aprotic solvents, the position of the absorption band of BPOH is independent of solvent polarity. The emission band is largely Stokes-shifted, its intensity being very weak and its spectral position is solvent-dependent *(Table 4)*. Emission in these solvents can be attributed to the excited monoketo tautomer ($^1MK^*$) possessing a non-zero dipole moment [159b, 166, 168b]. The weaker fluorescence of BPOH compared to $BP(OH)_2$ is mainly due to enhanced flexibility (possible TICT

Table 4
Spectroscopic properties of BPOH in some organic solvents and in aqueous solutions of different pH.

Main Species	Solvent	pK_a	$\tilde{\nu}$ (abs)	$\tilde{\nu}$ (exc)	$\tilde{\nu}$ (em)	$\Delta\tilde{\nu}$ (abs-em)	ϕ_f
			10^3 cm^{-1}	10^3 cm^{-1}	10^3 cm^{-1}	10^3 cm^{-1}	
BPOH	3-MP	-	30.8 [a]	n.r.	17.8 [a]	13.0 [a]	5.5 x 10^{-3} [b,c]
BPOH	Et_2O	-	30.8 [d]	n.r.	17.1 [d]	13.7 [d]	n.r.
BPOH	MeCN	-	30.9	30.9	16.9	14.0	1.3 x 10^{-4}
BPOH	EtOH	-	30.9 [e], 30.8 [d]	30.9 [e]	17.2 [e], 17.4 [d]	13.6 [e], 13.4 [d]	1.2 x 10^{-3} [e], 1.5 x 10^{-4} [d]
$[HBPOH]^+$	H_2O, pH 1	3.70 [f]	30.4	30.5	23.0	7.4	0.08
BPOH	H_2O, pH 6.5	9.68	31.3 (27.0)	27.6	23.0 [g]	8.3, 4.0 [g]	0.11 (5 x 10^{-3}) [h]
$[BPO]^-$	H_2O, pH 12.5		30.5	30.5	23.0	7.5	< 1 x 10^{-4}

[a] ref. [168b]; [b] ref. [169]; [c] The room temperature fluorescence lifetime data published so far is controversial: whereas *Tokumura* et al. report biexponential decay kinetics with time constants of 80 and 410 ps, *Kaczmarek* et al. report a value of 3.02 ns (cf. refs [168b, 169]). [d] ref. [166]; [e] this work; [f] pK_1 = 0.27; [g] excitation at 31300 cm^{-1} leads to tailing, Stokes shift of both bands included; [h] minor species (bands at ~ 27400 cm^{-1} and 23200 cm^{-1}) is higher fluorescent, ϕ_f = 0.11 with excitation at 26300 cm^{-1}; ϕ_f = 5 x 10^{-3} with excitation at 31200 cm^{-1}, no attempts were made to separate the single bands in absorption and emission

state formation) based on the lack of a second stabilizing H-bond and low-lying nπ^* transitions [159b, 166]. Thus, whereas in organic solvents only ^{1}DK* is observed for $BP(OH)_2$, ESIPT in BPOH produces the only possible ^{1}MK* excited tautomer.

3.2.4.2 BPOH in Protic Solvents

In protic solvents, solute-solvent interactions change the fluorescence behavior of BPOH, i. e., the emission spectrum is blue-shifted and the fluorescence quantum yield increases (cf. data in ethanol in *Table 4*). But on the other hand, the absorption spectrum in alcohols remains unchanged compared to aprotic solvents *(Table 4)*. Only water induces stronger effects and the pH-dependent behavior of BPOH is even more pronounced than that of $BP(OH)_2$ (for absorption spectra see Appendix C). The most striking features are the reduction in Stokes shift due to the hypsochromic shift in emission (from *ca.* 13500 cm^{-1} in organic solvents to *ca.* 7500 cm^{-1} in water), the strong increase in fluorescence quantum yield in acidic media, and the different changes in absorption and fluorescence excitation spectra over the whole pH range studied *(Table 4)*. Furthermore, throughout this pH range, the fluorescence excitation spectrum does not resemble the absorption spectrum closely. On the other hand, the changes in band shape and position of the emission spectrum are very small. Combining the behavior of both fluorescence excitation and emission spectra, excitation of different ground state species seems to generate spectrally very similar emissive transient species of BPOH at any pH. At pH 1, BPOH is moderately fluorescent (ϕ_f > 0.07) but the fluorescence excitation spectrum is similar in shape to the absorption spectrum at pH << 1 *(Fig. 9)* suggesting that the precursor of the emitting species is the doubly protonated BPOH (*Scheme 5*; emission with a Stokes shift of ca. 7500 cm^{-1}, in analogy to $BP(OH)_2$, Ch. 3.2.3.1).

With increasing pH, the absorption spectrum is shifted to higher energies, ϕ_f drops markedly, and the fluorescence excitation spectrum is changed completely (now centered at 27600 cm^{-1}; *Fig. 9*) whereas the shape of the emission spectrum remains nearly the same (*Fig. 6*, p. 24). Furthermore, excitation at 320 and 380 nm leads to identical emission spectra, the integral fluorescence of the two spectra being well-reflected by the corresponding intensities in the fluorescence excitation spectra *(Fig. 9)*.

Accordingly, measuring the fluorescence quantum yield with excitation at 380 nm yields a much higher value of 0.11 compared to 0.0055 with excitation at 320 nm (31200 cm^{-1}).[xxviii] No excited-state reaction from the majority of initially excited ^{1}ME* to the emitting species seems to take place. Moreover, keeping in mind the controversial discussion on fluorescent metal complex impurities, such an interference can be ruled out here when comparing the emission spectrum of the Zn^{II} complex of BPOH and that of free BPOH (*Fig. 9* and discussion in Ch. 3.4).[xxix] The Stokes shift of ≥ 4000 cm^{-1} obtained for the emitting species is very similar to that of the corresponding species of $BP(OH)_2$, ≥ 3900 cm^{-1} (minor species at medium pH, cf. Ch. 3.2.3.2) and does not suggest involvement of an ESIPT process (in acidic solution, where protonated ME is excited and ^{1}MK* emits, this shift is nearly twice as large).[xxx]

---

xxviii) No attempts were made here to separate the single overlapping absorption bands.

xxix) Ground state complex formation of pyridyl derivatives with water molecules is a field of high controversy, especially in the case of bipy. Whereas some authors favor such an explanation for the weak fluorescence of bipy in water [171], others reject this interpretation in favor of highly fluorescent $Zn^{II}\subset bipy_x$ complexes being present in the solution as impurities [158b, d]. Both positions were carefully considered in this work and contamination of the samples was strictly avoided (c_{Zn} < 1.5 nM, BAM Laboratory for Trace Elemental Analysis). Nonetheless, the effects still remained and the explanation given in the text seems the most probable. Furthermore, the observations made during the investigation of $Zn^{II}\subset$BPOH in water support this interpretation.

xxx) Note that here the Stokes shift is determined on the basis of corrected fluorescence excitation and emission spectra.

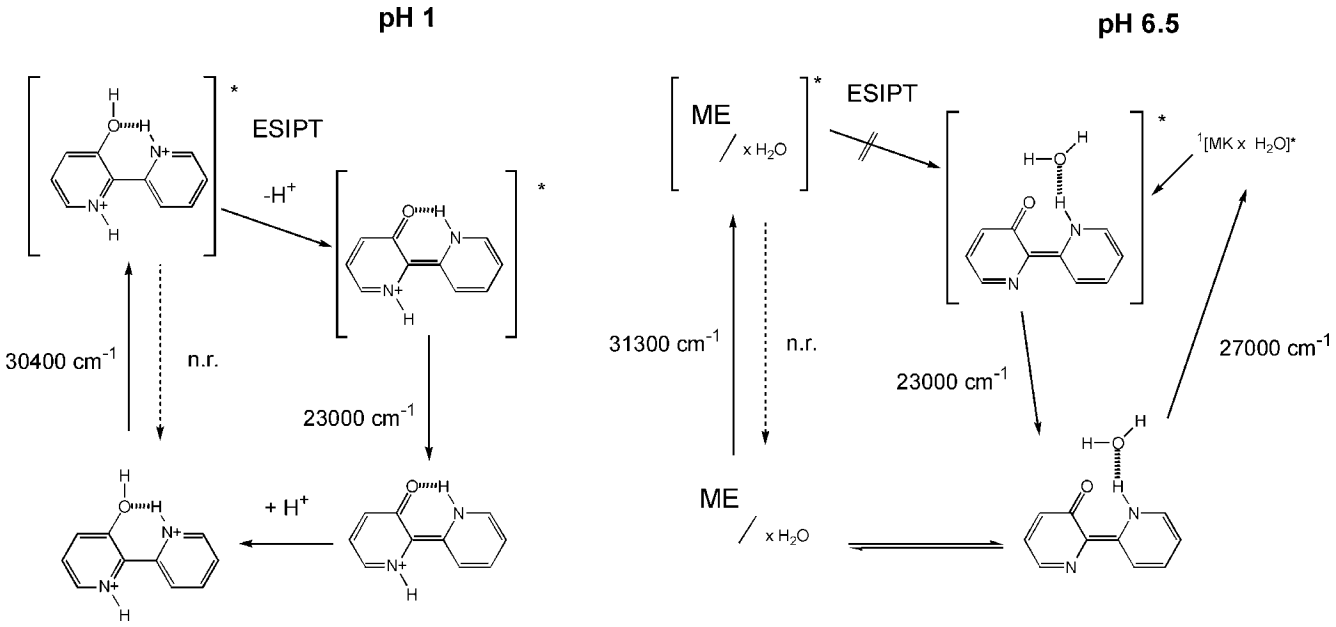

Scheme 5
Photophysical reaction mechanism of BPOH in acidic and neutral aqueous solution, explanation see text. The involvement of any solvent complexes has been omitted on the left side. At pH 6.5, a 1:2 solute-solvent complex/exciplex might as well be involved, the scheme shown representing only a model case. On the far right side, ^{1}[MK x H_2O] corresponds to the initially excited complex. Concerning the reduction in Stokes shift (from ca. 13500 cm^{-1} in organic solvents to ca. 7500 cm^{-1} in water) not only the differences between ^{1}MK* and its protonated or solvent-complexed analogues have to be considered but also the pronounced stabilization of MK with respect to ^{1}MK* in solvents of higher polarity [159b].*

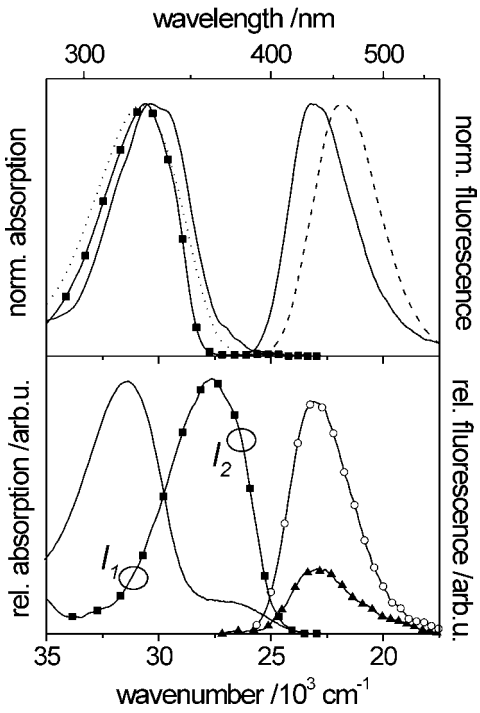

Fig. 9
Steady-state absorption and fluorescence spectra of BPOH in aqueous solution of pH 1 (upper part) and pH 6.5 (lower part). Upper part: — absorption and emission at pH 1, ■ fluorescence excitation spectrum at pH 1, ... absorption at pH ~ -1, - - - Zn^{II} complex of BPOH. Lower part (spectra at pH 6.5): — absorption, fluorescence excitation (■, for observation at 430 nm), and emission spectra for excitation at 380 (o, I_2) and 320 nm (▲, I_1);

$$\frac{I_1}{I_2} = \frac{\int F_{SS}(exc.320nm)}{\int F_{SS}(exc.380nm)} = 0.28$$

At higher pH, ϕ_f is further decreased and the red-shifted shoulder in the absorption spectrum disappears.

Arrived at this point, the possible mechanisms for the deactivation of excited BPOH can be described best by weak ^{1}MK* emission in organic solvents, (deprotonation and) stronger emission of (partly still protonated and/or solvent-complexed) ^{1}MK* at acidic pH, and by emission of a solute-solvent exciplex (of ^{1}MK*) at medium pH. Both latter mechanisms are depicted in *Scheme 5*.

3.2.4.3 Other Model Compounds

Similar observations as for BPOH in organic solvents were made for the other flexible model compounds. Although X-ray studies revealed in any case that these molecules are almost perfectly planar in the crystalline state, upon excitation in solution, non-radiative relaxation is by far the main route favored [159b, 166, 168b, 169]. Thus, besides close-lying $n\pi^*$ states, rapid torsional motions break up the thight intramolecular hydrogen bond, detected for these compounds in the ground state by a characteristic signal at low field in the ^{1}H-NMR spectra (BPOH δ 14.14 [172], oPP δ 14.3 [173], $BP(OH)_2$ δ 14.51 [172]). Additionally, the related compound HBA, being stabilized by a strong internal hydrogen bond as well, does not show any ESIPT fluorescence due to rapid rotational relaxation in the excited state [174]. However, HBQ and HdihBQ, where the molecule is fixed in planarity, display the typical largely Stokes-shifted ESIPT emission band in organic solvents [165, 168, 170].

The spectroscopic data on the other model compounds in aqueous solutions are very sparse. oPP is non-fluorescent between 0.5 < pH < 13.5.[xxxi] Similar results were obtained

xxxi) pK_a in water/dioxane (50/50) [175a]: 2.69, 12.01

by *Kábrt* and *Holzbecher* [175b]. As would be expected for a fixed model analogue with an internal hydrogen bond and a non-zero dipole moment, HBQ shows the same solvatochromic behavior as BPOH, i. e., nearly unchanged absorption and emission spectra [170b]. Forced to be planar, the fluorescence quantum yield is much higher than that of BPOH [170a]. The pH-dependent behavior shows the analogies as well [170a]. In this prefixed compound just the perturbations induced by the solvent on the internal hydrogen bond are observed.

In conclusion, comparison of the pH-dependent photophysical properties of $BP(OH)_2$, BPOH, and the other model compounds supports the explanations given above, i. e.,

(i) at acidic pH, one or both nitrogen atoms are protonated and the "prearranged PT conformation" leads to the most efficient ESIPT fluorescence (with the possible aid of solute-solvent complex formation),

(ii) at medium pH, deprotonation leads to a loss in fluorescence quantum yield (more pronounced for BPOH). A second emitting species, an exciplex with one or two solvent molecules, leads to fluorescence enhancement in BPOH but plays only a minor role in $BP(OH)_2$ (higher stability of the two internal hydrogen bonds). Water impedes the ESIPT process and the species decay separately. Whether one or two solvent molecules are engaged in such a complex could not be verified here, but the similarity of the behavior of BPOH and $BP(OH)_2$ suggests that, in the case of $BP(OH)_2$, the second ESIPT site does not play a major role in deactivation of this species.[xxxii] However, the complex absorption spectra and fluorescence decay behavior of $BP(OH)_2$ suggests that differently solvated tautomers are present in solution, and

(iii) at basic pH, both derivatives are (partly) deprotonated and the ESIPT fluorescence is drastically quenched.

The absence of interaction of intra- and intermolecularly hydrogen-bonded tautomers in the excited state has been found for several related dyes as well [176]. Moreover, the formation of a solute-solvent exciplex to be involved in the excited-state mechanisms governing PT and deactivation in both, $BP(OH)_2$ and BPOH, has been proposed by *Vollmer* and *Rettig* [166]. Other prominent examples, where solute-solvent hydrogen-bonding interactions in the ground state are precursors to proton transfer fluorescence are the related hydroxyquinolines or flavones [177].

Only recently, *Carballeira* and *Perez-Juste* showed with semi-empirical and ab initio calculations that complex formation between one $BP(OH)_2$ molecule and two water molecules is energetically favored in the ground state as well [162c]. As will be shown in the next subsections of this chapter, the photophysical behavior at medium pH is important for the spectroscopic characteristics of the metal complexes of these molecules because the changes observed for $BP(OH)_2$ and BPOH upon complexation to d^{10} metal ions are comparable.

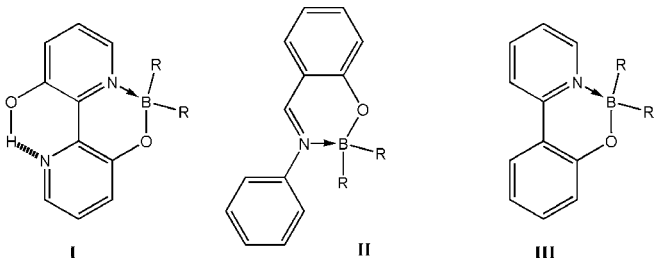

Scheme 6
Boron chelates of $BP(OH)_2$ (I), HBA (II), and oPP (III)

3.2.4.4 Buffer Solutions

As has already been mentioned in the caption of *Table 2,* p. 22, the extreme sensitivity of $BP(OH)_2$ towards pH causes the large differences in spectroscopic data published for $BP(OH)_2$ in aqueous solutions so far [159h, m, 165]. Thus, special attention has to be paid to pH adjustment in future investigations of this compound in aqueous solutions.

In contrast to pH, the influence of ionic strength (in terms of salts containing no heavy and transition metal cations) on the spectroscopic properties of $BP(OH)_2$ at a given pH is negligible. This is a very valuable characteristic since it allows the employment of buffer salts in order to guarantee a constant pH for the investigations involving metal ions. Only one class of buffer systems tested here had a remarkable effect on the absorption and emission behavior of $BP(OH)_2$, i. e., borate buffer systems (buffer region: $9.4 < pH < 11.0$). Borate derivatives strongly enhance the absorption bands centered at 24800 and 23200 cm^{-1} and lead to the appearance of another, even more hypsochromically shifted emission band, centered at 23200 cm^{-1}, respectively. Furthermore, the total fluorescence intensity is increased. The nature of the complex has not been investigated any further but binding of the borate anion to a deprotonated hydroxyl group and coordination to a pyridyl nitrogen is anticipated. Boron chelates of such a type (6-membered ring) are known for related structures, i. e., azomethines (namely HBA), and *Umland* et al. found boron chelates of a similar type in a number of *o*-(2-heterocycle)phenols (heterocycle: benzothiazolyl, benzoxazolyl, benzimidazolyl) [178]. Moreover, *Kábrt* and *Holzbecher* observed fluorescence enhancement in the presence of borates even for the non-fluorescent oPP [175b]. A schematic picture of the anticipated complex is given in *Scheme 6*. Therefore, borate buffers are not suitable for the application of $BP(OH)_2$ in metal ion analysis.

3.3 Complexes of $BP(OH)_2$ in Aqueous Solutions

The photophysical properties of $BP(OH)_2$ described in the preceeding subsections along with the analytically valuable properties such as its (moderate) water solubility and high photostability ($BP(OH)_2$ has been proposed as a fluorescence standard [159d] as well as a laser dye [159c, g]) render this compound a suitable candidate for an ion-sensitive fluorescent probe. Like its parent compound, bipy, $BP(OH)_2$ forms stable complexes with various heavy and transition metal ions. But until today, besides the work presented here and in refs [35-37], [167], and [172], metal ion complexes of $BP(OH)_2$ (and its model compound BPOH) have received

xxxii) This fact is well-supported by the similar behavior of M^{II} complexes of both dyes in water (Ch. 3.4). Note as well that the spectroscopic behavior of the $^1EK^*$ transient ($BP(OH)_2$) [163a] and $^1MK^*$ (BPOH) [168b] were found to be very similar.

little (or no) attention. Only *Cargill Thompson* et al. investigated two different mixed complexes of $BP(OH)_2$ with $Ru^{II}(bipy)_2$ [179], but these systems were only monitored in acetonitrile. The study presented here involves the metal ions Zn^{II}, Cd^{II}, Hg^{II}, Cu^{II}, Ni^{II}, Co^{II}, Fe^{II}, Mn^{II}, and Pb^{II} as well as Ca^{II}, Mg^{II}, and Na^{I} for reference experiments.

3.3.1 Steady-State Spectra

3.3.1.1 Absorption and Fluorescence

Complexation to the metal ions listed above leads to both a change in the absorption and the emission spectrum. Whereas the complexes $BP(OH)_2$ forms with paramagnetic transition metal ions, i. e., Cu^{II} or Ni^{II}, are non-fluorescent, in the case of the diamagnetic heavy metal ions of the d^{10} group, only Hg^{II} forms a non-fluorescent complex. The Zn^{II} and Cd^{II} complexes are highly fluorescent [35-37, 167, 172]. Part A of *Fig. 10* combines the absorption spectra of $BP(OH)_2$ in the presence of all the transition metal ions showing pronounced effects and in part B, both the steady-state absorption and emission spectra in the presence of the d^{10} metal ions are shown. The spectra resemble those of the 1:1-complexes at full complexation of the ligand.

From *Fig. 10*, the full overlap of the complexes' and the free ligand's absorption bands is obvious. For all the complexes investigated here, the absorption bands of lowest energy remain ligand-centered electronic transitions of $\pi\pi^*$ nature showing typical features of absorption bands of organic chromophores, i. e., broad structureless bands with relatively high extinction coefficients ($\varepsilon > 10^3\ M^{-1}\ cm^{-1}$). Metal-centered d-d transitions were not observed at the concentrations used and in the case of the paramagnetic ions, no MLCT or LMCT bands were found. However, due to its exceptional features (internal hydrogen bonds, enol-keto tautomerism, etc.), the characteristical shifts often observed upon complexation are obscured by the very broad absorption spectrum of $BP(OH)_2$ in aqueous solution of medium pH. In 8-hydroxyquinoline (8-HQ) for example, the absorption band of the complex is well separated and red shifted by 4520 cm^{-1}, most probably due to a more covalent nature of the transition metal-quinoline nitrogen bond [180]. Similar shifts as for 8-HQ are observed for the complexes of bipy (4460 cm^{-1} for the Zn^{II} complex, Ch. 3.4.1) but in the case of $BP(OH)_2$, the bands strongly overlap and only the maximum of the main band is shifted by 1600 cm^{-1}. The relevant data are included in *Table 5.*

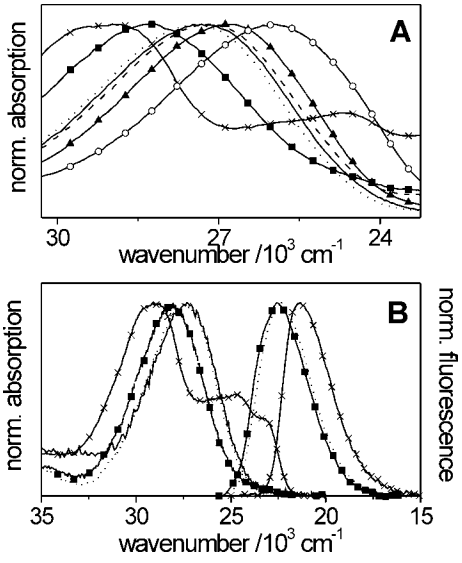

Fig.10
Normalized steady-state absorption spectra of [M^{II}⊂$BP(OH)_2$] in neat water. ***A****: free $BP(OH)_2$ (x) and complexes with Cd^{II} (■), Zn^{II} (·····), Hg^{II} (–), Co^{II} (- -), Ni^{II} (▲), and Cu^{II} (o).* ***B****: Spectra of the d^{10} metal ion complexes (excitation at 370 nm, c_L = 3 x 10^{-6} M; Hg^{II}⊂$BP(OH)_2$ is non-fluorescent).*

Table 5
Spectroscopic properties of the complexes of $BP(OH)_2$ in neat water.

M^{II}	$\tilde{\nu}$ (abs)	$\tilde{\nu}$ (em)	ϕ_f	τ_f
	10^3 cm^{-1}	**10^3 cm^{-1}**		**ns**
-	28.8, 24.8	21.3	0.04	0.45
Cu^{II}	26.0	-	-	-
Ni^{II}	26.9	-	-	-
Co^{II}	27.1	-	-	-
Hg^{II}	27.3	-	-	-
Zn^{II}	27.5	22.5	0.62	6.17
Cd^{II}	28.2	22.6	0.53	5.24

Opposite tendencies can be derived from the emission measurements, i. e., different effects of para- and diamagnetic cations with strong similarities within each group, the only exception being Hg^{II}. All the paramagnetic ions quench the fluorescence without any spectral shifts suggesting static quenching to be the main force (cf. Ch. 1.2). The emission spectra of the Zn^{II} and the Cd^{II} complex are very similar and largely overlap with the emission band of the free ligand (blue-shifted by *ca.* 20 nm (~ 1000 cm^{-1}), *Fig. 10*).[xxxiii] Addition of Hg^{II} ions to a solution containing $BP(OH)_2$ yields the same effect as has been observed for paramagnetic metal ions, i. e., static fluorescence quenching *(Table 5)*. Fluorescence excitation spectra recorded at full complexation resemble the absorption spectra of both cation complexes, the Zn^{II} and the Cd^{II} complex.

3.3.1.2 Titrations and Complex Stoichiometry

Figure 11 contains a set of titration spectra for $BP(OH)_2$ and Zn^{II} (part A) and Cu^{II} (part B), respectively. In both cases (and for all the other ions), the isosbestic points observed in a UV/Vis-spectrophotometric titration are not ideally sharp suggesting the formation of more than a single equilibrium. However, fitting the titration curves does only yield acceptable results for a sum of a 1:1 and a 2:1 complexation model in some cases (Zn^{II}, Cd^{II}), both complexes showing a spectroscopically similar behavior. For the other, more strongly coordinating ions, the complex stability constants are too high to be reliably determined by this method and the relatively poor solubility of $BP(OH)_2$ in terms of a c_{L0}-titration (Appendix B) made such a reverse titration (titration of M with L) impossible. Thus, in order to compare the binding strength of all the cations, the apparent complex stability constants were

xxxiii) The restriction on the pH working range mentioned above is obvious when comparing the absorption and emission bands of, e. g., the Mg^{II} with those of the Zn^{II} and the Cd^{II} complexes. The Mg^{II} complex absorbs at 27700 cm^{-1} and emits at 22800 cm^{-1}, strongly overlapping with the other two complexes (data for Mg^{II} complex at pH 11.0).

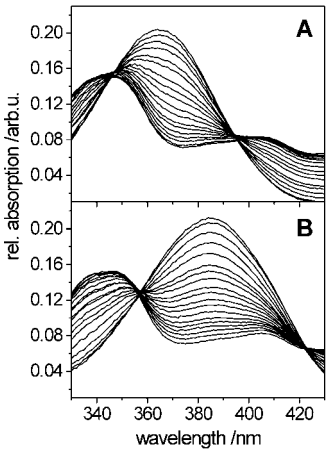

Fig. 11
*UV/Vis-spectrophotometric titration of $BP(OH)_2$ with Zn^{II} (**A**) and Cu^{II} (**B**) in neat water; c_L = 5 x 10^{-6} M ($x_{M/L}$ cf. Fig. 13)*

determined (Appendix B). In all the UV/Vis-spectrophotometric and fluorometric titrations performed with $BP(OH)_2$ and various metal ions, no divergent spectral features have been found making a discrimination between the 1:1 and 1:2 complex impossible in such a way (see Ch. 3.3.3 for ion selectivities and stability constants).[xxxiv] However, ML_2 formation is confirmed by an analysis of the complexation data according to the method of continuous variations which yields the stoichiometry of the complexes [181]. For a continuous variations diagram, the difference Y_λ between the measured absorbance A_λ and the calculated absorbance A_λ' is plotted vs. the molar fraction x of one reactand. The absorbances measured for the pure solutions of metal salt (subscript M) and ligand (subscript L) are used to calculate A_λ' according to eqn (1)). In the experiment, solutions of different molar ratios are prepared from equimolar solutions of M and L and the actual absorbance A_λ is measured. Then, Y_λ is calculated (eqn (2)) and when plotting Y_λ vs. x_L, maxima at x_L = 0.5, 0.67, and 0.75 are found for 1:1, 1:2, and 1:3 (M:L) complexes, respectively. An example of a Y_λ vs. x_L-plot is given in *Fig. 12*.

$$A_\lambda' = x_M \varepsilon(\lambda)_M c_M d + x_L \varepsilon(\lambda)_L c_L d \quad (1)$$

$$Y_\lambda = A_\lambda - A_\lambda' \quad (2)$$

with $c_{M0} = c_{L0}$ and $x_M + x_L = 1$.

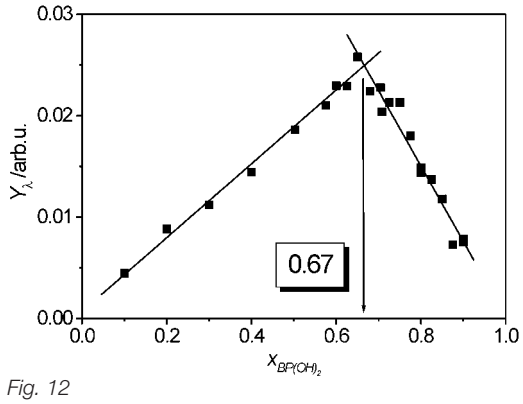

Fig. 12
Verification of the complex stoichiometry by the method of continuous variations (Y_λ vs. x_L- diagram for Cu^{II}); $c_{L0} = c_{M0}$ = 5 x 10^{-6} M.

xxxiv) A possible third complex species ($x_{M/L}$ = 3) was not found experimentally.

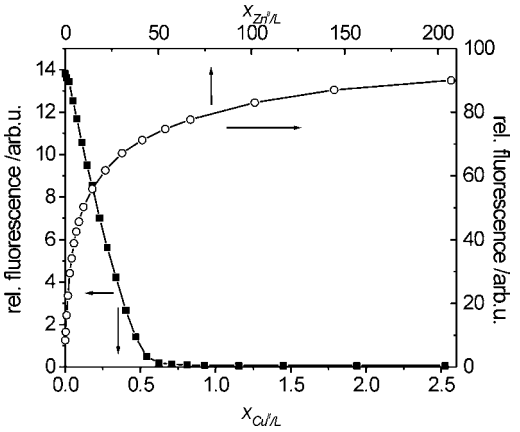

Fig. 13
Spectrofluorometric tiration of $BP(OH)_2$ with Cu^{II} (■) and Zn^{II} (o) in neat water (excitation at isosbestic points, c_L = 3 x 10^{-6} M)

Two fluorometric titrations, again for Cu^{II} and Zn^{II}, are shown in *Fig. 13*, clearly indicating both the higher stability constant of the Cu^{II} complex and the opposite effects of para- and diamagnetic cations on the fluorescence of $BP(OH)_2$.

When analyzing fluorescence excitation spectra recorded for solutions containing different amounts of free ligand and complex, the spectra could always be described by a linear combination of the fluorescence excitation spectra of the free ligand and the 1:1 complex. Thus, the 1:1 and 1:2 complexes behave fluorometrically identical and cannot be distinguished by steady-state emission spectroscopy either.

Those cations which do not or only weakly bind to $BP(OH)_2$, e. g., Pb^{II}, Fe^{II}, and Mn^{II}, do not influence the absorption and fluorescence behavior significantly. Having in mind the "dislike" of Mn^{II} for such coordination sites, the absence in spectroscopically observable complex formation for this ion is clear [182a].

3.3.2 Fluorescence Lifetimes

The effect of complexation on the fluorescence decay kinetics of $BP(OH)_2$ reflects the observations made for the steady-state fluorescence experiments. Addition of quenching ions such as Cu^{II} and Hg^{II} to a solution of $BP(OH)_2$ in water causes only a slight variation in the fluorescence lifetime but a strong decrease in the amplitude, when comparing the photons emitted over a certain time interval, i. e., static quenching occurs (this is observed at any excitation wavelength).

In contrast, for Zn^{II} and Cd^{II}, in agreement with an increase in fluorescence quantum yield, a chelation-induced increase in fluorescence lifetime is observed. As follows from *Fig. 14*, the presence of both Zn^{II} and Cd^{II} leads to the appearance of a new long-lived fluorescence decay component, its lifetime being cation-specific. At full complexation, the monoexponential decay kinetics of the complexes are visible. A time-resolved fluorometric titration reveals that with increasing metal ion concentration the relative amplitude of the short-lived decay component decreases and, correspondingly, the relative amplitude of the long-lived decay component increases. No ion concentration-dependent variations in the lifetime of the long-lived decay component are noticed thus completing the observations made by steady-state spectroscopy, i. e., identical spectroscopic behavior of the 1:1 and 1:2 complex. Accordingly, the relative fluorescence quantum

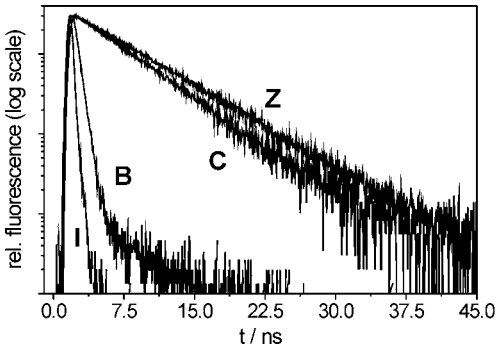

Fig. 14
*Fluorescence decay curves of $BP(OH)_2$ (**B**), its Zn^{II} (**Z**), and Cd^{II} (**C**) complexes (full complexation) in water of pH 7.6 (**I**: Instrumental response function; BESSY setup; excitation at absorption maximum; observation at emission maximum; c_L = 3 x 10^{-6}M).*

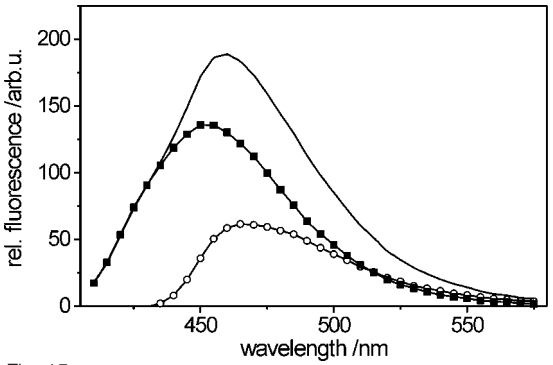

Fig. 15
$SAS_i(\lambda)$ of a mixture of $BP(OH)_2$: Zn^{II} ($x_{M/L}$ = 2) in water of pH 6.5; τ_1 = 0.45 ns (free ligand, o), τ_2 = 6.17 ns (complex, ■). The solid line corresponds to the steady-state emission spectrum (excitation at 360 nm; c_L = 3 x 10^{-6}M).

yield (Φ_{rel}, cf. Appendix B) of this slow decay component depends on cation concentration and can thus be used for the determination of both cations.

Emission wavelength-resolved fluorescence decay measurements were additionally performed with solutions containing both free and complexed probe molecules (to Zn^{II} and Cd^{II}) in order to separate the spectral contours of the single emitting species. The presence of two distinct species in both ground and excited state and the comparable shifts observed in absorption and emission suggest that fluorescence deactivation is fast compared to excited-state decomplexation. Thus, for the global analysis of the emission wavelength-resolved fluorescence decay data, ground state heterogeneity was assumed and the species associated spectra ($SAS_i(\lambda)$) are identical with the decay associated spectra ($DAS_i(\lambda)$) [183b]. The $DAS_i(\lambda)$ of the single emitting species are given according to eqns (3) and (63) (for abbreviations see Appendix A, for basic equations see Appendix B) [183]:

$$DAS_i(\lambda) = \frac{a_i(\lambda) F_{SS}^{tot}(\lambda)}{\sum_i a_i(\lambda)\tau_i} \qquad (3)$$

As an example, the spectra of the single compounds ($SAS_i(\lambda)$) of a solution containing $BP(OH)_2$ and Zn^{II} ions at a ratio of 1:2 are constructed by global analysis of the emission wavelength-resolved fluorescence decay profiles and are shown in *Fig. 15*. Here, i = 1 denotes component 1 (τ_f = 0.45 ns) attributed to $BP(OH)_2$, i = 2 denotes component 2 (τ_f = 6.17 ns) attributed to the Zn^{II} complex, and $F_{SS}^{tot}(\lambda)$ is the measured steady-state emission spectrum of the solution. The $SAS_i(\lambda)$ confirm the results obtained with the steady-state measurements, i.e., the fluorescent Zn^{II} (and Cd^{II}) complex(es) of $BP(OH)_2$ emit(s) at higher energies and reveal that the excited complex decays slower than the free probe *(Fig. 15)*.

All the fluorescence lifetime data are included in *Table 5*, p. 31. The faster decay of the fluorescence of the Cd^{II} complex can be understood on the basis of the heavy atom effect, introduced in Ch. 1.2. Assuming that in the complexes $k_{nr} \sim k_{isc}$, the heavy atom effect can be quantified by using a central field single electron approximation for the relationship between k_{isc} and the spin-orbit coupling constant ζ (eqn (4)). Here, Z is the atomic number and the term in the denominator includes screening of the nucleus and orbital penetration (n, l - quantum numbers). Accordingly, $\log k_{nr} + \log n^6$ is a measure for the heavy atom effect and the values calculated for the Zn^{II} and Cd^{II} complex amount to 11.4 and 12.1, in good agreement with values published for the related 8-HQ complexes of these ions [34a].

$$k_{isc} \propto \xi_{nl}^2 = \left(\frac{e^2h^2}{8\pi^2 m^2 c^2 a_0^2}\right)^2 \left[\frac{Z^4}{n^3\left(l+1\right)\left(l+\frac{1}{2}\right)l}\right]^2 \qquad (4)$$

The analytically most valuable effect is the difference in the fluorescence lifetimes of both complexes (Zn^{II} = 6.17 ns, Cd^{II} = 5.24 ns; and of the free ligand = 0.45 ns) allowing for the discrimination between species which can spectrally not be resolved. An example of an analytical application is given in Ch. 3.5.

3.3.3 Ion Selectivity

The complexation of metal ions by the fluorescent ligand is strongly pH-controlled reflecting the successive availability of possible coordination sites (cf. pK_a values in *Table 2*, p. 22) as well as the affinity of metal ions towards the chelation sites. Acidic pH prevent complexation, i. e., below pH 3, no noticeable complexation is observed for any of the cations studied here. From pH ~ 3 on, the cations are bound in the order of their complex stability constants *(Table 6)*. At ambient pH, all the other heavy and transition metal ions which show an effect, are complexed [35-37, 167]. However, no intensive complexation studies were carried out at basic pH > 9 because the fluorescence decay behavior of the free ligand is highly pH-sensitive in this pH region. Concerning

Table 6
Apparent complex stability constants of the complexes of $BP(OH)_2$ in aqueous solutions of neutral pH (see Appendix B for details).

M^{II}	$\log K^{app}$
Cu^{II}	5.9
Ni^{II}	5.0
Co^{II}	4.7
Hg^{II}	4.4
Zn^{II}	4.2
Cd^{II}	3.6

the main aim of this part of the work, the time-resolved fluorometric analysis of metal ions, the expense for pH adjustment in the basic pH range would be unfavorably high. Furthermore, at this pH, alkaline-earth metal ions such as Mg^{II} are bound as well and discrimination would be less efficient. Similar pH-dependent results were obtained when working with the aqueous buffer solutions described in Ch. 2.3. Thus, for most of the spectroscopic and analytical experiments, potassium dihydrogenphosphate/disodium hydrogenphosphate buffer solutions at various pH between 5.4 and 8.0 were used. The citric acid/sodium hydroxide buffer proved to be unsuitable because of the interference of competing complexation reactions.

The spectroscopically observable (apparent) complex stability constants ($\log K_{app}$) of the complexes formed are shown in *Table 6* and can be well-described by the Irving-Williams order [19], where the strongest complexation is observed for Cu^{II}. In the case of Fe^{II}, Mn^{II}, and Pb^{II}, only weak coordination-induced changes occur. No complexation was found for Na^{I}. The ion selectivity of $BP(OH)_2$ observed is comparable to other so-called "general" ligands with bidentate N,O-chelating sites. Among others, 8-HQ, pyridine-2-carboxylic acid, and a lot of aryl-azomethine ligands are the most widely used complexation reagents [182a, b, 184]. Provided that they are not much conformationally restricted, these ligands do not show any enhanced selectivity for particular ions [182].

3.4 Nature of the Complexes

Although the spectroscopic behavior of $BP(OH)_2$ and its complexes reported in Ch. 3.3 reveals certain tendencies, the real nature of the complexes is still unclear. Taking a closer look at the fluorescent probe itself, three different chelation mechanisms are possible *(Scheme 7)*.

Route C, the formation of a sterically unfavored 7-membered ring due to coordination to both hydroxyl groups, can be ruled out on the basis of thermodynamic considerations [185]. The necessary deprotonation of two hydroxyl groups at pH < 7 (complex formation with some M^{II}), the order of complex stability constants (the highest K_S is observed for the aminophile cation Cu^{II}), the general preferences of the "soft"[xxxv] metal ions complexed by "soft" donor heteroatoms, and the unfavored geometry of the resulting chelate render this mechanism very unlikely. However, chelate formation along route A and B has to be considered as has been shown by *Cargill Thompson* et al. [179].

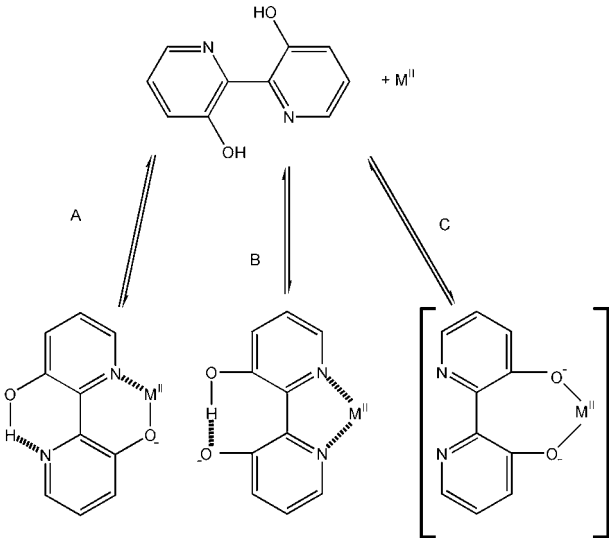

Scheme 7
Generalized scheme of possible chelation mechanisms being involved in metal ion complexation of $BP(OH)_2$ (The structures do not indicate actual complex stoichiometries.)

Thus, in order to get more insight into these processes, the (substituted) bipyridines and oPP shown in *Scheme 1*, p. 21 have been investigated with optical and ^{1}H-NMR spectroscopy in aqueous, ethanol, and acetonitrile solutions in the presence of the cations Zn^{II} and Cd^{II}.

3.4.1 Absorption and Fluorescence Spectroscopy

Whereas $BP(OH)_2$, BPOH, and bipy show complexation-induced spectroscopic effects upon addition of Zn^{II} and Cd^{II} in all the three solvents investigated, oPP, an only very weakly fluorescent molecule ($\phi_f < 10^{-5}$), does not show any pronounced changes in its photophysical properties upon complexation and even in organic solvents only small effects were observed at a high excess of metal ion (e. g., > 500-fold excess of Zn^{II}).

The spectroscopic data of the Zn^{II} and Cd^{II} complexes of BPOH and bipy are reported in *Table 7* along with the data of the corresponding $BP(OH)_2$ complexes.

3.4.1.1 Water

In neat water, the Zn^{II} and Cd^{II} complexes of both BPOH and $BP(OH)_2$ show a very similar absorption and emission behavior *(Fig. 16, Table 7)*. The spectral band positions in absorption as well as emission differ by only ≤ 1000 cm^{-1} and the fluorescence quantum yields and lifetimes are very similar as well. As a consequence, this results in similar rate constants for radiative and non-radiative deactivation.

On the other hand, the behavior of the corresponding complexes of bipy is clearly different. The Stokes shifts observed are only $^2/_3$ the size of those observed for the hydroxy bipyridyls, the fluorescence quantum yields are considerably lower, and especially the fluorescence decay times are faster by a factor of ca. 4.5.

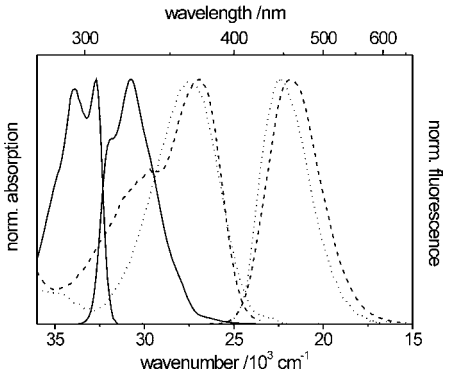

Fig. 16
Steady-state spectra of the Zn^{II} complexes of $BP(OH)_2$ (·····), BPOH (- -), and bipy (—) in neat water (full complexation, excitation at absorption maximum; $c_L = 3 \times 10^{-6}$ M).

xxxv) "soft" in terms of Pearson's HSAB concept [143]

Table 7
Spectroscopic properties of the Zn^{II} and Cd^{II} complexes of $BP(OH)_2$, BPOH, and bipy in neat water (W), ethanol (E), and acetonitrile (A).

Ion	Ligand	$\tilde{\nu}$ (abs)	$\tilde{\nu}$ (em)	$\Delta\tilde{\nu}$ (abs-em)	ϕ_f	τ_f	k_f	k_{nr}
		10^3 cm^{-1}	10^3 cm^{-1}	10^3 cm^{-1}		ns	10^8 s^{-1}	10^8 s^{-1}
Zn^{II} /	$BP(OH)_2$	27.5	22.5	5.0	0.62	6.17	1.00	0.61
W	BPOH	27.0	21.8	5.2	0.59	6.71	0.88	0.61
	bipy	33.9 [a]	30.8 [a]	3.1	0.34 [b]	1.43 [c]	2.38	4.61
Zn^{II} /	$BP(OH)_2$	25.6	21.5	4.1	0.55	6.07	0.91	0.74
E	BPOH [d]	25.2	20.8	4.4	(0.26)	-	-	-
	BPOH [e]	30.0 [f]	20.6 (26.6) [g]	9.4	0.47	6.21	0.76	0.85
	bipy	33.9	30.8	3.1	0.10	0.72 [h]	1.39	12.5
Zn^{II} /	$BP(OH)_2$ [d]	24.7	21.8	2.9	-	6.01	-	-
A	$BP(OH)_2$ [i]	30.5 [j]	25.5, 20.6	5.0, 9.9	n.d. [k]	1.37 [l]	-	-
	$BP(OH)_2$ [i]	24.7	21.8	2.9	0.47	5.87	(0.80)	(0.90)
	BPOH	30.4 [f]	27.5	2.9	0.36	1.31	2.75	4.88
	bipy	33.9	30.6	3.3	0.27	1.48	1.82	4.93
Cd^{II} /	$BP(OH)_2$	28.2	22.6	5.6	0.53	5.24	1.01	0.90
W	BPOH	27.2	22.0	5.2	0.48	5,79	0.92	0.99
	bipy	33.9	30.8	3.1	0.05	0.29	1.72	32.7
Cd^{II} /	$BP(OH)_2$	26.7	22.0	4.7	0.54	5.30	1.02	0.87
E	BPOH [d]	26.0	21.0	5.0	(0.26)	-	-	-
	BPOH [e]	30.2 [f]	21.1	9.1	0.45	5.50	0.82	1.00
	bipy	33.9	30.8	3.1	0.05	0.29	1.92	30.5
Cd^{II} /	$BP(OH)_2$	27.6	22.2	5.4	0.46	5.18	0.89	1.04
A	BPOH	30.7 [f]	27.4 (21.1)	3.3	0.10 [m]	0.26 [m]	3.85	34.6
	bipy	33.9	30.8	3.1	0.07	0.23	3.04	40.4

[a] Ohno and Kato reported values of 32500 and 30500 cm^{-1} [186a];
[b] *Kotlicka* and *Grabowski* published a value of 0.36 but used a higher tabulated fluorescence quantum yield for the fluorescence standard 2-AP (for ϕ_f of 2-AP cf. Ch. 2.5.2.1) [158b];
[c] *Castellucci* et al. measured a lifetime of 1.62 ns [186b];
[d] intermediate complex observed in the titration experiments at $x_{M/L} \leq 0.5$;
[e] data obtained at full complexation (ML complex);
[f] center of the band displaying a double maximum;
[g] intensity of the band at 26600 cm^{-1} = $^1/_{125}^{th}$ of the total fluorescence intensity;
[h] *Castellucci* et al. reported a decay time of 50 ps for Zn^{II}⊂bipy in methanol [186b];
[i] data obtained at highest Zn^{II} excess possible: two different absorption and emission bands;
[j] from fluorescence excitation spectrum;
[k] not determined because full complexation not obtainable;
[l] observed at 25500 cm^{-1}, τ_1 = 0.61 ns and τ_2 = 5.30 ns observed at 21800 cm^{-1};
[m] τ_2 = 5.44 ns, a_{rel} = 0.27 when observed at 21100 cm^{-1}; Φ_f^{rel} (band at 21100 cm^{-1}) = 0.02.

Accordingly, this effect should be predominantly reflected in different k_{nr}. Indeed, for example, the value found for Zn^{II}⊂bipy is nearly an order of magnitude higher than those obtained for Zn^{II}⊂BPOH and Zn^{II}⊂$BP(OH)_2$. This effect is even more pronounced in the case of Cd^{II}. Thus, the "activity" of $n\pi^*$ state interaction is higher in the bipy complexes than in the other two complexes and the influence of the heavy atom (or ion) Cd^{II} is more pronounced in the case of these smaller chelates with a 5-membered ring structure. Furthermore, besides the shift in absorption (electrostatic polarization induced by M^{II}), M^{II}⊂bipy shows the characteristically structured absorption band where the vibrational structure is better resolved [187]. On the other hand, comparing k_f and k_{nr} of M^{II}⊂$BP(OH)_2$ with those of free $BP(OH)_2$ it is obvious, that the rate constant for fluorescence deactivation remains constant (within experimental error; *Table 2*, p. 22) but the contributions of competing non-radiative deactivation channels of the first excited singlet state are markedly reduced.

It is interesting to note that tight binding of $BP(OH)_2$ in the complexes further reduces k_{nr} by a factor of 3.5 compared to k_{nr} in apolar solvents like cyclohexane (k_{nr} = 2.1, *Table 2*, p. 22).[xxxvi]

3.4.1.2 Ethanol

Ethanol, less polar than water but still capable of hydrogen bond formation, induces similar effects as water does but some noticeable differences in complex formation occur, especially in the case of BPOH. For M^{II}⊂$BP(OH)_2$ and M^{II}⊂bipy, a similar behavior compared to water is observed. The only deviations are slightly hypsochromically shifted spectra in the case of M^{II}⊂$BP(OH)_2$ and a marked drop in fluorescence quantum yield and lifetime of the Zn^{II} complex of bipy. The exceptional behavior of this complex in ethanol is unclear and will not be discussed any further. However, the data obtained for Zn^{II}⊂bipy are still different from those measured for the corresponding complexes of its hydroxy derivatives. Cd^{II}⊂bipy shows the expected features and in acetonitrile

xxxvi) It should, however, be noted that the striking similarity of the spectroscopic properties of M^{II}⊂$BP(OH)_2$ with those observed for Zn^{II}⊂bipy aggregates, could not be explained. *Dhanya* and *Bhattacharyya* found for aqueous solutions containing bipy (c_{bipy} = 8 x 10^{-3} M) and Zn^{II} (c_{Zn} = 8 x 10^{-2} M) at high concentrations absorption and emission bands centered at 27000 cm^{-1} and 22200 cm^{-1} (complex; 23200 cm^{-1} for free bipy at c_{bipy} = 8 x 10^{-3} M), respectively [158d]. Even more remarkable are the fluorescence lifetimes they measured, namely 5.17 ns (complex; 3.2 ns for free bipy). However, the concentrations used in the studies reported here lie in the range of $c_L \leq 5 \times 10^{-6}$ M and $c_M \leq 1 \times 10^{-3}$ M, making aggregation on the basis of π-stacking interactions unfavorable.

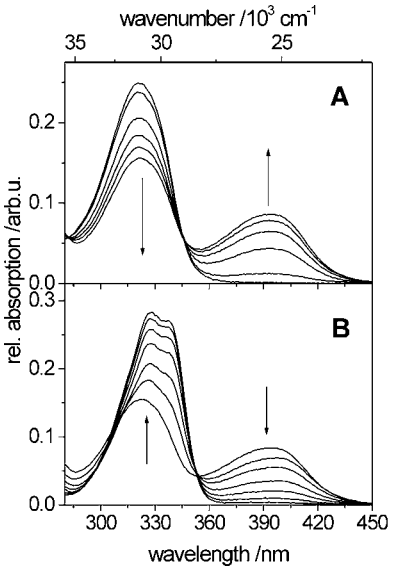

Fig. 17
*UV/Vis-spectrophotometric titration of BPOH with Zn^{II} in ethanol. **A**: Steps for $x_{M/L}$ = 0.1-0.5; **B**: for $x_{M/L}$ = 0.5-50 (arrows indicate changes upon Zn^{II} addition). Measurements were performed in 100 mm absorption cells with c_{BPOH} = 3.7 x 10^{-6} M.*

(see below), the behavior of Zn^{II}⊂bipy is again comparable to that in water.

For M^{II}⊂BPOH, complex formation is very remarkable. At low metal ion concentrations up to $x_{M/L}$ = 0.5, the formed complex resembles that of $BP(OH)_2$. In part A of *Fig. 17*, the UV/Vis-spectrophotometric titration spectra for BPOH with Zn^{II} up to $x_{M/L}$ = 0.5 are displayed and the characteristical features are obvious (see *Table 7* for corresponding data). Adding more Zn^{II} to the solution yields a decrease of the band at 25200 cm^{-1} and a new band builds up at 30000 cm^{-1} *(Fig. 17B)*. This band now displays the typical characteristics of the Zn^{II}⊂bipy complex (parts A, B in *Fig. 18*). However, the emission spectra measured up to a 1000-fold excess of Zn^{II} (corresponding to the spectrum at highest excess of Zn^{II} in *Fig. 17B*) resemble that of Zn^{II}⊂$BP(OH)_2$ and the fluorescence decays with nearly the same time constant *(Table 7)*.

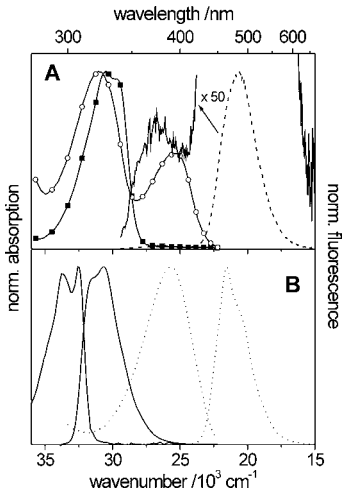

Fig. 18
*Steady-state spectra of the Zn^{II} complexes of the (substituted) bipyridines in ethanol. **A**: Absorption spectra of Zn^{II}⊂$(BPOH)_2$ (■), Zn^{II}⊂BPOH (o), and emission spectrum of Zn^{II}⊂BPOH (- -), the enlarged high energy side (—) of the emission spectrum is included as well (c_L = 3 x 10^{-6} M). **B**: Spectra of Zn^{II}⊂ $BP(OH)_2$ (.....) and Zn^{II}⊂bipy (—); full complexation, excitation at absorption maximum.*

Only at the high energy side, a weak band (of *ca.* $^1/_{125}{}^{th}$ intensity) centered at 26 600 cm^{-1} is visible. Having in mind the emission properties of Zn^{II}⊂bipy, i.e., low ϕ_f and fast decay kinetics, emission from a N,N-chelated Zn^{II}⊂BPOH might be weak in ethanol as well. However, the fluorescence excitation spectra recorded at 27 000 cm^{-1} and 20 800 cm^{-1} are similar and resemble the absorption spectrum of the 1:1 complex, centered at 30 000 cm^{-1}. Furthermore, a closer look at *Fig. 18* provides a possible explanation for the fluorometric results. At an equilibrium with intermediately formed complexes still in the solution, light emitted from the Zn^{II}⊂bipy-like complex is absorbed by this complex and reemitted with its characteristic fluorescence.

3.4.1.3 Acetonitrile

In acetonitrile, a solvent of comparable polarity lacking H-bond donating ability, the tendencies observed in ethanol are even more pronounced. Only the Cd^{II} complex of $BP(OH)_2$ shows nearly identical spectroscopic behavior in all three solvents. For Zn^{II}⊂$BP(OH)_2$, the metal ion concentration-dependent spectroscopic behavior resembles that of Zn^{II}⊂BPOH in ethanol. At low concentrations, the "normal" Zn^{II}⊂$BP(OH)_2$ features occur, but at a high excess of Zn^{II}, a blue-shifted band centered at 25 500 cm^{-1} appears in the emission spectrum *(Fig. 19)*. The changes in absorption are negligible but in the inset of *Fig. 19* the shift between the high-energy band of the fluorescence excitation spectrum (observation at 25 600 cm^{-1}) and the absorption band is visible. Observation at 19 200 cm^{-1} yields a band corresponding to the absorption band of the 1:2 complex. Furthermore, emission wavelength-dependent fluorescence decay data support the results as well (1.37 ns at 25 500 cm^{-1} vs. *ca.* 6 ns at 21 800 cm^{-1}; *Table 7*).[xxxvii]

For Zn^{II}⊂BPOH, only the absorption band at 30 400 cm^{-1} and an emission band at 27 500 cm^{-1} are found, independent of Zn^{II} concentration *(Fig. 20)*. The similarity of the photophysical properties of Zn^{II}⊂bipy and Zn^{II}⊂BPOH, including typical

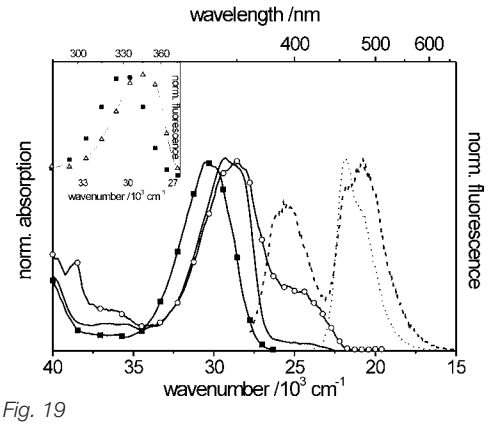

Fig. 19
Steady-state spectra of Zn^{II}⊂$BP(OH)_2$ in acetonitrile. Absorption spectrum (—), emission spectrum of the ML_2-complex (·····, excitation at 24500 cm^{-1}), emission spectrum at high Zn^{II} excess (both complexes present, - -, excitation at 29500 cm^{-1}), fluorescence excitation spectra at high Zn^{II} excess (observation at 25 600 cm^{-1}, ■; observation at 19200 cm^{-1}, o). In the inset, the absorption spectrum of the ML_2-complex (—) and the fluorescence excitation spectra of the free ligand (Δ) and at high Zn^{II} excess (observation at 25600 cm^{-1}, ■) are included (c_L = 3 x 10^{-6} M).

xxxvii) Note that the spectra presented in any case of complexation study are not spectra of pure compounds since at nearly any concentration, (some of) the species are in equilibrium and thus present in solution.

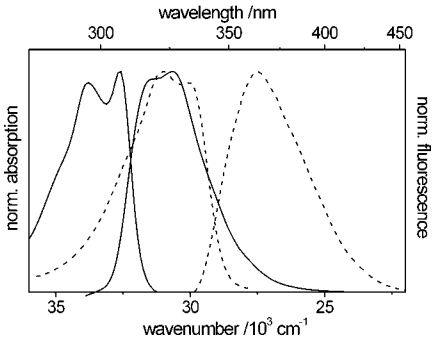

Fig. 20
Steady-state spectra of the Zn^{II} complexes of BPOH (- -) and bipy (–––) in acetonitrile (excitation at absorption maximum; c_L = 3 x 10^{-6} M).

characteristics (vibrational structure) of the M^{II}⊂bipy absorption band, is remarkable (*Table 7* and *Fig. 20*).

The higher-energy emission band, absent in ethanol, indicates the formation of a Zn^{II}⊂bipy-like chelate in acetonitrile. In accordance with the different behavior of the Zn^{II} and the Cd^{II} complex of $BP(OH)_2$, for Cd^{II}⊂BPOH still some Cd^{II}⊂$BP(OH)_2$-like chelate is observed at low Cd^{II} concentrations. For a comparison, the spectra of the bipy and BPOH complexes are shown in *Fig. 20*.

The data presented so far lead to the conclusion that the complexes investigated can be devided into two groups according to their spectroscopic behavior in the different solvents (these "spectroscopic reference structures" are labeled "Zn^{II}⊂bipy-like" and "Cd^{II}⊂$BP(OH)_2$-like").

Zn^{II}⊂$BP(OH)_2$	"Cd^{II}⊂$BP(OH)_2$-like" in all the solvents except in acetonitrile at high excess of Zn^{II};
Zn^{II}⊂BPOH	"Cd^{II}⊂$BP(OH)_2$-like" in water and at low metal ion concentrations in ethanol, "Zn^{II}⊂bipy-like" in acetonitrile and ethanol at high metal ion concentrations;
Cd^{II}⊂BPOH	"Cd^{II}⊂$BP(OH)_2$-like" in water and at low metal ion concentrations in ethanol and acetonitrile, "Zn^{II}⊂bipy-like" at high metal ion concentrations in ethanol and acetonitrile;
Cd^{II}⊂bipy	"Zn^{II}⊂bipy-like".

The fact that the complexes of bipy display their characteristical behavior in all the solvents and that the only other possible chelate structure formed in the complexes of the hydroxy derivatives is N,O-chelation points to this structure as being the favorable one for the chelates of the *o*-hydroxy bipyridyls in solvents capable of H-bond formation. Unfortunately, due to the different behavior of oPP (see below), N,O-chelates could not directly be detected employing optical spectroscopy and thus ^{1}H-NMR experiments were additionally performed.

3.4.1.4 Stability of the Complexes

Analyzing titrations of $BP(OH)_2$, BPOH, and bipy with Zn^{II} in the three solvents studied, the apparent complex stability constants determined support the conclusions drawn on the basis of the photophysical properties.

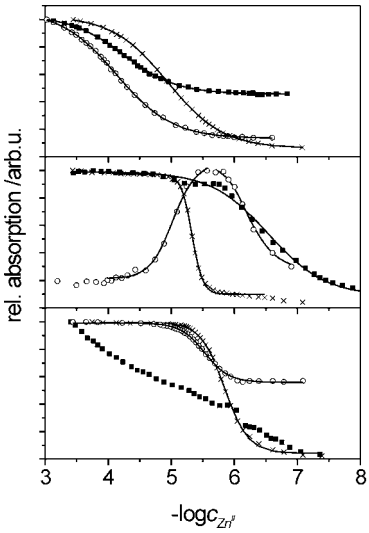

Fig. 21
Titrations curves ($A(\lambda)_{norm}$ vs. -logc_{Zn}) for $BP(OH)_2$, BPOH, and bipy with Zn^{II} in water (top), ethanol (middle) and acetonitrile (bottom). $BP(OH)_2$ ■ at 365 nm (H_2O), 370 nm (EtOH), and 405 nm (MeCN); BPOH o at 371 nm (H_2O), 360 nm (EtOH), and 335 nm (MeCN); bipy x at 307 nm (H_2O), 307 nm (EtOH), and 305 nm (MeCN). Solid lines represent fits according to the procedure described in Appendix B.

In water, BPOH and $BP(OH)_2$ yield comparable logK^{app} of 4.1 and 4.2 and the value of bipy/Zn^{II} amounts to 4.9. The outstanding behavior of BPOH in ethanol is well reflected in the shape of the titration curve monitored at 360 nm (*Fig. 21*, middle section) and in acetonitrile, the similarity of the complexes of Zn^{II}⊂bipy and Zn^{II}⊂BPOH is evident. Here, the Zn^{II} complex of $BP(OH)_2$ shows a very different behavior. Furthermore, whenever N,O-chelation occurs, not only the work necessary for desolvation of cation and ligand and the enthalpic and entropic contributions gained by complex formation have to be considered but the work necessary for deprotonation is additionally important.

3.4.1.5 oPP

As mentioned above, for oPP, only very small cation-induced effects on its photophysical properties were found during these investigations. This is consistent with results reported in the literature so far, where oPP was described as being non-fluorescent at room temperature and the only complexation reaction in water to yield spectroscopic effects was observed for Be^{II} ions [169, 175b]. Besides *Kábrt* and *Holzbecher, Johnston* and *Freiser* reported on the complexation of oPP with Cu^{II} in a water/dioxane (50/50) mixture but for all the *o*-(2-heterocycle)phenol derivatives (with heterocycle = pyridyl, imidazolinyl, benzimidazolyl, isoquinolinyl) investigated in that work, the stability constant obtained for oPP was the smallest one [175a]. In the crystalline state, the strong internal hydrogen bond (oPP shows the shortest N-O-distance in X-ray structures of the o-hydroxy bipyridyls) [169] is a force against the conformation oPP has to adopt in all the complexes synthetically prepared so far (e. g., twist of ~ 25° between the aryl rings in a Co^{III} complex [188] and 34° in a [$Ru^{II}bipy_2$oPP] complex [173]). Furthermore, for the Co^{III} complex of oPP, Ganis et al. observed a broad distribution of twist angles (22-29°) for the ligand in the crystalline state suggesting that in the complex, the rotational energy barrier for oPP is low [188]. In accordance with our observations, this could point to the formation of a complex in solution

which is spectroscopically not accessable. Nevertheless, the low acidity of the phenolic hydroxyl group in oPP does not favor complexation at medium pH and the pK_a values of 2.69 and 12.01 are an evidence for strong internal hydrogen bonding in solution [175] (for pK_a of $BP(OH)_2$ and BPOH, *Tables 2* and *4*, pp. 22, 28).

3.4.2 NMR Spectroscopy

For the verification of the chelate structures anticipated for $M^{II}\subset BP(OH)_2$ in polar solvents, the ^{1}H-NMR spectra of $BP(OH)_2$, BPOH, bipy as well as their Zn^{II} and Cd^{II} complexes were measured in deuterated acetonitrile (CD_3CN). The results are summarized in *Table 8*.

Due to their typical coupling patterns, assignment of the ^{1}H-NMR spectra of the free ligands presented no problem. Especially the signals from H-6 (in α-position of the pyridyl nitrogen atom), showing a decreased vicinal coupling constant ^3J(H-5, H-6) [189a], were easily identified. Application of the method of incremental schemes [189a], well-known for pyridyl systems, revealed a good agreement between measured and tabulated data and the coupling constants obtained correspond well with the data reported for pyridyl systems in the literature [189a]. In the case of BPOH, additional measurements were necessary in order to assign all the seven ^{1}H-signals properly. A two- dimensional ^{1}H-^{1}H correlation spectrum (COSY) allowed the separation of the three-spin system of the hydroxy-pyridyl moiety and the four-spin system of the pyridyl ring. The close neighborhood of the H-4 and H-5 signals (AB-part of an ABX-spectrum) and of the H-3‘ and H-6‘ signals could be resolved employing hetero-correlated ^{1}H-^{13}C spectra (partly including ^{1}H-^{1}H homo-coupling).

Another important feature for the determination of the nature of the complexes is the presence and the position of the OH-signal, being involved in internal hydrogen bond formation (*Scheme 2*, p. 22). For the free ligands, this signal was found at the expected position at low field, i. e., at δ 14.14 (BPOH) and δ 14.51 ($BP(OH)_2$), respectively. In the case of BPOH, addition of Zn^{II} ions induced a drastic shift of the position of this signal, appearing now at δ 9.22. In contrast to this observation, the signal maintains its position at δ 14.5 in $Zn^{II}\subset BP(OH)_2$ but is broadened. Thus, the “proton chelate” in BPOH is cracked by Zn^{II} complexation but remains at least partially intact in $Zn^{II}\subset BP(OH)_2$ (case A in *Scheme 7*, p. 34; ref. [179] and, concerning the effects of internal hydrogen-bonding, cf. the ^{15}N- and ^{17}O-NMR studies by *Sitkowski* et al. [159n]).

The same results could be derived from the changes in the chemical shifts of the signals of the heteroaromatic protons. It is well known that upon complexation, the conformation of bipy changes from its favored trans form in inert solvents to the corresponding cis form in the complex (bidentate chelate) [186b, 190a]. Although complex formation in bipy is accompanied only by minor changes in chemical shifts [190], especially the shifts to lower field in the case of H-4 and H-5 are characteristic.

For BPOH, these shifts are of the same magnitude as for bipy *(Table 8* and *Fig. 22)*. This result further supports the explanation that Zn^{II} is bound by BPOH in acetonitrile via N,N-coordination, accompanied by the loss of the intramolecular hydrogen bond in BPOH. On the other hand, for $BP(OH)_2$, nearly no changes in the positions of the chemical shifts of the aromatic protons are observed upon complexation. The signals are only broadened due to the dynamics of exchange effects. This broadening is still more pronounced in the Cd^{II} complex but the effects induced by both ions are similar *(Table 8)*.

Unfortunately, due to the relatively high concentrations required for the NMR measurements and the relatively poor solubility of Zn^{II} salts in acetonitrile, it was not possible to identify the proposed N,N-chelate for high excess of Zn^{II} over $BP(OH)_2$ (see above). In the case of Cd^{II}, no such complex was observed in neither experiment[xxxviii].

Table 8
^{1}H-NMR chemical shifts (ppm from TMS) of the heteroaromatic protons of $BP(OH)_2$, BPOH, and bipy (solvent - CD_3CN, counter ion - perchlorate, c_L = 1 x 10^{-4} M, c_{Zn} = 2 x 10^{-3} M, c_{Cd} = 0.185 M).

	Position							
	3	4	5	6	3‘	4‘	5‘	6‘
bipy	8.410	7.875	7.371	8.647	-	-	-	-
+ Zn^{II}	8.492	8.314	7.828	8.793	-	-	-	-
+ Cd^{II}	8.491	8.262	7.800	8.721	-	-	-	-
BPOH	-	7.304	7.292	8.184	8.564	8.014	7.451	8.575
+ Zn^{II}	-	7.819	7.669	8.386	9.072	8.259	7.746	8.794
+ Cd^{II}	-	7.769 [a]	7,624 [a]	8.266 [a]	9.1 [b]	8.188	7.702	8.691
$BP(OH)_2$	-	7.441	7.385	8.116	-	-	-	-
+ Zn^{II}	-	7.472	7.409	8.131	-	-	-	-
+ Cd^{II}	-	7.54	7.540	8.140	-	-	-	-

[a] broad; [b] very broad

xxxviii) It is interesting to note that complexation of $BP(OH)_2$ to Cu^{II} in acetonitrile does not lead to the formation of a N,N-chelate. The main absorption band remains centered at ca. 29 000 cm^{-1} but the shape of the spectrum resembles very much that of $BP(OH)_2$ in water at medium pH, i. e., the Cu^{II} complex displays a second maximum at 23 800 cm^{-1} ($\varepsilon \sim {}^1/_2\ \varepsilon_{max}$) and a shoulder at ca. 22 600 cm^{-1} ($\varepsilon \sim {}^1/_3\ \varepsilon_{max}$), respectively. Thus, it seems possible, that with the aid of complex formation, even the study of different enol(ate) and keto tautomers in solvents of different polarity and proticity is possible. As would have been expected, the Cu^{II} complex is non-fluorescent.

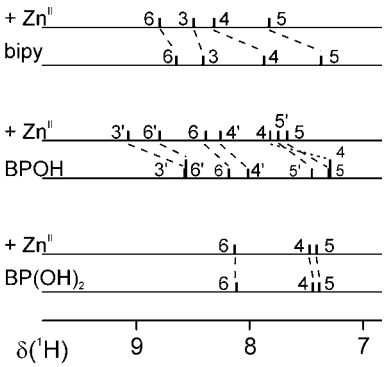

Fig. 22
Graphical representation of ^{1}H-NMR chemical shifts (ppm from TMS) of the heteroaromatic protons of BP(OH)$_2$, BPOH, and bipy (for experimental conditions, see Table 8).

3.4.3 Mechanistic Considerations

In order to explain the observed chelation behavior of the compounds, i. e., the unusual complex formation with the o-hydroxy bipyridyls, some mechanistic considerations are made. The violation of two basic laws in coordination chemistry, the formation of a 6-membered ring in spite of the (usually) more stable 5-membered ring and the preference for N,O-chelation vs. N,N-chelation, will be addressed. “Soft” (cf. footnote [xxxv], p. 34) metal ions usually prefer coordination via π-donating (heterocyclic) nitrogen atoms over that via σ-donating oxygen atoms [191]. Moreover, it is well-known for other *o*-(2-heterocycle)phenol derivatives (with heterocycle = benzopyrroleninyl, benzimidazolyl, benzoxazolyl, benzothiazolyl) that their complex formation reflects the coordinating behavior of other N,O-chelating reagents like for example 8-HQ, only the stability of the 6-membered chelates being generally lower than those of the corresponding 5-membered chelates [192].

3.4.3.1 BP(OH)$_2$

In the case of BP(OH)$_2$, the chelate with a 5-membered ring, being the only possible structure for M^{II}⊂bipy, is only favored to some extent in solvents possessing no H-bond donating ability, e. g., acetonitrile. Only in such a solvent, the possibility for formation of the relatively unstable 7-membered “proton chelate” (case B in *Scheme 7*, p. 34) with an O-H-O-bridge exists. If it is formed or not, could not really be clarified in this work. All attempts to grow crystals of this complex species were unsuccessful and the observation of a characteristical signal at δ ~ 18 (O-H-O-bridge) [179] in the ^{1}H-NMR measurements was not possible due to the limited solubility of Zn^{II} salts in acetonitrile. Thus, the fact that the stability of hydrogen bond bridges (“proton chelates”) is largely enhanced for 6-membered rings compared to 5- or 7-membered rings seems to be the main driving force here [184a, 185a]. The strong 7-membered “proton chelate” reported by *Cargill Thompson* et al. seems to be the weaker structure in the present complexes [179]. Mainly the increase in mesomeric stabilization and resonance in the 6-membered ring (higher degree of aromaticity) renders the hydrogen bond stable in 6-membered rings and accounts for this structural preference. The stablizing mesomeric effect in the N, O-chelate can be rationalized as a “tautomeric electron pair shift” leading to enhanced electron delocalization. Stabilization of 6-membered metal ion chelates by 6-membered “proton chelates” has been observed before, e. g., in *peri*-dinaphtholazo reagents [193]. Furthermore, for 6-membered chelates in azomethine derivatives, only minor differences between the “proton chelate” and the metal ion chelate have been observed, i. e., mainly the lone electron pair of the nitrogen atom takes part in coordination and the aromatic ring π electrons are not much required for binding of the metal ion [192]. Here, again, 6-membered “proton chelates” are more stable than 5-membered ones [184a, b]. Moreover, all the observations for enhanced stability in 6-membered chelates listed above have been made for systems in aqueous solutions. In the case of the Ru^{II}bipy$_2$-BP(OH)$_2$-complex in acetonitrile described by *Cargill Thompson* et al., the limited possibilities in a Ru^{II}bipy$_2$ prearranged coordination sphere seem to favor deprotonation and cis chelation of BP(OH)$_2$ as the third ligand. Unfortunately, the low solubility of Zn^{II} in acetonitrile prevented the estimation of both fluorescence quantum yield and lifetime of the 1:1 complex. These values along with the spectral data of this complex should have made a verification of the ligands conformation possible. Compared to planarity in the type of chelate *Cargill Thompson* et al. reported, a twisted but N,N-chelated conformation of BP(OH)$_2$ would result in blue-shifted spectra and a change in rate constant as has been observed for the complexes of 3,3‘-dimethyl-2,2‘-bipyridyl [194].

3.4.3.2 BPOH

The results obtained for BPOH support the findings for BP(OH)$_2$. Even this ligand, where N,N-chelation should be more easily achievable due to reduced steric hindrance (lack of one *o*-hydroxyl group), favors N,O-chelation in aqueous solutions and for the primarily formed ML$_2$-complexes in ethanol. The formation of an additional “proton chelate” is not possible but (a) solvent molecule(s) can saturate the second pyridyl nitrogen by hydrogen bonding. The only slightly lower logK^{app} of Zn^{II}⊂BPOH compared to Zn^{II}⊂BP(OH)$_2$ in water suggests that the stabilization due to intramolecular hydrogen bonding is very limited in water in the latter.

3.4.3.3 Excited-State Deactivation, Summarized

For the fluorescent complexes, a comparison of k_f and k_{nr} of M^{II}⊂BP(OH)$_2$ with those of the free ligand reveals that the stability of the planar ligand is increased in the complex, resulting in comparable rate constants for fluorescence deactivation (cf. *Tables 2* and *7*, pp. 22, 35) but reduced rate constants of non-radiative deactivation. k_{nr} of the complexes is even smaller than that of the free ligand in apolar solvents like cyclohexane. The strong similarity of the mono-enolate complex M^{II}⊂BPOH and of M^{II}⊂BP(OH)$_2$ do not favor any major contribution of the second PT site in the latter. This is consistent with the observations made for the solvent-solute complexes in Ch. 3.2.4. Moreover, the similarity of the photophysical properties of M^{II}⊂BPOH and M^{II}⊂BP(OH)$_2$ in water (and partly in ethanol) and the completely different behavior of most M^{II}⊂oPP suggests that the second pyridyl nitrogen atom (not the whole PT site) may be important for stabilization in both the ground and the excited state in water. Parallel to BP(OH)$_2$, upon charge transfer in the excited state, the charge density on both nitrogen atoms is increased in BPOH.

Correspondingly, the observed drastic decrease in fluorescence intensity in the complexes with paramagnetic ions is due to the formation of a stable, non-fluorescent complex. As already mentioned above, for Cu^{II}, Ni^{II}, and Co^{II}, no decay

component with a fluorescence lifetime > 10 ps has been found, thus indicating that the observed decrease in $BP(OH)_2$ fluorescence intensity is caused by static quenching. In the case of these ions, the main quenching mechanism is assumed to be acceleration of intersystem crossing transitions due to their paramagnetic nature.

Complexation of Hg^{II} results in the same static quenching effect, only this time the heavy atom effect accounts for the higher intersystem crossing rate.

3.5 Analytical Applications

In the following subsection of this chapter, the analytical application of $BP(OH)_2$ as a fluorescent probe for the d^{10} metal ions Zn^{II} and Cd^{II} is described [36b]. The main emphasis is put on the comparison of steady-state and time-resolved fluorometry. Especially for this system with strongly overlapping absorption and emission bands, the advantages of time-resolved emission spectroscopy (TRES) are demonstrated. TRES in this case does not only mean recording a single decay at a given excitation and emission wavelength but the two-dimensional measurement of a set of decays at several emission wavelengths. With this technique and simultaneous analysis of all the decays registered for a certain sample employing a global analysis algorithm, the quality of the result of the chemical analysis is further enhanced.

3.5.1 Experimental Details

For the measurements reported here, a buffer system was employed (see Ch. 2.3). The spectral band position of the steady-state spectra of $Zn^{II}\subset BP(OH)_2$ and $Cd^{II}\subset BP(OH)_2$ remained the same whereas the fluorescence decay times were determined to 0.55 ns, 7.26 ns, and 6.22 ns for $BP(OH)_2$, its Zn^{II} and Cd^{II} complex.

In order to have comparable total experiment times for the time-resolved and steady-state analytical measurements the CPC were generally lower than those given in Ch. 2.6. But as the results of the time-resolved measurements are always based on global analysis combining data of 5 decays (with ≤ 4000 CPC per decay) or 20 decays (with ≤ 1000 CPC per decay), a sufficient level of statistical confidence is reached. For all the steady-state analytical measurements, the data acquisition time was limited to intervalls up to 15 minutes per spectrum and for the time- resolved analytical experiments, data were acquired up to 3 minutes per decay. In order to resolve the overlapping emission bands of $BP(OH)_2$ and its complexes, emission wavelength-dependent decay curves were recorded from 420 to 500 nm in steps of 20 nm (measurement time of 15 min required) and from 410 to 600 nm in steps of 10 nm (measurement time of 1 h required).

Steady-state emission spectra were analyzed employing a linear singular value decomposition algorithm and fluorescence decay data were analyzed globally (Ch. 2.8). The data record analyzed consisted of 500 and 1024/2048 data points for the single steady-state spectrum and single decay (BESSY/ps-LIF), respectively.

Prior to analyical measurements, a twenty-point calibration curve for each ion and each experimental technique was recorded and yielded correlation coefficients of $r \geq 0.998$ in all cases. Then the samples containing unknown amounts of both metal ions were measured according to the following procedure:

(i) steady-state emission spectrum

(ii) fluorescence decays at 5 different emission wavelengths (≤ 4000 CPC; 15 min measurement time)

(iii) fluorescence decays at 20 different emission wavelengths (≤ 1000 CPC; 1 h measurement time)

(iv) steady-state emission spectrum.

The second steady-state emission spectrum was recorded in order to exclude experimental errors due to photodecomposition of the sample.

For the analysis of a steady-state emission spectrum of a certain mixture of Cd^{II} and Zn^{II}, the spectrum was fitted with the spectra of the three single components (singular value decomposition) and a measurement error of 1 % was assumed.

3.5.2 Results

The results of six experiments are shown in *Table 9* and two graphical examples for steady-state fits are given in *Fig. 23*. In the upper part of *Fig. 23* the measured curve (full line), the fit (dotted line) and the contributions of the single components to the fit (dashed line) of sample #3 containing 3.59 mg l^{-1}

Table 9
Results of the determination of Zn^{II} and Cd^{II} in aqueous solutions with $BP(OH)_2$ and steady-state (SSF) or time-resolved (TRF) fluorometry.

Sample	*c* /Cd^{II}				*c* /Zn^{II}			
	mg l^{-1}				mg l^{-1}			
	given	found SSF	found TRF [a]	found TRF [b]	given	found SSF	found TRF [a]	found TRF [b]
#1	1.45	2.56	1.40	1.42	0.26	0.13	0.25	0.25
#2	0.94	2.84	0.92	0.93	0.52	0.31	0.53	0.52
#3	3.59	4.67	3.65	3.54	0.06	0.01	0.02	0.04
#4	0.75	0.50	0.74	0.75	0	0.02	0.006	0.001
#5	0.20	1.18	0.10	0.23	0.23	0.16	0.24	0.23
#6	3.59	6.05	3.50	3.60	0.71	0.33	0.74	0.70

[a] 5 decays from 420 to 500 nm in steps of 20 nm analyzed; [b] 20 decays from 410 to 600 nm in steps of 10 nm analyzed

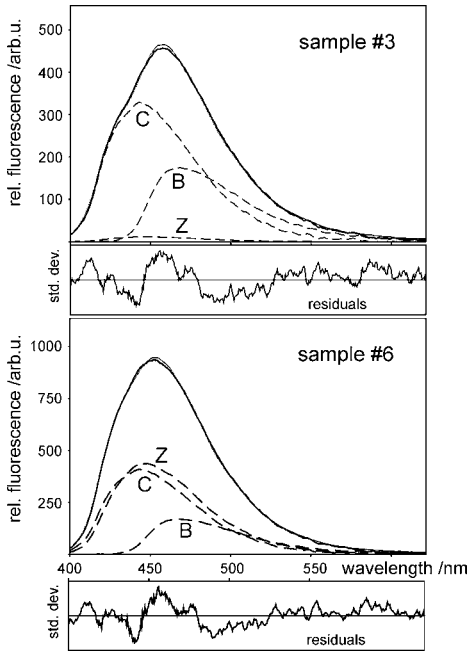

Fig. 23
*Fitting results obtained by analyzing the steady-state emission spectra of the samples #3 and #6 (—, measured spectra; ·····, fits; - -, single components attributed to uncomplexed $BP(OH)_2$ (**B**), its Cd^{II} (**C**), and Zn^{II} (**Z**) complexes).*

Cd^{II} and 60 µg l^{-1} Zn^{II} (60-fold excess of Cd^{II} over Zn^{II}) are presented. A comparison of the plot and the data for sample #3 listed in *Table 9* shows that the high excess of Cd^{II} over Zn^{II} is overrated in the fit although the fit describes the measured spectrum well. The contributions of the components associated with the emission of free $BP(OH)_2$, the Zn^{II}, and the Cd^{II} complex are labeled B, Z, and C, respectively.

The same effect is still observed for a 5-fold excess of Cd^{II} over Zn^{II} in sample #6 (lower part of *Fig. 23*). Both examples illustrate the poor correlation between a goodness of the fit and the accuracy of the analytical result for the steady-state technique.

In the case of the time-resolved measurements, single decays were fitted to three fixed exponentials performing ten trial fits with different initial estimates for the amplitudes in order to exclude optimizations into local minima. The wavelength-resolved recorded decay curves were then analyzed globally [183]. Taking into account the ground state heterogeneity, global analysis allows the construction of the decay associated spectra ($DAS_i(\lambda)$) of the single emitting species according to eqns (3) and (63) (pp. 33, 114) (i = 1 - component 1 (τ_f = 0.55 ns) - $BP(OH)_2$, i = 2 - component 2 (τ_f = 7.26 ns) - Zn^{II} complex, i = 3 - component 3 (τ_f = 6.22 ns) - Cd^{II} complex). Here, within the global analysis algorithm, the decay times of the species are fixed (i. e., values obtained for the single components in pure solutions) and linked for the analysis of all the decays while the program varies the pre-exponential factors until changes in the error surface (χ^2 surface) are minimal, i. e., convergence is reached (cf. Ch. 2.8.2). The errors for all the measurements presented here were below global χ_R^2 = 1.5. The results of the determination of Zn^{II} and Cd^{II} with time-resolved fluorometry (decays collected at 5 emission wavelengths; 15 min measurement time) are included in *Table 9* and the resulting decay associated spectra of sample #5 are shown in *Fig. 24*.

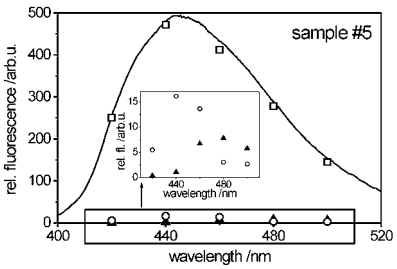

Fig. 24
Fitting results obtained by globally analyzing five decays of sample #5. The measured steady-state spectrum (—) and the spectral contributions ($DAS_i(\lambda)$) of the single species are displayed (▲- $DAS_1(\lambda)$, $BP(OH)_2$; □ - $DAS_2(\lambda)$, Zn^{II} complex; o - $DAS_3(\lambda)$, Cd^{II} complex). For a better representation of $DAS_1(\lambda)$ and $DAS_3(\lambda)$, the region of weak fluorescence is enlarged in the inset.

Comparison of the analytical results shown in *Table 9* clearly reveals the improvement in the determination of chemically very similar compounds, e. g., the complexes of Zn^{II} and Cd^{II} with $BP(OH)_2$, when employing time-resolved instead of steady-state fluorometry. Whereas the mean deviation from the true value for all the single concentrations equals 105 % in the case of steady-state fluorometry, the use of time-resolved techniques leads to considerably smaller deviations, 13 % (for the 5 emission wavelength measurements) and 6 % (for the 20 emission wavelength measurements), respectively. When recording a time- and wavelength-resolved emission matrix of a sample, even the detection of a relatively small amount of Zn^{II} besides a large amount of Cd^{II} (*Table 9*, sample #3) and the quantification of Cd^{II} in solutions containing both ions at nearly the same concentration (*Table 9* and *Fig. 24*, sample #5) is possible.

The apparent mismatch between the spectral contributions of the single complexes in *Fig. 24* ($DAS_2(\lambda) >> DAS_3(\lambda)$) and the concentrations of Zn^{II} and Cd^{II} in sample #5 given in *Table 9* ($c_{Zn} \cong c_{Cd}$) is due to the higher complex stability constant (cf. *Table 6*, p. 33) and fluorescence quantum yield (cf. *Table 5*, p. 31) of the Zn^{II} complex. Although the fitting of the steady-state data always yielded small errors in terms of describing the shape of a spectrum, the analytical validity of the fits is rather poor. The strongly overlapping emission bands of all the three compounds and especially the two complexes exclude the application of steady-state spectroscopy in this field of analytics. For the same temporal expense, i. e., a measurement time of 15 min, the employment of time-resolved emission spectroscopy at five different emission wavelengths leads to an improvement in the validity of the analytical result of nearly one order of magnitude. This is mainly based on the increased precision of the measured fluorescence lifetime ($<\tau_f>$ = 6.7 ns, temporal resolution ≤ 0.05 ns) compared with the spectral resolution of the steady-state emission measurements. Employing time-resolved fluorometry it was possible to detect Zn^{II} (Cd^{II}) accompanied by an up to 5-fold (2-fold) molar excess of Cd^{II} (Zn^{II}).

A further increase in sensitivity is achievable when decreasing the step size in the wavelength-resolved recording of fluorescence decays but aiming at an on-line and in situ application of this technique the prolongation of the time for both the analytical measurement and data evaluation is not favored. Depending on the photostability of the fluorescent probe employed and the complex formed as well as the

sensitivity and capability of the detection system, higher count rates due to higher excitation intensities could lead to an increase in CPC and thus an additional increase in sensitivity. This is especially possible with the high excitation rates used (ps-LIF in the 4 MHz mode or BESSY in the 4.8 MHz single-bunch mode) which exceed the observed count rates (≤ 10 kHz) by orders of magnitude. For this system, due to the differences in complex stability constants and fluorescence quantum yields, the determination of Cd^{II} in the presence of Zn^{II} will always be less sensitive then vice versa. An analytically more favorable discrimination between both ions spanning for example three or more orders of magnitude in a simultaneous determination is not possible due to the relatively small temporal difference between the fluorescence lifetimes of the two complexes ($\Delta \tau_f$ = 1 ns).

Concerning analytical applications, due to its molecular size and non-selective complexation properties, $BP(OH)_2$ is not a candidate for in situ analysis but can be used in fluorometric HPLC or IEC detection, especially when aiming at the determination of Zn^{II} and Cd^{II}.

3.6 $BP(OH)_2$ in Conclusion

The investigation of the outstanding ESIPT properties of $BP(OH)_2$ in aqueous solution of different pH revealed that, although the intramolecular hydrogen bonds are weakened, the main fluorescence arising from the diketo tautomer is conserved at acidic and medium pH. A second emitting species acconts for a blue-shifted emission band at medium pH and a similar behavior of BPOH suggests that emission occurs from a solute-solvent exciplex. At higher pH, deprotonation quenches the PT fluorescence markedly. The heavy and transition metal ion-binding properties of $BP(OH)_2$ are rather non-selective and chelation- induced fluorescence enhancement is only observed for the d^{10} metal ions Zn^{II} and Cd^{II}. Upon complexation to paramagnetic ions, static quenching occurs. The characterization of two different chelates of the Zn^{II} and Cd^{II} complexes of the *o*-hydroxy bipyridyls was possible employing solvent-dependent optical spectroscopic and NMR studies. The analytically valuable occurrence of two different fluorescence lifetimes for the spectrally very similar Zn^{II} and Cd^{II} complexes of $BP(OH)_2$ allowed to show the potential of TRES and global analysis in discriminating between spectrally non-resolvable emitting species.

4 Chalcone-Analogue Intrinsic Fluorescent Probes

4.1 Chalcones & Receptors - Introductory Words

Intrinsic fluorescent probes which absorb and emit in the visible and/or NIR region of the spectrum are of major interest in the field of fluoroionophore design for analytical chemistry (Ch. 1.1.2, 1.3). Interfering matrix effects such as, e. g., matrix autofluorescence can be circumvented, if the fluorescent sensor employed is excitable and its fluorescence detectable in the visible/NIR range of the spectrum (Ch. 1.1.2, 1.3). Due to the rapid development in laser technology, today, excitation at wavelengths ≥ 450 nm is possible even with low-cost pulsed laser diodes and fluorescent probes emitting with a sufficiently large Stokes shift permit the collection of fluorescence at wavelengths ≥ 600 nm. The class of dyes presented here was mainly chosen because D-A-chalcones substituted with an annelated heteroaromatic acceptor (e. g., benzothiazole) fulfil both requirements, i. e., absorption at ≥ 450 nm and a strongly Stokes-shifted emission in solvents of high polarity. Moreover, the tuning of the wavelengths of chalcones by exchanging donor and acceptor moieties is synthetically well feasible. Furthermore, in order to improve receptor-controlled cation selectivity, a new receptor specifically binding heavy and transition metal ions was integrated in a D-A-chalcone ICT probe.

Chalcones are known until the turn of the century [195]. They are precursors of many naturally occuring pigments, i. e., their (poly)hydroxylated derivatives or flavones, and their hydroxy-methoxy substituted derivatives play a major role in plant metabolism.[xxxix] Today, they are used as precursors in organic synthesis [197a], UV absorption filters in polymers [197b], NLO materials for SHG [197c], photorefractive polymers [197d], photosensitizers in color films [197e], antioxidants in both lipids [197f] and polymers [197g], sweeteners in food technology [197h, i], and in holographic recording technology [197j]. Due to their valuable biological activities, the main commercial field of application is medical therapy.[xl]

For purposes of clarification, the chemical structure, substitution pattern, and nomenclature of the chalcones is given in *Scheme 8* and *Table 10*.

4.1.1 Choice of the Receptors

The cation selectivity of modular fluorescent probes is to a large extent controlled by the specificity of the receptor. The great majority of the systems described so far was designed for s-block alkali and alkaline-earth metal ions which are classified as hard cations by *Pearson's* concept of "Hard and Soft Acids and Bases" (HSAB) [143]. Thus, these probes typically contain macrocycles with hard oxygen donor atoms such as polyoxa monoaza and benzo crown ethers (see Ch. 1.3.3 for references). Substitution of oxygen atoms of the crown ether for soft nitrogen atoms yields mixed polyoxa polyaza crown ethers or macrocyclic polyamines. Whereas the latter form complexes with heavy and transition metal ions [109, 110a-e, g, 113c, 119e, f], the former have been-reported to bind also alkali and alkaline-earth metal ions (polyoxa diaza crowns; see Ch. 1.3.3 for references). However, complexation of metal ions by these diaza crowns and macrocyclic polyamines is rather non-selective [199].

xxxix) Some examples of occurence are the root bark of liquorice *(Glycyrrhiza glabra)* [196a], the heartwood of the dwarf cherry *(Prunus cerasus L.)* [196b], the buds of the green alder *(Alnus viridis)* [196c], and the leaves and fruits of the bog-myrtle *(Myrica gale)* [196d].

xl) Aminochalcones are, e. g., bacteriostatic for *Staphylococcus aureus, Escherichia coli,* and *Bacillus subtilis* [198a], α-nitro-/bromo- and β-bromo-/hydroxy-chalcone are used as antibiotics [198b], 2',4,4'-trimethoxy-chalcone has choleretic activity [198c], and dialkylamino-alkoxy-chalcones are potential adrenergic blockers [196d].

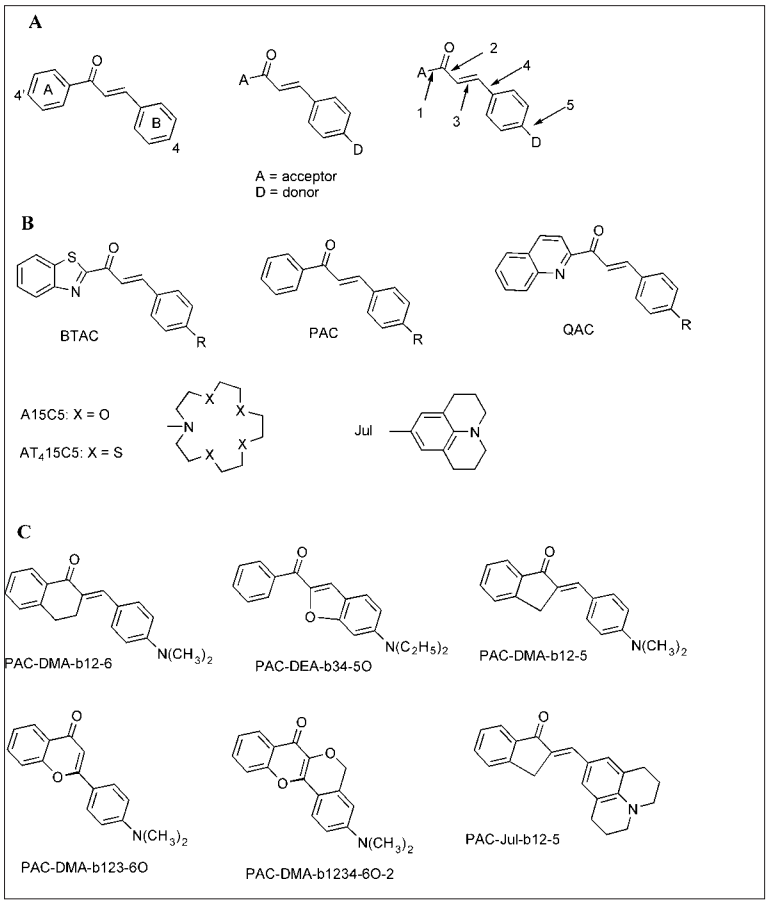

Scheme 8
A: *General structure of substituted chalcones [197a], structure used for labeling of chalcones in this work (for nomenclature, see Table 10), and numbering of the flexible bonds in the chromophore (see bridging scheme in Table 10).*
B: *Examples of acceptor and donor moieties.*
C: *Examples of chemical structures (explanation see caption to Table 10).*

An alternative way for selectively binding soft heavy and transition metal ions requires the use of macrocyclic or acyclic ligands where some or all of the hard oxygen atoms are replaced by soft sulfur and/or nitrogen atoms [110b, e-g]. Only recently, two examples of fluorescent probes which contain oxygen, nitrogen and/or sulfur donor atoms have been reported, $BT_2$18C6 [90d] and $T_4$14C4 [110e, f]. In order to extend this concept within the framework of this thesis, the four oxygen donor atoms of fluorescent probes carrying A15C5 were literally replaced by sulfur atoms to yield the corresponding $AT_4$15C5-substituted probes. The synthesis as well as the absorption and cation extraction properties of chromoionophores containing aza thia crowns as cation specific ligating sites were recently described [200]. However, such macrocycles have never been employed before as cation-specific receptors in ion-responsive fluorescent probes. Polythia crown ethers are especially suited for binding soft thiophilic heavy and transition metal ions, e. g., Ag^{I} and Hg^{II}, and the alkali and alkaline-earth metal ions are not expected to interfere in cation complexation [122a, 199a, 201]. Furthermore, the system aza thia crown/transition metal ion also shows considerably higher cation binding constants compared to the system aza oxa crown/alkali or alkaline-earth metal ion and should thus permit lower detection limits.

Table 10
Nomenclature and abbreviations used in this work. The compounds are labeled according to an AX-D system, where A denotes the acceptor moiety, D the corresponding donor in 4-position of ring B, and X is always "AC" which stands for "acceptor" and "chalcone". Thus, BTAC-A15C5 is the benzothiazolyl-acceptor substituted chalcone with a 4-tetraoxa-monoaza-15-crown-5 donor or, according to IUPAC nomenclature, 1-benzothiazol-2-yl-3-[4-(1,4,7,10-tetraoxa-13-aza-cyclopentadec-13-yl)-phenyl]-prop-2-en-1-one. Simple functional groups are abbreviated by their structural formulae, i. e, the 4-methoxy derivative of BTAC is BTAC-OCH_3. Bridged compounds carry the suffixes given in the right part of the table.

Label	Moiety	Label	Bridge
BT	benzothiazolyl	b12-5	bonds 1 & 2, bridged by a 5-membered ring (a -CH_2- group)
P	phenyl	b12-6	bonds 1 & 2, 6-ring (-CH_2-CH_2-)
Q	quinolinyl	b34-5O	bonds 3 & 4, 5-ring (-O-)
DMA	dimethylamino	b123-6O	bonds 1, 2 & 3, 6-ring (-O-)
A15C5	tetraoxa-monoaza-15-crown-5	b1234-6O-2	bonds 1, 2 & 3 (6-ring, -O-) and bonds 3 & 4 (6-ring, -O-CH_2-)
$AT_4$15C5	tetrathia-monoaza-15-crown-5		
Jul	julolidyl	**Label**	**Middle Section of, e.g.,** BT**AC**-H
H	hydrogen	AC	acceptor substituted chalcone

4.2 Photophysics - Literature Review

The photophysical properties of chalcones have been studied by numerous researchers[xli] involving mostly asymmetrical D-A-chalcones but additionally symmetrical D-A-D-chalcones [205-214]. Whereas in the former case, the acceptor is usually exemplified by a 4'-substituted PAC derivative, in the latter case the carbonyl group is the acceptor part and the two 4-donor substituted B-rings serve as bis-donor, i. e., these molecules are of the 1,5-diphenyl-1,4-pentadien-3-one type [207a, 209c, 212a, b]. Until today, only very few heteroaromatic moieties have been introduced to the acceptor part of the chalcones [207a].

According to their photophysical behavior, substituted chalcones can be divided into two groups, those with a (substituted) amine donor in the 4-position of ring B and those without. Only the (substituted) amino group possesses a donating ability strong enough to induce CT absorption bands in the visible region of the spectrum. Moreover, only such D-A-chalcones are known to emit fluorescence of reasonable intensity. All the other PAC derivatives, regardless of the acceptor strength of the 4'-substituent, are only weakly fluorescent at best. PAC-OH [214d] and PAC-OCH_3 [207b, 209e] are non-fluorescent as well as 4'-O_2N-PAC-H [209e]. The same accounts for derivatives with a reversed A-D-substitution pattern such as 4'-DMA-PAC-Cl [209e] and 4'-DMA-PAC-NO_2 [209e] as well as for 4-acceptor substituted PAC-NO_2 [209e] and PAC-Cl [207b, 209e]. Plain PAC-H is non-fluorescent as well [207b, 209e, 214d]. Accordingly, even in the relatively polar solvent CH_2Cl_2[xlii] their energetically lowest-lying absorption bands still lie in the UV region of the spectrum, ranging from 32 600 cm^{-1} for PAC-H to 24 400 cm^{-1} for 4'-DMA-PAC-NO_2 [209e]. On the other hand, unsubstituted PAC-DMA shows a $S_0 \rightarrow S_1$ absorption band at 24 200 cm^{-1} and the corresponding band of 4'-O_2N-PAC-DMA is centered at 22 300 cm^{-1} [209e].

Both the absorption and fluorescence of the PAC-DMA derivatives show the usual ICT characteristics connected with a charge transfer from the amine donor to the arylcarbonyl acceptor fragment. The fluorescence quantum yield of PAC-DMA amounts to 0.013 in ethanol[xliii] and until today, only PAC-DMA has been used as a fluorescent probe for sensing the micro environment in micelles [213a], cyclodextrins [213b], and in flow cytofluorometry [215].

Thus, besides studying potential ion sensing properties, the investigation of a series of differently substituted D-A-chalcones promised to give more insight into fluorescence enhancement and/or quenching processes observed for this type of fluorescent ICT dyes. *Table 11* covers the range of D-A-chalcones investigated in this work.

4.3 Photophysics – Own Results

The absorption and emission spectra of the BTAC and PAC derivatives in selected solvents are shown in Fig. *25* to *29* (pp. 45-46). *Tables 12* to *14*, pp. 46-47, combine the spectroscopic data on the D-A-chalcones investigated here and in *Table 15*, p. 48, some photophysical properties of the model systems taken from the literature are given.

It is apparent that introduction of a donor to the 4-position leads to a strong shift of the main absorption band to lower energies (*Tables 12* to *14*, pp. 46-47). The charge transfer character of the energetically lowest-lying absorption band is further exemplified by a comparison of the steady-state spectra of BTAC-H, BTAC-DMA, and PAC-DMA in three solvents of different polarity in *Fig. 27*. However, during the studies of these chalcones, the photophysical behavior proved to be rather complex, especially as a function of solvent polarity and when monitoring the deactivation of the excited singlet state(s) by time-resolved fluorometry (see below). Thus, for a better insight, two bridged PAC-DMA

xli) All the research groups being involved with hydroxylated derivatives, i. e., the large group of flavones and flavylium compounds are not enumerated here. Due to a hydroxyl group in the 2-position of ring B, cyclization reactions are possible yielding flavylium analogues and for the 2'-hydroxy derivatives, strong internal hydrogen bond formation occurs (and, to a lesser extent, cyclization) [202]. Thus, the photophysical properties and behavior observed for these chalcone derivatives are very different to those of the 4,4'-D-A-chalcones studied here. Readers interested in the chalcone-flavylium interconversion process are referred to the works of Matsushima et al. and *Pina* et al. [203, 204].

xlii) The solvent-dependent photophysical data on these types of chalcones are considerably sparse, the most comprehensive work being that of *Gustav* et al. [209e]. For all the chalcones, the solvent of highest polarity used by these authors was CH_2Cl_2.

xliii) Studying the literature on fluorescence properties of D-A-chalcones, the high degree of scattering of both, the emission band position and fluorescence quantum yield is apparent. For PAC-DMA in ethanol, ϕ_f of 0.02 [209e] and 0.15 [207b] have been published, in contrast to 0.013 found by us. Often, the fluorescence standards employed remain obscure or are doubtful.

Table 11
D-A-chalcones investigated in this work and selected model systems studied by other researchers

4'-Acceptor	Bridge	4-Donor	4'-Acceptor	Bridge	4-Donor	Ref.
BT	-	H	P	b12-5	DMA	[210], [212f]
	-	OCH_3		b123-6O	DMA	[212f]
	-	DMA		b1234-6O-2	DMA	[212f]
	-	A15C5		b12-5	Jul	[210]
	-	$AT_4$15C5				
	-	Jul				
Q	-	DMA				
P	-	H				
	-	DMA				
	b12-6	DMA				
	b34-5O	DMA				
	-	A15C5				

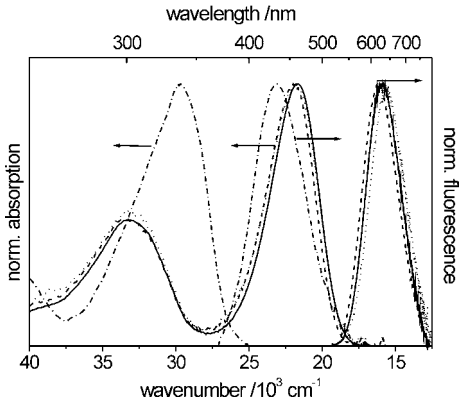

Fig. 25
Normalized steady-state absorption and emission spectra of BTAC-AT$_4$15C5 (- -), BTAC-A15C5 (—), BTAC-DMA (·····), and BTAC-H (- · - ·) in acetonitrile.

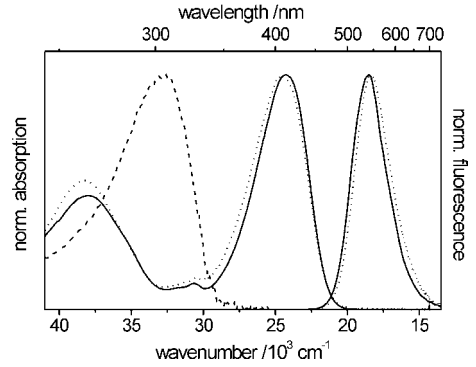

Fig. 26
Normalized steady-state absorption and emission spectra of PAC-A15C5 (—), PAC-DMA (·····), and PAC-H (- -) in acetonitrile (PAC-H is non-fluorescent).

derivatives have been investigated as well. The comparison of the photophysical behavior of the PAC derivatives with selectively bridged single or double bonds has been further extended by taking into account spectroscopic properties (steady-state) published on other model systems by *Wang* [210] and *Wang* and *Wu* [212f] (*Table 15*, p. 48). PAC-DMA-b12-6 and PAC-DMA-b34-5O have only recently been synthesized by Dr. *Bricks* and studies concerning their dynamic fluorescence behavior have not yet been carried out. Despite the amount of data accumulated during the experimental part of this thesis, an elaborate explanation of the processes being operative in these compounds is still not possible yet and further work is clearly needed. Moreover, describing and discussing the mechanistical studies in great detail here would go beyond the scope of this thesis and only a concise description of the main findings will be reported here.

4.3.1 Steady-State Spectra

4.3.1.1 Effect of *N,N*-Alkylamino Substitution

The uncomplexed fluorescent probes BTAC-AT$_4$15C5, BTAC-A15C5, PAC-A15C5 and the corresponding dimethylamino compounds BTAC-DMA and PAC-DMA display rather similar spectral properties, i. e., broad absorption bands and a strongly Stokes-shifted emission band in polar solvents (*Fig. 25* and *26*). Only in apolar hexane, the spectra show some vibronic structure (*Fig. 27* and *29*). Substitution of oxygen for sulfur obviously does not largely alter the electronic character of the substituent and thus does not lead to any considerable shifts in the spectra (*Fig. 25* and *26*). A similar, negligible effect has been observed by Ishikawa et al. for the spectral shifts in absorption in the case of 4-dinitrophenylhydrazones of Ph-A15C5 and Ph–AT$_4$15C5 [216].

As shown in *Table 12* and as can be deduced from a comparison of *Fig. 27* and *29*, the intramolecular charge transfer (ICT) character (transition from the nitrogen donor of ring B to the benzothiazol-carbonyl acceptor moiety) of the absorption and emission bands of these molecules follows from the solvent-dependent spectral shifts in absorption and emission [217]. Both bands undergo a red shift with increasing solvent polarity, the spectral shift of the fluorescence band being more pronounced. This increase in Stokes shift with increasing solvent polarity indicates that the fluorescent excited singlet state(s) is (are) more strongly stabilized in polar solvents than the ground state thus pointing to a larger dipole moment of the excited state [218a].

4.3.1.2 Solvatochromic Behavior

For the *N,N*-alkylamino substituted BTAC and PAC derivatives the fluorescence excitation spectra in non H-acidic, polar solvents resemble closely the absorption spectra. In alcohols and apolar solvents such as hexane or 3-methylpentane, deviations occur. In the case of alcohols, this behavior is also reflected in the emission spectra, i. e., measuring the emission spectrum at constantly increasing excitation wavelengths

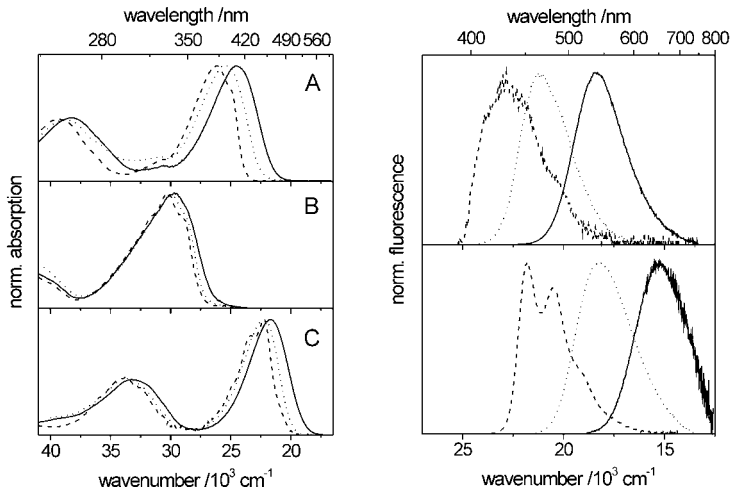

Fig. 27
*Left part: Normalized steady-state absorption spectra of PAC-DMA (**A**), BTAC-H (**B**), and BTAC-DMA (**C**) in hexane (- -), diethylether (·····) and acetonitrile (—).*
Right part: Normalized steady-state emission spectra of PAC-DMA (upper part) and BTAC-DMA (lower part) in the same solvents. For the emission band positions of BTAC-H, see Fig. 25 and Table 14, p. 48.

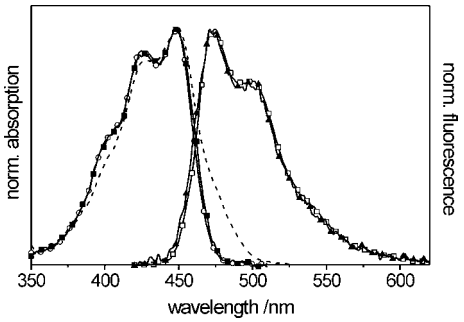

Fig. 28
Absorption spectrum (- -), fluorescence excitation spectra (λ_{obs} = 470 nm - o; 560 nm - ■), and fluorescence emission spectra (λ_{exc} = 370 nm - ▲; 470 nm - □) of BTAC-A15C5 in hexane.

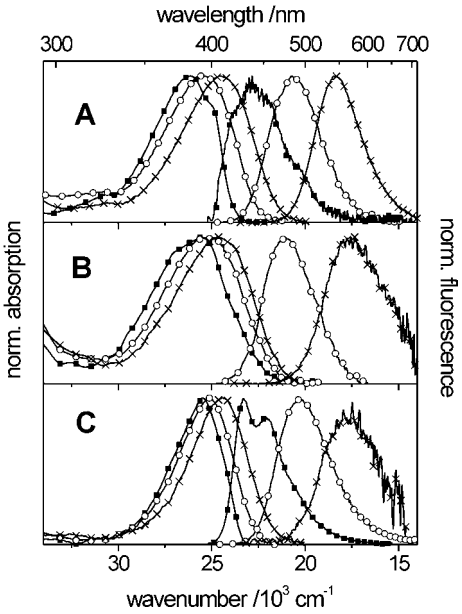

Fig. 29
*Normalized absorption and emission spectra of PAC-DMA (**A**), PAC-DMA-b12-6 (**B**, emission spectrum in hexane not included), and PAC-DMA-b34-5O (**C**) in hexane (■), diethylether (o) and acetonitrile (x).*

Table 12
Selected spectroscopic data of BTAC derivatives with substituted 4-amino donor groups

	Solvent	$\tilde{\nu}$ (abs)	ε [$\tilde{\nu}$ (abs)]	$\tilde{\nu}$(em)	$\Delta\tilde{\nu}$(abs-em)	ϕ_f
		10^3 cm^{-1}	10^3 M^{-1} cm^{-1}	10^3 cm^{-1}	cm^{-1}	
BTAC-DMA	MeOH	21.46	29.3	15.24	6220	0.0007
	EtOH	21.55	30.7	15.80	5750	0.004
	MeCN	21.83	34.1	15.22	6610	0.002
	CH_2Cl_2	21.60	35.0	16.21	5390	0.10
	Et_2O	22.78	35.9	18.25	4530	0.52
	Diox	22.17	34.2	18.07	4100	0.61
	Hex	23.87, 22.78	35.7	21.79, 20.53	2080	0.04
BTAC-A15C5	EG	20.83	n.d. [a]	15.24	5590	0.004
	MeOH	21.46	33.3	15.43	6030	0.002
	EtOH	21.50	34.7	15.75	5750	0.007
	i-PrOH	21.37	32.5	16.05	5320	0.018
	MeCN	21.69	38.6	15.48	6210	0.007
	CH_2Cl_2	21.55	36.3	16.37	5180	0.11
	Et_2O	22.32	39.1	18.12	4200	0.61
	Toluene	21.74	38.1	18.55	3190	0.49
	Hex	22.17, 23.36	n.d. [a]	21.19, 20.00	2170	0.11
BTAC-$AT_4$15C5	EtOH	21.88	n.d. [a]	15.70	6180	0.01
	MeCN	21.98	37.9	15.70	6280	0.02
	CH_2Cl_2	22.12	n.d. [a]	16.83	5290	0.42
	Et_2O	22.83	n.d. [a]	18.52	4310	0.51
BTAC-Jul	EtOH	20.04	33.3	14.97	5070	0.005
	MeCN	20.16	39.4	14.07	6090	0.001
	CH_2Cl_2	19.88	37.3	15.04	4840	0.014
	Et_2O	21.15	37.9	16.70	4450	0.25
	Hex	21.23	n.d. [a]	20.37, 19.03	1510	0.43

[a] n.d. - not determined due to low solubility

Table 13
Selected spectroscopic data of PAC derivatives

	Solvent	$\tilde{\nu}$ (abs)	ε [$\tilde{\nu}$ (abs)]	$\tilde{\nu}$(em)	$\Delta\tilde{\nu}$(abs-em)	ϕ_f
		10^3 cm^{-1}	10^3 M^{-1} cm^{-1}	10^3 cm^{-1}	cm^{-1}	
PAC-DMA	EtOH	23.92	26.6	18.12	5800	0.011
	MeCN	24.43	29.0	18.38	6050	0.15
	CH_2Cl_2	24.27	n.d.	19.26	5010	0.24
	THF	24.70	25.0	20.04	4660	0.09
	Et_2O	25.34	33.5	20.60	4740	0.020
	Hex	26.00	33.7	22.85	3150	0.0001
PAC-DMA-b12-6	EtOH	23.98	n.d.	18.26	5720	0.006
	MeCN	24.66	n.d.	17.43	7230	0.027
	CH_2Cl_2	24.41	n.d.	18.86	5550	0.013
	THF	24.98	n.d.	19.89	5090	0.007
	Et_2O	25.60	n.d.	20.95	4650	0.002
	Hex	26.29	n.d.	22.53	3760	0.0001
PAC-DMA-b34-5O	EtOH	23.98	n.d.	18.09	5890	0.003
	MeCN	24.47	n.d.	17.57	6900	0.0014
	CH_2Cl_2	24.13	n.d.	18.50	5630	0.003
	THF	24.69	n.d.	19.19	5500	0.041
	Et_2O	25.13	n.d.	20.27	4860	0.051
	Hex	25.49	n.d.	22.76	2730	0.046
PAC-A15C5	MeCN	24.27	31.6	18.50	5770	0.25
PAC-H	MeCN	32.57	21.4	-	-	-

Table14
Selected spectroscopic data of other D-A- and 4'-A-chalcones.

	Solvent	$\tilde{\nu}$ (abs)	ε [$\tilde{\nu}$ (abs)]	$\tilde{\nu}$(em)	$\Delta\tilde{\nu}$(abs-em)	ϕ_f
		10^3 cm^{-1}	10^3 M^{-1} cm^{-1}	10^3 cm^{-1}	cm^{-1}	
BTAC-H	EtOH	29.85	26.4	23.22	(6970) [a]	0.0002
	MeCN	29.67	26.3	23.29	(6580) [a]	0.0001
	CH_2Cl_2	29.59	24.5	23.31	(6760) [a]	0.0002
	Et_2O	29.98	30.7	23.90	(6080) [a]	0.0002
	Hex	30.30	33.0	23.92	(6380) [a]	0.0002
BTAC-OCH_3	EtOH	27.03	25.3	18.87	8160	0.0001
	MeCN	27.10	25.9	19.61	7490	0.0002
	CH_2Cl_2	26.74	26.2	20.53	6210	0.0001
	Hex	27.86	31.7	25.45	2410	0.0002
QAC-DMA	EtOH	22.83	26.8	16.18	6650	0.005
	MeCN	23.09	28.5	15.62	7470	0.008
	CH_2Cl_2	22.83	28.9	17.04	5790	0.18
	Et_2O	24.10	27.1	18.94	5160	0.29
	Hex	25.13	29.8	22.57 (21.37)	3160	0.002

[a] main emitting species is different from main absorbing species (explanation concerning fluorescence excitation spectra see text)

Table 15
Selected spectroscopic data of PAC derivatives studied by other researchers.

	Solvent	$\tilde{\nu}$ (abs)	$\tilde{\nu}$ (em)	$\Delta\tilde{\nu}$(abs-em)	ϕ_f	ref
		10^3 cm^{-1}	10^3 cm^{-1}	cm^{-1}		
PAC-DMA	MeCN	24.10	18.66	5440	0.13	[212f]
	Et_2O	n.r	(21.3)	n.r.	0.054	[212f]
	CH	26.11	n.r.	n.r.	0.0007	[212d]
PAC-DMA-b12-5	MeCN	24.0	18.7	5300	0.045	[212f]
	Et_2O	24.4, 25.1	21.8	2900	0.007	[210]
	Hex	26.2, 25.1	24.1	1500	0.0001	[210]
PAC-Jul-b12-5	MeCN	24.5	18.2	6300	0.005	[210]
	Et_2O	n.r	20.5	-	0.024	[210]
	Hex	26.0	22.8	3200	0.011	[210]
PAC-DMA-b123-6O	MeCN	26.8	21.1	5700	1	[212f]
	Et_2O	n.r.	23.9	-	0.87 [a]	[212f]
	Hex	28.6	n.r.	-	0.007	[212f]
PAC-DMA-b1234-6O-2	MeCN	25.2	20.4	4800	0.86	[212f]
	Et_2O	n.r.	22.4	-	1	[212f]
	Hex	n.r.	n.r.	-	0.50	[212f]

[a] in ref. [212e], the same authors report a ϕ_f of 0.32

shifts the emission band to lower frequencies (BTAC-A15C5: excitation at 420 nm and 470 nm yields bands centered at 599 nm and 603 nm, respectively).

The behavior in apolar solvents is different. Only slight changes were detectable for fluorescence excitation and emission spectra recorded with different emission or excitation wavelengths. Singular value decomposition analysis of a set of either spectra yielded only one single component of high significance.[xliv] However, the absorption spectrum has a pronounced shoulder on the low energy side which is not found in the excitation spectra *(Fig. 28)*.

4.3.1.3 Solvatochromic Plots and Dipole Moments

A measure for the strength of the ICT process is obtained by analysis of the spectroscopic data as a function of solvent polarity employing the Lippert-Mataga formalism as described in Appendix B in more detail [218]. Plots of the Stokes shift vs. solvent polarity functions $f(\varepsilon_r) - f(n)$ (cf. eqn (71)) are shown in *Fig. 30* for the different 4-DMA-substituted chalcones. Similar good correlations are observed for the other amino-substituted compounds as well, yielding straight lines with a single slope. The dipole moments obtained are included in *Table 16*, p. 49.

The deviations between the values calculated for (μ_{es} - μ_{gs}) by the different solvatochromic methods are almost the same for all the compounds studied, i. e., the permanent electric dipole moment of the solvent free molecule in the fluorescent state (eqn (75)) equals ca. 65 % of the dipole moment in solution (eqn (73)). A comparable influence of the solute's

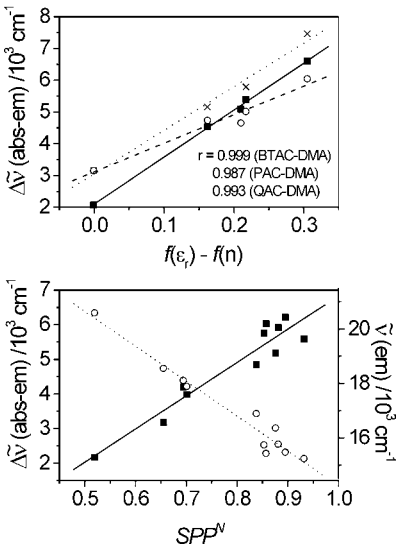

Fig. 30
Upper part: Solvatochromic plots (and fits) according to eqn (70a) for BTAC-DMA (■—), PAC-DMA (o, - -), and QAC-DMA (x, ·····). For better clearness, only the data obtained in acetonitrile, dichloromethane, THF, diethylether, and hexane are included; the correlation coefficients are indicated. Lower part: Plots of Stokes shift (■) and emission band maximum (o) vs. empirical solvent polarity parameter SPP^N for BTAC-A15C5 in the solvents listed in Table 12, p. 46, acetone, THF, and 1,4-dioxane. The fits (—, Stokes shift; - -, emission band maximum) include all data points.

polarizability has been found for related D-A-stilbenes, respectively [219]. Since eqn (70a) assumes that emitting and initially excited Franck-Condon state are of the same nature, a comparison with the dipole moments calculated by eqn (73) gives a first hint for the involvement of possible other excited states, i. e., for example a highly polar state. Although

xliv) A second component of minor significance was observed but could not be verified any further with the simple method employed.

Table 16
Dipole moments obtained from the slope of solvatochromic plots according to eqns (70a), (73), (75), and (70b). In the case of eqn (70b), the value of $\beta = 2\alpha / a_O^3$ *was taken to 1 for isotropic polarizability.*

	Eqn	a_O [a]	μ_{gs} [b]	μ_{es}	$(\mu_{es} - \mu_{gs})$
		Å	D	D	D
BTAC-DMA	(70a)	6.4	2.9	22.6	19.7
	(73)	6.4	2.9	24.5	21.6
	(75)	6.4	2.9	16.5	13.6
	(70b)	6.4	2.9	14.5	11.6
BTAC-A15C5	(70a)	7.3	4.6	27.2	22.6
BTAC-Jul	(70a)	6.5	4.3	24.5	20.2
QAC-DMA	(70a)	6.2	2.6	20.6	18.0
PAC-DMA	(70a)	5.7	3.9	16.7	12.8
	(73)	5.7	3.9	16.7	12.8
	(70b)	5.7	3.9	11.5	7.6
[c]	(70b)	-	-	-	5.9 [c]
PAC-DMA-b12-6	(70a)	5.7	3.8	17.7	13.9
	(73)	5.7	3.8	17.6	13.8
	(70b)	5.7	3.8	12.2	8.4
PAC-DMA-b34-5O	(70a)	5.7	4.7	20.5	15.8
	(73)	5.7	4.7	20.5	15.8
	(70b)	5.7	4.7	14.1	9.4
PAC-DMA-b12-5 [c]	(70b)	-	-	-	5.6 [c]
[d]	[d,e]	8 [d]	6 [d]	16 [d,e]	10 [d,e]
PAC-DMA-b123-6O [c]	(70b)	-	-	-	8.2 [c]
PAC-DMA-b1234-6O-2 [c]	(70b)	-	-	-	5.8 [c]

[a] according to ref. [224];
[b] for optimized ground state geometry by AM1;
[c] taken from ref [212f];
[d] taken from ref. [210];
[e] determined by Wang according to a method proposed by Varma and Groenen on the basis of correlating the absorption maxima [210, 225]

a definite conclusion concerning the real values of the dipole moments cannot be drawn since their determination is critically dependent on the choice of the right Onsager cavity radius[xlv] and the ground state dipole moment used, the data agree quite well suggesting formation of an already polar localized or delocalized excited state.

The correlations found in the solvent polarity plots with the newly developed empirical solvent polarity *SPP*^{N} scale [220, 221] (see Appendix B) demonstrate the linear dependence of both the Stokes shift and fluorescence band maximum on solvent polarity as well *(Fig. 30)*. The *SPP*^{N} scale deals with both dipolar nature and polarizability of solvents and describes the observed changes sufficiently well. Applying the $E_T(N)$ or $E_T(30)$ scale leads to worse fits, especially for hydrogen-bonding solvents (cf. Ch. 5.2.2 and Appendix B).

xlv) Especially in the case of the crown ether receptors, bulky but flexible subunits, considerations based on X-ray data or optimized geometries obtained by quantum chemical calculations can yield largely differing values. Whereas BTAC-AT$_4$15C5 crystallizes in (more or less) flat layers, for BTAC-A15C5, an L-type crystal structure is found where the flexible crown ether ring is tilted for about 80° forming the bottom line of the "L" [85b]. The difficulties in determining the real value of the excited-state dipole moment is further exemplified by a comparison of the values given for PAC-DMA and PAC-DMA-b12-5 (*Table 16*, p. 51).

4.3.1.4 Fluorescence Quantum Yields

For the compounds studied, the fluorescence quantum yield largely depends on both the nature of the 4-substituent of ring B and the solvent polarity. In polar aprotic solvents such as acetonitrile, the fluorescence quantum yields of BTAC-AT$_4$15C5, BTAC-A15C5, BTAC-DMA, and BTAC-Jul are rather low and decrease on the order of BTAC-AT$_4$15C5 > BTAC-A15C5 > BTAC-DMA > BTAC-Jul (*Table 12*, p. 46). In contrast, PAC-DMA and PAC-A15C5 emit moderate fluorescence with quantum yields of ca. 0.2 in acetonitrile, respectively *(Table 13)*. Here, again, the crowned compound is higher fluorescent than the DMA compound and the julolidyl substituted compound shows the weakest fluorescence (ϕ_f = 0.029 of PAC-Jul[xlvi]) [214c]. Similar effects have been observed for other ICT fluorescent probes, their dimethylamino and julolidyl derivatives [76, 77a, 222]. The reduced mobility of the donor group, i. e., its bulkiness, and the different electron donating properties of these tertiary amine substituents account for these results. For these three dyes,

xlvi) The actual value might be even smaller since Itoh et al. determined a value of ϕ_f = 0.34 for PAC-DMA in acetonitrile [214c], distinctly higher than the values obtained by *Wang* and *Wu* (0.13) [212f] and in this work (0.15, *Table 12*, p. 46).

the bulkiness of the substituents increases on the order of DMA << Jul < A15C5 < $AT_4$15C5 [124a] and the donor strength of the amino nitrogen decreases on the order of Jul > DMA ~ A15C5 > $AT_4$15C5 as follows from the bathochromic shifts of the corresponding spectra (*Table 12*, p. 46).

The lines in *Fig. 31*, although they are only guides to the eye, indicate an opposite behavior concerning the solvent polarity dependence of the fluorescence quantum yields. Coming from the apolar region, the quantum yield increases and after crossing a certain polarity, decreases *(Fig. 31)*. In alcohols, all the compounds show low fluorescence quantum yields (*Tables 12* to *14*, pp. 46-47). A maximum in a ϕ_f vs. $E_T(N)$ plot is seen for most compounds and appears for the D-A-chalcone with the strongest ICT character (BTAC-Jul) in hexane (no rising edge) and for those with weaker ICT character (PAC-DMA, PAC-DMA-b12-5, and PAC-DMA-b12-6) in acetonitrile. The largely bridged compounds show no pronounced dependence and fluorescence quenching only in hexane. Besides the latter, only PAC-DMA-b34-5O and PAC-Jul-b12-5 show an exceptional behavior with a maximum on the apolar and medium polar side in diethylether, $E_T(N)$ = 0.117, and THF, $E_T(N)$ = 0.207, respectively. Due to the linear correlation of the Stokes shift with solvent polarity, plots of ϕ_f vs. Stokes shift yield curves with equal trends, i. e., a maximum at a certain Stokes shift indicative of the corresponding solvent.

A reduction in solvent polarity strongly enhances the fluorescence quantum yield of all the BTAC derivatives but leads to a loss in fluorescence intensity for PAC-DMA. Moreover, from plots of the fluorescence quantum yield of all the *N,N*-alkylamino substituted D-A-chalcones as a function of solvent polarity, some interesting tendencies can be derived *(Fig. 31)*. The trends in the two regions can be ascribed to the so-called "negative solvatokinetic behavior", i. e., increasing fluorescence quantum yield with increasing solvent polarity, and the "positive solvatokinetic behavior" where the decrease in emission results from excited-state population of a highly polar charge transfer transient species (see Appendix B for more details) [225]. Both possibilities will be discussed in Ch. 4.4.2.

Before describing the results of the time-resolved fluorescence measurements, the most prominent features of the steady-state spectroscopic behavior of the D-A-chalcones are summarized. The strong ICT character is well-documented for all the (substituted) anilino derivatives by the large difference in dipole moment of ground and excited state *(Table 16)* and the resulting photophysical consequences manifested in shape and position of the spectra. Whereas in polar aprotic solvents a single species seems to be present in solution, the possible involvement of different ground state species can be derived from the differences between absorption and fluorescence excitation spectra in alcohols and less polar solvents. However, the most striking features are the different solvatokinetic behaviors observed within the PAC series and for the 4-DMA substituted compounds with different acceptors, i. e., PAC-DMA, BTAC-DMA, and QAC-DMA.

4.3.2 Fluorescence Lifetimes

Owing to the weak fluorescence of most chalcones, the time-resolved emission data published in the literature until today are very sparse. Generally, the fluorescence lifetimes are referred to as being "within the temporal resolution of the instrument", i. e., (much) shorter than 1 ns [210]. Only recently, *Wang* and *Wu* published fluorescence decay times of PAC-DMA, PAC-DMA-b12-5, and PAC-DMA-b123-6O in various solvents at room temperature and reported single exponential decay kinetics for all three compounds in all the solvents studied, i. e., for instance, 0.70 ns for PAC-DMA in acetonitrile [212e]. However, the time-resolved emission studies carried out for some of the D-A-chalcones by us give a more complicated picture but will not be described in detail here [226]. Moreover, the partly unexpected findings in the emission behavior of some of the recently synthesized bridged PAC derivatives (especially PAC-DMA-b34-5O, showing a completely different behavior than PAC-DMA despite bridging of the most probable quenching channel, i. e., the central double bond) require some additional time-resolved studies in order to test the validity of the model developed within the framework of the present results (see Ch. 4.4.2). Thus, only the main features are summarized here.

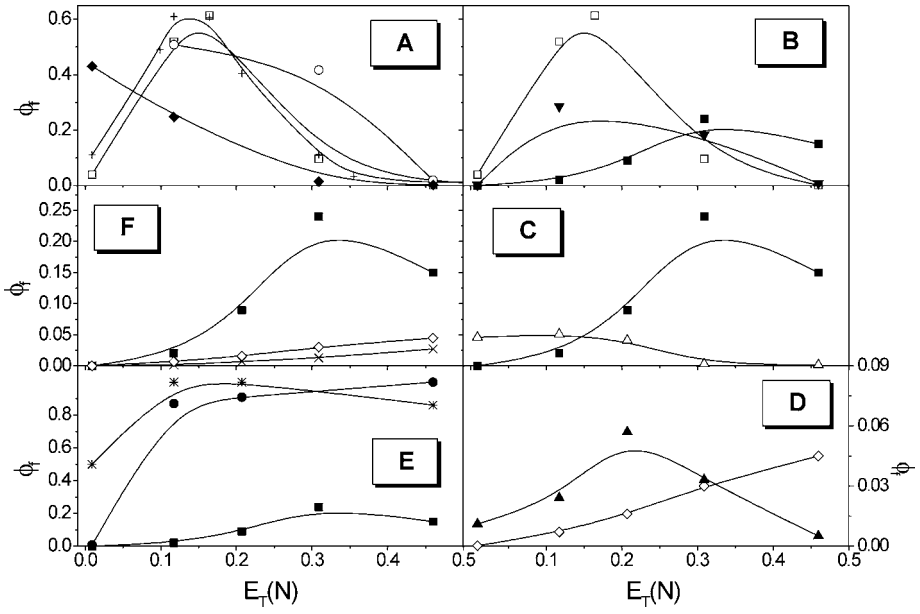

Fig. 31
Plots of ϕ_f vs. $E_T(N)$ for the D-A-chalcones investigated.
***A:** BTAC-DMA (□), BTAC-A15C5 (+), BTAC-$AT_4$15C5 (o), BTAC-Jul (◆);*
***B:** BTAC-DMA (□), QAC-DMA (▼), PAC-DMA (■); **C:** PAC-DMA (■), PAC-DMA-b34-5O (Δ);*
***D:** PAC-DMA-b12-5 (◊), PAC-Jul-b12-5 (▲); **E:** PAC-DMA (■), PAC-DMA-b123-6O (•), PAC-DMA-b1234-6O-2 (*);*
***F:** PAC-DMA (■), PAC-DMA-b12-5 (◊), PAC-DMA-b12-6 (x). PAC-DMA is included in most of the plots for a better comparison. The solid lines are only guides to the eye and data in protic solvents are omitted. Data for PAC-DMA-b123-6O, PAC-DMA-b1234-6O-2, PAC-DMA-b12-5, and PAC-Jul-b12-5 taken from refs [210] and [212f].*

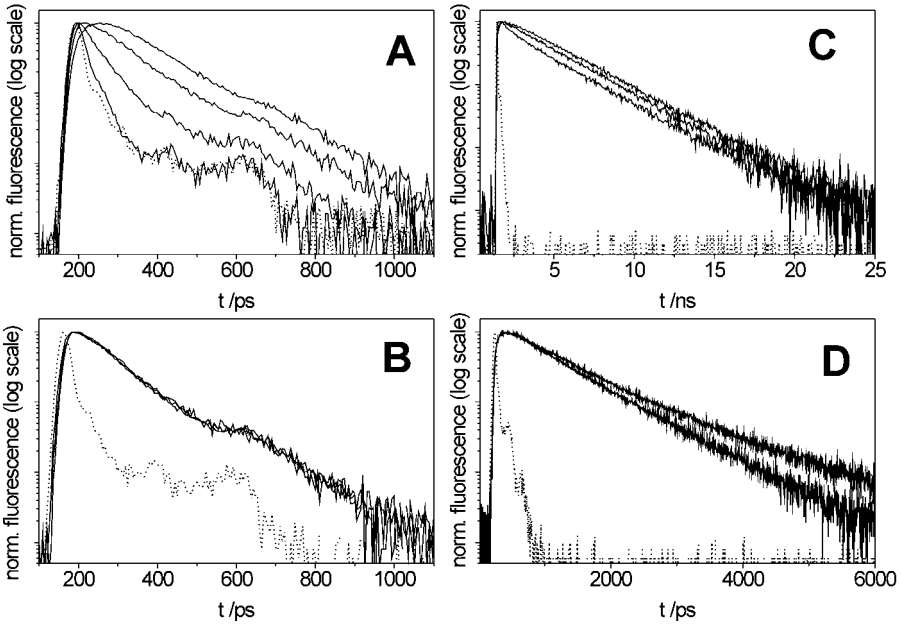

Fig. 32
Fluorescence decay curves of BTAC-A15C5 in different solvents at 298 K.
***A:** i-propanol, excitation at 456 nm, emission at 710, 605, 560, and 500 nm (from top to bottom);*
***B:** acetonitrile, excitation at 456 nm, emission at 720, 640, and 560 nm;*
***C:** diethylether, excitation at 428 nm, emission at 640, 560, and 500 nm (from top to bottom);*
***D:** hexane, excitation at 428 nm, emission at 560 and 480 nm (from top to bottom); dotted curve - IRF.*

For all the compounds investigated here, monoexponential decay kinetics were observed only in highly polar, aprotic solvents, i. e., acetonitrile or acetone *(Fig. 32B)*. In all the other cases, the fluorescence decay profiles could only be fitted to at least two exponentials *(Fig. 32A, C, D)*. In medium and apolar solvents, a main decay component is observed and the minor species have either a positive amplitude over the whole emission spectrum (e. g., hexane) or a negative amplitude at the low energy side of the emission spectrum (e. g., diethylether). In some cases, extrapolation of the $DAS_i(\lambda)$ ratio does not converge to a value of -1 at the red edge, pointing to a more complex behavior than a simple two-state reaction scheme with a single excited species as precursor (cf. Ch. 6.4). Moreover, for BTAC-DMA and BTAC-A15C5, two decaying species with distinctly different decay times and only slightly changing (with observation wavelength) positive relative amplitudes are found in hexane, respectively.[xlvii] For a comprehensive overview, the decay times of the main emitting species are included in *Table 17*. The behavior in alcohols will be discussed separately in Ch. 4.3.2.1.

Furthermore, excitation wavelength-dependent time-resolved studies suggest, that either different ground state species are excited or that CT formation rates depend on the frequency of incident light [227].

Generally, the data given in *Table 17* agree with the solvent dependence of the fluorescence quantum yields, i. e, e. g., an increase in lifetime with decreasing solvent polarity for amino substituted BTAC derivatives. Although a determination of the rate constants for radiative and non-radiative deactivation (k_f and k_{nr}) is not possible without separating the

Table 17
Main decay species of BTAC and PAC derivatives in aprotic solvents at 298 K.

	Solvent	ϕ_f ps		Solvent	τ_f ps
BTAC-DMA	MeCN	25	BTAC-$AT_4$15C5	MeCN	170
	Et_2O	950, 3090		CH_2Cl_2	2240
	Hex	180, 690 [a]		Et_2O	1060, 2790
BTAC-A15C5	MeCN	74	QAC-DMA	MeCN	100
	Acetone	270		CH_2Cl_2	1550
	CH_2Cl_2	850		Et_2O	750, 2080
	THF	2230		Hex	11
	Et_2O	780, 3090	PAC-DMA	MeCN	870
	Toluene	1000, 3060		CH_2Cl_2	1120
	Hex	600, 1120 [a]		Et_2O	150, 550 [b]

[a] $a_{rel}1\ (\lambda)$ of +0.4 to +0.6;
[b] 290 K

xlvii) A similar decay behavior has been found for BTAC-H in polar solvents, only slightly solvent polarity-dependent, yielding a fast decay component of 30-200 ps and a slow decay component of ca. 1.6 ns (a_{rel} ~ 0.6), both with positive amplitudes throughout the whole emission range measured.

Table 18
Main decay species of BTAC and PAC derivatives in alcohols at 298 K. Decay times obtained by simultaneously fitting N decays to i linked lifetimes (the program varies only the preexponential factors). Although global analysis is not the adequate model to describe the relaxation behavior, this fitting routine was used in order to obatin comparable quantities, i. e., apparent lifetimes (in all the cases global $\chi_R^2 < 1.3$).

EtOH	τ_f^{app}	N		Solvent	τ_f^{app}	N
	ps				ps	
BTAC-DMA	10, 22	19	BTAC-A15C5	MeOH	7, 14	17
QAC-DMA	23, 31	12		EtOH	19, 35	24
PAC-DMA	9, 33, 41	20		i-PrOH	13, 46, 91	27
BTAC-$AT_4$15C5	11, 22, 64	14		EG	11, 45	17

rate constants by evaluation and analysis of the excited-state reaction model, the parallel trends suggest a more drastic change (decrease) in k_{nr} compared to k_f upon going to apolar solvents for the emitting species of BTAC-DMA and related compounds and the vice versa behavior for PAC-DMA.

4.3.2.1 Decay Behavior in Alcohols

Comparing the fluorescence decay traces recorded for BTAC-A15C5 in *i*-propanol and acetonitrile (shown in *Fig. 32A* and *B*) and comparing the fluorescence lifetimes in these solvents in *Tables 17* and *18*, the question of the origin of the nonexponential decay behavior in alcohols arises. Besides an excited-state reaction involving population of (several) transient species, relaxation of the solvent molecules of the inner and outer solvation sphere ((strong or weak) dipolar interaction with the solute or in the bulk) has to be considered. Moreover, regarding the deactivation of an excited ICT molecule with a large excited-state dipole moment and a carbonyl group in the acceptor part in a polar solvent capable of hydrogen bond formation, i. e., alcohols, solute-solvent interactions can occur in the form of exciplex formation (with the precursor complexes possibly being already present in the ground state). After a brief introduction of the characteristic solvent relaxation times and an exemplary analysis of the spectral response function of two chalcones, the contributions of these different effects are discussed.

When a strong dipole, e. g., the excited dye molecule interacts with the inner solvation sphere, those solvent molecules lose their (dipolar and long-range) orientational correlations and relax in an individual manner. On the other hand, solvent molecules in the bulk (outer solvation shell) maintain their properties and relax in a collective way. Whereas the latter process is comparably fast and can be quantified by the solvent longitudinal relaxation time τ_l, the former process can be much slower depending on the degree or strength of direct interaction of solvent molecule and solute and is referred to as the microscopic reorientation time or (average) solvation time (τ_M, $<\tau>$) [228b, c, 229-231]. For weakly interacting solvents such as acetonitrile or acetone, τ_l and $<\tau>$ are rather similar and in the order of a few hundred fs [228b], but for alcohols at room temperature both times are in the order of a few ps [228b, c, 229, 230]. Especially for alcohols which are “aggregated solvents” capable of strong hydrogen bond formation, the temporal relaxation phenomena largely depend on the location of the single solvent molecule with respect to the solute.

Usually, for fluorescent molecules with $\tau_f >> \tau_l$, measurement of the time-dependent fluorescence (Stokes) shift or determination of the spectral response function of the dye molecules in a certain solvent yields the characteristic solvation times within relatively good agreement [228b, 230b].[xlviii]

On the other hand, when an excited-state reaction with two or three species is operative, the rate constants are predominantly dependent on the molecular structure of the dye itself and often lead to largely different fluorescence decay times (and thus largely different time-dependent spectral shifts) for related molecules [233].

In order to compare the nonexponential decay behavior and the time dependence of the emission band, the spectral evolution of TRES was followed for BTAC-A15C5 in *i*-propanol and BTAC-$AT_4$15C5 in ethanol.

$$C_\nu(t) = \frac{\nu(t) - \nu(\infty)}{\nu(0) - \nu(\infty)} \qquad (5)$$

The time-dependent solvation process can be monitored by the spectral response function $C_\nu(t)$ according to eqn (5), where $\nu(t)$, $\nu(0)$, and $\nu(\infty)$ are the characteristic frequencies at the corresponding observation time (Appendix B). As an example, TRES and a plot of $C_\nu(t)$ of BTAC-$AT_4$15C5 in ethanol are given in *Fig. 33* and the corresponding plot for BTAC-A15C5 in *i*-propanol is included in *Fig. 34*.

Comparing the fitting results of the correlation function $C_\nu(t)$ (τ_1, τ_2 indicated in *Fig. 33*, $<\tau>$ = 19 ps) the data obtained in ethanol are comparable to the times found by *Horng* et al. in the same solvent at 295 K for the spectral response function of a coumarin dye, i. e., slow components τ_i of 5.03 and 29.6 ps and $<\tau>$ = 16 ps [228b]. Room temperature data on i-propanol are sparse but a comparison of low-temperature data on n- and i-propanol and extrapolation of the data for the latter suggests, that the τ_i of 13 and 54 ps ($<\tau>$ = 35 ps) found here *(Fig. 34)* are of the same order of magnitude [228b, 230b]. However, as in the case of the fluorescence lifetimes given in *Table 18*, the values obtained here for $<\tau>$ are apparent values and do not reflect the real solvent relaxation times.

Combining these observations the following can be derived. For the D-A-chalcones, the fluorescence decay times in

xlviii) Note that for a series of highly fluorescent coumarin dyes, *Gustavsson* et al. observed spectral response functions with largely varying τ_i of 1.05 to 3.36 ps (short) and τ_i of 11.17 to 20.13 ps (long time in methanol) for the different dyes employed [232].

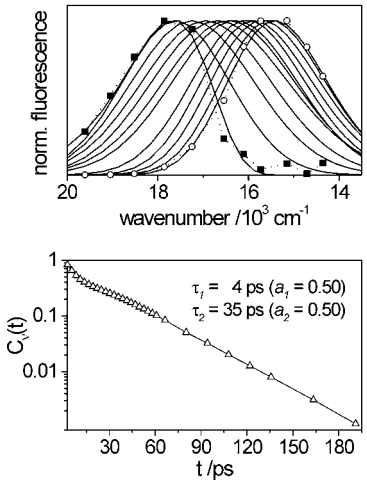

Fig. 33
Upper part: Spectral reconstruction of the wavelength-resolved fluorescence decay of BTAC-AT$_4$15C5 in ethanol at 298 K. Solid lines correspond to lognormal fits and dotted lines to the actual data points converted to the frequency scale (■ at t = 0, o at t = ∞). Lower part: Fit of the spectral response function C$_v$(t) to two exponentials indicated in the plot.

alcohols are of similar magnitude as the relaxation times of the protic solvents (e. g., τ_l = 16 ps, τ_M = 47 ps for ethanol [231] and data in *Table 18*) [228b, 229, 230b]. Moreover, hydrogen bond formation at an acceptor carbonyl group (found for coumarins which are very similar in this respect to the D-A-chalcones) was found to be operative on the same time scale as well (e. g., *ca.* 15 ps in methanol) [232]. On the other hand, the differences in fluorescence lifetime data in alcohols (e. g., τ_f *(BTAC-AT$_4$15C5)* ~ 3 x τ_f (BTAC-DMA) for the slow components; *Table 18*) are evident but less pronounced compared to those in a "fast" solvent such as acetonitrile where only the excited state relaxation is monitored (here, solvent relaxation is > 100 times faster than fluorescence; τ_l *(MeCN)* = 0.2 ps [234]; τ_f (BTAC-AT$_4$15C5) ~ 7 x τ_f (BTAC-DMA); *Table 17*, p. 51). The monoexponential decay kinetics in acetonitrile suggest that in these polar solvents only a single emitting species is present in the excited state pointing to a straightforward excited-state reaction mechanism (e. g., fast population of a single highly polar transient species).

As a consequence, the prerequisites accounting for the large differencies in acetonitrile (see above a factor of 7 between the DMA and the AT$_4$15C5 derivative) are still present in alcohols but obscured by another effect. This presence of another effect besides solvent relaxation is obvious when taking a look at the fluorescence lifetimes of PAC-DMA in both solvents (870 ps in acetonitrile and a long-lived component of 41 ps in ethanol). Most favorably the crucial effect is hydrogen bond formation.

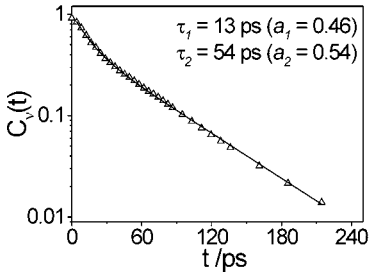

Fig. 34
Fit of the spectral response function C$_v$(t) of BTAC-A15C5 in i-propanol at 298 K to two exponentials indicated in the plot.

Thus, solvent relaxation, hydrogen bond formation, and deactivation of the emitting singlet state are on the same time scale for the D-A-chalcones and the effects cannot be monitored or analyzed separately. Accordingly, the fluorescence decay times given in *Table 18* are only apparent τ_f describing the superimposed processes best and global analysis of the wavelength-resolved fluorescence decay data according to an excited-state reaction mechanism involving discrete species is misleading in this case. A statement concerning a possible excited-state reaction mechanism (involving, e. g., twisted transient species) cannot be given. However, the dependences reported for the fluorescence excitation spectra in Ch. 4.3.1.2 suggest a more complex (ground and excited-state) reaction scheme than simple solvent relaxation.

4.3.3 Temperature-Dependent Behavior

The temperature-dependent emission behavior of BTAC-DMA, BTAC-A15C5, BTAC-AT$_4$15C5, BTAC-Jul, and PAC-DMA was investigated in ethanol and the DMA compounds were additionally studied in diethylether.

Steady-State Spectra in Ethanol. Upon cooling, the steady-state spectra of BTAC-DMA, BTAC-A15C5, and BTAC-AT$_4$15C5 show very similar tendencies. Above the glass point of ethanol (T_g^{EtOH} = 159 K), the Stokes shift is slightly decreased (both bands shift into opposite directions) and line-narrowing of the bands is observed. Selected spectroscopic data of the five compounds investigated are combined in *Table 19*.

The fluorescence quantum yield increases for all the derivatives studied upon reducing the temperature and only at T < 90 K, nearly constant values for ϕ_f of ca. 0.9 (BTAC-DMA, BTAC-A15C5, BTAC-AT$_4$15C5), 0.7 (BTAC-Jul), and 1.0 (PAC-DMA) are obtained *(Fig. 35)*.

Steady-State Spectra in Diethylether. In diethylether, with decreasing temperature, the fluorescence quantum yield of BTAC-DMA changes only to a minor extent. However, both the absorption and the emission spectrum are shifted to lower energies with the Stokes shift remaining nearly constant *(Fig. 36)*. When freezing the sample, a drastic hypsochromic shift in both absorption and emission is observed and the band positions remain nearly constant upon cooling down to 10 K. The tendency found for the fluorescence quantum

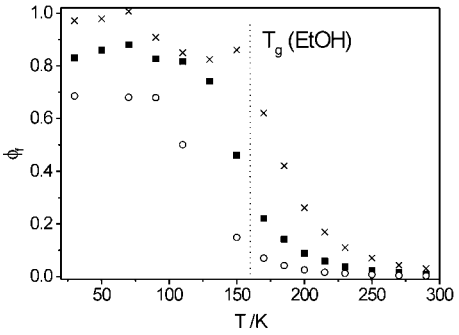

Fig. 35
Fluorescence quantum yields of BTAC-DMA (■), BTAC-Jul (○), and PAC-DMA (x) in ethanol as a function of temperature. The dotted line marks T_g^{EtOH}.

Table 19
Steady-state spectroscopic data of some D-A-chalcones in ethanol at various temperatures.

	T	$\tilde{\nu}$ (abs)	fwhm (abs)	$\tilde{\nu}$ (em)	fwhm (em)	ϕ_f
	K	10^3 cm^{-1}	10^3 cm^{-1}	10^3 cm^{-1}	10^3 cm^{-1}	
BTAC-DMA	290	21.54	4.46	15.84	3.85	0.01
	230	21.33	4.14	15.96	3.67	0.04
	185	21.22	3.75	16.21	3.41	0.14
	150	21.04	3.40	16.71	3.07	0.46
	30	20.16	2.75	18.83	2.31	0.87
BTAC-A15C5	290	21.41	4.41	15.73	3.99	0.02
	230	21.19	3.83	15.82	3.63	0.07
	185	21.05	3.50	16.36	3.49	0.24
	150	20.96	3.30	17.08	3.09	0.60
	30	20.24	2.37	19.01	2.29	0.89
BTAC-AT$_4$15C5	290	21.72	4.08	15.69	3.87	0.03
	230	21.34	3.758	15.92	3.70	0.09
	185	21.06	3.39	16.34	3.50	0.29
	150	20.80	3.07	17.10	3.06	0.68
	30	19.96	2.65	18.73	2.20	0.90
BTAC-Jul	290	19.72	4.10	14.99	3.66	0.002
	230	19.52	3.95	15.11	3.21	0.01
	185	19.44	3.75	15.32	2.86	0.04
	150	19.37	3.42	15.74	2.66	0.15
	30	18.80	2.79	17.42	2.34	0.71
PAC-DMA	290	23.85	4.42	18.15	3.45	0.03
	230	23.39	4.30	18.15	3.30	0.11
	185	23.11	4.16	18.18	3.19	0.42
	150	23.09	4.15	18.80	3.17	0.86
	30	22.78	3.62	20.41	2.83	0.97

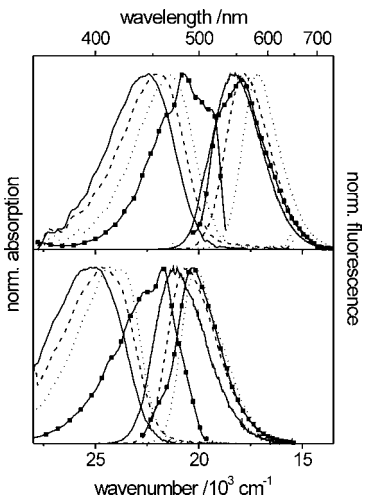

Fig. 36
Steady-state absorption and emission spectra of BTAC-DMA (top) and PAC-DMA (bottom) in diethylether at 290 K (—), 230 K (- -), 170 K (····). At 30 K (■), the fluorescence excitation and emission spectrum are displayed; T_g^{Et2O} = 156 K).

yields in diethylether glass is similar to that in ethanol glass, i. e., a further increase from ca. 150 to 90 K and a nearly constant value at $T < 90$ K.

The spectroscopic properties of PAC-DMA, weaker fluorescent in diethylether at room temperature, undergo very similar spectral changes upon reducing the temperature. In contrast, the changes in fluorescence quantum yield are much more pronounced and emission increases upon decreasing the temperature from ϕ_f = 0.02 (290 K) via 0.14 (250 K), 0.60 (210 K), 0.86 (130 K) to ca. 1.0 at 30 K. In the glass, PAC-DMA behaves similar to BTAC-DMA.

Dynamic Emission Behavior in Ethanol and Diethylether. Generally, the room temperature behavior is conserved above the glass point in both diethylether and ethanol and the tendencies reported for the fluorescence quantum yields are reflected by the fluorescence lifetimes, i. e., an increase in lifetime(s) upon cooling. Following once more the description of the fluorescence decays by fitting them to two or three exponentials (which is necessary to obtain acceptable results), decay times of 92, 416, and 730 ps are found for

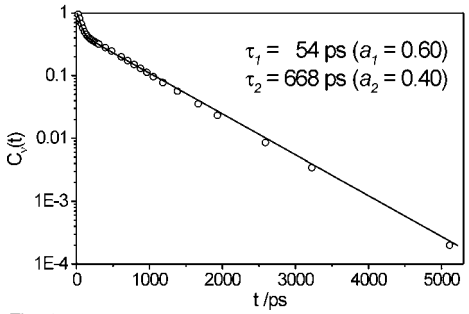

Fig. 37
Fit of the spectral response function $C_v(t)$ of BTAC-A15C5 in ethanol at 185 K to two exponentials indicated in the plot.

BTAC-A15C5 in ethanol at 185 K, respectively. At the same temperature, the fluorescence decays of the other derivatives can be described by 53, 265, and 516 ps (BTAC-DMA), 90, 490, and 800 ps (BTAC-AT$_4$15C5), 100 and 375 ps (BTAC-Jul), and 590 and 1070 ps (PAC-DMA), reflecting the behavior at 298 K. At 183 K, the relaxation time τ_l of ethanol amounts to 728 ps (τ_M = 3.7 ns) [231] and the times found in an analysis of the spectral response function of, e. g., BTAC-DMA at 185 K, are 54 and 668 ps, respectively *(Fig. 37)*. Thus, even in an alcohol solution at low temperature, solvent dynamics intermingle with fluorescence deactivation obscuring a straightforward analysis of a possible excited-state reaction mechanism involving molecular motions and different excited-states. Nevertheless, the dependence of the excited-state deactivation on molecular structure is not only obvious from the differences in fluorescence lifetimes (cf., e. g., BTAC-Jul and BTAC-AT$_4$15C5) but especially from the shape of the curve in the ϕ_f vs. *T* plot in *Fig. 35*. Whereas PAC-DMA reaches a ϕ_f of ~ 1 at *T* = 30 K, for BTAC-Jul still 30 % of the relaxation is radiationless. Whether this comparably large contribution of radiationless deactivation is only due to an enhanced rate constant of internal conversion could not be clarified here.

For a better illustration, at this point, the main spectroscopic features of the D-A-chalcones are summarized. The 4-*p*-*N,N*-anilino-substituted D-A-chalcones show a typical ICT behavior manifested in a large increase in dipole moment upon excitation and the corresponding effects on the spectroscopic properties, i. e, for instance, an increase in Stokes shift with solvent polarity. Most remarkable is the dependence of the fluorescence quantum yield on solvent polarity for the single derivatives, being strongly affected by changes in both donor and acceptor strength and bridging pattern. The behavior ranges from purely positive solvatokinetics (e. g., BTAC-Jul) to mainly negative solvatokinetics (e. g., PAC-DMA). Bridging of the central double bond does not necessarily lead to strong fluorescence enhancement and the fluorescence decay kinetics reveal a more complex behavior in medium and apolar solvents. Furthermore, for all the D-A-chalcones except BTAC-Jul, fluorescence quenching is observed in apolar hexane and in polar H-acidic solvents, the fluorescence is strongly quenched as well. Here, in alcohols, the fluorescence deactivation is largely controlled by solvent relaxation and hydrogen bond formation.

4.3.4 BTAC-H

Before discussing possible excited-state reaction or deactivation mechanisms, the spectroscopic behavior of the reference compound BTAC-H containing only the phenyl ring as considerably weak donor is described in the following paragraph.

The solvent-dependent shifts in absorption and emission are much less pronounced (*Fig. 25*, p. 45, *Tables 12* and *14*, p. 46, 47) and a similar behavior has been previously described for other chalcones carrying weak donors in position 4 of ring B [207b, 209e]. BTAC-H shows both a strongly blue-shifted absorption and emission band compared to the other BTAC derivatives and has the lowest fluorescence quantum yield of the chalcone series in all the solvents investigated. Additionally, its main absorption band centered at ca. 29 700 cm^{-1} has an asymmetrical shape in all the solvents employed and resembles a linear combination of a stronger absorption band at ca. 31 800 cm^{-1} and a weaker band at ca. 29 100 cm^{-1}, respectively. Both subbands show a similar, slight dependence on solvent polarity. Concerning the origin of the bands, the absorption band of 2-acetyl-benzothiazole (the acceptor composite) ($\tilde{\nu}$ (abs) = 34 010 cm^{-1}, ε [$\tilde{\nu}$ (abs)] = 11700 M^{-1} cm^{-1} in acetonitrile; $\tilde{\nu}$ (abs) = 34 250 cm^{-1}, ε [$\tilde{\nu}$ (abs)] = 12 100 M^{-1} cm^{-1} in diethylether) is found in a different frequency region and a transition localized on the 4-substituted cinnamoyl fragment of the chromophore should appear in the same wavelength region. Thus, in accordance with results obtained by *Szmant* and *Basso* who intensively studied series of PAC derivatives [206], no hints for such localized transitions were found. This is further supported by the mismatch of absorption and luminescence excitation spectrum, i. e., the excitation spectrum is shifted to lower frequencies (*ca.* 27 700 cm^{-1}; note that 2-acetyl-benzothiazole is non-fluorescent).

4.4 Photophysics - Mechanistic Considerations

When trying to construct an excited-state reaction mechanism for the D-A-chalcones one has to be aware of a complex equilibrium involving different stereoisomers already in the ground state.

As depicted in *Scheme 9*, s-cis ("c") and s-trans ("t") single bond isomerism (bond b2) is possible and in the case of the BTAC derivatives, a further *syn* and *anti* isomerism concerning the BT nitrogen and the CO oxygen atom can occur (to avoid "cis" and "trans" misunderstandings, the double bond isomers are labeled *E* and *Z* and the single bond isomers *c* and *t*, arriving at *cE*, *tE*, *cZ*, and *tZ* isomers).[xlix]

However, the discussion of stereoisomerism in the literature is inconsistent. Whereas most articles published on the photophysics of chalcones disregard the topic, the mechanisms are intensively discussed in connection with isomerization reactions in 2-hydroxy-chalcones yielding cyclic flavylium compounds [202-204]. Moreover, scanning the chemical structures given in many publications on chalcones, some authors prefer to use the *cE* conformation, others the *tE*

xlix) The occurence of trans-cis isomerization in the ground state was excluded by recording the emission spectrum as a function of laser excitation energy up to 10 mW (CW). Furthermore, HPLC analysis with UV/Vis diode array detection of an irradiated sample of BTAC-A15C5 showed only one peak, its absorption spectrum being identical to that of a reference sample kept in the dark. Chalcone cis isomers described in the literature so far show a strongly blue-shifted absorption spectrum [209a].

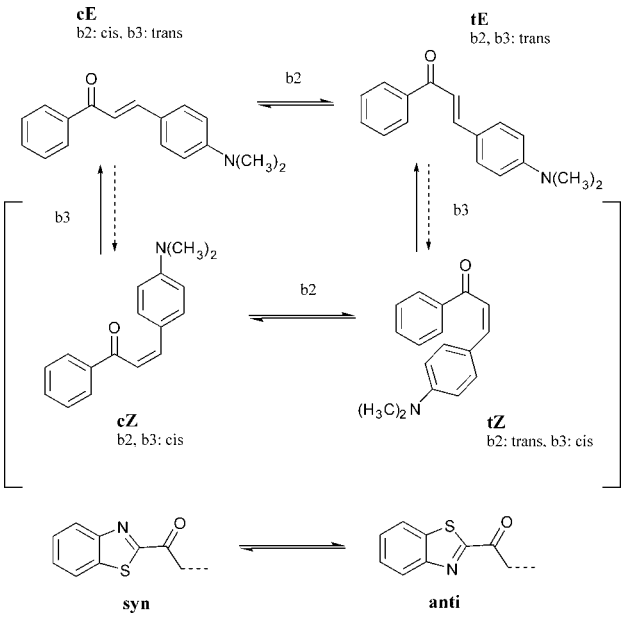

Scheme 9
Chemical structures of possible chalcone isomers. In the top row, the two stable s-isomers of the b3-double bond E isomer, in the middle row the sterically unfavored Z isomers are shown. The conformation of bonds b2 and b3 is indicated and the labels on the arrows denote the bonds which have to rotate for the respective transition. In the bottom row, the syn / anti isomerism of BTAC derivatives is shown.

conformation without going into detail on the real isomerism [208, 211, 214c]. On the other hand, from X-ray studies of numerous chalcones it is known that either *cE* or *tE* isomers are preferred in certain molecules in the crystalline state. PAC-H and *p*-Br-PAC were found to crystallize in *cE* [235], but NO_2-PAC-Br and certain PyrAC (Pyr = pyridine) derivatives show *tE* conformation in the solid state [236, 237a]. Moreover, for PylAC (Pyl = pyrrole) and SeAC (Se = selenophene) derivatives, syn and/or anti conformations (in *cE* or *tE*) were reported [237b, c]. In one of the few photophysical studies concerning stereoisomerism, *Nicodem* and *de Matos* proposed s-isomerism in the ground state to be responsible for wavelength-dependent photoproduct formation in PAC-H in apolar solvents [209a].

Concerning the compounds investigated here, X-ray studies of BTAC-A15C5 and BTAC-$AT_4$15C5 showed the molecules to crystallize in the *anti-cE* conformation [85b] and in recent ^{1}H-NMR investigations of PAC-DMA in $CDCl_3$, coupling of *o*-phenyl protons was only observed for H-α (CH adjacent to CO group), favoring a *cE* conformation as well.

4.4.1 Quantum Chemical Calculations

Ground state geometry optimizations for both *s*-isomers converge in the case of the b2-unbridged compounds (with the excpetion of PAC-DMA-b4-5) and yield no pronounced energy differences (ΔE (s-iso) = 6 kJ mol^{-1} at most) for any pair of *tE* and *cE* isomers *(Table 20)*.[l] The corresponding ground state dipole moments ($\Delta\mu$ (*s*-iso) = 2.6 D at most) and transition energies ($\Delta E_{S0\text{-}S1}$ (*s*-iso) ≤ 750 cm^{-1}) are of comparable magnitude as well. Geometry optimizations for the *tZ* and *cZ* conformers do not converge and these isomers are highly unfavored from this point of view. With fixed *Z*-geometries at b3, energy differences with respect to the most stable geometry of 35 kJ mol^{-1} (PAC-DMA-b12-6) at minimum are found for the *cZ* isomers (e. g., several 100 kJ mol^{-1} in the case of some BTAC derivatives) and of more than several 100 kJ mol^{-1} for the *tZ* isomers, rendering the latter very unstable.[li]

l) The same is observed for the *syn* and *anti* isomers.

li) The only relatively stable *cZ* isomer is found for PAC-DMA-b4-5 with ΔE *(s-iso)* = 10 kJ mol^{-1}.

Table 20
Calculated relative ground state energies and dipole moments of the s-isomers of D-A-chalcones (AM1/HyperChem). Transition energies obtained by 1SCF calculation (CI of 6, AM1/HyperChem).

	Most Stable Isomer	ΔE(s-iso) [a]	$\Delta\mu$(s-iso) [b]	$\Delta E_{S0\text{-}S1}$ (s-iso) [c]
		kJ mol^{-1}	D	cm^{-1}
PAC-DMA	cE	6.3	+0.7	320
PAC-DMA-b12-6	cE	-	-	-
PAC-DMA-b12-5	cE	-	-	-
PAC-Jul-b12-5	cE	-	-	-
PAC-DMA-b34-5O	cE	1.9	-0.6	80
PAC-DMA-b123-6O	tE	-	-	-
PAC-DMA-b1234-6O-2	tE	-	-	-
PAC-Jul [d]	cE	6.5	+0.8	170
PAC-DMA-b34-5 [d]	tE	2.6	-1.4	130
PAC-DMA-b4-5 [d, e]	cE	-	-	-
BTAC-DMA	cE	4.4	+2.6	340
BTAC-$AT_4$15C5	cE	6.1	+2.2	20
BTAC-Jul	cE	5.9	+1.3	750

[a] energy level difference of the second s-isomer ΔE *(s-iso) = E (tE) - E (cE)*;
[b] difference in ground state dipole moment $\Delta\mu$ *(s-iso) = μ (tE) - μ (cE)*;
values used for μ_{gs} in the solvatochromic analysis (*Table 16*, p. 49) are obtained for *cE*;
[c] difference in calculated excitation energies $\Delta E_{S0\text{-}S1}$ *(s-iso)* = $E_{S0\text{-}S1}$ *(tE)* - $E_{S0\text{-}S1}$ *(cE)*;
[d] molecules have only been modeled theoretically (see Appendix D for chemical structure);
[e] optimization for tE starting geometry converges into *cE*

In most cases, *cE* is the slightly more stable ground state isomer but for *tE* the higher ground state dipole moment is calculated. The trend is different for the b34-bridged compounds, i. e., for PAC-DMA-b34-5O, *cE* has a higher dipole moment and is the more stable isomer (for the only theoretically studied methylene bridged PAC-DMA-b34-5, *tE* is found to be more stable but cE has a distinctly higher dipole moment).

Transferred to the observations made in solution, the small differences in excitation energies given in *Table 20* suggest the occurrence of largely overlapping bands (at least in apolar solvents) whenever more than one isomer is present.

If restriction is opposed on the bonds by bridging, in most cases the torsion angles (and bond lengths) obtained for optimized ground state structures of *cE* and *tE* are very similar for all the PAC derivatives *(Table 21)*. Energy barriers for twisting of the aryl acceptor moiety are generally low (15 kJ mol^{-1} for PAC derivatives, 5 kJ mol^{-1} for BTAC derivatives), the smaller value in the case of the BTAC derivatives owing to the absence of aromatic *o*-protons. Rotation around b3 is connected with the usual high activation barrier for C-C double bonds and for rotation around b2, two possibilities have to be considered. If only rotation around this bond is considered, an activation barrier of > 40 kJ mol^{-1} is found but if simultaneous rotation around b1 and b2 is inspected, energy barriers of ca. 15 kJ mol^{-1} are obtained and the volume required for rotation (the cone of rotation) is considerably reduced. A more detailed theoretical study of PAC-DMA is found in ref. [139].

In conclusion, the quantum chemical calculations reveal that energetically and electronically similar rotamers (*s*-isomers) can be expected to complicate the photophysical behavior of the chalcones, especially in less polar solvents,[lii] but on the other hand, energetically unfavored ground state Z isomers seem to play no role here.

4.4.2 Mechanistic Considerations

In an attempt to interpret the photophysical behavior of the D-A-chalcones, the role of possible deactivation routes of the initially excited singlet state are discussed. Here, rotations around certain bonds, the nature of populated states, and isomerization reactions need to be considered. Due to the differently bridged compounds and data available the discussion will mainly be based on the behavior of the PAC derivatives and their steady-state spectroscopic properties.

4.4.2.1 Excited-State Transient Species

The main deactivation routes of the excited state can be divided into weakly and (highly) polar transient species.

Weakly Polar Transient Species and Interacting States. In these D-A-chalcones, non-radiative loss of excitation energy is possible via two such mechanisms, i. e., vibronic coupling of energetically close-lying $n\pi^*$ states (proximity effect) [239] or population of a weakly polar, biradicaloid P* state. The latter requires twisting around the C-C double bond [240, 241]. Consecutively, the triplet state can be populated via P*.

The plots of ϕ_f vs. $E_T(N)$ in *Fig. 31*, p. 50 reveal that the fluorescence of all the compounds investigated here (except BTAC-Jul) is considerably lower in hexane than in diethylether. The fluorescence quantum yields given for BTAC-DMA and BTAC-A15C5 in *Table 12*, p. 46, further underline this trend, i. e., upon going from 1,4-dioxane or toluene to hexane, the fluorescence intensity drops markedly (e. g., for BTAC-A15C5: ϕ_f = 0.61 in 1,4-dioxane and ϕ_f = 0.11 in hexane). Only for BTAC-Jul, an increase in fluorescence quantum yield is observed in this polarity region. Thus, the fact that the maximum of a ϕ_f vs. $E_T(N)$ plot (or, equally, a ϕ_f vs. $\tilde{\nu}$ (abs-em) plot) is shifted to less polar solvents with increasing charge transfer character points directly to the involvement of a non-polar, non-emissive state in the excited-state deactivation. The more polar the fluorescing state, the less efficient is the population of or interaction by this quenching state. The

lii) Such phenomena are well-known, for instance, in the case of naphthyl phenyl-substituted ethylenes [238] and for the related BOZ derivatives [222] (see Appendix D for chemical structure). For these systems, largely overlapping bands are found in solution.

Table 21
Calculated torsion angles (Θ) of PAC derivatives in the ground state (AM1/HyperChem). For chemical structures of the molecules, see Scheme 8, Ch. 4.1.

	cE			*tE*		
	b1	**b2**	**b4**	**b1**	**b2**	**b4**
	Θ /°	**Θ /°**	**Θ /°**	**Θ /°**	**Θ /°**	**Θ /°**
PAC-DMA	-33	-10	-10	-33	149	-173
PAC-DMA-b12-6	-4	-19	53	-	-	-
PAC-DMA-b12-5	-2	6	28	-	-	-
PAC-DMA-b34-5O	-31	-9	0	-35	161	0
PAC-DMA-b123-6O	-	-	-	0	179	26
PAC-DMA-b1234-6O-2	-	-	-	1	0	9
PAC-Jul [a]	-33	-10	-11	-35	151	5
PAC-DMA-b34-5 [a]	-54	-14	0	-34	157	0
PAC-DMA-b4-5 [a]	34	7	-179	16 [b]	53 [b]	176 [b]

[a] molecules have only been modeled theoretically (see Appendix D for chemical structure);

[b] data of the *cZ* isomer

decrease in fluorescence quantum yield which is observed in this region of the polarity scale even for the PAC derivatives with a bridged C-C double bond, i. e., PAC-DMA-b34-5O, PAC-DMA-b123-6O, and PAC-DMA-b1234-6O-2, indicate the influence of both mechanisms enumerated above. P* state formation is not possible in these derivatives but the emitting, polar state is sufficiently destabilized to experience perturbation by the proximity effect. Furthermore, rotation of the carbonyl group is possible in PAC-DMA-b34-5O, but especially the large difference between the fluorescence quantum yields of the totally bridged compound PAC-DMA-b1234-6O-2 and PAC-DMA-b123-6O (ca. two orders of magnitude) cannot be explained by rotation of the CO group. However, for BTAC-Jul the emissive state is still of considerably lower energy in hexane and both interaction by the latter effect and population of the P* state is suppressed to a major extent. Similar maxima (ϕ_f vs. $E_T(N)$ plot) of BTAC-DMA, the crowned BTAC derivatives, and PAC-DMA-b34-5O, unable to rotate around the double bond, suggest that the P* state plays only a minor role in the deactivation of these BTAC ICT compounds aswell.

The temperature dependence of the fluorescence quantum yields and lifetimes of BTAC-DMA and PAC-DMA in diethylether (Ch. 4.3.3) give further evidence in favor of this explanation. Whereas PAC-DMA shows a behavior known for compounds displaying reduced emission due to P* state formation [219], i. e., strong increase in fluorescence quantum yield upon cooling, this tendency is absent in BTAC-DMA. Only for PAC-DMA, freezing of the radiationless relaxation channel P* requiring a relatively high activation energy (and large free volume for rotation) leads to enhanced emission (ϕ_f 0.02 at 290 K and 0.74 at 170 K). BTAC-DMA is already highly fluorescent at room temperature (ϕ_f 0.52).

Furthermore, direct experimental evidence for the formation of a “dark” P* state has been reported in the case of bis(*p-N,N*-dimethylaminobenzylidene)acetone by *DeVoe* et al. employing transient absorption spectroscopy [209f].

In accordance with previously published investigations on amino donor-substituted D-A-chalcones [209b], population of a non-polar emissive triplet state, preferably from the P* state, was not directly observed. No phosphorescence could be detected in either room or low temperature measuremens[liii]. Luminescence emission of BTAC-H, decaying with a lifetime of < 1.7 ns, appears in a wavelength region where *Caldwell* and *Singh* detected the triplets of, e. g., PAC-H (430 nm in heptane), but the decay time measured here is much shorter than the triplet depopulation times of > 12 ns given by these authors [209b]. The real nature of this weakly emissive state of BTAC-H is still obscure, yet its lifetime is much shorter than that of styrene[liv] [242a] or cyclohexenone triplets [242c].

Furthermore, no photoproducts (neither by addition reactions nor by *trans-cis* isomerization) were found in any of the measurements performed. Due to the loss in π electron conjugation within the molecule, such addition products absorb in the UV region of the spectrum and should have been easily detectable but no drastic changes of this kind were observed upon irradiation.[lv] Moreover, the molecular structure of the BTAC derivatives does not favor a stable cis isomer (*Scheme 9*, p. 56) and any species formed by C-C double bond twisting should undergo a very rapid backward reaction leading to the *trans* isomer in the ground state.

<u>*Polar Transient Species and Interactions.*</u> The polar transient species and interactions that might be involved in excited-state deactivation of the D-A-chalcones comprise rotation around C-C single bonds, i. e., emissive or non-emissive TICT states, and hydrogen-bonding interactions in H-acidic solvents, i. e., alcohols. TICT state (A* state) formation is widely but controversely discussed for PAC derivatives [209f, 210, 212d, f, 213] but here, comparative investigation of the bridged compounds provide a means to encircle possible and probable pathways.

<u>*Amino Bond b5.*</u> A major influence of the C-N bond b5 (*Scheme 8*, p. 43) on the excited state deactivation of D-A-chalcones can be directly excluded by comparing the largely differing fluorescence quantum yields of PAC-DMA, PAC-DMA-b12-X (X = 5,6), and PAC-DMA-b34-5O in solvents of any polarity. Whereas PAC-DMA and the b12-X derivatives show a negative solvatokinetic behavior, PAC-DMA-b34-5O exhibits positive solvatokinetics (see Appendix B for details). Furthermore, a comparison of the solvatochromic behavior of BTAC-Jul and BTAC-DMA suggests that the stronger ICT in the former compound leads to red-shifted spectra and lower fluorescence quantum yields owing to the energy gap law [243]. When plotting $\log k_{nr}$ of BTAC-DMA and the crowned derivatives as a function of emission energy (for solvents of polarity between acetonitrile and THF), a linear correlation is obtained pointing mainly to a dependence of non-radiative deactivation on donor strength according to CT character and energy gap rule *(Fig. 38)*. Under the simplified assumption that no other process contributes to excited-state depopulation, a decrease in energy gap between the emissive and corresponding ground state leads to an increased probability for internal conversion (ic) and only k_{ic} is accelerated. The absence of a major influence of rotation around b5 is stressed by the small differences between bulky BTAC-A15C5 and BTAC-DMA. Similar explanations have been given by *Wang* in a comparison of PAC-DMA-b12-5 and PAC-Jul-b12-5, his data being partly included in *Table 15*, p. 49 [210]. Results published recently by F*ery-Forgues* et al. on BOZ derivatives (see Appendix D for chemical structure) and by *Itoh* et al. on chalcones point into the same direction [214c, 222].

<u>*Anilino Bond b4.*</u> Considering the anilino bond, the formation of a polar transient state can occur via twisting around b4. This is possible for all PAC derivatives except PAC-DMA-b34-5O and fully bridged PAC-DMA-b1234-6O-2. Whereas highly fluorescent PAC-DMA-b123-6O excludes any non-radiative deactivation via b4-twisting, the impossibility of populating such a fluorescent state can account (partly) for the positive solvatokinetic behavior and quenched fluorescence of PAC-DMA-b34-5O. If such a (highly) polar emis-

liii) *Caldwell* and *Singh* found a low triplet formation rate for PAC-DMA only in heptane at 77 K (decay time of 500 ns) [209b] but no such transients were found during the studies reported here for BTAC-DMA and BTAC-A15C5 in 3-methylpentane at 77 K.

liv) Decay via a twisted conformation is generally accepted for styrene triplets [242a] and more planar triplets have even longer lifetimes [242b].

lv) Photochemical products have been reported for PAC-H [205, 209a] and bis(*p-N,N*-dimethylaminobenzylidene)acetone [209c].

sive state (A*) exists, an increase in solvent polarity should stabilize this state to a larger extent than, e. g., a weakly polar P* state and should thus accelerate the reaction of initially excited E* towards A*. Accordingly, the fluorescence quantum yield should increase with solvent polarity according to the negative solvatokinetic effect. Comparing the solvent-dependent fluorescence quantum yield data of the PAC derivatives (*Fig. 31*, p. 50), such a negative solvatokinetic behavior is only observed for all the compounds with an unbridged anilino bond suggesting the involvement of such a transient state. Furthermore, the differences between PAC-DMA-b123-6O and the fully bridged derivative would support such an explanation as well (The steeper slope of a plot of Stokes shift vs. the *Bilot-Kawski* solvent polarity parameter for PAC-DMA-b123-6O given by *Wang* and *Wu* in ref. [212f] is another hint for the population of a more polar emissive state in derivatives with an unbridged b4).

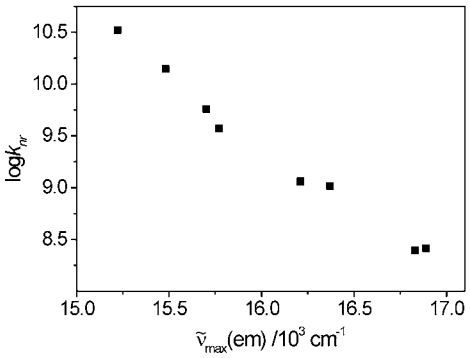

Fig. 38
Plot of $\log k_{nr}$ vs. $\tilde{\nu}$ (em) for the BTAC derivatives (DMA, A15C5, $AT_4$15C5) in solvents of polarity between acetonitrile and THF Table 12, p. 46)

Bonds at the Carbonyl Group b1 and b2. Bridging of the C-C single bonds b1 and b2 (*Scheme 8*, p. 43) does not strongly alter the shape of the ϕ_f vs. $E_T(N)$ plot. The curve has a nearly identical shape but is of lower amplitude for PAC-DMA-b12-5, and especially for PAC-DMA-b12-6 (*Fig. 31*, p. 50). Accordingly, for the single bonds b1 and b2, two contradictory observations are made *(Fig. 31)*, i. e.,

(i) bridging leads to fluorescence quenching (PAC-DMA-b12-X compared to PAC-DMA),

(ii) but the lack of a bridge opens an efficient non-radiative funnel for depopulation of initially excited (relaxed) state E* as well (in weakly fluorescent PAC-DMA-b34-5O).

The generally lower fluorescence quantum yield in the case of PAC-DMA-b12-6 can be understood on the basis of the higher flexibility of the cyclohexene ring undergoing a nearly barrierless ring inversion (boat-chair interconversion) [244]. But the higher fluorescence of PAC-DMA compared to PAC-DMA-b34-5O cannot be explained by population of a fluorescent polar, b1- or b2-twisted transient species since in both derivatives rotation around b1 and b2 is possible. In contrast, the positive solvatokinetic behavior of PAC-DMA-b34-5O with bridged double and anilino single bond (and a less “active” bond b5, see above) points directly to the formation of a polar, non-emissive state K* by twisting around b1 and/or b2. Since D-A-stilbenes containing a central double bond fixed by a 5O-bridge on the donor side (“benzofuran-bridged” fura derivatives as in PAC-DMA-b34-5O, see Appendix D for chemical structure) exhibit moderate fluorescence in polar solvents, such compounds fluoresce with a quantum yield of 0.13 in aqueous solution [72a], no intrinsic O-bridge-specific quenching channel is very probable. Furthermore, both bridged derivatives PAC-DMA-b123-6O and PAC-DMA-b1234-6O-2 are highly fluorescent despite an intramolecular oxygen bridge as in PAC-DMA-b34-5O.

Thus, the contradictory observations stated in (i) and (ii) above suggest that for PAC-DMA and its b12-bridged derivatives, different reactivities for P* and A* state formation should occur. The torsion angles around b4 given in *Table 21*, p. 57, are much larger in the case of the two b12-bridged derivatives and thus not only population of a fluorescent A* state but also reaction towards a non-emissive P* state might be accelerated. Another possible explanation involves more efficient P* formation from initially populated A*. For PAC-DMA, population of polar emissive A* and polar non-emissive K* (b1- or b2-twisted transient species) compete and the negative solvatokinetic behavior suggests that A* is more polar, hence more stabilized and more efficiently populated in polar solvents leading to a higher fluorescence quantum yield.

4.4.2.2 Stereoisomerism

Returning to stereoisomerism, which has been completely neglected during the preceeding mechanistic discussion for the sake of simplicity, the implications can be rationalized as follows.

According to their bridging pattern, the PAC derivatives can be divided into three groups, i. e., possible ground state *s*-isomers, *cE*-only, *tE*-only, and *cE* and/or *tE* (*Scheme 9*, p. 56).

Fixed tE Isomers. The only two derivatives fixed in this conformation are the highly fluorescent and largely bridged PAC-DMA-b123-6O and PAC-DMA-b1234-6O-2. Here, in apolar solvents, mainly the proximity effect should lead to fluorescence quenching but in all the more polar solvents, only a polar fluorescent, rigidized *tE** state emits (cf. change in dipole moment upon excitation, *Table 16*, p. 49) and, in the case of PAC-DMA-b123-6O, a highly fluorescent *tA** transient species possibly plays a role.[lvi]

Fixed cE Isomers. Synthesis and investigation of molecules in a fixed *cE* conformation and with a bridged double bond is not possible without largely altering the electronic nature of the compounds and thus the rate of intrinsic *cE* fluorescence remains unknown. Emission in the fixed *cE* isomers with a flexible double bond, i. e., PAC-DMA-b12-X (X = 5,6), occurs most favorably via A* population, counterbalanced by (parallel or consecutive) reaction towards non-emissive P*.

Molecules Forming cE and/or tE Isomers. Besides the unbridged BTAC derivatives and PAC-DMA, PAC-DMA-b34-5O is left in this third group. Concerning these compounds, the ground state equilibrium between both isomers will be largely dependent on their stabilization by the respective solvent. Upon increasing solvent polarity, the isomer with the higher dipole moment will be more strongly

lvi) The large difference of the fluorescence quantum yields of both compounds in hexane remains unclear at present and *Wang* and *Wu* did not give any explanation as well [212].

stabilized. If both ground state isomers exist and are excited they can theoretically interconvert via K* formation and the corresponding "backward" reaction yielding the other *xE** isomer. However, the yield of such a reaction will be rather low (e. g., for BTAC derivatives in polar solvents where fast deactivation is observed) and the NEER (non-equilibration of excited rotamers) principle put forth by Havinga for excited-state reaction mechanisms of polyenes is assumed to maintain its validity in the case of the D-A-chalcones [245a, b]. If more than one ground state isomer is present, the excited-state reaction scheme extends to a dual scheme with individual species *tA*, cA*, tP**, and *cP**.

4.4.2.3 Generalized Excited-State Reaction Model

Combining the reaction mechanisms mentioned so far, one arrives at a modified, enlarged three-state scheme discussed for D-A-stilbenes *(Scheme 10)* [241]. For the BTAC derivatives, the general scheme proposed is consistent including stronger stabilization of the polar states with increasing solvent polarity compared to the PAC derivatives.

According to the interpretations given in the preceeding sections the polarity of the states increases in the order of E* ~ P* < K* < A* for the D-A-chalcones. Besides possible population of these transient states, the influence of both the proximity effect and the energy gap rule govern the relaxation behavior of these compounds.

Coming back once more to the results of the time-resolved emission measurements, i. e., the noticeable $DAS_i(\lambda)$ ratios in largely overlapping bands (e. g., hexane or diethylether, *Fig. 32*, p. 51), stereoisomerism already in the ground state might account for the findings. The close spectroscopic relation of both *s*-isomers is exemplified by the spectrally similar absorption and emission characteristics of, e. g., PAC-DMA-b12-5 (fixed *cE*) and PAC-DMA-b123-6O (fixed *tE*) and is supported by the quantum chemical calculations (Ch. 4.4.1). Such a case would give rise to an excitation wavelength dependence of the relative amplitudes as was observed in some of the TRES measurements. Furthermore, when two ground state species are simultaneously excited (and populate another emitting species A* as well as possibly interact via K*) and in the case of largely overlapping bands, the values obtained by extrapolation of the $DAS_i(\lambda)$ ratios into the blue and red region[lvii] could not reach -1 or ∞. Depending on the concentration of initially populated *cE** and *tE**, $c_0(cE^*)$ and $c_0(tE^*)$, their radiative and non-radiative deactivation pathways, a complex expression involving the rate constants could be obtained for the decay times measured in the experiment *(Scheme 10)* [246]. However, a detailed analysis of the fluorescence decay behavior will be given elsewhere [226].

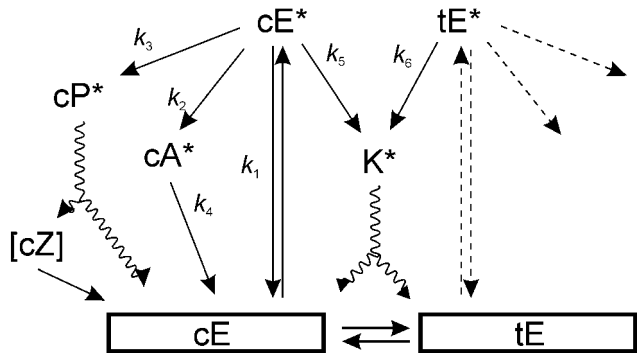

Scheme 10
Generalized excited-state reaction model for D-A-chalcones (triplet states, backward reactions, and consecutive population of two transient species are omitted for clearness). Dashed arrows indicate the second branch, coming into play when two ground state s-isomers are excited. Solid arrows denote reactions and radiative deactivations and wiggled arrows mark non-emissive decays. Theoretically, cE and tE* can interconvert when considering backward reactions from K* (see text for discussion). Any triplet formation would occur most probably from P*.*

4.4.2.4 BTAC-H Revisited

A further hint for the presence of different ground state species follows from the spectroscopic behavior of BTAC-H (*Table 14*, p. 47)[lviii]. No noticeable CT interactions are operative and the initially excited state undergoes very fast non-radiative deactivation which may be either ascribed to the "proximity effect", i. e., vibronic coupling of energetically close-lying nπ* and ππ* states [210] or efficient P* state formation (with or without consecutive triplet population; see above) [209b]. Assuming a certain analogy to stilbene derivatives, excitation of BTAC-H would lead to the formation of weakly polar E* but the corresponding P* state should be of higher polarity [223b]. Accordingly, the energy level position of P* should be stronger stabilized by polar solvents leading to enhanced quenching in polar solvents. However, from the generally low fluorescence quantum yields of BTAC-H, no such trend can significantly be derived (see *Table 14*, p. 47). A comparison with BTAC-OCH_3 (*Table 14*, p. 47), spectrally displaying CT characteristics but still being weakly fluorescent in solvents of any polarity, indicates that most probably efficient P* state formation is operative in both molecules regardless of substitution pattern. Since all the other D-A-chalcones are only weakly fluorescent at best (see Ch. 4.2), the formation of a fluorescent A* state can be excluded for any other D-A-chalcone besides the amino-substituted ones. For the corresponding PAC derivatives, the high photochemical trans-cis isomerization rates, low fluorescence quantum yields, and efficient triplet formation published by other authors point to efficient P* formation and support these findings [209a, b]. In contrast, for the 4-*p*-*N,N*-alkylamino substituted chalcones, no trans-cis isomerization has been reported and was found in this work [209b].

However, the emission spectrum of BTAC-H is largely red-shifted compared to the main absorption band (despite CT) and yields a different fluorescence excitation spectrum with a center in the low-energy tail of the absorption spectrum. And, besides a short decay component, a second long decay component has been found (and no rise times, see above). A possible explanation might again involve different ground state isomers.

---

lvii) blue region: λ (blue)→0, $\lim_{\lambda \to blue} \frac{DAS_1(\lambda)}{DAS_2(\lambda)} \leq \infty$;

red region λ (red)→∞, $-1 < \lim_{\lambda \to red} \frac{DAS_1(\lambda)}{DAS_2(\lambda)} \leq 0$.

For BTAC-DMA in diethylether at 298 K, λ(blue) → 0.29 and λ (red) → -0.28, for BTAC-$AT_4$15C5, the corresponding values are 0.30 and -0.20.

lviii) As well as that of PAC-H, which has been described by numerous other researchers, e. g., in ref. [209a, e] and will not be discussed here any further.

4.4.2.5 Alcohols Revisited

In H-acidic solvents, i. e., alcohols, the fluorescence of all the compounds investigated here is weak (no data were reported by *Wang* and *Wu* on PAC-DMA-b123-6O and PAC-DMA-b1234-6O-2) and the deactivation of the excited state is intermingled with solvent relaxation and hydrogen bond formation, i. e., all processes occur on a similar time scale (see Ch. 4.3.2.1). Whereas the emission of the BTAC derivatives is already weak in acetonitrile, the fluorescence of PAC-DMA is quenched (factor 15) when going from acetonitrile to ethanol (*Table 13*, p. 47). Thus, the deactivation of the excited state is attributed to hydrogen-bonding interactions (of A*), preferably occurring at the carbonyl group of the acceptor, solute-solvent complexes being possibly (already) present in the ground state [210, 247]. Accordingly, any H-bond interaction (with the acceptor fragment of the molecule) should increase in size upon a charge transfer process taking place after excitation [177a, 248].

A more elaborate explanation of the mechanisms involved cannot be given here within the scope of this thesis and furthermore, additional investigations, i. e., dynamic and temperature-dependent studies of some of the bridged PAC derivatives are required. Especially synthesis and experimental investigation of PAC-DMA-b4-5 and PAC-DMA-b124-5-2 (see Appendix D for chemical structure) would yield very valuable data for the verification of the model given in *Scheme 10*. In the former derivative, only twisting around the single bond capable of forming the emissive A* state is blocked by bridging and in the latter derivative, the only unbridged bond is the central double bond allowing, for instance, to draw a conlusion on the solvent-dependent rate of P* formation.

4.5 Complexes of Chalcone-Analogue Fluorescent Probes

For both fluorescent probes, BTAC-AT$_4$15C5 and BTAC-A15C5, spectroscopic complexation studies were carried out in order to investigate the effect of the receptor on cation selectivity and complex stability constant. Furthermore, the spectroscopic properties of their cation complexes were compared. These studies involved the alkali and alkaline-earth metal ions Li^{I}, Na^{I}, K^{I}, Mg^{II}, Ca^{II}, Sr^{II}, and Ba^{II} as well as the heavy and transition metal ions Ag^{I}, Cu^{I}, Cu^{II}, Ni^{II}, Co^{II}, Zn^{II}, Cd^{II}, Hg^{II}, and Pb^{II}. The complex stability constants reported here were determined from both absorption and fluorescence measurements and, in the case of Li^{I} and Ca^{II}, also conductometrically. Furthermore, the fluorescence behavior of the cation complexes of both probes are compared to that of other ICT fluorescent probes such as DCM-A15C5, DCS-A15C5, and BOZ-A15C5.[lix]

4.5.1 Complexation Behavior of BTAC-AT$_4$15C5

Before discussing the complexation behavior of the BTAC derivatives in acetonitrile, it is important to recall the features in this polar solvent, i. e., monoexponential decay kinetics and no wavelength dependences in their steady-state spectra (Ch. 4.3). Thus, on the basis of the mechanistic considerations (Ch. 4.4.2) and in analogy to observations made for polyenes [245c], it is assumed that a single (preferably *cE*) isomer is predominantly present in solution and the excited-state behavior involves mainly A* formation (and partly competing K*).

4.5.1.1 Steady-State Spectra

The fluorescent probe carrying the tetrathia monoaza macrocycle AT$_4$15C5 is expected to show much stronger coordination tendencies towards “soft” heavy and transition metal ions, especially the thiophilic ions Ag^{I}, Cu^{I}, and Hg^{II}, than towards “hard” main group metal ions. As expected, a comparison of the data given in *Table 22* and the spectra shown in *Fig. 39* reveals that BTAC-AT$_4$15C5 shows complexation-induced changes of its optical properties only with “soft” metal ions, the only exception being Cu^{I} (see Ch. 4.5.7 for discussion).

As can be deduced from both *Fig. 39* and *Table 22*, the hypsochromic shifts observed in absorption are rather large compared to the corresponding shifts in emission. Moreover, the shifts are much more pronounced in the case of the divalent metal ion Hg^{II} (7 320 cm^{-1} in absorption, 1 300 cm^{-1} in emission) compared to monovalent Ag^{I} (900 cm^{-1} in absorption, 790 cm^{-1} in emission). The total abstraction of the nitrogen lone electron pair from the chromophore system in the case of Hg^{II} (cf. absorption spectra of the Hg^{II} complex and BTAC-H in *Fig. 39*) indicates the strong electrostatic interaction between the ion bound in the cavity of the receptor and the nitrogen donor atom of the latter. Furthermore, the high selectivity of this receptor for the thiophilic metal ions such as Ag^{I} and Hg^{II} is demonstrated by the lack of spectroscopic changes upon addition of Zn^{II}, Cd^{II}, Ni^{II}, or Pb^{II} salts (see footnote [lxii]).The isosbestic points observed in both cases in a UV/Vis spectrophotometric titration experiment indicate the formation of a single equilibrium, i. e., 1:1-complexes (*Fig. 45*, p. 68).

Even more interestingly, not only in the case of the Ag^{I} but also in the case of the Hg^{II} ion, commonly known as a fluorescence quencher due to the heavy atom effect, fluorescence enhancement along with an increase in fluorescence lifetime is observed.

Moreover, in the case of this well-known fluorescence quencher (cf., e. g., quenching of BP(OH)$_2$ emission by Hg^{II}, Ch. 3.3.1.1), the FEF = 6 is considerably high for an ICT

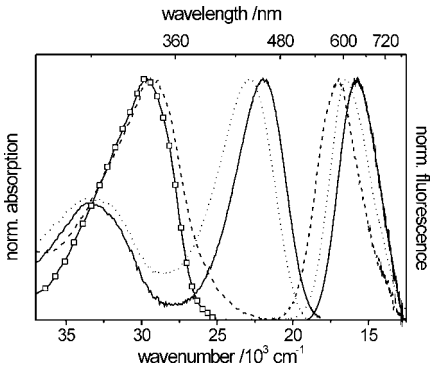

Fig. 39
Normalized steady-state absorption and emission spectra of BTAC-AT$_4$15C5 (–) and its Ag^{I} (·····) and Hg^{II} (- -) complexes in acetonitrile. The absorption spectrum of BTAC-H (□) is included for comparison.

lix) For chemical structures, see Appendix D.

fluorescent probe (see below and in refs in Ch. 1.3.3)[lx]. Of all the metal ions employed in these studies, only Cu^{II} was found to interfere with the observed selectivity, i. e., complexation-induced changes occur also in the presence of Cu^{II} (see discussion in Ch. 4.5.7).

4.5.1.2 Fluorescence Lifetimes

Time-resolved fluorescence measurements performed with BTAC-$AT_4$15C5 and Ag^{I} as well as Hg^{II} show that in accordance with the observed increase in fluorescence quantum yield, cation complexation of the probe is also accompanied by the appearance of a new (Ag^{I}) or two new (Hg^{II}) long-lived decay component(s) with cation specific fluorescence lifetimes between 350 ps and 1 ns *(Table 22)*.

Under conditions where complex formation is complete, biexponential decay kinetics are noticed for Ag^{I} and the kinetics of the Hg^{II} complex involve three decay components. In the case of Hg^{II}, both long-lived decay components show a positive amplitude through the whole range of the emission spectrum and largely overlapping spectra.

When analyzing the wavelength-resolved fluorescence decay data of the complexes at full complexation, at the far blue edge of the spectrum a fast decay component of 55 ps (for Ag^{I}) and 90 ps (Hg^{II}) with a positive amplitude is found. In the middle and red region of the spectrum, this component is found as a rise time. For the Hg^{II} complex, recording TRES as a function of excitation wavelength (within the excitation range of the second harmonic of the ps-LIF), two additional time constants with positive amplitudes through the whole spectral region are found.

Globally analyzing a set of 20 decay curves, 10 recorded for excitation at 380 and 410 nm each, yields three components of 90 ps, 568 ps, and 1.1 ns, respectively (*global* χ_R^2 = 1.1; for two components: *global* χ_R^2 = 1.9)[lxi]. Thus, with both

Table 22
Spectroscopic properties of the cation complexes of BTAC-$AT_4$15C5 in acetonitrile. The experiments were carried out up to the µM concentration range for the heavy and transition metal ions and up to the mM concentration range for the alkali and alkaline-earth metal ions[lxii] (c_L = 3 x10^{-6} M; the short decay components are not included).

	$\tilde{\nu}$ (abs)	$\tilde{\nu}$ (em)	$\Delta\tilde{\nu}_{cp\text{-}fp}$ (abs)	$\Delta\tilde{\nu}_{cp\text{-}fp}$ (em)	ϕ_f
	10^3 cm^{-1}	**10^3 cm^{-1}**	**cm^{-1}**	**cm^{-1}**	
BTAC-$AT_4$15C5 [a]	21.98	15.70	-	-	0.02
⊂Hg^{II}	29.30	17.00	7320	1300	0.12
⊂Zn^{II}, Cd^{II}, Ni^{II}, Co^{II}	-	-	-	-	-
⊂Cu^{II}	30.11 [b]	18.15 [c]	8130	2450	(0.009) [c]
⊂Cu^{I}	-	-	-	-	-
⊂Ag^{I}	22.88	16.49	900	790	0.05
	τ_2	τ_3	logK_S	r_M [d]	χ_m^2 x r_M [e]
	ps	**ns**	**abs**	**Å**	
BTAC-$AT_4$15C5 [a]	170	-	-	-	-
⊂Hg^{II}	568	1.07	> 5.5 [f]	1.02	4.08
⊂Zn^{II}, Cd^{II}, Ni^{II}, Co^{II}	-	-	-	0.74, 0.95, 0.69, 0.74	2.01, 2.71, 2.52, 2.61
⊂Cu^{II}	202	1.15	n.d.	0.73	2.64
⊂Cu^{I}	-	-	-	0.96 (4)	3.46
⊂Ag^{I}	348	-	4.51	1.15	4.28

[a] no effects observed for Li^{I}, Na^{I}, K^{I}, Mg^{II}, Ca^{II}, Sr^{II}, Ba^{II}, and Pb^{II} ;

[b] For BTAC-$AT_4$15C5⊂Cu^{II}, various subbands, exemplified by shoulders in the absorption spectrum (e. g., at 36 000 and 23 000 cm^{-1}) were found, their origin being unclear at present (see text);

[c] For BTAC-$AT_4$15C5⊂Cu^{II}, a second emission band at 23 200 cm^{-1} is observed, whose origin is unclear at present (see text);

[d] All the radii were taken from ref. [249a] and are for six-coordination except where the coordination number is indicated in brackets [250a] and for Cu^{I} [250b]. For Cu^{I}, tetrahedral coordination is found in most polythia ether complexes [251].

[e] The electronegativity values given in the literature differ largely in units [252a]. Here, the softness or class B parameter [253] was calculated with the electronegativity values of *Allred* and *Rochow* [252b, c]

[f] too high to be determined with acceptable accuracy with the method employed (Appendix B)

lx) At higher excess of Hg^{II} in the solution quenching is observed. The concentration dependence of fluorescence quenching points to a diffusion-controlled process (typically observed for "heavy atoms" in a solution containing a fluorescent dye) but might as well be due to the formation of another chelate-like complex (see Ch. 4.5.7 for discussion).

lxi) Note that employing a fourth decay component is possible but does not significantly improve the fit (see for discussion in Ch. 4.5.3).

lxii) Due to the heterocyclic donor atoms being present in the chromophore (and in form of the nitrogen in the receptor), at higher concentrations, i. e., at $x_{M/L}$ > 100, slight spectroscopic changes are observable for other heavy and transition metal ions such as, e. g., Ni^{II} as well. However, the occurence of these trace metal ions at such concentrations is barely found in matrices where fluorescence sensing is commonly employed.

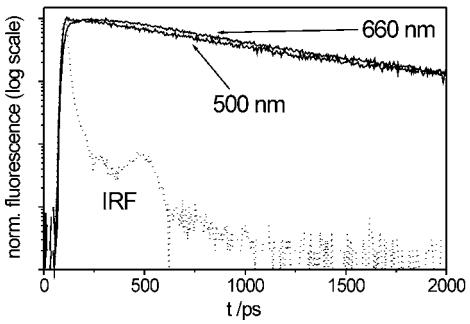

Fig. 40
Fluorescence decay curves of BTAC-AT$_4$15C5⊂Hg^{II} in acetonitrile. Excitation at 380 nm, emission at 500 (DAS$_2$ / DAS$_3$ = 0.8) and 660 nm (DAS$_2$ / DAS$_3$ = 1.2).

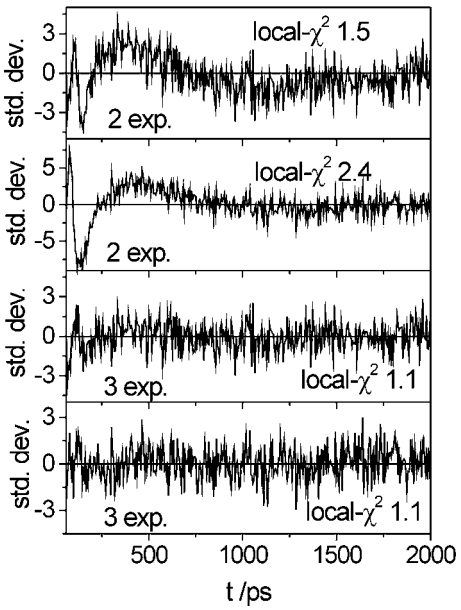

Fig. 41
Residuals of the fit results of the decay curves shown in Fig. 40. From top to bottom: decays at 500 nm and 660 nm fitted to two exponentials and the same decays fitted to three exponentials (decay times given in the text, local χ_R^2 indicated).

excitation wavelengths employed, only the complex(es) is (are) excited. For a better illustration, two decays of the Hg^{II} complex are shown in *Fig. 40*.

4.5.1.3 Cu^{II} and Cu^{I}

In the case of Cu^{II}, the spectroscopic changes are more complex and involve the appearance of two fluorescence emission bands and various subbands in the absorption spectrum. Additionally, the Cu^{II} complex shows fluorescence quenching and a nonexponential fluorescence decay behavior, the single decay components depending on both excitation and observation wavelength. Due to its weak fluorescence, the comparably low temporal resolution of the BESSY setup (55.5 ps chn^{-1} and a short decay component with τ_1 = 42 ps), and the gap in the excitation range of the ps-LIF (330-370 nm), the spectroscopic behavior of this complex was not further studied. Explanations for the nature of the Cu^{II} complex will be given in Ch. 4.5.7 dealing with a possible second coordination site in D-A-chalcones.

Furthermore, it is interesting to note that no spectroscopically detectable complexation reaction was found for Cu^{I} in the investigated µM concentration range (no spectroscopic interference by this ion).

4.5.2 Complexation Behavior of BTAC-A15C5

4.5.2.1 Steady-State Spectra

Addition of alkali and alkaline-earth metal ions to an acetonitrile solution of BTAC-A15C5 affects both its absorption and emission behavior. As follows from *Table 23*, binding of BTAC-A15C5 to the monovalent cations Li^{I}, Na^{I}, and K^{I} leads to a small hypsochromic shift in absorption accompanied by a decrease in molar absorptivity whereas for divalent cations, the hypsochromic shift is much more pronounced and leads to the appearance of a strongly blue-shifted absorption band of the cation complex located at 28 680 cm^{-1} for Mg^{II}, 27 890 cm^{-1} for Ca^{II}, 27 250 cm^{-1} for Sr^{II}, and 26 320 cm^{-1} for Ba^{II}.

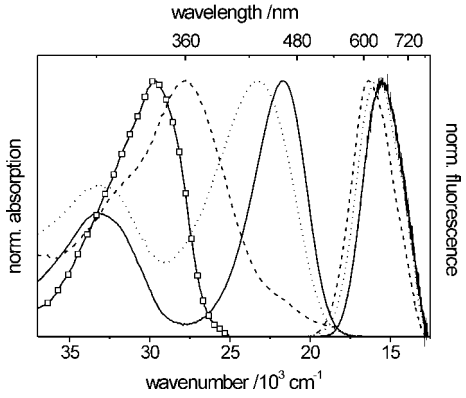

Fig. 42
Normalized steady-state absorption and emission spectra of BTAC-A15C5 (—) and its Na^{I} (·····) and Ca^{II} (- -) complexes in acetonitrile. The absorption spectrum of BTAC-H (□) is included for comparison.[lxiii]

This effect is again indicative of pronounced removal of the lone electron pair of the nitrogen atom of the receptor from the conjugated π system as can be derived from a comparison of the absorption bands of BTAC-H and the Ca^{II} complex in *Fig. 42*. Besides for Mg^{II}, isosbestic points are observed in all the cases studied indicating a single equilibrium and thus, the formation of well-defined 1:1-complexes. For Mg^{II}, in addition to the blue-shifted absorption band located at 28 680 cm^{-1} the appearance of a red-shifted absorption band with a maximum at 17 300 cm^{-1} is noticed[lxiv]. Similar effects as described for Mg^{II} are observed in the presence of Pb^{II}, Hg^{II}, and Cu^{II} at $x_{M/L}$ > 5 (i. e., in the µM concentration range) suggesting the formation of a second complex of different nature. The special complexation behavior of Mg^{II} along with the interfering complexation reactions of some of the heavy and transition metal ions will be discussed in detail in the subsection about the nature of the complexes, Ch. 4.5.7.

---

lxiii) The remaining absorption at ca. 22 000 cm^{-1} (shoulder) at large excess of metal ion is attributed to uncomplexed dye molecules in the equilibrated state. Similar effects have been described for other ICT probes [84, 91b]. *Mateeva* et al. discussed nπ* transitions being responsible for these bands but this assumption could not be supported here [91b].

lxiv) Interestingly, such effects were not observed for BTAC-AT$_4$15C5 and Mg^{II} in the mM concentration range.

Table 23
Spectroscopic properties of the cation complexes of BTAC-A15C5 in acetonitrile. The experiments were carried out up to the mM concentration range for the alkali and alkaline-earth metal ions and up to the µM concentration range for the heavy and transition metal ions[lxii] (c_L = 3 x 10^{-6} M; short decay components not included).

	$\tilde{\nu}$ (abs)	$\tilde{\nu}$ (em)	$\Delta\tilde{\nu}_{cp\text{-}fp}$ (abs)	$\Delta\tilde{\nu}_{cp\text{-}fp}$ (em)	ϕ_f	τ_f
	10^3 cm^{-1}	10^3 cm^{-1}	cm^{-1}	cm^{-1}		ps
BTAC-A15C5 [a]	21.69	15.48	-	-	0.007	71
⊂Li^{I}	22.78	15.78	1090	300	0.04	171
⊂Na^{I}	23.07	15.95	1380	470	0.04	102
⊂K^{I}	22.39 [b]	15.70 [b]	700	220	0.03 [b]	87
⊂Mg^{II} [c]	28.68, 17.30	16.81, -	6990, -4390	1330, -	n.d.	86
⊂Ca^{II}	27.89	16.38	6200	910	0.06	192
⊂Sr^{II}	27.25	16.08	5560	600	0.05	201
⊂Ba^{II}	26.32	16.02	4630	540	0.03	n.d.
⊂Pb^{II}	27.93	16.50	6240	1020	0.06	n.d.
⊂Hg^{II}, Cu^{II}	30.20, 16.83	-	8510, -4860	-	-	-
	$\log K_S$	$\log K_S$	$\log K_S$	r_M [d]	n^2 / r_M	
	abs.	em.	cond.	Å	$Z^2Å^{-1}$	
BTAC-A15C5 [a]	-	-	-	-	-	
⊂Li^{I}	2.57	2.42	2.80	0.76	1.32	
⊂Na^{I}	1.79	1.85	n.d.	1.02	0.98	
⊂K^{I}	1.4 [b]	n.d.	n.d.	1.46	0.68	
⊂Mg^{II} [c]	n.d.	n.d.	n.d.	0.72	5.55	
⊂Ca^{II}	3.69	3.37	3.29	1.06 (7)	3.77	
⊂Sr^{II}	2.82	2.82	-	1.21	3.31	
⊂Ba^{II}	2.80	2.38	-	1.47 (9)	2.72	
⊂Pb^{II}	n.d.	n.d.	n.d.	1.19	3.36	
⊂Hg^{II}, Cu^{II}	n.d.	n.d.	n.d.	1.02, 0.73	3.92, 5.48	

[a] no effects on the ICT band observed for Zn^{II}, Cd^{II}, Ni^{II}, Co^{II}, Cu^{I}, Ag^{I};

[b] extrapolated values because full complexation could not be achieved due to solubility problems;

[c] excitation at the bathochromically shifted absorption band does not yield any measurable fluorescence; ϕ_f and $\log K_s$ have not been determined because no full complexation could be achieved. Additionally, the low-energy absorption and emission band largely overlap.

[d] All the radii were taken from ref. [249a] and are for six-coordination except where the coordination number is indicated in brackets [250a]. The values given in brackets have been found by Jonker in X-ray analyses of related MAP-A15C5 complexes [250a, 254]; cavity size of the aza crown: 1.7-1.8 Å [249b, c]

Chelation to the alkali and alkaline-earth metal ions is further accompanied by a blue shift of the emission band of BTAC-A15C5 and an increase in fluorescence quantum yield by a factor of 4 to 8.5 depending on the cation bound, see *Table 23*, respectively.

The size of both effects is clearly affected by the charge of the cation bound, the strongest hypsochromic shift of 1 330 cm^{-1} occuring for Mg^{II} and the highest increase by a factor of 8.5 occuring for Ca^{II}. Furthermore, in the case of Mg^{II}, excitation at the long-wavelength absorption band does not yield any measurable fluorescence (this is also observed for the other ions forming this complex, see *Table 23*).

4.5.2.2 Fluorescence Lifetimes

Time-resolved fluorescence measurements performed with some alkali and alkaline-earth metal ion complexes of BTAC-A15C5 show that in accordance with the observed increase in fluorescence quantum yield, cation complexation of BTAC-A15C5 is also accompanied by the appearance of a new long-lived decay component with a cation specific fluorescence lifetime of 90-200 ps which exceeds that of the uncomplexed fluorescent probe by a factor of 1.2 to 3. Again, under conditions where complex formation is complete, a behavior as reported above for Ag^{I} is observed for the divalent ions, i. e., a second fast decay component is observed. For the monovalent ions, this species was not detectable with a reasonable confidence owing to the temporal resolution of the instrument. The fast time trace detected for Ca^{II}

amounts to 50 ps, respectively. In the low energy region of the spectrum, negative amplitudes are found for these species.

4.5.3 Excited-State Deactivation

Cation complexation in the donor part of ICT chromo- and fluoroionophores generally leads to a reduction in the chromophoric π system resulting in hypso- and hypochromic shifts. This behavior can be rationalized in the general framework of triad theory [255a, b] and the theory on linear conjugated systems [255c] as the step from a more asymmetric polymethinic character to a more asymmetric polyenic character.

The much less pronounced shifts in the emission spectra of the complexes point to a weakening of the cation nitrogen coordinative bond in the excited state. This can be understood on the basis of the charge redistribution taking place within the lifetime of the excited state leading to a radical cation-like donor fragment (see mechanistic considerations in Ch. 4.4.2). Thus, the cation-nitrogen coordinative bond is weakened due to electrostatic repulsion.

4.5.3.1 Cation Repulsion in the Excited State

The large Stokes shift of the cation complexes, especially for divalent ions (e. g., 11 510 cm^{-1} for the Ca^{II} complex, *Table 23*), suggests that absorbing and emitting species are different. In combination with the fast ICT process in these probes, this behavior indicates that the electrostatic repulsion between cation and crown nitrogen atom occurs parallel to the CT on the sub-ps time scale. Thus, the (red-shifted) emission spectrum measured does not correspond to the initially excited complex with strong ion-probe interaction (LM)* but to its successor (in terms of an excited-state reaction), a relaxed species with weaker cation-donor atom interaction. This is consistent with the time-resolved emission data, where a fast component is found as a decaying species in the high-energy part of the spectrum and as a rising species (rise time; negative amplitude) in the low-energy part. The lifetime of this species is relatively short, i. e., for instance, 50 ps for Ca^{II} or 55 ps for Ag^{I}, and the reconstructed spectra of both components overlap largely for all the cations studied (e. g., maximum at 580 nm for the 90 ps species and 584 nm for the 568 ps species in the case of Hg^{II}). But especially the last features, the strong spectral overlap implying a large Stokes shift for the fast decay component as well, do not favor attribution of this decay time to the initially excited (LM)*. However, due to limitations of the experimental setup, a faster and further hypsochromically shifted transient species could not be detected here for these metal ions.

4.5.3.2 Excited-State Reaction Mechanism of Model Systems

Thus, for a better understanding of the photophysics of the BTAC probes, it is helpful to consider related ICT probe systems studied by time-resolved absorption (on the sub-ps time scale) and emission spectroscopy and described in the literature.

Similar photophysical effects of cation complexation (in absorption and emission) as for the BTAC probes have been reported for DCS-A15C5 and DCM-A15C5 (see Appendix D for chemical structures) [77b, d, 96a-c]. For both probes, fast decay components have been found in the fluorescence decays recorded at the high-energy side of the complex' spectrum (e. g., 400 ps in the case of Ca^{II} and DCM crown; τ_f (fp) = 2.1 ns) [77d, 96b, c]. Furthermore, the sub-ps transient absorption measurements carried out by *Martin* et al. (for DCM-A15C5) and *Rullière* et al. (for DCS-A15C5) revealed that another species showing a strongly blue-shifted spectrum is involved in the excited state process on the fs time scale (< 2 ps for DCM-A15C5; similar lifetimes have been reported for DCS-A15C5) [77b, d, 96a-c]. The interpretation given by these authors can be summarized as follows.

Excitation leads to initial formation of (LM)* with strong cation-probe interaction followed by an ultrafast "internal dissociation" (< 700 fs for M^{n+}/DCM-A15C5) yielding the excited cation-probe contact pair (L*M). Reorientation of the solvation sphere finally leads to a ternary complex (L*/S/M) where the coordination site of the cation formerly inhabited by the crown nitrogen atom is now occupied by a solvent molecule (S) [96a-c]. The latter process occurs on the ps time scale and was found to depend on the coordinating ability of the cation, i. e., (L*/S/M) formation is observed in 2 ps for Li^{I}/DCM-A15C5 and 30 ps for Ca^{II}/DCM-A15C5, respectively [77b, d]. The fluorescence of this last species decays with a lifetime of ca. 1.9 ns (for the cation complexes of DCM-A15C5) and displays the spectral features of the steady-state emission spectrum.

4.5.3.3 Excited-State Reaction Mechanism of BTAC Complexes

Transferring this model scheme to the observations made here, for BTAC-A15C5 and BTAC-$AT_4$15C5 the following mechansim is anticipated.

Detection of locally excited (LM)* escapes the limited temporal resolution of the instrument and the fast decay component found in the case of Ca^{II}, Ag^{I}, and Hg^{II} is attributed to the loose contact pair (L*M). After reorientation in the ion's coordination sphere, the main emissive species (L*/S/M) is formed and emits with a characteristic lifetime of, e. g., 348 ps in the case of Ag^{I} (*Table 22,* p. 62), the value of the latter lifetime reflecting the coordinative strength of the cation best (τ_2 (Hg^{II}) >τ_2 (Ag^{I}), see logK_S values in *Table 22*, p. 62). The formation of an outer-sphere complex (i. e., complete cation ejection form the crown), a much slower process itself [77d], does not seem to be operative in these systems on this ps time scale (for excitation and emission of inner- and outer-sphere complexes cf. Ch. 6.5) [77b, d].

Behavior of Hg^{II}⊂BTAC-$AT_4$15C5. For this complex, two largely overlapping species with fluorescence lifetimes in the ns time range (568 and 1066 ps) and comparable amplitudes are found (for $DAS_i(\lambda)$ ratios see caption to *Fig. 40*, p. 63). However, evaluation of the global analysis results assuming a simple three-state reaction scheme (Appendix B) shows large deviations from 1 for extrapolation of the $SAS_i(\lambda)$ ratios according to eqns (82) and (83) into the high- and low-energy regions of the spectrum. Furthermore, the results obtained when assuming a parallel reaction mechanism deviate distinctly from 1 in the blue region as well [183]. Thus, another rearrangement in the complex during the excited-state lifetime (according to a consecutive reaction mechanism) can be excluded as well as the formation of two different loose complexes in a parallel reaction mechanism. Moreover, the

UV/Vis-spectrophotometric titrations revealed a constant decrease (increase) of the absorption band of the free probe (complexed probe) up to $x_{M/L} = 1$, suggesting only the formation of a 1:1 complex.

A possible explanation, which lacks experimental verification in this case (cf. footnote lxi, p. 62), is the occurrence of two ground state complexes in different conformations (a well-known fact for crown ether receptors, see discussion in Ch. 4.5.7 or 6.5.3). In such a case, when both complexes show largely overlapping bands, simultaneous excitation leads to two parallel (individual for each species) decoordination reactions on a similar time scale and hence four decay components could be expected. As already mentioned in footnote lxi (p. 62), analysis of the fluorescence decay curves employing four components improved the fit to a minor extent but did not yield reliable results concerning a possible model.

Another possible explanation involves a second chelating site in the chromophore, although its direct detection was not possible for BTAC-AT$_4$15C5⊂Hg^{II} employing optical spectroscopy (see Ch. 4.5.7 for discussion). Thus, the real nature of the dynamic emission behavior of the Hg^{II} complex(es) remain(s) obscure at present.

4.5.4 Complex Stability Constants and Spectroscopic Effects

4.5.4.1 Correlation of Cation-Induced Spectral Shifts and Charge Density

In the ground state, the size of the chelation-induced blue shift of the ligand absorption band reflects the reduction of the electron donating character of the nitrogen atom of the monoaza crown due to cation coordination. Thus, it depends on charge density and electron affinity of the cation bound, the strongest changes occuring here for Hg^{II} (BTAC-AT$_4$15C5) as well as for monovalent Na^{I} and divalent Mg^{II} (BTAC-A15C5; cf. resemblance of the absorption spectra of BTAC-H and the complexes in *Figures 39* and *42*, pp. 61, 63).

For BTAC-A15C5, the same order is found as has been reported for other probes such as DCS-A15C5, DCM-A15C5, and MAP-A15C5 [77a, 96a, c, 254]. The influence on the complexation-induced shifts in absorption decreases on the order of Mg^{II} > Ca^{II} > Sr^{II} > Ba^{II} >> Na^{I} > Li^{I} (> K^{I}) whereas for the stability constants of the complexes, the following order of Ca^{II} >> Sr^{II} > Ba^{II} > Li^{I} >> Na^{I} > K^{I} is observed (*Table 23*, p.64; In the case of Mg^{II}, logK_S could not be determined spectroscopically.).

The good correlation observed for a plot of the cation-induced spectral shifts $\Delta\tilde{\nu}_{cp\text{-}fp}$ (abs) and the complex stability constants logK_S vs. the so-called class A or ionic index (the ratio of charge and ion radius n^2/r^{n+} as a measure for electrostatic attraction) [253] shown in *Fig. 43* suggests that for a certain ICT probe both effects depend mainly on electrostatic interaction.

<u>*Behavior of Li^{I}.*</u> However, an exceptional behavior is observed for Li^{I} *(Fig. 43)*. Due to its higher charge density $\Delta\tilde{\nu}_{cp\text{-}fp}$ (abs) should be larger for Li^{I} compared to Na^{I}. Instead, the opposite is noticed. On the other hand, Li^{I} shows a higher complex stability constant than Na^{I}. This is in agreement with the *Pearson* hardness parameter [143b], but seems to contradict a second quantity affecting the stabilization of macrocyclic

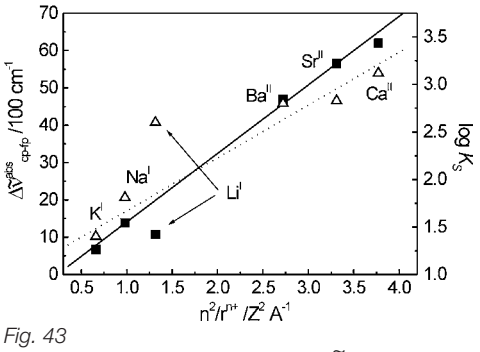

Fig. 43
Cation-induced shift in absorption $\Delta\tilde{\nu}_{cp\text{-}fp}$ (abs) (—, ■) and logK_S (·····, Δ) as a function of charge density (class A index) for BTAC-A15C5 and its alkali and alkaline-earth metal ion complexes in acetonitrile. Fits do not contain the values for Li^{I}.

complexes, the optimum fit of the ion bound into the cavity of the macrocyclic receptor [256]. Na^{I} (ionic diameter of 2.04 Å for a coordination number of 6) fits considerably better into the A15C5 cavity (1.7-2.2 Å) than Li^{I} (ionic diameter of 1.52 Å for a coordination number of 6) [249a]. This suggests that in the case of Li^{I}, coordination is most likely due to binding to the four macrocyclic oxygen atoms while the other two coordination sites of the cation are saturated with oxygen atoms of the counter ion and/or solvent molecules.

This is consistent with X-ray data of the alkali metal ion complexes of MAP-A15C5 reported by *Jonker* et al. where the distance between the nitrogen atom of the crown and the cation decreases on the order K^{I} > Li^{I} > Na^{I} [78b, 254]. Furthermore, extraction experiments carried out for 15C5 by *Iwachido* et al. revealed that 15C5⊂Li^{I} is extracted as a dihydrate (2.0 water molecules per complex molecule, four coordinative bonds to only four donor oxygens) whereas for 15C5⊂Cs^{I} coextraction of only 0.2 water molecules occurs [257]. For the alkaline-earth metal ions, all the tendencies discussed correlate well (spectral shifts, K_S values, n^2/r^{n+}), the enhanced K_S value for Ca^{II} compared to those for Sr^{II} and Ba^{II} stressing the optimum fit of this ion into the cavity of the receptor.

<u>*Empirical Correlation.*</u> The single factors governing the absolute values of logK_S for the Ph-A15C5 receptor unit in ICT probe molecules have been discussed by *Fery-Forgues* et al. for BOZ- and DCM-A15C5 [258]. The interplay between the degree of conjugation in the whole chromophore (orbital overlap between aniline nitrogen and aniline phenyl ring due to the twist between the fragments and/or pyramidalization at the nitrogen atom) and the inductive effect of the para substituent of the aniline moiety, i. e., the basic chromophore, accounts for the fact that correlation of complex stability, spectroscopic, and NMR data are not straightforward. However, this research group found an empirical relationship linking the Δ (Ca^{II}) shifts of the ^{1}H-NMR signals of the *ortho* and *meta* protons to the complex stability constants for a series of para substituted Ph-A15C5 derivatives [258]. Using this relationship (eqn (6)), a value of logK_S = 3.67 is calculated being in good agreement with the experimentally found value of 3.69 (*Table 23*, p. 64; for NMR data see *Tables 25* and *26*, pp. 72, 73).

$$\log K_S = 1.79(\pm 0.17) + 5.36(\pm 0.59)[\Delta(Ca^{II})_{ortho} - \Delta(Ca^{II})_{meta}] \qquad (6)$$

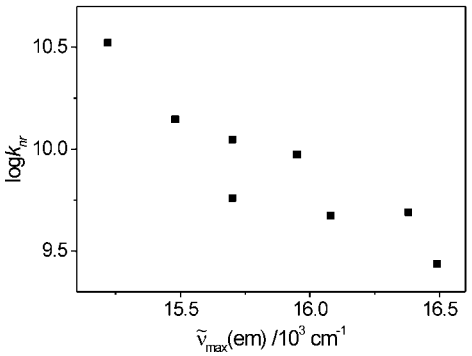

Fig. 44
Plot of $\log k_{nr}$ vs. $\tilde{\nu}$ (em) for BTAC-DMA, BTAC-A15C5, and BTAC-AT$_4$15C5 as well as the Na^I, K^I, Ca^{II}, and Sr^{II} complexes of BTAC-A15C5 and the Ag^I complex of BTAC-AT$_4$15C5 in acetonitrile. The complexes showing cation-induced peculiarities are omitted.

BTAC-AT$_4$15C5. Although the complex stability constant of BTAC-AT$_4$15C5⊂Ag^I is even larger than those observed for the divalent alkaline-earth metal ions (*Tables 22* and *23*, pp. 62, 64), the shift of 900 cm^{-1} found for Ag^I in absorption is rather small. This behavior stresses the high preference of Ag^I for sulfur donor atoms compared to nitrogen donor atoms which was found for other dithia diaza crown ethers as well [259]. In the case of Hg^{II} showing a stronger coordination to nitrogen donor atoms, the spectral shifts are much more pronounced.

4.5.4.2 Cation-Induced Fluorescence Enhancement

In Ch. 4.4, the fluorescence emission of D-A-chalcones in polar solvents has been attributed to the population of a highly polar, single bond-twisted transient species A* (twisted anilino bond) during the lifetime of the excited state (with possible competition of non-emissive K* state formation, Ch. 4.4.2.3). Moreover, involvement of a non-emissive P* state (twisted double bond) has been found to be of minor importance for the BTAC derivatives (Ch. 4.4.2.1). Accordingly, as in the free probes, the single bonds are unbridged in the complexes and thus population of A* (and K*) should be possible. Moreover, under the assumption that rotation around the double bond (towards P*) is negligible, the bulkiness of the complexed receptor should slow down rotational motions around all single bonds to a comparable degree. Having in mind the correlation of emission band maximum and rate constant of radiationless deactivation for the BTAC derivatives in polar solvents (*Fig. 38*, p. 59), i. e., a decrease in fluorescence quantum yield and lifetime is mainly connected to the S_1-S_0 energy gap and k_{ic}, the free and complexed probes should show a comparable correlation. Indeed, such a correlation can be derived from *Fig. 44*. Under the assumption, that the influence of all the other possible excited-state deactivation routes is negligible, this leads to the conclusion that the cation-induced fluorescence enhancement can be predominantly attributed to a change of the donor strength and does not seem to involve the blocking off or slowing down of excited-state reactions connected with a specific rotational motion.

4.5.5 Comparison of BTAC-AT$_4$15C5 and BTAC-A15C5

Upon exchanging the macrocyclic sulfur heteroatoms for oxygen, the negative charge on the heteroatom increases and thus the electrostatic attraction between the heteroatom and the "hard" alkali or alkaline-earth metal cation via ion-dipole forces is enhanced resulting in complexation of these ions. On the contrary, for soft Ag^I and Hg^{II} (with a high class B or covalent index) the effects are opposite, i. e., less electrostatic but rather covalent bonding is involved, especially with the nitrogen atom[lxv] [249b].

The considerably higher complex stability constants found for Ag^I and Hg^{II} support the spectroscopic results, i. e., these ions are more tightly bound than main group metal ions by the A15C5 receptor resulting in cation-induced photophysical effects already at lower ion concentrations [122a, 199a, 201].

Both observations clearly reflect the different binding constants and cation selectivities of the two macrocyclic receptors A15C5 and AT$_4$15C5 and thus demonstrate the crucial effect of the choice of an appropriate receptor for the design of cation-selective fluorescent probes.

4.5.6 Comparison with Other ICT Fluorescent Probes

The other ICT probes of comparable type investigated so far can be divided into two groups according to their ionic nature, i. e., positively charged [90, 91, 93, 94, 104c] (styryl or stilbazolium dyes) and neutral probes [72, 76, 77, 80, 84, 96]. Whereas for the former type usually smaller cation-induced shifts in absorption and emission are observed the effects are comparable to those of the BTAC crowns in the case of the latter.

On the other hand, nearly all of the probes studied so far show complexation-induced quenching. As an example, a decrease in fluorescence quantum yield of a factor of 2.7 was reported for the Ca^{II} complex of DCM-A15C5. Moreover, the effects on the fluorescence lifetime are considerably small and binding to Ca^{II} leads to a reduction by 12 % (maximum value observed for M^{n+}⊂DCM-A15C5) [77a, b, d]. In the case of the Ca^{II} complex of DCS-A15C5, the decrease in both ϕ_f and τ_f is even more pronounced [96a-c].

An increase in both fluorescence quantum yield and lifetime has only been reported for very few ICT fluorescent probes [76, 93d, 94], for instance, for related BOZ-A15C5 (factor of 2 in ϕ_f and 160 % increase in τ_f) [76]. Accordingly, the cation-induced fluorescence enhancement factors of 2-8.5 along with the cation-specific increase in fluorescence lifetime of 140-630 % render the crowned BTAC derivatives a powerful example of ICT fluorescent probes. Moreover, this is strikingly stressed by the fact that these features are preserved upon complexation to the well-known fluorescence quencher Hg^{II}.

---

lxv) Accordingly, the addition of Ag^I to BTAC-A15C5, even at a high excess, does not yield any measurable spectral changes. *Létard* et al. described similar effects for the complexation of Ag^I to a D-A-substituted fluorescent probe with an A15C5-receptor in acetonitrile [96a]. Even for lariat ethers, where a methylene spacer between the phenyl ring and the A15C5 receptor allows an encapsulation of Ag^I, the complex stability constants in acetonitrile reported for Li^I and Na^I were at least 10- and at most 100-times higher than those reported for Ag^I [260]. Strong coordination of Ag^I ions by solvent molecules is the main reason for this behavior in acetonitrile [261].

4.5.7 Nature of the Complexes

For a more detailed understanding of the spectroscopic behavior of BTAC-A15C5⊂Mg^{II} and the interfering reactions of some heavy and transition metal ions, the complexation behavior of other D-A-chalcones were investigated and compared to those mentioned above. When taking a closer look at the fluorescent probes carrying a benzothiazole acceptor, complex formation at a second coordination site in the acceptor part of the molecule is possible *(Scheme 11)*. In such a case, a bidentate chelate with a 5-membered ring structure could be formed involving the oxygen atom of the carbonyl group and either the sulfur or the nitrogen atom of the benzothiazole ring (cf. *syn / anti* stereoisomerism discussed in Ch. 4.4.2.2).

The experiments described in the following part of this chapter include steady-state absorption and emission measurements of Mg^{II}, Hg^{II}, Cu^{II}, protons and BTAC-DMA, BTAC-OCH_3, BTAC-H, PAC-A15C5, PAC-DMA, PAC-H, QAC-DMA, and 2-acetylbenzothiazole as well as ^{1}H-NMR investigations of BTAC-A15C5, BTAC-DMA, QAC-DMA, as well as their Mg^{II} and Ca^{II} complexes (in Ch. 4.5.7.2).

4.5.7.1 Absorption and Fluorescence Spectroscopy

At $x_{M/L} \leq 5$, no effects are found for ions such as Zn^{II}, Ni^{II}, or Pb^{II} and only at higher concentrations a behavior similar to that of the "red" Mg^{II} complex is observed. In order to introduce the possible coordination sites for the single derivatives, a short list is given here (the capital letter in brackets denotes all possible coordination routes according to *Scheme 11*): BTAC-DMA (B,C), BTAC-OCH_3 (B,C), BTAC-H (B,C), 2-acetylbenzothiazole (B,C), QAC-DMA (B), crowned BTAC derivatives (A,B,C), PAC-A15C5 (A). Moreover, for PAC-DMA and PAC-H, no complex formation according to routes A, B, C is possible and only loose coordination of an ion to the carbonyl oxygen atom can occur.

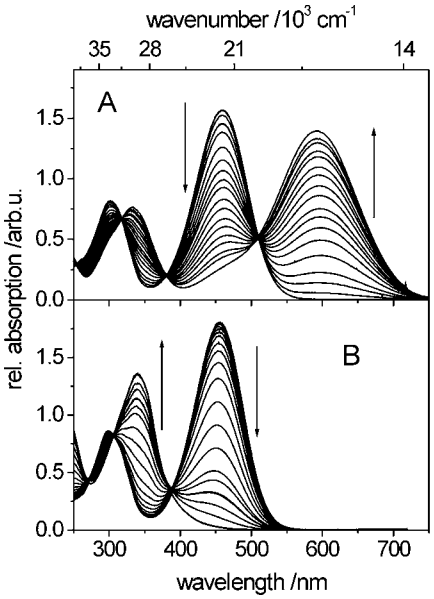

Fig. 45
*UV/Vis-spectrophotometric titration spectra of BTAC-DMA (**A**) and BTAC-$AT_4$15C5 (**B**) with Hg^{II} perchlorate in acetonitrile (c_L = 9 x 10^{-6} M, Hg^{II} addition in the range of 0.04 ≤ $x_{M/L}$ ≤ 20 (BTAC-DMA) and 0.008 ≤ $x_{M/L}$ ≤ 20 (BTAC-$AT_4$15C5)).*

Figure 45 combines the UV/Vis-spectrophotometric titration spectra of BTAC-$AT_4$15C5 and BTAC-DMA with Hg^{II}. The absorption spectra of BTAC-DMA, PAC-DMA, PAC-A15C5, and QAC-DMA in the presence of a large excess of Mg^{II} are displayed in *Fig. 46*, p. 70 and *Table 24* contains other relevant spectroscopic data.

As follows from the titrations shown in *Fig. 45*, the shifts induced by Hg^{II} are clearly different for BTAC-DMA and BTAC-$AT_4$15C5 suggesting a second coordination site being operative in these derivatives. Furthermore, from *Table 24* follows that protonation of both BTAC derivatives leads to

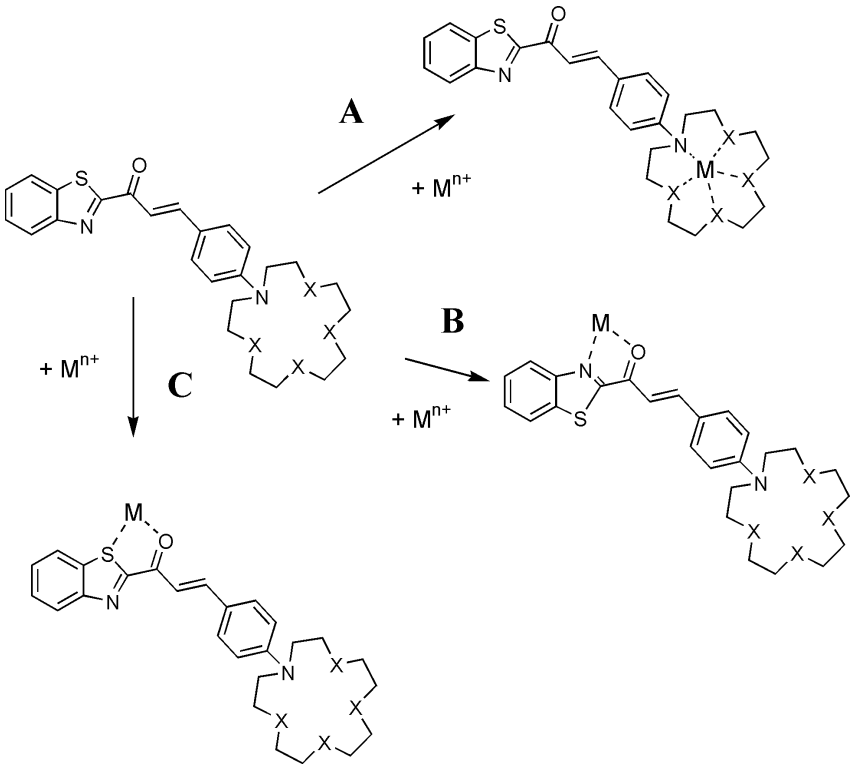

Scheme 11
*Possible coordination sites in D-A-chalcones containing a benzothiazole acceptor and a monoaza crown ether donor. Formation of the ion-macrocycle complex (route **A**), a N,O-chelate (route **B**) or a S,O-chelate (route **C**) (formation of a 5-membered S,O-chelate (route C) is considered as being more or less only theoretically possible).*

similar hypsochromic shifts, i. e., abstraction of the nitrogen lone electron pair upon protonation results in an absorption band resembling that of BTAC-H. The appearance of a new absorption band for BTAC-DMA⊂Hg^{II}, shifted into the opposite direction (bathochromic shift) as for the crowned complex indicates an increase of the intramolecular charge transfer pointing to a higher strength of the acceptor for this complex. Moreover, the electronic nature of the Hg^{II} ion (closed-shell d^{10} configuration) and the high molar absorptivity of the red-shifted band ($\varepsilon \sim 31\,000\ M^{-1}\ cm^{-1}$) exclude any coordination of Hg^{II} to the DMA nitrogen atom or ligand field transitions. Formation of an acceptor-based chelate is further supported by comparison of the protonation and Hg^{II} complexation data of BTAC-DMA and BTAC-OCH_3, a similar D-A-chalcone with a weaker donor. At the acid concentration employed (0.1 M $HClO_4$), no protonation occurs at the benzothiazole nitrogen atom and thus in the absence of a nitrogen containing amino group, no hypsochromic shifts are observed for BTAC-OCH_3. In contrast, addition of Hg^{II} induces very similar bathochromic shifts of 4 900 cm^{-1} for both compounds *(Table 24)*. Obviously, complexation to the acceptor part increases its strength and correspondingly shifts the $S_0 \rightarrow S_1$ transition to lower energies (stronger ICT character).

These findings are in good agreement with the results obtained for the main group metal ion Mg^{II} and various D-A-chalcone derivatives. A closer look at *Fig. 46* suggests that the appearence of the red-shifted band is predominantly connected to the presence of a heteroatom in the aromatic acceptor part of the chalcones. QAC-DMA, mimicking closely the M^{n+}-favored chelating reagent 8-HQ (see Appendix D for chemical structure) shows the most pronounced effect, i. e., the largest increase in the red-shifted band and correspondingly, the largest decrease of the free dye's absorption band (reduced to ca. $^1/_5{}^{th}$ of the initial intensity) [51, 262]. Additionally, the bathochromic shift observed is the strongest for this series of D-A-chalcones (4 940 cm^{-1}). The second most pronounced effect is seen for BTAC-DMA, carrying the benzothiazole moiety with a heterocyclic nitrogen atom showing reduced basicity compared to the quinoline nitrogen atom and hence, being a weaker coordination site in a chelate [263]. In the case of the absence of a heterocyclic nitrogen atom in PAC-DMA and PAC-A15C5 (phenyl ring as acceptor), only coordination to the carbonyl oxygen atom can induce a bathochromic shift. The absorption spectra recorded for the complex of PAC-DMA indicate that coordination of Mg^{II} to the carbonyl group has an effect in absorption. However, this

Table 24
Spectroscopic properties of some D-A-chalcones in acetonitrile in the presence of Mg^{II}, Hg^{II}, and H^+.

	$\tilde{\nu}$ (abs)^{blue}	$\tilde{\nu}$ (abs)^{red}	$\tilde{\nu}$ (em)	$\Delta\tilde{\nu}_{cp\text{-}fp}$ (abs)^{blue}	$\Delta\tilde{\nu}_{cp\text{-}fp}$ (abs)^{red}	rel. fluo. [a]
	$10^3\ cm^{-1}$	$10^3\ cm^{-1}$	$10^3\ cm^{-1}$	cm^{-1}	cm^{-1}	
BTAC-$AT_4$15C5 [b]		21.98	15.70	-	-	-
⊂Hg^{II}	29.3	-	17.00	7320	-	E
BTAC-A15C5 [b]		21.69	15.48	-	-	-
⊂Mg^{II}	28.68	17.30	16.81	6990	-4390	E
⊂Hg^{II}	30.20	16.83	-	8510	-4860	-
BTAC-DMA		21.83	15.22	-	-	-
⊂Mg^{II}	-	17.45	-	-	-4380	-
⊂Hg^{II}	-	16.83	-	-	-5000	-
H^+	30.30	-	19.61	8470	-	Q
BTAC-H [c, d]		29.67	23.29	-	-	-
BTAC-OCH_3 [e]		27.10	19.61	-	-	-
⊂Hg^{II}	-	22.22	-	-	-4880	-
PAC-A15C5		24.27	18.50	-	-	-
⊂Mg^{II}	31.54	(21.19)	18.76	7270	(-3080)	Q
PAC-DMA [f]		24.51	18.45	-	-	-
⊂Mg^{II}	-	21.19	-	-	-3320	-
QAC-DMA [f]		23.09	15.62	-	-	-
⊂Mg^{II}	-	18.15	-	-	-4940	-

[a] in the case of the relative fluorescence an "E" denotes enhancement and a "Q" denotes quenching;

[b] the effects observed for protons are similar to those of BTAC-DMA;

[c] the effects observed for PAC-H are similar;

[d] no effects observed for Mg^{II}, Hg^{II}, H^+;

[e] no effects observed for H^+;

[f] the effects observed for protons and Hg^{II} are similar to those of BTAC-DMA, in the case of Hg^{II} only stronger for QAC-DMA and weaker for PAC-DMA

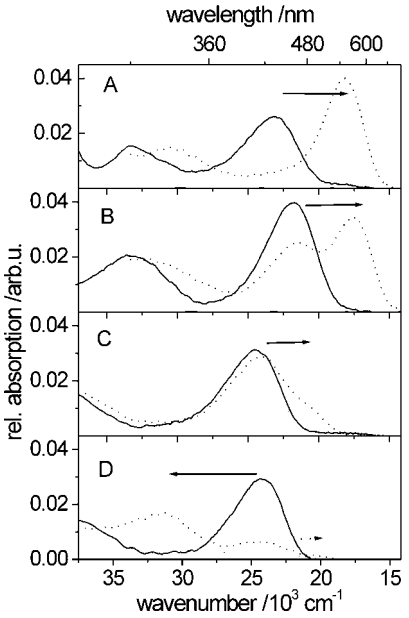

Fig. 46
*Steady-state absorption spectra of QAC-DMA (**A**), BTAC-DMA (**B**), PAC-DMA (**C**), and PAC-A15C5 (**D**) in the absence and the presence of a high excess of Mg^{II} ($x_{M/L}$ = 85 000, c_L = 1 x 10^{-6} M). The thick solid line resembles the free dye, the dotted line the spectrum in the presence of Mg^{II}. The thin solid lines describe the single components. The spectra were fitted by modeling the band of the free dye and including one (or two in the case of PAC-A15C5) additional band(s) as lognormal function(s). In the case of PAC-A15C5 and Mg^{II}, a weak shoulder at the low-energy edge of the absorption band was also found at this high excess of cation. The arrows denote the shifts observed.*

effect is rather weak because the formation of a stabilizing bidentate chelate is not possible. Furthermore, introducing a crown in this simple chalcone structure (PAC-A15C5) yields the "normal" complexation behavior observed for the other alkaline-earth metal ions and BTAC crowns, i. e., a cation-induced hypsochromic shift of the absorption band. Only a very weak red-shifted shoulder is seen in the spectrum of PAC-A15C5⊂Mg^{II}.

The same holds true for other heavy and transition metal ions such as Zn^{II}, Ni^{II}, and Pb^{II} as was already mentioned at the beginning of this subchapter. Here, generally lower cation concentrations are required to induce similar effects as discussed for Mg^{II}. This correlates well with the generally higher complex stability constants of these ions in chelates of such a type [18, 262-264] (This is also expressed by the relatively high class A or ionic index of these ions, *Table 23*, p. 64.). Moreover, as in the case of BTAC-A15C5⊂Mg^{II}, excitation in the low-energy absorption band does not yield a measureable fluorescence for any of the complexes studied here.

Chalcones Lacking a Donor. For BTAC-H, 2-acetylbenzothiazole, and PAC-H, no spectroscopic changes are observed in any case. However, this does not imply that no chelate formation occurs but a possible product is not spectroscopically detectable. Here, like in many other complexes of diamagnetic (main) group metal ions, the absorption and emission spectra of the possible complexes should closely resemble those of the free ligand [32b].

Hg^{II} Revisited. Returning once more to the remarkable time-resolved emission behavior of BTAC-$AT_4$15C5⊂Hg^{II}, i. e., the occurence of at least three decay components, coordination in the acceptor part of the complex by a second ion or the formation of complexes of higher order are possible. Considering both the titration spectra given in *Fig. 45*, p. 68 and the facts mentioned in the preceeding paragraph on BTAC-H, such species should escape a UV/Vis-spectrophotometric detection[lxvi]. Moreover, when comparing the relative amplitudes[lxvii] found in a time-resolved fluorescence experiment for the 1.1 ns component at $x_{M/L}$ = 1 and $x_{M/L}$ = 10, the values of 0.48 ($x_{M/L}$ = 1) and 0.42 ($x_{M/L}$ = 10) indicate no drastic changes[lxviii]. Since no fluorescence of the "red" complex was detected in any case *(Table 24)*, these complexation studies could not clarify the time-resolved emission behavior of BTAC-$AT_4$15C5⊂Hg^{II} described in Ch. 4.5.3.3.

Complexation Involving Cu^{II}. The behavior of Cu^{II} ions led to some additional studies involving Ph-$AT_4$15C5 and Ph-A15C5. Upon addition of Cu^{II}, the absorption spectrum of the former compound is changed drastically and instead of the two lowest transitions at 38 500 cm^{-1} (ε ~ 17 800 M^{-1} cm^{-1}) and 33 100 cm^{-1} (ε ~ 2 200 M^{-1} cm^{-1}) in free Ph-$AT_4$15C5, bands centered at 38 700 cm^{-1} (m), 29 100 cm^{-1} (m), 23 000 cm^{-1} (m), and 17 600 cm^{-1} (w) are found in acetonitrile, respectively[lxix]. In accordance with other data published on the electronic spectra of Cu^{II}-thioether coordination compounds, the two low-energy bands are assigned to σ(S)→Cu LMCT as well as (possibly superimposed) π(S)→Cu LMCT and/or d-d* ligand field transitions. For $AT_4$15C5, *Westerby* et al. reported bands at 24 100 cm^{-1} (ε = 6 100 M^{-1} cm^{-1}) and 17 800 cm^{-1} (ε = 1 900 M^{-1} cm^{-1}) [265a] and in comparable crown ethers, the σ(S)→Cu LMCT transitions are located at 24 100 cm^{-1} (ε = 8 000 M^{-1} cm^{-1}; $T_4$15C5 and ε = 7 000 M^{-1} cm^{-1}; $T_5$15C5) [265b], 27 400 cm^{-1} (ε = 6 000 M^{-1} cm^{-1}; $AT_3$14C4) [265a], 25 500 cm^{-1} (ε = 2 500 M^{-1} cm^{-1}; $A_2T_4$18C6) [266], and the weaker transitions at 17 700 cm^{-1} (ε = 1 100 M^{-1} cm^{-1}; $T_4$15C5) [265b], 17 700 cm^{-1} (ε = 2 000 M-1 cm-1; T515C5) [265b], 18 200 cm^{-1} (ε = 1 000 M^{-1} cm^{-1}; $AT_3$14C4) [265a], and 16 300 cm^{-1} (ε = 202 M^{-1} cm^{-1}; $A_2T_4$18C6) [266]. The latter band centered at ca. 17 200 cm^{-1} is assigned to various transitions of π(S)→Cu LMCT and/or d-d* ligand field type[lxx] by different authors for certain complexes [267]. Although theoretical considerations predict that changes in the coordination sphere, e. g., going from tetragonal to tetrahedral coordination, result in bathochromic shifts [267a, b] only a minor dependence of the band's position on complex geometry was found [265b, 266, 268, 269a, b]. Furthermore, such

lxvi) In the case of BTAC-DMA and Hg^{II}, analysis of the titration spectra given in *Fig. 45* yielded acceptable fits for a 1:1 model (according to eqn (57)) with a logK_S of 5.0.

lxvii) $a_{rel}(3) = a(3) / (a(2) + a(3))$ with the 0.5 ns (1.1 ns) decay component as species 2 (3)

lxviii) Note that excitation between 330 and 370 nm is not possible with the ps-LIF setup employed thus limiting fluorescence decay studies as a function of excitation wavelength to a great extent in this case. In the experiments reported here, no pronounced trends in the relative amplitudes of the decay components were observed. Furthermore, the lifetimes are similar (within experimental error) for both $x_{M/L}$.

lxix) The spectra were fitted to multiple gaussian peak functions and the molar absorptivities were only roughly determined by fitting two spectra: (s) denotes strong (> 5 000 M^{-1} cm^{-1}), (m) medium (5 000 M^{-1} cm^{-1} > x > 1 000 M^{-1} cm^{-1}), and (w) weak bands (< 1 000 M^{-1} cm^{-1}); "ε ~ xy" indicates determination from two measurements.

lxx) Due to the small overlap between sulfur π orbitals and Cu^{II} d orbitals, π(S)→Cu LMCT transitions are generally weaker than σ(S)→Cu LMCT transitions [267a].

a change in coordination sphere, induced for example upon substitution of a hydrogen atom at the macrocyclic nitrogen donor by an alkyl or aryl group, is reflected by a change in the intensity of the band [266, 269a, b].

With this knowledge in mind, the spectral contours of a UV/Vis-spectrophotometric titration of BTAC-$AT_4$15C5 with Cu^{II} were followed in order to characterize the species formed. Due to the strong overlap of Cu^{II}-thioether or Cu^{II}-amine bands with those of the chromophore, assignments of the higher-energy absorption bands were not possible. Up to $x_{M/L} = 1$, the bands of the free probe (33 200 cm^{-1} and 21 900 cm^{-1}) are diminished and new bands at 31 900 cm^{-1} (s) and 16 700 cm^{-1} (m) are observed[lxxi]. In the course of the titration, these bands decrease and the bands at 23 900 cm^{-1} (ε = 2 400 M^{-1} cm^{-1}) and 18 100 cm^{-1} (ε = 2 000 M^{-1} cm^{-1}) (at full complexation) build up. Having in mind the discussion on acceptor chelate formation (band centered at 16 900 cm^{-1} for Hg^{II}) and the previous paragraph about sulfur-Cu^{II} transitions, partly consecutive, partly parallel formation of a chelate and a macrocyclic inclusion complex is anticipated. This is further supported by the comparatively low complex stability constant of $\log K_S$ = 3.86 for $AT_4$15C5⊂Cu^{II} [265a]. Accordingly, both reactions, binding to the donor and thus weakening its strength as well as coordination to the acceptor, result in a very complex photophysical behavior.

The situation is even more complicated for BTAC-DMA and Cu^{II}. Here, in a complexometric titration, four different regions are observed, i. e., $x_{M/L} \leq 0.5$, $0.5 < x_{M/L} \leq 1$, $1 < x_{M/L} \leq 3$, and $3 < x_{M/L}$[lxxi]. For the first two regions, the typical chelate band at ca. 16 700 cm^{-1} is observed again, but upon further increasing the Cu^{II} concentration, a band at 30 800 cm^{-1} and several strongly overlapping bands exemplified by various shoulders in the range of 28 600 cm^{-1} to 14 300 cm^{-1} were found. Although the results obtained for Ph-A15C5 and PAC-DMA point to coordination of Cu^{II} to the DMA group, assignment of any of these bands was impossible for BTAC-DMA due to their strong overlap. For Ph-A15C5 and PAC-DMA, bands of comparable intensity are found at 20 900 cm^{-1} (Ph-A15C5) and 21 200 cm^{-1} (PAC-DMA), respectively, suggesting coordination to the anilino nitrogen atom. Moreover, no effects were found in a UV/Vis-spectrophotometric titration of PAC-H and BTAC-H with Cu^{II}.

Titrations performed with BTAC-OCH_3 (donor does not contain a nitrogen atom) and Hg^{II} as well as Cu^{II} support these findings. In both cases, sharp isosbestic points are observed and both the decrease as well as increase of the bands at 27 100 cm^{-1} and 22 200 cm^{-1} are similar for both ions. Here, no other coordination site interferes in the Cu^{II} titration.

In summary, comparing the molar absorptivities and size of the hypso- and bathochromically shifted absorption bands of the Hg^{II} (*Fig. 45*, p. 68) and Cu^{II} complexes of BTAC-$AT_4$15C5 and BTAC-DMA, respectively, it is obvious that Hg^{II} coordinates (mainly) to the donor in the former and to the acceptor in the latter but Cu^{II} shows mixed coordination for both compounds, possibly involving rearrangements of the complexes.

Complexation Involving Cu^{I}. Apparently, Cu^{I} induced no spectral shifts for any of the chalcone derivatives studied. However, in the case of BTAC-$AT_4$15C5, complexation is anticipated but lacks spectroscopic detection. For several other polythia crown ethers, Cu^{I} complexation was observed the complex geometry preferably being a tetrahedral geometry [251]. *Corfield* et al. observed tetrahedral coordination for $T_5$15C5⊂Cu^{I} with the remaining fifth sulfur donor atom lacking any binding to the central ion [265c]. Even for macrocyclic dithia diaza ligands of different ring sizes, exclusive thioether coordination of Cu^{I} was reported [269c]. With respect to BTAC-$AT_4$15C5 this suggests, that complexation occurs but no shifts are detectable due to the absence of Cu^{I}-nitrogen interaction[lxxii]. Furthermore, the possibilities to detect any Cu^{I}-thioether MLCT transitions in the absorption spectrum are poor because such bands appear in the region of 43 500-33 300 cm^{-1} [270], strongly overlapping with the intense absorption of the organic probe molecule.

Complexation Involving Other Ions. It is noteworthy that the presence of only a single nitrogen in the receptor sufficiently prevents complexation of those transition metal ions which show pronounced preference for nitrogen donor atoms, e. g., Zn^{II} and Ni^{II}. In the case of a diaza dioxa crown ether with adjacent alkylated nitrogen atoms, *Lindoy* et al. found in an X-ray diffraction study that the Zn^{II} ion is even situated on the outside of the crown ether and only coordinates to the two nitrogen atoms in a large ring, quasi chelate-like structure [271]. Thus, with the receptors employed in the D-A-chalcone fluorescent probes, complexation of these ions is not enhanced by a macrocyclic effect [272]. Furthermore, this is exemplified by the absence of a blue-shifted band for BTAC-DMA in the prescence of these ions.

In the case of BTAC-$AT_4$15C5, complexation to Pb^{II} is not favored despite the high class B index of this ion (*Table 22*, p. 62) [253]. Instead, the exchange of oxygen for sulfur donor atoms leads to enhanced binding selectivities for the “soft” metal ions Ag^{I} and Hg^{II} compared to Pb^{II}, possessing borderline character [143a, 273]. Similar observations have been made for a large number of mixed mono- or diaza polyoxa/thia crown ethers [123b, 274]. Here, in all cases, binding to Pb^{II} (as well as Cd^{II} and Co^{II}) is much weaker than complex formation with Cu^{II} and Ag^{I} [123b]. Furthermore, only in the case of Pb^{II}, alkylation of the nitrogen donor atoms resulted in a significantly lower complex stability constant [123b].

The lack of formation of a bidentate chelate (5-membered ring) in the case of the other alkaline-earth metal ions can be rationalized in terms of the complexation behavior of 8-HQ. This reagent forms a bidentate complex (5-membered ring) with Mg^{II} which shows a much higher complex stability constant than all the other alkaline-earth metal ions complexes [264].

Similar effects, i. e., complexation-induced red shifts in absorption upon coordination to a carbonyl group in the acceptor part of a molecule, have been observed for coumarin- [86c] and flavonol-based [275] fluorescent probes.

4.5.7.2 NMR Spectroscopy

In order to verify the results obtained with optical spectroscopy and to get more information about the chemical structure of the above mentioned complexes, ^{1}H-NMR spectra of

lxxi) Note that these regions are not defined by sharp isosbestic points indicating mixed complex formation.

lxxii) The shifts observed for Ag^{I} are already comparatively small, see *Table 22*, p. 62.

BTAC-DMA, QAC-DMA, and PAC-DMA were recorded in the absence and presence of Mg^{II} and Ca^{II} perchlorates in CD_3CN, respectively. In contrast to optical spectroscopy, complex formation and dissociation are comparably fast on NMR time scale and thus, the chemical shifts measured are only average values. Also, the additionally observed shifts are not directly related to the strength of the complex formed.

A prerequisite for any structural statement on the complexes is the unequivocal assignment of the signals for the free chalcones. The alternating electron density between the carbonyl and DMA group, the characteristical splitting of the signals of the CH-α and CH-β group ($^3J_{a,\beta}^{trans}$ = 16 Hz) and the AA'XX'-system of the aromatic *o*- and m-protons facilitated this assignment. In the case of the heterocyclic acceptors BT and Q, additional COSY spectra were recorded, and for the quinoline system, long range coupling ^5J of the protons H-4 and H-8 induced a cross peak. Thus, definite assignment of the signals was possible in all cases and coupling constants as well as splitting patterns found correlate well with literature data [189b].

For the complexation experiments, Mg^{II} ions were added in a 180-fold excess (c_L = 1.5 x 10^{-3} M) and the additional chemical shifts ($\Delta = \delta_{cp} - \delta_{fp}$; Δ-shifts) measured are given in *Table 25*.

The Δ-shifts are comparatively small for PAC-DMA, but especially in the case of QAC-DMA, strong shifts to lower field are observed for the aromatic protons adjacent to the quinoline nitrogen atom, i. e., H-3, H-4, and H-6. This fact supports the proposed formation of a bidentate acceptor N,O-chelate (5-membered ring chelate). However, BTAC-DMA⊂Mg^{II} does not show such pronounced shifts of the BT protons. Here, only the proton signals of H-α and H-β of the -CO-CH=CH-fragment are shifted into opposite directions suggesting dominant interaction of Mg^{II} and the carbonyl oxygen atom. Having in mind the results obtained for PAC-DMA (less changes upon addition of Mg^{II}) and the effects measured with optical spectroscopy (*Fig. 46,* p. 70), this explanation is contradictory. In such a case, i. e., coordination only to the carbonyl group, the adjacent electrophilic BT moiety should decrease the electron density at the oxygen atom and should thus deactivate the coordinating ability of the carbonyl group in BTAC-DMA compared to PAC-DMA (and hence, the shifts in both, ^{1}H-NMR and absorption spectra should be more pronounced for PAC-DMA).

In contrast to this, another explanation is anticipated. Complex formation in BTAC-DMA is possible without further rotation of the BT moiety (*syn* conformation of the N,O-chelate, low barrier for rotation), but the quinoline ring in QAC-DMA has to adopt the less favored *syn* conformation prior to complexation (in the *anti* conformation, the steric hinderance of H-3 and H-α is minimized). Accordingly, the same coordination (N,O-chelate) takes place in BTAC-DMA and QAC-DMA, but the additional conformational reorientation induces stronger shifts for QAC-DMA.

The other important complexation site for Mg^{II} in BTAC-A15C5, the monoaza crown ether receptor, was characterized by ^{1}H-NMR spectroscopy as well. Here, a comparison of the data presented in *Table 26* and *Fig. 47* for the Mg^{II} and the Ca^{II} complex provide additional evidence for a second, "normal" coordination site in BTAC-A15C5⊂Mg^{II}. For both,

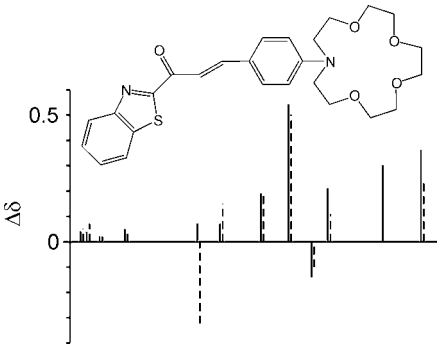

Fig. 47
Graphical representation of the Δ-shifts induced by Ca^{II} (solid line) and Mg^{II} (dashed line) at the corresponding proton positions of BTAC-A15C5 (for experimental conditions, see Table 26).

Mg^{II} and Ca^{II}, drastic shifts are observed for the signals of the methylene groups of the crown ether moiety (with opposite signs for the methylene group adjacent to the nitrogen atom) and for those of the aromatic protons in o-position but in the case of Ca^{II}, only minor shifts are observed for the vinylenic protons (with an opposite sign for H-α, s. *Fig. 47*).

In accordance with the absorption effects, addition of Mg^{II} produces again the above described Δ-shifts for H-α and H-β suggesting the presence of two active binding sites in BTAC-A15C5, the crown ether moiety and the N,O-chelate. However, some of the signals are broadened for BTAC-A15C5⊂Mg^{II} indicating slow exchange kinetics.

As has been mentioned before, coordination according to route C (*Scheme 11*, p. 68), i. e., the formation of an S,O-chelate (a chelate with one "soft" and one "hard" donor atom) is not likely to occur for these D-A-chalcones.

Before discussing some analytical aspects, the results of the complexation experiments are briefly summarized. Both fluorescent probes investigated show the expected cation selectivities for complexation at the crown ether receptor, i. e., BTAC-$AT_4$15C5 binds to thiophilic cations and BTAC-

Table 25
^{1}H-NMR chemical shifts δ (ppm from TMS) of BTAC-DMA, QAC-DMA, and PAC-DMA and the respective Mg^{II}-induced shifts Δ (ppm; solvent - CD_3CN, counter ion - perchlorate, c_L = 1.5 x 10^{-3} M, c_{Mg} = 0.27 M; D, A denote molecular fragments).

		BTAC-DMA		QAC-DMA		PAC-DMA	
Position		δ	Δ	δ	Δ	δ	Δ
D	DMA	3.047	0.035	3.035	0.084	3.012	-0.001
	ortho	6.778	0.027	6.791	0.051	6.756	-0.003
	meta	7.680	0.060	7.689	0.155	7.617	0.008
	a	7.997	0.126	8.289	0.056	7.716	0.034
	b	7.800	-0.175	7.886	0.026	7.464	-0.005
A	2	-	-	-	-	8.027	0.000
	3	-	-	8.189	0.388	7.516	-0.014
	4	8.197	0.040	8.434	0.314	7.595	0.013
	5	7.575	0.047	8.004	0.129	-	-
	6	7.630	0.048	7.710	0.106	-	-
	7	8.104	0.047	7.859	0.099	-	-
	8	-	-	8.243	0.230	-	-

A15C5 to the "hard" main group metal ions. Complexation in the donor part of the molecule leads to the well-known shifts in both absorption and emission for these typical ICT probes. But in contrast to the great majority of ICT probes, both crowned BTAC derivatives show a cation-induced increase in both fluorescence quantum yield and lifetime, the latter resulting in a cation-specific lifetime of the complex. Analytically even more valuable is the fluorescence enhancement for BTAC-AT$_4$15C5 in the presence of the well-known fluorescence quencher Hg^{II}. Here, the excited-state deactivation behavior of the complex is more complicated possibly involving different ground state conformers or complexes of mixed stoichiometry. For the alkali and alkaline-earth metal ion complexes of BTAC-A15C5 and the Ag^{I} complex of BTAC-AT$_4$15C5, fast decoordination in the excited state leads to formation of a loose complex as the main emitting species. Finally, for some heavy and transition metal ions and various BTAC derivatives, N,O-chelation occurs at the benzothiazole-carbonyl acceptor leading to a non-fluorescent, bathochromically absorbing species.

4.6 Analytical Applications

Potential analytical applications could be directly derived from the selectivities and spectroscopic properties discussed so far. Due to the enhanced selectivity of its receptor, BTAC-AT$_4$15C5 is a promising candiate for Ag^{I} and Hg^{II} detection.

The formation of well-defined complexes[lxxiii] is reflected by a simple relationship of fluorescence (or absorption) signal and metal ion concentration and leads to linear calibration graphs (shown for a fluorometric titration of Ag^{I} in *Fig. 48*).

Table 26
^{1}H-NMR chemical shifts δ (ppm from TMS) of BTAC-A15C5 and the Ca^{II}- and Mg^{II}-induced shifts Δ (ppm; solvent - CD_3CN, counter ion - perchlorate, c_L = 1.5 x 10^{-3} M, c_{Ca} = 0.30 M, c_{Mg} = 0.27 M; D, A denote molecular fragments).

		BTAC-A15C5		
Position		δ	Δ (Ca^{II})	Δ (Mg^{II})
D	ε-CH_2	3.588	0.36	0.24 [a]
	δ-CH_2	3.59	} 0.30	
	γ-CH_2	3.58		
	β-CH_2	3.723	0.21	0.11
	α-CH_2	3.619	-0.14	-0.10 [a]
	Ortho	6.785	0.54	0.50 [a]
	Meta	7.652	0.19	0.19
	β-CH	7.984	0.07	0.15
	α-CH	7.793	0.09	-0.33 [b]
A	4	8.198	0.05	0.04
	5	7.596	0.02	0.02
	6	7.610	0.04	0.07
	7	8.103	0.04	0.05

[a] broad;
[b] very broad

lxxiii) For Hg^{II}, these complexes are only well-defined in terms of steady-state spectroscopy (see discussion in the subchapters above).

Since addition of the hard metal ions Li^{I} and Ca^{II} even at a high excess does not cause any measurable changes of the absorption and emission properties of BTAC-AT$_4$15C5, their presence should not interfere with the fluorometric determination of thiophilic heavy metal ions such as Ag^{I} or Hg^{II}. On the other hand, the complexation behavior of aminophilic heavy and transition metal ions such as Cu^{II} is often problematic for fluorescent probes carrying substituted amine receptor sites since these metal ions (especially Cu^{II}) coordinate to simple alkylated amino groups without chelate formation [264]. However, complex formation of such a type is often encountered for these ions only in concentration ranges above those occurring in most natural liquid media and thus, provided that Cu^{II} ions are not present in a μM concentration range, BTAC-AT$_4$15C5 could be directly employed for sensing purposes. Otherwise, the aid of masking reagents is required. However, incorporation of the dye to any kind of sensor matrix and equipping that matrix with a covalently bound masking reagent for Cu^{II} should be feasible.

For both ions, the dynamic working range covers between one and two orders of magnitude for a conventional steady-state fluorometric titration and can be increased by a factor of *ca.* 5 employing time-resolved fluorometry. In the case of BTAC-AT$_4$15C5, simultaneous determination of Ag^{I} and Hg^{II} is possible employing time-resolved fluorometry with a sufficiently high temporal resolution because the differences in the decay times of the single species are considerably large ($\tau(3)_{Hg\text{-}complex}$ = 3 x $\tau_{Ag\text{-}complex}$ = 4 x τ_{fp} and $\tau(2)_{Hg\text{-}complex}$ = 1.6 x $\tau_{Ag\text{-}complex}$ = 3.3 x τ_{fp}).

Furthermore, any application of BTAC-AT$_4$15C5 in polar solvents with increased "hardness", e. g., water or methanol, leads to larger complexation-induced shifts for Ag^{I} (due to

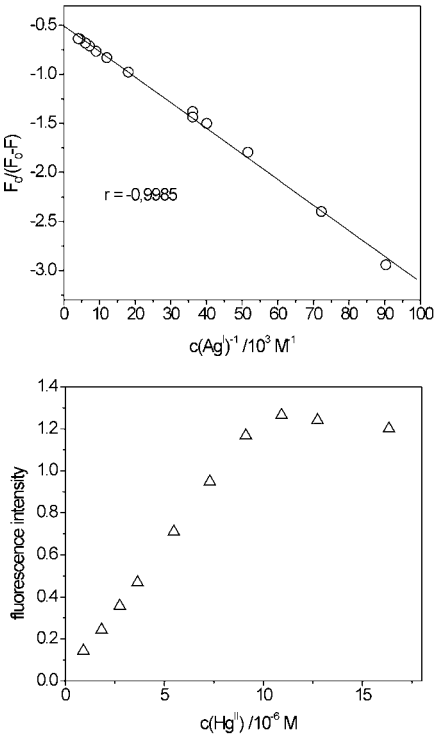

Fig. 48
Fluorometric titration of BTAC-AT$_4$15C5 with Ag^{I} (top) and Hg^{II} (bottom) in acetonitrile (c_L = 9 x 10^{-6} M, excitation at isosbestic point). Whereas in the case of Ag^{I} analysis of the data according to eqn (56) (assuming that during the titration $c_M \sim c_{M,tot}$) still yields acceptable fits, in the case of Hg^{II} eqn (57) has to be used (Appendix B).

reduced ion-solvent interaction) [96e]. In methanol, the shift observed in absorption equals 2 290 cm^{-1} compared to a value of 900 cm^{-1} in acetonitrile. Accordingly, the complex stability constant should be similar or higher in these solvents lacking nitrogen donor atoms. For Ag^{I} binding by diaza polyoxa crown ethers such an effect was observed by *Cox* et al. [276]. In the case of sulfur donor atoms, the effect should be less pronounced. However, recalling the spectroscopic behaviour of the D-A-chalcones in highly polar, strongly hydrogen-bonding solvents, time-resolved fluorescence detection is not very favorable.

The ion sensing characteristics of BTAC-A15C5 are comparable to those found for many other ICT fluorescent probes carrying the A15C5 receptor. Discrimination between all the alkali and alkaline-earth metal ions is not possible with steady-state spectroscopy and even empolying TRES, the relatively small differences in fluorescence lifetimes of the single complexes do not favor a simultaneous determination. However, compared to most other ICT probes, all the alkali and alkaline-earth metal ion complexes of BTAC-A15C5 show enhanced fluorescence quantum yields and fluorescence lifetimes, the latter being cation-specific. Thus, separating the ions or the complexes prior to fluorescence detection (for instance, upon employing ion chromatography combined with fluorometric detection) makes it possible to use these advantages, i. e., specific fluorescence decay times, as additional analyte-specific parameters. In a HPLC experiment with pre- or post-column derivatization, time-resolved fluorescence detection should allow the quantification of a species via the amplitude of the signal and the analyte could be unequivocally identified by both retention time and fluorescence lifetime.

A set of fluorometric titration curves for Li^{I}, Na^{I}, Ca^{II}, and Sr^{II} perchlorates in acetonitrile is shown in *Fig. 49* the correlation coefficients demonstrating the well-defined 1:1-complexation and good applicability.

Concerning analytical applicability in time-resolved fluorometry, both probes absorb in an analytically useful spectral region and excitation with low-cost (pulsed) laser diodes should be possible. However, due to the comparably short fluorescence lifetimes (in the ps time range), detection of the fluorescence decay curves with an acceptable accuracy is not possible employing low-cost detection methods such as boxcar or sampling detection. Thus, single photon timing detection has to be employed. Moreover, especially in the case of the alkali and alkaline-earth metal ions, fast photomultipliers are required in order to resolve decaying species with different fluorescence lifetimes in the order of ≥ ± 20 ps.

Nevertheless, the studies presented here demonstrate the enormous potential of carefully directed receptor design for the development of highly selective fluorescent probes. In the case of the BTAC derivatives, the choice of $AT_4$15C5 does not only lead to a higher selectivity but additionally to analytically more favorable spectroscopic properties, i. e., higher fluorescence quantum yields and lifetimes while maintaining the cation-induced fluorescence enhancement factors.

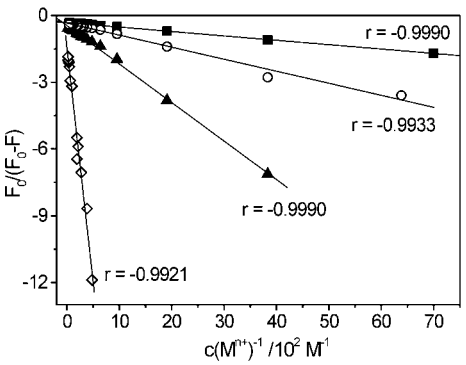

Fig. 49
Fluorometric titration of BTAC-A15C5 with Li^{I} (▲), Na^{I} (◊), Ca^{II} (■), and Sr^{II} (o) in acetonitrile (c_L = 1 x 10^{-5} M, excitation at isosbestic points).

Another aspect which needs careful consideration is acceptor complexation. Although in the present case, this type of complexation leads to the formation of non-fluorescent complexes[lxxiv], with the right choice of donor and acceptor, e. g., modified PAC derivatives, analytically more valuable effects might be achieved[lxxv]. The development of fluorescent probes showing cation-induced bathochromic shifts in emission while maintaining (at least partly) their fluorescence quantum yield is of major importance.

4.7 D-A-Chalcones in Conclusion

In the first part of this chapter, the photophysical behavior of several donor-acceptor-substituted chalcones was studied in order to get a better insight into the photophysical processes being operative in these compounds. In the case of the PAC derivatives, showing spetroscopic effects typical for a strong ICT process and partly positive, partly negative solvatokinetics, the excited-state deactivation behavior is tentatively ascribed to the involvement of three different, highly twisted transient species, an emissive (highly polar A*) and two non-emissive states (weakly polar P* and polar K*). For the BTAC derivatives, showing a more pronounced ICT behavior, population of P* seems to play a minor role and the weak fluorescence in highly polar solvents was mainly ascribed to an accelerated rate constant for internal conversion due to a small S_0-S_1 energy gap. The latter effect points directly to the main advantage of the crowned BTAC derivatives as fluorescent probes, i. e., cation-induced fluorescence enhancement. The cation is bound in the donor part of the molecule and increases the S_0-S_1 energy gap by (weak) interaction with the donor moiety (reduction of donor strength) in the excited state. Accordingly, this leads to increased, cation-specfic fluorescence lifetimes of the complexes. The analytically most valuable results of these studies are the selective complexation behavior (for thiophilic Ag^{I}, Hg^{II}) of the probe equipped with the $AT_4$15C5 receptor and the fact that the mechanism leading to fluorescence enhancement in these probes is not perturbed by binding to the heavy metal ion Hg^{II}. In contrast to most fluorescent probes, a higher fluorescence quantum yield and longer lifetime are also found in the presence of Hg^{II}.

lxxiv) Note however that BTAC-OCH_3 (and to a minor extent BTAC-DMA and QAC-DMA) is an excellent chromoionophore!

lxxv) Such effects are known for crowned flavonols [275].

5 Substituted Triaryl-Δ^2-Pyrazolines - ET Fluorescent Probes

Since utilization of an electron transfer (ET) mechanism for fluorescence sensing allows for a complexation-induced "switching on/off" of a fluorescent probe, the main aim of the studies described in this chapter was the development of a fluorescent ET probe for metal ions showing favorably high fluorescence enhancement factors. 1,3,5-Triaryl-Δ^2-pyrazolines, with their rigid but only partly unsaturated central Δ^2-pyrazoline ring, are known for their bright fluorescence and the molecular structure permits the introduction of a substituent in the 5-position which is electronically largely decoupled from the actual chromophore. Furthermore, equipping this substituent with an oxidizable donor group should present a promising way of controlling the charge transfer process within the main chromophore by a second intramolecular process, an ET. Having in mind that the corresponding chalcone derivatives are used as precursor compounds for the synthesis of Δ^2-pyrazolines (Ch. 2.1.3) and with the crowned D-A-chalcones described in the preceeding chapter already at hand, the 3-benzothiazol-2-yl substituted triaryl-Δ^2-pyrazolines were synthesized and their spectroscopic and complexation behavior investigated.

5.1 Photophysics - Literature Review

The chromophore of the triaryl-Δ^2-pyrazolines involves only three atoms of the pyrazoline 5-membered ring and two aryl moieties in 1- and 3-position, i. e., the $\pi p\pi$-conjugated Ar-C(3) R=N(2)-N(1)R-Ar fragment. Position 4 of the pyrazoline ring is occupied by a methylene group, and the carbon atom at position 5 (sp^3 hybridized) carries a hydrogen atom and the third aromatic substituent (*Scheme 12*, part A). *Table 27* and *Scheme 12* contain the nomenclature of the triaryl-Δ^2-pyrazolines investigated, the substitution pattern, and representative examples of the possible chemical structures.

1,3,5-Triphenyl-Δ^2-pyrazoline and most of its derivatives are highly fluorescent compounds. They are widely used as whitening or brightening reagents for paper, textile fibres, and plastics [277, 278a] as well as wavelength shifters in scintillation counting [279]. Other fields of research include electrogenerated chemoluminescence [280a] and singlet oxygen quenching [281]. Only recently, *Reddy* et al. investigated possible applications of some triaryl-Δ^2-pyrazolines as laser dyes but lasing activity was not found [282].

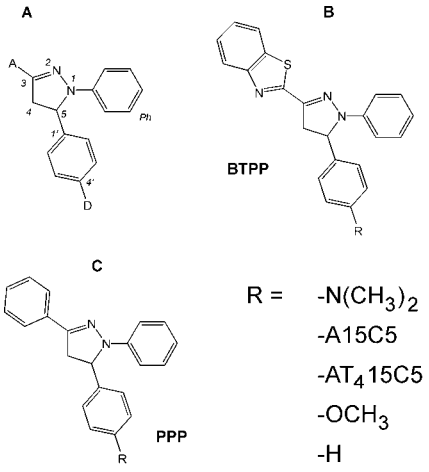

Scheme 12
*General structure and labeling of the substituted 1,3,5-triaryl-Δ^2-pyrazolines (**A**) and chemical structure of the BTPP (**B**) and PPP (**C**) derivatives. The substituents are given in the lower right part. A and D denote the acceptor of the chromophore and the 5-donor group (for labeling and nomenclature, see Table 27).*

Since the extensive works of *Rivett* et al., the crucial role of the *para* substituent of the 5-phenyl group on the fluorescence quantum yield of this class of dyes is known [283a]. Without a strong donor at the 5-position rather intense CT absorption (ε_{max} ~ 25 000 M^{-1} cm^{-1}) and fluorescence (ϕ_f ~ 0.8) bands were observed by this research group. They were also the first to report that either a strong donor (e. g., amino group) or a strong acceptor (e. g., nitro or carboxyl group) at the 5-*p*-position causes considerable fluorescence quenching in polar solvents such as methanol [283a]. In the 1,3,5-triphenyl-Δ^2-pyrazoline derivatives, in contrast to a simple methylene or ethylene spacer, fluorophore and receptor are separated by a "bridged ethylene group", i. e., the CH_2-CHR-group of the pyrazoline ring. This arrangement prevents pronounced electronic interaction in the ground state but allows interaction via long-range processes in the excited state, i. e., electron transfer (ET). Accordingly, the observation of *Rivett* et al. that exchange of the *para* hydrogen atom in this position (5-*p*-H) for a donor or acceptor group capable of ET interaction does not alter the ICT characteristics of the absorption and emission behavior significantly but only quenches the fluorescence, inspired other groups to test possible applications of triphenyl-Δ^2-pyrazoline derivatives as fluorescent probes [284a, b, 285]. The switching "on" or "off" of such a quenching channel allows fluorescence signal generation and led to the application of triaryl-Δ^2-pyrazolines as fluorescent sensors showing comparatively large FEF of 10 to 70 [61, 62, 114, 284a, b].

Further inspection of the literature investigations on the triaryl-Δ^2-pyrazolines shows that most investigations were concerned with substituted triphenyl-Δ^2-pyrazolines whereas only few works include other (hetero)aromatic acceptors at the 3-position. Moreover, for the efficiency of the fluorescence quenching process not only the donor strength of the isolated 5-substituent is important but the character of the ICT process in the 1,3-diaryl-Δ^2-pyrazoline chromophore as well.

A large number of triphenyl-Δ^2-pyrazolines carrying various kinds of electron donating and accepting substituents as well as substituents possessing "heavy atom character" have been investigated spectroscopically in the past forty years [278, 279b, 280, 281, 283-288]. Besides simple (donor and acceptor) substituents, the variety of acceptors employed in the 3-position comprise biphenylyl [279b, 280b] and styryl groups [278, 280b, 281a, 285c] as well as pyridyl [284b, 287a], furyl [280b, 287b], thienyl [278a, 280b, 287b], quinolinyl [287b], and naphthoylene-benzimidazolyl substituents [287f]. Other studies include symmetric bis-derivatives [280, 287e] and triazolyl substituted triphenyl-Δ^2-pyrazolines [287d].

Whereas hydrazones are non-fluorescent, unsubstituted triaryl-Δ^2-pyrazolines are (highly) fluorescent in solvents of any polarity, mainly due to sterical fixation of donor and acceptor

Table 27
1,3,5-Triaryl-Δ^2-pyrazolines investigated in this work. The compounds are labeled according to their three aromatic substituents and their corresponding donor group in the para position of the 5-substituent. Due to phonetic reasons, the order of the aromatic substituents is 3-1-5, i.e., BTPP-DMA (which is 3-benzothiazol-2-yl-1-phenyl-5-phenyl-triaryl-Δ^2-pyrazoline with a p-N,N-dimethylamino donor group at the 5-substituent or, according to IUPAC nomenclature, 2-[1-Phenyl-5-(4-dimethylamino-phenyl) 4,5-dihydro-1H-pyrazol-3-yl]-benzothiazole. Simple functional groups are abbreviated in the same way as in the case of the D-A-chalcones, i.e., the methoxy derivative of BTPP-DMA is BTPP-OCH_3. For abbreviations of the functional groups, see Table 10, p. 43. The PPP derivatives served as reference compounds only.

3-p-Acceptor	5-p-Donor
BT	H
	OCH_3
	DMA
	A15C5
	$AT_4$15C5
P	DMA
	H

by the pyrazoline ring[lxxvi] [283b, 286a]. Introduction of a nitro group in the *para* position leads to fluorescence quenching for the 1- and 5-substituent [280b, 286a, 287a, 288a] but for the cyano, methoxycarbonyl, and methylsulfonyl groups, quenching is only observed upon introduction to the 5-*p*-position[lxxvii] [283a, 284c, 287h]. Furthermore, heavy atom quenching was found for the iodo derivatives [283a] and it is interesting to note, that 1-*p*-amino substitution leads to drastic fluorescence quenching in polar solvents (and in combination with a 3-*p*-CN acceptor even in apolar solvents) [283a, c].

In addition, the CT absorption and fluorescence intensity is strongly decreased upon substitution at the *ortho* position of the 5-phenyl ring due to electronic interaction with the N(1) donor atom [286b] (or hydrogen bonding in the case of *o*-hydroxyl) or by 3-*o*-substituents influencing the CT by interacting with N(2) [280b]. When a pyridine acceptor is introduced to the 3-position, the 2-pyridino derivative shows reduced and the 4-pyridino derivative shows enhanced (and further bathochromically shifted) fluorescence in polar solvents [287a]. For substituents in both important positions of the chromophore (1, 3), linear correlations have been observed for their emission energies and *Hammett* substituent constants [283a, 289b].

Moreover, the nature of the excited-state charge transfer process has been well documented by a correlation of electrochemical and spectroscopic data by *Pragst* and *Weber* [280b].

lxxvi) Only the rigidity of a 5-membered ring suppresses fluorescence quenching and, e. g., 1,3-diphenyl-1,4,5,6-tetrahydro-1,2-diazine is non-fluorescent in apolar solvents [289a].

lxxvii) In all cases, various quenching mechanisms are discussed involving, e. g., vibrational modes, low-lying nπ^* transitions, intramolecular electron transfer, hydrogen bonding, or "mixing" of different states. Here, only relevant references will be made and the reader is referred to the original articles for further discussion concerning these compounds. Moreover, introduction of an electron acceptor in the 1-*p*-position enhances fluorescence but leads to hypsochromic shifts, unfavorable in terms of long-wavelength sensor design [280b, 283a].

5.2 Photophysics - Own Results

5.2.1 Steady-State Spectra

The measured photophysical data of the compounds investigated are collected in *Table 28*.

The first prominent features which render the BT-sub-stituted probes analytically more valuable than most of their triphenyl derivatives are their red-shifted absorption and emission bands accompanied by high fluorescence quantum yields. For example, in acetonitrile, the absorption band is centered at ca. 25 000 cm^{-1} and emission occurs at *ca.* 19 500 cm^{-1}, while for PPP-DMA, the corresponding transitions are found at 27 800 cm^{-1} and 21 300 cm^{-1}, respectively. As derived from the quantum chemical calculations below (Ch. 5.2.5), the nature of the electronic transition ($\pi\pi^*$ nature) involves an intramolecular charge transfer from the donor moiety exemplified by the 1-phenyl-N(1) fragment to the acceptor part of the molecule, i. e., Ar-C(3)=N(2). Along with the CT, increased charge densities are found for the pyrazoline ring atoms N(2) and C(3) in the first excited singlet state. As already mentioned above and as can be derived from the data in *Table 28*, the position of the bands is significantly influenced only by the 1-*p*- and 3-*p*-substituents of the pyrazoline ring whereas the fluorescence quantum yield dependends on the *para* substituent at all three positions [283a, 284b, 287b].

The fact that in the case of the BTPP derivatives introduction of a strong donor to the 5-*p*-position has only a negligible influence on the spectral position of both the absorption and emission band can be derived from a comparison of the data listed in *Table 28* and the spectra displayed in *Fig. 50*. Additionally, the excited-state CT process is connected with a more dipolar nature of the excited compared to the ground state. For all the compounds listed in *Table 28*, the absorption and fluorescence excitation spectra match in all the solvents employed.

The characteristic structure of the absorption spectra of the triphenyl-Δ^2-pyrazolines, i. e., three transitions of different intensities in the UV/Vis region of the spectrum, is observed for the BTPP derivatives as well *(Fig. 50)* [280b]. In accordance with the stronger CT character of the BTPP compounds, the absorption bands lie at the low-energy side of the 240-260 nm, 290-325 nm, and 350-480 nm regions found by *Pragst* and *Weber*[lxxviii] [280b]. The comparison of the absorption spectra of BTPP-H with those of the anilino-substituted derivatives (e. g., BTPP-DMA) in *Fig. 50* reveals that for the 5-*p*-amino-substituted derivatives, the high-energy band of the pyrazoline chromophore and the most intense transition in the alkylated aniline chromophore (at ca. 37 700 cm^{-1}) are superimposed.

In all the solvents studied here, both absorption and emission spectrum show no vibrational structure and even in hexane a slightly more structured band is only seen in the emission spectrum. Here, the intensity ratio of the 0-0-band to the second vibronic band is smaller than unity[lxxix] indicating a difference between ground and excited-state minimum prob-

lxxviii) Since the ET quenching characteristics of the BTPP derivatives are of main interest, no attempts were made to assign any of the high-energy bands.

lxxix) Fitted to a progression of j = 3 gaussian bands.

Table 28
Experimental spectroscopic data of the substituted triaryl-Δ^2-pyrazolines.

	Solvent	$\tilde{\nu}$ (abs)	ε [$\tilde{\nu}$(abs)]	$\tilde{\nu}$(em)	$\Delta\tilde{\nu}$(abs-em)	ϕ_f	τ_f
		10^3 cm^{-1}	10^3 M^{-1} cm^{-1}	10^3 cm^{-1}	cm^{-1}		ns
BTPP-H	MeOH	24.81	28.8	19.17	5640	0.38	2.54
	MeCN	25.13	29.4	19.61	5520	0.72	4.02
	Acetone	25.06	29.3	19.73	5330	0.75	3.91
	THF	24.88	29.4	19.90	4980	0.71	3.88
	Et_2O	25.19	25.7	20.46	4730	0.87	4.17
	Toluene	24.81	28.2	20.33	4480	0.84	3.45
	Hexane	25.32	24.9	21.19	4130	0.73	3.32
BTPP-DMA	MeOH	24.51	27.7	19.36	5150	0.003	0.03
	MeCN	24.94	29.0	19.34	5600	0.006	0.03
	Acetone	24.81	28.4	19.60	5210	0.08	0.20
	THF	24.75	28.5	19.80	4950	0.55	3.00
	Et_2O	25.00	27.9	20.30	4700	0.86	4.02
	Toluene	24.57	29.8	20.12	4450	0.84	3.39
	Hexane	25.13	25.8	21.03	4100	0.78	3.31
BTPP-A15C5	MeOH	24.51	26.3	19.42	5090	0.006	0.05 [a]
	MeCN	25.00	28.2	19.52	5480	0.016	0.11 [a]
	Toluene	24.57	27.3	20.00	4570	0.85	3.34
	Hexane	25.06	25.1	21.05	4010	0.75	3.27
BTPP-$AT_4$15C5	MeCN	24.94	29.7	19.47	5470	0.10	1.07 [a]
	Toluene	24.63	27.8	20.26	4370	0.87	3.46
BTPP-OCH_3	MeOH	24.75	26.1	19.17	5580	0.36	2.42
	MeCN	25.00	27.5	19.57	5430	0.77	4.05
	Hexane	25.25	25.2	21.16	4090	0.85	3.32
PPP-DMA	MeOH	27.93	17.7	20.54	7390	0.19	1.56
	MeCN	27.70	19.0	21.34	6360	0.69	4.19
	Hexane	27.70	18.8	23.01	4690	0.52	2.90
1-p-NH_2-PPP-H	MeOH [b]	26.5	n.r.	20.2	6280	< 0.05	n.r.
	CH [b]	26.7	n.r.	20.7	6000	0.68	n.r.
1-p-CN-PPP-H	MeOH [b]	28.0	n.r.	23.5	4640	0.79	n.r.
	CH [b]	27.8	n.r.	25.4	2330	0.86	n.r.
PPP-H	MeOH	28.09	18.9	20.81	7280	0.38	n.d.
	MeCN	28.09	19.1	21.50	6590	0.62	4.33 [c]
	CH [b]	28.1	n.r.	23.4	4730	0.82	n.r.

[a] $\langle\tau_\phi\rangle$ calculated according to eqn (66) given in Appendix B, explanation see text;
[b] ref. [283a];
[c] ref. [287h]

ably due to conformational reorientation in the excited state. The Stokes shift increases with solvent polarity indicating a higher dipole moment in the excited-state than in S_0 *(Fig. 51)* and in aprotic solvents, all the BTPP and PPP derivatives have high fluorescence quantum yields. Thus, in all solvents, emission is due to an allowed charge transfer transition $S_1(CT)\rightarrow S_0$. These observations are in agreement with those reported by other research groups for 1,3-di- and 1,3,5-triaryl-Δ^2-pyrazolines [280, 284a, b, 285a, d, 286, 287b, h, 288, 289c, d, 290].

The negligible spectroscopic effect upon introduction of a 5-*p*-donor substituent, exemplified by weak ground state CT interactions and a shift of ca. 200 cm^{-1} in absorption, suggests a predominantly electronically decoupled arrangement

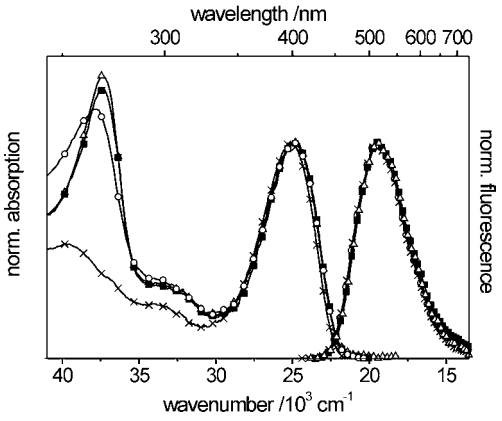

Fig. 50
Normalized steady-state absorption and emission spectra of BTPP-$AT_4$15C5 (Δ), BTPP-A15C5 (■), BTPP-DMA (o), and BTPP-H (x) in acetonitrile.

of the main 1,3-chromophore and the 5-chromophore (5-*p*-substituted aryl moiety). This effect is even observed for the bulky crown ether groups and gives further evidence for the rigidity of the "Δ^2-pyrazoline-bridge" and the prearrangement of 1-, 3-, and 5-substituents in a conformation preventing orbital overlap. In contrast to spectral similarity with the reference compounds, the fluorescence quantum yield is drastically quenched for the BTPP derivatives with a strong 5-*p*-donor (aniline) in solvents of high polarity (i. e., acetonitrile). Furthermore, the strength of this (long-range) quenching process is very sensitive to the nature of the 3- and the 5-substituent as can be read from the data in *Table 28*. For a 3-phenyl group, no quenching is observed and for the 5-*p*-(substituted) anilino BTPP derivatives, the process is accelerated on the order of DMA > A15C5 > $AT_4$15C5 (and not existent for the 5-*p*-methoxy derivative).

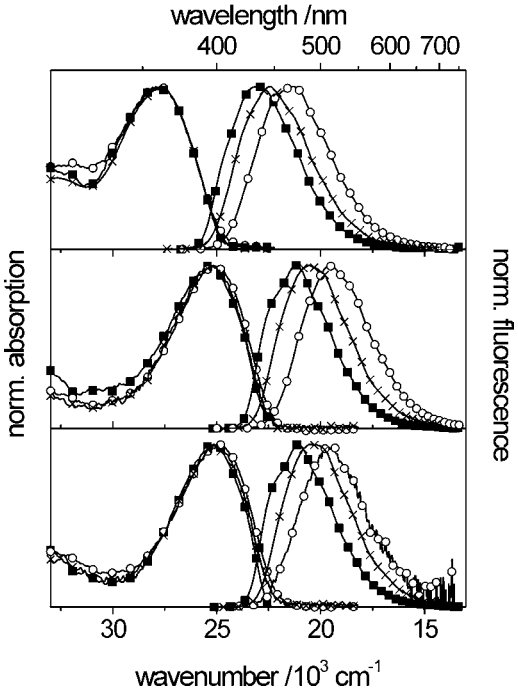

Fig. 51
Normalized steady-state absorption and emission spectra of PPP-DMA (top), BTPP-H (middle), and BTPP-DMA (bottom) in hexane (■), diethylether (x), and acetonitrile (o).

In protic solvents such as methanol the situation is different. Quenching, less pronounced compared to quenching by ET, occurs regardless of the 3- or 5-substituent. A similar behavior has been observed for other Δ^2-pyrazolines before [283a, 284a, b]. Upon excitation, the CT process leads to an increase in electron density at N(2) inducing a higher availability of the lone electron pair for solvent interactions such as hydrogen bonding. Such phenomena are often encountered for fluorescent CT states [291-293].

Since all the triaryl-Δ^2-pyrazolines display enhanced radiationless deactivation of the excited state in protic solvents, such H-bond formation should occur at N(2). Sterical hinderances seem to play no role in this increased non-radiative loss of excitation energy in H-acidic solvents, since a less planar arrangement of the 1-aryl and the Δ^2-pyrazoline moiety (as, e. g., in 1-(2-methylphenyl) [290] or 1-(2,6-dimethylphenyl) [289d, e] derivatives) only leads to slightly reduced fluorescence quantum yields even in highly viscous solvents. Even a pretwisted 3-Ar group has only a weak influence on the fluorescence quantum yield (the influence of both, pretwisted 1- and 3-substituent is much more pronounced for the spectral band positions) [287b, 289a, d, e, 290]. Nonetheless, the effect of hydrogen bonding on the fluorescence of the PPP chromophore is more pronounced since here only N(2) has a high charge density in the excited state and a lone electron pair. In the BTPP derivatives, dissipation of the negative charge in the N(2)=C(3)-thiazole acceptor fragment reduces the charge density at the particular nitrogen atom (cf. *Fig. 56*, p. 82).

5.2.1.1 Transition Dipole Moments

The degree of similarity between the nature of the absorbing and emitting state, i. e., if they differ in the average twist angle around bonds N(1)-Ar and C(3)-Ar, can be derived from a comparison of the transition dipole moments M_{abs} and M_{em} obtained by analyzing steady-state and dynamic photophysical data according to eqn (38) and (39) (cf. Appendix B and *Table 29*)[lxxx].

The nearly constant values of M_{abs} and M_{em} (within experimental error of ± 0.1 D) independent of solvent polarity indicate that the geometry of the absorbing and the emitting state do not differ largely with respect to these particular angles. Furthermore, the solvent-independent ratio of $M_{em}/M_{abs} \cong 1$ in the aprotic solvents suggests that the geometry of the initially excited *Franck-Condon* and emitting CT state are the same. Only in protic solvents such as methanol, the ratio of 0.88 for BTPP-DMA suggests intramolecular rearrangements involving most favorably hydrogen bond formation. A better tool for the detection of angular differences in ground and excited-state conformations is provided by combination of eqns (38) and (44) and rearrangement of eqn (39) to give eqns (45) and (46) (see Appendix B), which exclude the $\tilde{\nu}^3$ dependence of k_f. Here, the ratio of 1.1 ± 0.1 (for the BTPP derivatives) in hexane suggests a relaxation of the initially excited *Franck-Condon* state towards a more planar conformation of the emitting CT state. But with increasing solvent polarity this tendency is reversed and in acetonitrile

lxxx) The transition energy is an inadequate parameter since both changes in the twist angle and changes in the solvation sphere affect this parameter.

Table 29
Transition dipole moments $M_{abs,em}$ and photophysical parameters of the substituted triaryl-Δ^2-pyrazolines.

	Solvent	M_{abs}	M_{em}	M_{em} / M_{abs}	k_f	k_{nr}	k_f^{SB}	k_f / k_f^{SB}
		D	D		10^8 s^{-1}	10^8 s^{-1}	10^8 s^{-1}	
BTPP-H	MeOH	5.8	5.4	0.93	1.5	2.4	1.7	0.87
	MeCN	5.8	5.6	0.96	1.8	0.7	1.9	0.93
	Et_2O	5.4	5.6	1.05	2.1	0.3	1.9	1.09
	Hexane	4.9	5.4	1.10	2.3	0.8	1.9	1.21
BTPP-DMA	MeOH	5.7	5.1	0.88	1.4	450	1.7	0.78
	MeCN	5.9	5.7	0.97	1.8	300	1.9	0.94
	Et_2O	5.6	5.7	1.03	2.1	0.4	2.0	1.06
	Hexane	5.1	5.6	1.09	2.4	0.7	2.0	1.18
BTPP-A15C5	MeCN	5.7	5.1	0.88	1.5	89	1.9	0.78
	Hexane	5.3	5.5	1.04	2.3	0.8	2.1	1.08
BTPP-$AT_4$15C5	MeCN	5.9	4.1	0.69	0.9	8.3	1.9	0.48
	Toluene	5.2	5.4	1.04	2.5	0.4	2.3	1.09
BTPP-OCH_3	MeOH	5.7	5.4	0.94	1.5	2.6	1.7	0.89
	MeCN	5.8	5.8	0.99	1.9	0.6	1.9	0.98
	Hexane	5.3	5.6	1.06	2.4	0.6	2.2	1.12
PPP-DMA	MeOH	4.5	4.4	0.97	1.2	5.2	1.3	0.94
	MeCN	4.7	4.7	1.00	1.6	0.7	1.6	1.00
	Hexane	4.2	4.2	1.00	1.8	1.7	1.8	1.01

ratios of 0.95 ± 0.1 point to a less planar structure[lxxxi]. However, the differences in the conformation of these states seem to be rather small. In contrast, the influence of protic solvents is well reflected by the distinct decrease in k_f /k_f^{SB} (and thus M_{em}^2/M_{abs}^2) for BTPP-H, BTPP-DMA, and PPP-DMA upon going from acetonitrile to methanol.

The same tendency is revealed by the rate constants of radiative and non-radiative deactivation, i. e., a slight decrease in k_f with increasing solvent polarity but a much more pronounced increase in k_{nr}.

5.2.2 Excited-State Solvatochromism and Dipole Moments

In order to estimate the strength of the charge transfer process and to compare BTPP-H and BTPP-DMA more closely the spectroscopic data obtained in different solvents were analyzed as a function of solvent polarity employing the *Lippert-Mataga* formalism described in Appendix B in more detail [218]. A plot of the Stokes shift vs. the solvent polarity functions *f (ε_r) - f(n)* (cf. eqn (71)) is shown in *Fig. 52* and the dipole moments obtained are included in *Table 30*.

The good agreement between the dipole moments obtained by eqn (70a) and (73) suggest the equal (CT) character of emitting state and initially excited state for both molecules. Thus, a 5-*p*-donor has obviously no substantial influence on the CT process in the 1,3-chromophore. The same is found when taking into account the polarizability of the solute (cf. Appendix B). Although eqn (75) yields lower values for μ_{es}, the dipole moments of BTPP-H and BTPP-DMA are still similar. Comparison with other (μ_{es} - μ_{gs}) data published for Δ^2-pyrazolines in the literature is so far only possible regarding the order of magnitude of the change in dipole moment (cf. footnote cxix, p. 113). *Güsten* et al. reported a value of (μ_{es} - μ_{gs}) = 11.5 D for 1-*p*-chloro-3-*p*-cyano-diphenyl-Δ^2-pyrazoline and *Yan* et al. found (μ_{es} - μ_{gs}) = 8.9 D for 3-*p*-nitro-triphenyl-Δ^2-pyrazoline [285d, 289c]. The former group analyzed their data according to *Bakhshiev's* and the latter according to the *Bilot-Kawski* formalism (taking into account the polarizability of the solute (cf. Appendix B)), which yields nearly similar results as eqn (75)[lxxxii]. Being aware of the crucial choice of the *Onsager* cavity radius, the changes in dipole moment are of similar magnitude. The correlations found in the solvent polarity plots demonstrate the power of the newly developed SPP^N scale to deal with both, dipolar nature and polarizability of solvents sufficiently well (see Appendix B).

lxxxi) *Strähle* et al. observed a slightly different solvatochromic behavior for the (substituted) 1,3-diphenyl-Δ^2-pyrazolines, i. e., adoption of a planar structure in the excited state [289d]. Such a conformation is less favored in the triaryl analogues since it requires cooperative rotation of the 5-substituent to avoid steric crowding. Furthermore, quantum chemical calculations reveal higher energy barriers for rotation around Ar-C(3) and N(1)-Ar in the case of BTPP-H (9.0 and 14.2 kJ mol^{-1}) than in the case of 3-benzothiazol-2-yl-1-phenyl-Δ^2-pyrazoline (2.8 and 11.3 kJ mol^{-1}). On the other hand, planarization of N(1) does not necessarily imply planarization of the whole Ar-C(3)=N(2)-N(1)-Ar fragment. In the optimized ground state geometry of $[MeBTTP\text{-}OCH_3]^+$ (see Ch. 5.5.3 and *Scheme 15*, p. 92), the fragment Ar-C(3)=N(2)-N(1) is almost perfectly planar (and the oscillator strength of the $S_0 \rightarrow S_1$ transition is higher than in the uncharged BTPP derivatives) but the 1-phenyl group is twisted for ca. 20° (in contrast to ca. 13° in BTPP-H, PPP-H and 5.4° in 1,3-diphenyl-Δ^2-pyrazoline) [294].

lxxxii) The quadratic term of the Stark effect taken additionally into account by *Bilot* and *Kawski* is small compared to the other terms.

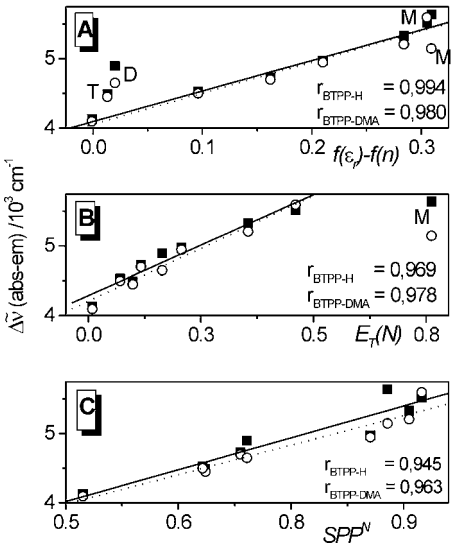

Fig. 52
*Solvatochromic plots (and fits) according to eqn (70a) (**A**) and plots of Stokes shift vs. empirical solvent polarity parameters $E_T(N)$ (**B**) and SPP^N (**C**) for BTPP-H (■,—) and BTPP-DMA (o,·····) in the solvents listed in Table 28, di-n-butylether, and 1,4-dioxane. For the fit of the solvatochromic plot the values for toluene (T), 1,4-dioxane (D), and methanol (M) were excluded; the fit in **B** excludes only methanol (M) and the fit of Stokes shift vs. SPP^N includes all data points.*

For PPP-DMA, BTPP-H, and BTPP-DMA, the increasing Stokes shift with increasing solvent polarity, already traceable in *Fig. 51*, p. 78, yields a difference (μ_{es} - μ_{gs}) of ca. 13 D for BTPP-H as well as BTPP-DMA. Such a change in dipole moment of ca. 13 D for the BTPP 1,3-chromophore corresponds to a charge separation distance of ca. 3.0 Å equaling a (theoretical) distance from N(1) to the C(3)-BT bond reflecting the charge shift within the 1,3-chromophore.

The results described in this subchapter (e. g., on the conformational change between absorbing and emitting species) so far support the explanation given by *Sahyun* et al. for related systems, i. e., most probably electron transfer occurs via the tilted "pseudo-spiro" arrangement of 1,3- and 5-chromophore [288]. In such an arrangement of the two chromophores a through-space ET via spacially close orbitals of the 5-aryl moiety and N(1) is possible [288b, 295]. According to the rule of minimum overlap, ET via such a configuration implies rotation of the 5-moiety towards perpendicularity in order to stabilize the product and leads to low rates for the backwards process [240].

5.2.3 Fluorescence Lifetimes

The time-resolved emission behavior of the triaryl-Δ^2-pyrazolines investigated here is relatively straightforward. The fluorescence lifetime data are included in *Table 28*, p. 77. In apolar solvents, the decay kinetics can be described by a single exponential. This is also valid for all the derivatives without a 5-*p*-amino donor in all the polar solvents investigated here. For the derivatives showing fluorescence quenching in polar solvents, in the case of the crowned BTPP derivatives biexponential decay kinetics were found (a second, long-lived decay component with a low relative amplitude). However, global analysis of fluorescence decay curves recorded as a function of emission wavelength revealed no rise times and unchanged amplitude ratios with relative

Table 30
Dipole moments obtained from the slope of solvatochromic plots according to eqns (70a), (73), and (75). The Onsager radius a_O was taken to 7.1 Å (BTPP-DMA) and 6.8 Å (BTPP-H) on the basis of the AM1-optimized geometry and the method proposed by Edward for spherical molecules (gs - ground state, es - excited state) [224].

	Eqn	μ_{gs} [a]	μ_{es}	(μ_{es} - μ_{gs})
		D	D	D
BTPP-H	(70a)	0.8	12.5	11.7
	(73)	0.8	13.7	12.9
	(75)	0.8	9.2	8.4
BTPP-DMA	(70a)	1.7	14.3	12.6
	(73)	1.7	14.8	13.1
	(75)	1.7	10.2	8.5

[a] for optimized ground state geometry by AM1

amplitudes for the longer component (3 ns) of only 5 % over the whole spectral range measured *(Fig. 53)*. This fact points to partial non- or multiexponential decay behavior of the crowns. Assuming similarity of the electronic structure for the crowned derivatives and the parent molecule BTPP-DMA, a possible explanation for this interesting behavior may arise from conformational flexibility of the crown unit (which can induce varying basicity of the amino electron lone pair). Keeping in mind the *endo-exo* isomerization of crown ethers, differences in the interaction between nitrogen lone electron pair and the 5-phenyl π system could result in different ET rates and hence different fluorescence decay times. In the classical *endo* conformation, i. e., in unsubstituted A15C5 with a secondary amino nitrogen, the lone electron pair is directed into the crown's cavitiy and in the exo conformation away from the crown's cavity [296]. Here, in the case of a tertiary amine both "extreme" conformations are not possible but only an exo conformation with considerable overlap between the phenyl π plane and the hybrid orbital (lone electron pair) of the sp^3 nitrogen atom would allow a fast ET process.

5.2.4 Temperature-Dependent Behavior

In order to verify the electron transfer process and its dependence on molecular motions, steady-state and time-resolved fluorescence measurements were carried out with BTPP-DMA in ethanol as a function of temperature. At room temperature (298 K), the spectroscopic properties of BTPP-DMA in ethanol are comparable to those in methanol.

As can be seen in *Fig. 54*, the structureless spectroscopic features are maintained during the temperature range of 290-30 K, the spectra at 30 K resembling closely those of BTPP-DMA in hexane (*Fig. 51*, p. 78). No phosphorescence was detected at any temperature. *Fig. 55* combines the corresponding fluorescence quantum yield and lifetime data. Monoexponential fluorescence decay kinetics are observed over the whole temperature region. Furthermore, from a comparison of the kink point in the ϕ_f and τ_f vs. *T* plots with the glass temperature of the solvent it is clear, that a rotational deactivation process is frozen in BTPP-DMA. Accordingly, upon analyzing the temperature-dependent emission data in terms of the well-known Arrhenius equation (eqn (7)) a linear correlation is obtained for a plot of $\ln k_{nr}$ vs. T^{-1} down to the

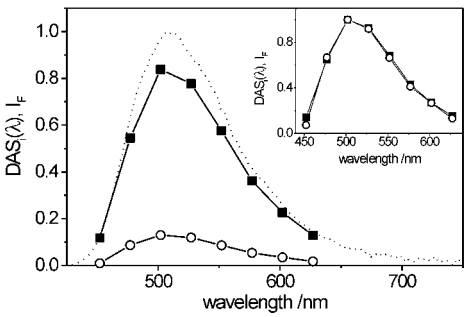

Fig. 53
DAS$_i$(λ) (solid lines with symbols) and steady-state emission spectrum (·····) of BTPP-AT$_4$15C5 in acetonitrile (excitation at 415 nm, c_L = 3 x 10^{-6} M). The inset contains the normalized DAS$_i$(λ). The global analysis revealed decay times of 0.98 ns (⟨ a_{rel} ⟩ = 0.95; DAS$_1$(λ), ■) and 2.96 ns (DAS$_2$(λ), o), respectively[lxxxiii].

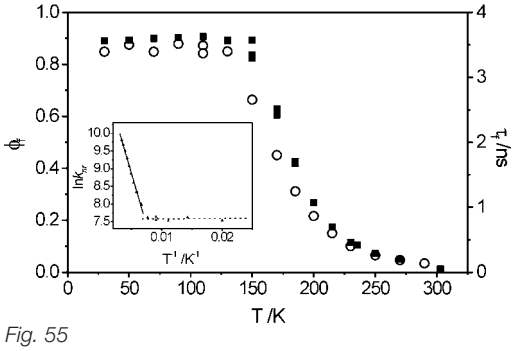

Fig. 55
Temperature dependence of fluorescence quantum yield (o) and lifetime (■) of BTPP-DMA in ethanol. The inset shows the temperature dependence of lnk_{fr} before (—) and after (constant,·····) the glass temperature of ethanol (T_g^{EtOH} = 158 K).

glass temperature of ethanol (T_g^{EtOH} = 158 K; *Fig. 55*). In consequence, an activation barrier of 11.3 kJ mol^{-1} is found for the non-radiative processes. k_i does not show a distinct temperature dependence with values of 2 (± 0.3) x 10^8 s^{-1} over the temperature range studied.

$$\ln k = \ln A - \frac{E_A}{RT} \qquad (7)$$

In the glass, the constant values obtained for both fluorescence quantum yield and lifetime suggest that no other process (except possibly a barrierless down-hill process) is operative and ET is frozen. Furthermore, the absence of any detectable phosphorescence leads to the conclusion that the remaining 10 % of non-radiative deactivation can be attributed to internal conversion from S1 to the ground state [116]. In solution, the temperature dependence points to a mainly viscosity-controlled process.

5.2.5 Quantum Chemical Calculations

5.2.5.1 Ground State Geometries

In order to get more insight into the geometric arrangements, the charge distribution and nature of the molecular orbitals in the triaryl-Δ^2-pyrazolines, quantum chemical calculations were employed. The molecules studied comprise of BTPP-DMA, BTPP-H, PPP-DMA, PPP-H, and their methylated or protonated derivatives being important for a better understanding of the complexation experiments (Ch. 5.5).

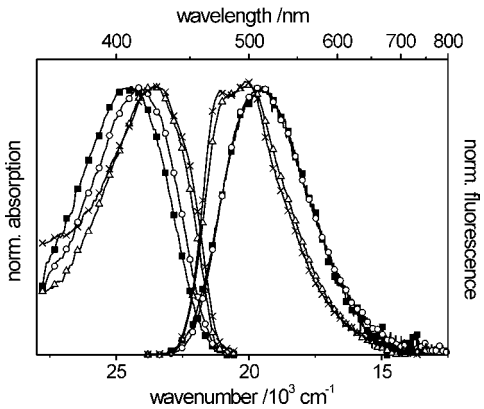

Fig. 54
Normalized steady-state absorption and emission spectra of BTPP-DMA in ethanol at 290 K (■), 200 K (o), 110 K (Δ), and 30 K (x).

lxxxiii) The corresponding values obtained for BTPP-A15C5 by global analysis of 8 decays are 0.03 ns (⟨a_{rel}⟩ = 0.82) and 0.34 ns.

Ground state geometry optimizations were performed on a semiempirical AM1 level and the relevant torsion angles and bond lengths of some of the molecules are summarized in *Table 31*, p. 83 (labeling of the atoms according to *Scheme 13*).

The 1,3-diaryl-Δ^2-pyrazoline chromophore is found nearly planar in the A-C(3)R=N(2)-N(1) fragment but the more tetrahedral conformation of N(1) induces a distortion for the 1-phenyl substituent (twist of ca. 12°). This is in agreement with data given by *Blair* et al. for PPP-H on the basis of AM1/MOPAC calculations [288b]. Furthermore, the energy barriers for rotation around the sterically unrestricted single bonds are generally low for all the molecules studied. The activation barriers are calculated to 14.2 and 16.3 kJ mol^{-1} (N(1)-Ph) and 9.0 and 7.3 kJ mol^{-1} (C(3)-A) for the corresponding single bonds of BTPP-H and PPP-H, respectively. In contrast, rotation around the sterically restricted single bond (C(5)-C(1')) is connected with a high barrier, i. e., 164 kJ mol^{-1} and 159 kJ mol^{-1}. The torsion angles N(1)-C(5)-C(1')-C(2') and N(1)-C(5)-C(1')-C(6') are -50° and 131°, respectively. This results in a tilted, "pseudo"-spiro arrangement of the pyrazoline and the 5-phenyl planes (for comparison: *Blair* et al. obtained a nearly perpendicular prearrangement of 93.1° for the molecular planes of the central Δ^2-pyrazoline and the 5-phenyl ring of PPP-H). The bond lengths are generally in good agreement for the PPP derivatives with those obatined by *Duffin* in an X-ray study of 1,3-diphenyl-Δ^2-pyrazoline despite the distortions imposed by the 5-substituent [294] and especially the C(3)-C(1^A) bond displays a certain double-bond character in the case of the BTPP derivatives [297]. The protonated and methylated compounds will be discussed further below.

Regarding the degree of pyramidalization at the aza crown or DMA nitrogen atom, the differences are small for the DMA, A15C5, and AT$_4$15C5 derivatives in the optimized ground state geometry (sum of the bond angles at N^{DMA} of 350.9°, 355.5°, and 352.6°). But whereas for BTPP-DMA maximum interaction between the nitrogen lone electron pair (hybrid AO) and the π orbitals of the phenyl ring is possible, the energetically most favorable conformation for the aza crown ethers involves considerable twisting around the C(4')-N^{DMA} bond (folded conformation of phenyl ring and crown ether)

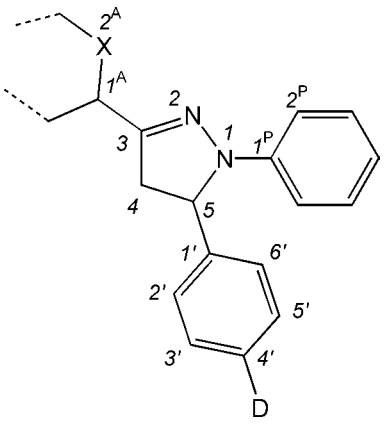

Scheme 13
Labeling of the atoms in the triaryl-Δ²-pyrazolines calculated

and the orbital overlap is reduced. This folded confirmation of the *N*-phenyl crowns was also found in X-ray studies of *N*-phenyl-A15C5 [85b, 298], MAP-A15C5 derivatives [254], and BTAC-A15C5 (cf. footnote xlv, p. 49) [85b]. Calculation of the energy barriers for rotation around this bond in the isolated donors *N,N*-dimethylaniline, *N*-phenyl-A15C5, and *N*-phenyl-AT$_4$15C5 yields an order of 15.8 kJ mol^{-1} < 124 kJ mol^{-1} > 72 kJ mol^{-1}.

Assuming that the crowned BTPP derivatives exist in two conformers, isomerization is connected to the highest barrier in BTPP-A15C5. The loss of pyramidalization at N(1) in the excited state reduces the distance between 1- and 5-substituent. Thus, (concerted) rotational movement of both groups is theoretically possible leading to a quasi parallel arrangement between these moieties giving rise to π-π interactions. However, such a process involving cooperative action and dramatic changes in the geometry of the excited state could not be verified in the mechanistic studies. Furthermore, small deviations from the optimum spiro geometry would result in comparatively large differences in ET rates.

5.2.5.2 Molecular Orbitals and Differences of CT and ET States[lxxxiv]

Figure 56 combines the HOMO-1, HOMO, and LUMO of both molecules. In contrast to PPP-DMA, where HOMO (and LUMO) are only localized on the 1,3-chromophore, in BTPP-DMA the highest occupied MO is delocalized on both fragments of the molecule. Furthermore, HOMO-1 is only located on the anilino fragment and thus, any ET is connected to the HOMO-1 - LUMO gap.

To analyze the effect of the differences of ET and CT states on the nature of the fluorescence quenching process in BTPP-DMA, calculations were employed for the optimized and 90° (ET) geometries of BTPP-DMA and PPP-DMA in the gas phase and in a reaction field (SCRF calculations for ε_S = 37.5 and a_O = 6 and 8 Å). However, the results obtained are not straightforward yielding no pronounced differences for optimized and ET geometries. Furthermore, the SCRF results stress the tendencies observed in the gas phase calculations but do not clarify the picture. Thus, only the prominent features of the calculations with the optimized geometries will be given here.

The $S_0 \rightarrow S_1$ transition shows a > 90 % HOMO - LUMO contribution for both molecules with high oscillator strengths *f* of 1.03 and 0.80 for BTPP-DMA and PPP-DMA, respectively. In contrast, for both molecules *f* ~ 0.02 is found for transitions involving ET configurations. Furthermore, the HOMO-1 - LUMO configuration is distributed on more than one transition for both molecules. A pronounced difference in ET-CT energy gap is also not found for the state (and configuration) energies of both molecules. The results given so far are consistent with the similarity of both molecules in an apolar environment. However, considering dipole moments the situation changes. The dipole moments (along the DMAn axis) obtained for the

lxxxiv) calculated employing HyperChem AM1 (CI = 8) and ZINDO/S (CI = 10) see Ch. 2.11

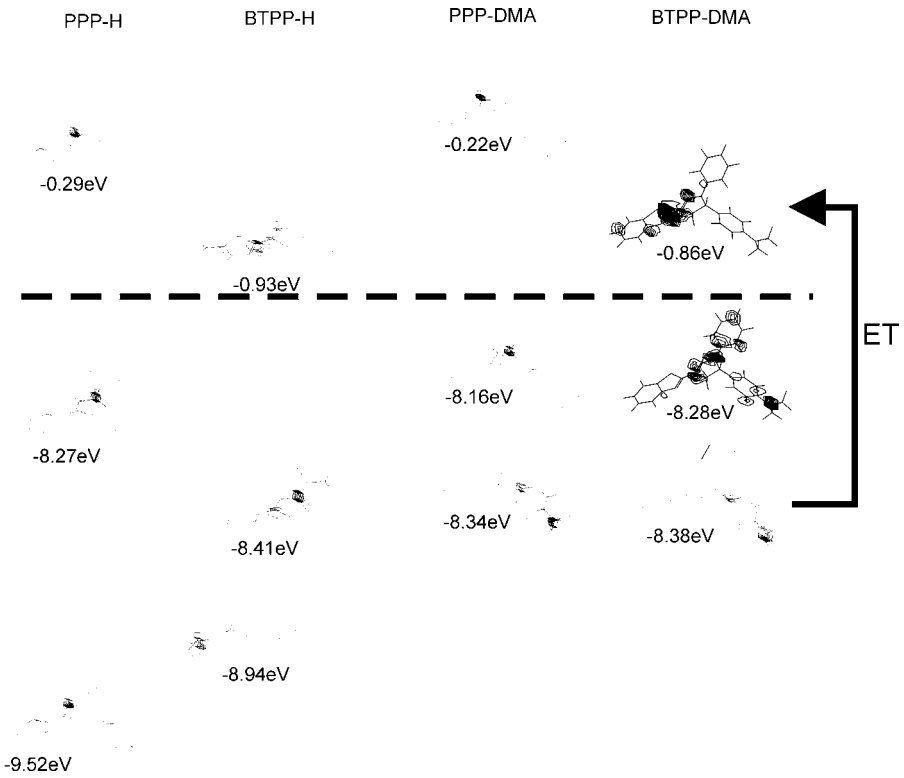

Fig. 56
Frontier MOs (HOMO-1, HOMO, LUMO) of PPP-H, BTPP-H, PPP-DMA and BTPP-DMA. The orbital coefficients are squared for a better visualization and the energy levels are indicated (AM1/ Hyperchem). Not shown are the HOMO-1, HOMO, and LUMO of BTPP-A15C5 (-8.36 eV, -8.26 eV, -0.84 eV) and BTPP-AT$_4$15C5 (-8.51 eV, -8.32 eV, -0.86 eV), which are nearly identically localized on the molecular fragments as in BTPP-DMA.

ET configuration are larger than those for the corresponding CT configuration (31 D vs. 8 D for BTPP-DMA and 32 D vs. 12 D for PPP-DMA). Furthermore, the dipole moments (for ET configuration, along the BT or P acceptor axis) are determined to 10 D (BTPP-DMA) and 4 D (PPP-DMA), respectively. On the other hand, the dipole moments for the CT configuration (8 D and 12 D) are elongated in the acceptor axis by 3 D in BTPP-DMA and 9 D in PPP-DMA, respectively. Thus, taking into account solvent stabilization (quenching is observed in highly polar solvents only), the thermodynamic driving force is stronger in BTPP-DMA compared to PPP-DMA.

5.3 Intramolecular Electron Transfer and Charge Transfer Reaction

The experimental and theoretical results indicate the competition of two photophysical processes on a (sub) ps time scale, governing the spectroscopic behavior of BTPP-DMA. The initially excited[lxxxv] ^{1}CT* experiences solvent relaxation and is able to fluoresce with a certain quantum yield and lifetime but non- or weakly adiabatic ET can quench this emission markedly in BTPP-DMA. In this chapter the rate constants of the two processes are examined closer.

5.3.1 Non- or Weakly Adiabatic ET

Assuming that the only other process governing the excited-state behavior of BTPP-DMA compared to BTPP-H is non- or weakly adiabatic electron transfer,[lxxxvi] the rate constant for ET in acetonitrile can be determined according to eqns (8), (9), and (10).

$$\phi_f^{noET} = \frac{k_f}{k_f + k_d} \text{ and } \tau_f^{noET} = \frac{1}{k_f + k_d} \quad (8)$$

$$\phi_f^{aET} = \frac{k_f}{k_f + k_d + k_{et}} \text{ and } \tau_f^{aET} = \frac{1}{k_f + k_d + k_{et}} \quad (9)$$

$$k_{et} = \frac{1}{\tau_f^{aET}} - \frac{1}{\tau_f^{noET}} \quad (10)$$

Here, *"noET"* refers to the photophysical parameters of the unquenched molecule (e. g. τ_f = 4.0 ns for BTPP-H and BTPP-OCH_3) and *"aET"* to those of the molecule with "active electron transfer", i. e., BTPP-DMA. With the fluorescence lifetime data given in *Table 28*, p. 77, the rate constant for the ET process is determined to k_{et} = 3 x 10^{10} s^{-1} in acetonitrile.

5.3.2 Strongly Adiabatic ET (CT)

Having in mind the homogeneous emission spectrum and the lack of a second decaying species in the time-resolved experiments, it is possible to obtain the rate constant for the adiabatic ET process (the CT) from initially excited *Franck-Condon* to the solvent-relaxed emitting ^{1}CT state employing (modified) classical electron transfer theory [299, 300]. Taking into account various parameters such as solvent relaxation (longitudinal solvent relaxation time τ_l) and reorganization energy (λ_S) as well as activation barriers ($\Delta G^{\#}$) the rate constant of an adiabatic, solvent diffusion-controlled electron transfer can be derived from eqn (11) [301].

lxxxv) or ultrafast populated; Note, however that no reaction of a localized or delocalized excited state towards a CT state was traceable.

lxxxvi) This simplification is justified by nearly identical radiative rate constants for all BTPP derivatives and non-radiative rate constants for BTPP-H and BTPP-OCH_3 in any given solvent.

Table 31
Calculated torsion angles (Θ) and bond lengths (l) of BTPP-DMA, BTPP-H, PPP-DMA, PPP-H, and their methylated or protonated derivatives in the ground state (AM1/HyperChem). The results obtained for the methylated and protonated species of BTPP are similar (torsion angles ± 0.5° and bond lengths ± 0.005 Å).

	-R$^+$ [a]	N(2)-N(1)-C(1^P)-C(2P)		C(4)-C(3)-C(1^A)-X(2^A)		C(4)-C(5)-C(1')-C(2')		C(3)-N(2)	N(2)-N(1)	N^{BT}-C(1^A)
		Θ /°	l /Å	Θ /°	l /Å	Θ /°	l /Å	l /Å	l /Å	l /Å
BTPP-DMA [b]	-	12.9	1.428	2.8, X = S	1.447	65.9	1.496	1.327	1.351	1.331
BTPP-H [b]	-	13.1	1.429	2.5, X = S	1.447	66.7	1.499	1.327	1.352	1.331
[MeBTPP-OCH_3]$^+$	N^{BT}	20.1	1.431	1.2, X = N	1.414	58.8	1.491	1.363	1.295	1.371
[HBTPP-OCH_3]$^+$	N(2)	62.8	1.452	0.3, X = S	1.439	58.3	1.492	1.337	1.396	1.348
[HBTPP-OCH_3]$^+$	N(1)	58.2	1.479	2.0, X = S	1.448	50.0	1.484	1.322	1.421	1.344
PPP-DMA	-	13.3	1.429	3.6, X = C	1.456	66.5	1.496	1.325	1.358	-
PPP-H	-	13.3	1.430	4.5, X = C	1.456	67.1	1.499	1.325	1.359	-
1,3-diph.-pyraz. [c]	-	5.4	1.423	7.5, X = C	1.408	-	-	1.333	1.336	-
1,3-diph.-pyraz.	-	12.5	1.428	6.4, X = C	1.455	-	-	1.325	1.361	-
[HPPP-H]$^+$	N(1)	56.6	1.479	2.1, X = C	1.451	52.8	1.489	1.324	1.421	-
[HPPP-H]$^+$	N(2)	62.2	1.453	0.8, X = C	1.441	60.0	1.495	1.339	1.395	-

[a] position of protonation or methylation;

[b] The *anti* (X = S, *Scheme 13*) stereoisomer is energetically favored (6 kJ mol^{-1}) but the optimized geometry of the *syn* isomer shows comparable features, e. g., the corresponding torsion angles of syn-BTPP-H amount to 13.1°, 5.0°, and 67.5°, respectively.

[c] X-ray results reported by *Duffin* for 1,3-diphenyl-Δ^2-pyrazoline [294]

$$k_{et} = \frac{1}{\tau_l}\sqrt{\frac{\lambda_S}{16 k_B T \pi}}\, e^{\frac{-\Delta G^{\#}}{k_B T}} \qquad (11)$$

In acetonitrile, where solvent relaxation is fast and for the classical "outer-sphere" ET, where the "outer-sphere" barrier (i. e., solvent reorganization) is large compared to the vibrational (bond) changes ("inner-sphere" barrier), this simplified model can be applied and λ_S can be determined according to eqn (12) using $(\mu_{es} - \mu_{gs})^2 / a_O^3$ from the solvatochromic plots[lxxxvii].

$$\lambda_S = \frac{(\mu_{es} - \mu_{gs})^2}{a_O^{\,3}}(f(\varepsilon_r) - f(n)) \qquad (12)$$

Furthermore, assuming a low activation barrier of $\Delta G^{\#} \sim k_B T$ (e. g., $\Delta G^{\#} \sim 170$ cm^{-1} as for biaryls in acetonitrile) [302] a rate constant $k_{et} = 5.9 \times 10^{11}$ s^{-1} (= k_{ct}) is obtained for the 1-phenyl-3-benzothiazol-2-yl-Δ^2-pyrazoline derivatives in acetonitrile.

Thus, the processes governing the excited-state behavior of BTPP-DMA in a "fast" polar solvent such as acetonitrile ($\tau_l = 0.2$ ps) can be rationalized like this. After excitation, the initally populated *Franck-Condon* state forms the ^{1}CT state in < 2 ps. Besides other non-radiative energy losses, emission from this state has to compete with a fast ET reaction from the 5-*p*-amino donor ($\tau_{et} = 33$ ps).

5.4 BTPP-DMA vs. PPP-DMA

BTPP-DMA vs. PPP-DMA or the question, why ET quenching is observed only for the former derivative still persists. Based on the (solvatochromic) experimental data, the CT process in the main Δ^2-pyrazoline chromophore is assumed to be completed on the sub-ps time scale for both derivatives. Thus, other factors determining the efficiency of the intramolecular quenching process must govern the behavior of these molecules. Upon applying *Marcus* ET theory, the driving force of the quenching ET process will be determined for both Δ^2-pyrazoline derivatives and compared with respect to the experimentally observable results.

The ET process involves the transfer of an electron from the donor to the acceptor resulting in an intramolecular radical ion pair $D^{\bullet+}$-$A^{\bullet-}$ of oxidized donor (D) and reduced acceptor (A). With the ionization potential *IP* of D and the electron affinity *EA* of A being related to the corresponding oxidation and reduction potentials (eqns (13), (14)) the driving force of an ET process is given by eqn (15).

$$IP = E_{1/2}(D^+ / D) - \Delta G(D^+) + const. \qquad (13)$$

$$EA = E_{1/2}(A / A^-) - \Delta G(A^-) + const. \qquad (14)$$

$$\Delta G_{ET} = e[E_{1/2}(D^+ / D) - E_{1/2}(A / A^-)] - \Delta E_{00} + E_{solv} - E_C \qquad (15)$$

ΔE_{00} corresponds to the free energy of the equilibrated excited state, E_{solv} denotes a solvation term,[lxxxviii] and E_C represents the Coulombic interaction between the oppositely charged ions[lxxxix] [300, 303]. For highly polar media and neutral reactants, the solvation term is negligible and $E_C < 0.1$ eV for charge separation distances of ≥ 4 Å in acetonitrile (it is assumed that the separation distance of ≥ 4 Å derived from the optimized ground state geometry is maintained in the excited state due to the rigidity of the spacer). *Table 32* combines the calculated (theoretical) ET driving forces for some of the investigated Δ^2-pyrazolines.

Even though the distinctly more negative ΔG_{ET} value for BTPP-DMA is in line with the experimentally obtained results, the negative ΔG_{ET} value for PPP-DMA in *Table 32* contradicts the corresponding observations in solution. Moreover, in less polar solvents such as diethylether quenching is absent for both 5-*p*-DMAn derivatives. The thermodynamic quantity ΔG_{ET} alone seems to be insufficient to explain why ET takes place only in BTPP 5-*p*-anilino derivatives. *Fig. 57* schematically depicts the processes being involved in an intramolecular non- or weakly adiabatic ET reaction. A more general model of the ET process takes into account the kinetic effects which can be quantified by eqn (16) for the non- or weakly adiabatic case [299, 306]. Here, λ_0 is the energy of reorganization in the whole ensemble, consisting of a so-called "inner sphere (barrier)" term λ_i and an "outer sphere (barrier)" term λ_S. The former accounts for reorganization in the solute, i. e., for example bond length changes and the latter describes the solvent reorganization energy ($\lambda_0 = \lambda_i + \lambda_S$) [300, 301b]. Since no data for λ_i are available for the molecules under investigation and with the assumption that changes of this type are comparable for both rigid molecules, this term is neglected in the further treatment. The solvent reorganization energy is given by eqn (18) where the single quantities are explained in footnote[lxxxviii]. *V* is the electronic coupling matrix element and quantitizes the degree of electronic coupling or interaction between donor and acceptor part. In these "pseudo" spiro-arranged D-A-assembly, *V* is not expected to be large but weak electronic coupling is known to play a significant role in classical spiro compounds (spiroconjugation) [307] involving both, spiro-conjugated π systems or π systems and adjacent orbitals with lone electron pairs of heteroatoms such as oxygen or nitrogen. Thus, *V* cannot be neglected in a process via "pseudo" spiro orientation as is expected for the Δ^2-pyrazolines.

$$\Delta G^{\#} = \frac{\lambda_0}{4}\left(1 + \frac{\Delta G_{ET}}{\lambda_0}\right)^2 - V \qquad \text{in the form of} \qquad (16)$$

lxxxvii) The longitudinal solvent relaxation time in acetonitrile was taken to 0.2 ps [234].

lxxxviii) $E_{solv} = \frac{e^2}{4\pi\varepsilon_0}\left(\frac{1}{2r_{D^+}} + \frac{1}{2r_{A^-}}\right)\left(\frac{1}{\varepsilon_S} - \frac{1}{\varepsilon_{MeCN}}\right)$;
r_{D+} and r_{A-} are the ionic radii and e_S is the dielectric constant of the solvent. If the solvation term is written in this way, i. e., normalized on acetonitrile, comparison of the data is easier because most oxidation and reduction potentials are obatined in this solvent

lxxxix) $E_C = \frac{e^2}{4\pi\varepsilon_0\varepsilon_S d_{DA}}$; d_{DA} is the charge separation distance.

Table 32
Calculated ET driving forces for BTPP-DMA, BTPP-OCH_3, and PPP-DMA in acetonitrile as well as BTPP-DMA in diethylether.

	Solvent	ΔE_{00}	$E_{1/2}(D^+/D)$	$E_{1/2}(A/A^-)$ [a]	E_{solv} [b]	E_C [c]	ΔG_{ET}
		eV V	(MeCN, Fc/Fc$^+$)	V (MeCN, Fc/Fc$^+$)	eV	eV	eV
BTPP-DMA	MeCN	3.09	0.44 [d]	-2.22	0	0.05	-0.48
	Et_2O	3.10	0.44	-2.22	0.87	0.41	-0.02
BTPP-OCH_3	MeCN	3.10	1.45 [e]	-2.22	0	0.05	0.52
PPP-DMA	MeCN	3.43	0.39 [f]	-2.83	0	0.06	-0.27

[a] experimentally determined to -2.19 V and -2.82 V for the parent compounds PPP-H and BTPP-H in MeCN vs. Fc/Fc$^+$; [116]

[b] $1/2r_{D^+} + 1/2r_{A^-}$ estimated from the spherical molecule [304]

[c] a charge separation distance of 8.3 Å corresponds to the core-core distance of 5-*p*-substituent to BT, 6.6 Å for PPP-DMA;

[d] 3-BT-1-P-Δ^2-pyrazoline is oxidized at 0.68 V [116]

[e] value for methoxybenzene taken from ref. [305];

[f] 1,3-PP-Δ^2-pyrazoline is oxidized at 0.57 V [116]

$$\Delta G^{\#} \approx \frac{\lambda_S}{4}\left(1+\frac{\Delta G_{ET}}{\lambda_S}\right)^2 - V \qquad (17)$$

$$\lambda_S = e^2\left(\frac{1}{2r_{D^+}}+\frac{1}{2r_{A^-}}-\frac{1}{d_{DA}}\right)\left(\frac{1}{n^2}-\frac{1}{\varepsilon_S}\right) \qquad (18)$$

Indeed, the quantities for $\Delta G^{\#} + V$ provide an improved agreement with the different quenching behavior *(Table 33)*. Whereas in the case of BTPP-DMA in acetonitrile, $\Delta G^{\#} + V \sim 4.5 \times k_BT$, the energy barriers in PPP-DMA (*ca*. 6.5 x k_BT) and in BTPP-OCH_3 (ca. 25 x k_BT) are distinctly higher. Even for BTPP-DMA in diethylether, where the destabilization of the ion pair is less compensated by the gain in energy due to Coulombic attraction (which increases in solvents of low dielectric constant), ET is connected with a barrier comparable to that for PPP-DMA in MeCN. The "borderline" behavior is further exemplified by the sensitivity of the ET process towards substitution of the DMAn donor. Both, the A15C5 and $AT_4$15C5 crown slow down the ET process (in the case of the latter drastically) as could be derived from the fluorescence quantum yield and lifetime data in *Table 28*, p. 77. Besides other important ET parameters, in the case of a sensible ET quenching reaction, a comparison of different substituted anilino derivatives should take into account the actual redox potentials.[xc]

Again, considering the molecular orbitals provides a possible explanation. The localization is similar to that in BTPP-DMA for all three MOs of interest, but the energy gap between the HOMO and HOMO-1 is larger for BTPP-AT415C5 inducing a larger gap between the initially populated CT state and the quenching ET state (see caption of *Fig. 56*, p. 82). For the examples presented here, the simple consideration could only qualitatively explain the difference upon exchanging a 5-*p*-methoxy for an amino donor.

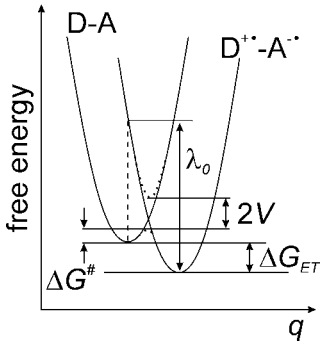

Fig. 57
Free energy curves for an unsymmetrical ET as a function of a general reaction coordinate q. The solid parabola denote the diabatic potential surfaces and the dotted parabola denote the adiabatic surfaces in the region of intersection.

In conclusion, the relative differences of the kinetic and thermodynamic ET properties as well as the quantum chemical calculations are in line with the experimental observations that by tuning the intramolecular CT in the main chromophore of the triaryl-Δ^2-pyrazolines it is possible to accelerate or slow down an excited-state ET process, which can be utilized for sensing activities.

5.5 Complexes of Triaryl-Δ^2-Pyrazoline Fluorescent Probes

In analogy to the BTAC crowns, the complexation behavior of the BTPP crowns was investigated with the main group metal ions of the first two groups of the periodic table as well as with the heavy and transition metal ions already mentioned in Ch. 4.5, i. e., Ag^I, Cu^I, Cu^{II}, Ni^{II}, Co^{II}, Zn^{II}, Cd^{II}, Hg^{II}, and Pb^{II}. Due to the nature of the ET sensing process, most of the complex stability constants reported in this chapter were determined only from fluorescence measurements. Furthermore, a comparison of the crowned BTPP derivatives with other ET ion sensing systems reported in the literature is given at the end of this chapter.

5.5.1 Complexation Behavior of BTPP-$AT_4$15C5

A comparison of the fluorescence quantum yields given in *Table 28*, p. 77 clearly indicates that if complexation-induced

xc) Note that the oxidation potentials given in the literature for *N,N*-dimethylaniline (e. g., 0.85 V [308a] or 0.81 V [308b], both in MeCN vs. SCE) are shifted for about 100 and 150 mV or 60 and 110 mV compared to BTPP-DMA (0.44 V vs. Fc/Fc$^+$; Fc Fc$^+$ + 0.31 V = SCE) or PPP-DMA (0.39 V vs. Fc/Fc$^+$). Moreover, any simplifications made when employing the *Weller* equation have to be carefully considered.

Table 33
ET parameters for BTPP-DMA in different solvents, BTPP-OCH_3, and PPP-DMA in acetonitrile.

	Solvent	ΔG_{ET} eV	λ_S [a] eV	$\Delta G^{\#} + V$ cm^{-1}
BTPP-DMA	MeCN	-0.48	1.25	960
	Et_2O	-0.02	0.73	1390
BTPP-OCH_3	MeCN	0.52	1.28	5100
PPP-DMA	MeCN	-0.27	1.14	1340

[a] for parameters see *Table 32*

fluorescence enhancement occurs, large FEF can be expected. Whereas PPP-DMA is highly fluorescent in acetonitrile and still moderately fluorescent in methanol, BTPP-DMA and its crowned analogues are less fluorescent in these solvents.

Furthermore, both 5-*p*-H derivatives, i. e., BTPP-H and PPP-H (and the 5-*p*-donor derivative BTPP-OCH_3) are highly fluorescent (PPP-H: ϕ_f = 0.38 in MeOH, ϕ_f = 0.62 in MeCN; BTPP-H: ϕ_f = 0.38 in MeOH, ϕ_f = 0.75 in MeCN)[xci].

5.5.1.1 Steady-State Spectra

The spectroscopic changes induced upon complexation of metal ions to BTPP-$AT_4$15C5 are strongly dependent on the metal ion. As will be discussed in detail below, for metal ions with a strong tendency for chelate formation, complexation at two different coordination sites in the molecule is possible. However, only complexation to the crown ether moiety is reminiscent of a behavior expected for an "ET analogue" of BTAC-$AT_4$15C5. *Table 34* combines the spectroscopic data of the metal ion complexes of BTPP-$AT_4$15C5.

Whereas no changes in fluorescence quantum yield occur in the presence of all the alkali and alkaline-earth metal ions, binding to heavy and transition metal ions leads to fluorescence enhancement in the case of Ag^{I} and, to a minor extent, Hg^{II}. For Hg^{II} and Cu^{II}, the appearance of a second absorption and corresponding emission band is observed at higher cation concentration/excess ($x_{M/L} \geq 2$).

xci) The changes are comparably drastic in acidic solution, i. e., the ET process is "switched off" by protonation. Here, electrochemical investigations support the spectroscopic observations. For protonated PPP-DMA and BTPP-DMA the first step in the cyclovoltammogram disappears, i. e., the oxidation of the anilino group. Only the irreversible oxidation of the pyrazoline moiety (BTPP-DMA: 0.72 V in MeCN vs. $Fc/Fc^{+\cdot}$, PPP-DMA: 0.49 V in MeCN vs. Fc/Fc^{+}) was detectable. Accordingly, protonation, like complexation, leads to a "switching on" of fluorescence for the BTPP derivatives.

Table 34
Spectroscopic properties of the cation complexes of BTPP-$AT_4$15C5 in acetonitrile (for the concentration range used and further comments, see caption to Table 22, p. 63; $c_L = 3 \times 10^{-6}$ M).

	$\tilde{\nu}$ (abs)	$\tilde{\nu}$ (em)	$\Delta\tilde{\nu}_{cp\text{-}fp}$ (abs)	$\Delta\tilde{\nu}_{cp\text{-}fp}$ (em)	ϕ_f	τ_f (blue) [a]
	10^3 cm^{-1}	10^3 cm^{-1}	cm^{-1}	cm^{-1}		ns
BTPP-$AT_4$15C5 [b]	24.94	19.47	-	-	0.10	0.98, 2.96 [c]
⊂Hg^{II} [d]	25.13, 21.69	19.61, 16.61	190, -3250	140, -2860	0.22, 0.03	1.23, 2.88 [e]
⊂Zn^{II}, Cd^{II}, Ni^{II}, Co^{II}	-	-	- -	-	-	-
⊂Cu^{II} [d]	25.06, 21.32 [f]	19.57, 16.60	120, -3620	100, -2870	n.d. [g]	3.2
⊂Cu^{I}	24.9	19.8	0 0	0.12	n.d	-
⊂Ag^{I}	25.06	19.61	120 140	0.65	3.70	-

	τ_f (red) [a]	logK_S	r_M [h]	$\chi_m^2 \times r_M$ [i]
	ns	(em)	Å	
BTPP-$AT_4$15C5 [b]	-	-	-	-
⊂Hg^{II} [d]	0.59	5.3, 3.6	1.02	4.08
⊂Zn^{II}, Cd^{II}, Ni^{II}, Co^{II}	-	-	0.74, 0.95, 0.69, 0.74	2.01, 2.71, 2.52, 2.61
⊂Cu^{II} [d]	0.7	n.d.	0.73	2.64
⊂Cu^{I}	-	n.d.	0.96 (4)	3.46
⊂Ag^{I}	-	4.92	1.15	4.28

[a] "blue" denotes excitation and emission wavelength set in the high-energy bands, "red" denotes excitation and emission wavelength set in the low-energy bands;

[b] no effects observed for Pb^{II}, Mg^{II}, Ca^{II}, Sr^{II}, Ba^{II}, Li^{I}, Na^{I}, K^{I};

[c] $a_{rel}(1) = 0.95$ (cf. *Fig. 53*, p. 81);

[d] The low-energy bands are only observed at a metal ion excess of $x_{M/L} > 2$ (upper µM concentration range). Excitation at the high-energy absorption band yields the high-energy emission band and excitation at the low-energy absorption band yields the low-energy emission band.

[e] $a_{rel}(1) = 0.85$;

[f] For BTPP-$AT_4$15C5⊂Cu^{II}, various subbands, exemplified by shoulders in the absorption spectrum were found, whose origin is unclear at present (see text).

[g] not determined;

[h] All radii were taken from ref. [249a] for six-coordination except where the coordination number is indicated in brackets [250a] and except for Cu^{I} [250b]. For Cu^{I}, tetrahedral coordination is found in most polythia ether complexes [251].

[i] The electronegativity values given in the literature differ largely in units [252a]. Here, the softness or class B parameter [253] was calculated with the electronegativity values of *Allred* and *Rochow* [252b, c].

During a titration of BTPP-AT$_4$15C5 with these two ions, first the absorption band centered at 24 940 cm^{-1} remains nearly unchanged and only at $x_{M/L} > 2$, a second band centered at ca. 21 500 cm^{-1} appears. Parallel to the slight hypsochromic shift of the absorption band (to ca. 25 100 cm^{-1}) in the first part of the titration, the aniline absorption band at 37 700 cm^{-1} is diminished. The resulting absorption spectrum at $x_{M/L} = 1$ is identical with the absorption spectrum of BTPP-H suggesting efficient complexation in the crown ether moiety *(Fig. 58)*. In all the cases where the ion is bound to the macrocycle and the nitrogen lone electron pair participates in cation binding, this band is diminished (*Fig. 60*, p. 91). The origin of the second red-hifted absorption band will be discussed in detail in Ch. 5.5.3.

As has already been mentioned for BTAC-AT$_4$15C5, complex formation with the Cu^{II} ion follows comparatively slow kinetics, i. e., the immediately formed complex undergoes rearrangement, and time-dependent changes in the absorption spectrum are observed.[xcii] For both complexes, BTPP-AT$_4$15C5⊂Hg^{II} and Cu^{II}, excitation in the high-energy absorption band yields the "blue" fluorescence emission (typical for such Δ^2-pyrazolines) and the same accounts for the low-energy bands. This is in agreement with the dependence of the fluorescence excitation spectra on emission wavelength. A fluorescence excitation spectrum recorded at an emission wavelength of 20 000 cm^{-1} yields a spectrum being similar to that of the uncomplexed probe. When gradually bathochromically shifting the observation wavelength, the low-energy band builds up and the band centered at 19 600 cm^{-1} gradually decreases. The results of a fluorometric titration shown in *Fig. 59* are very similar to the UV/Vis-spectrophotometric titration.

BTPP-AT$_4$15C5⊂Cu^{II} shows the same spectroscopic features as the Hg^{II} complex only with reduced fluorescence quantum yields for both emission bands. The FEF for the complex at Hg^{II} $x_{M/L} = 1$ (Hg^{II} resides in the crown) equals 2.2. A higher

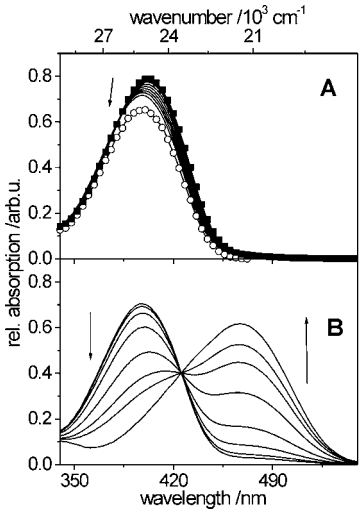

Fig. 58
*UV/Vis-spectrophotometric titration spectra of BTPP-AT$_4$15C5 with Hg^{II} perchlorate in acetonitrile. Hg^{II} addition in the range of $0.02 \le x_{M/L} \le 1$ (**A**) and $2 \le x_{M/L} \le 100$ (**B**). The spectrum of uncomplexed BTPP-AT$_4$15C5 (■) and the absorption spectrum of BTPP-H (o) are included for better comparison ($c_L = 5 \times 10^{-6}$ M).*

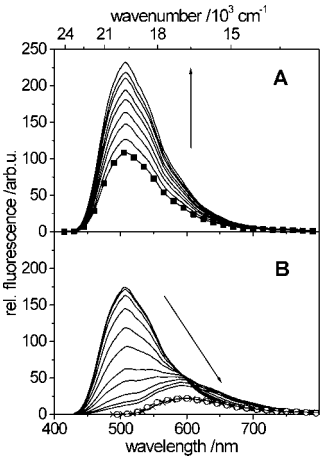

Fig. 59
*Fluorometric titration spectra of BTPP-AT$_4$15C5 with Hg^{II} perchlorate in acetonitrile. HgII addition in the range of $0.02 \le x_{M/L} \le 1$ (excitation at 400 nm, **A**) and $2 \le x_{M/L} \le 100$ (excitation at isosbestic point 425 nm, **B**). Solid squares (■) denote the spectrum of uncomplexed BTPP-AT$_4$15C5 and the emission spectra of BTPP-AT$_4$15C5⊂Hg^{II} at large ion excess excited at 480 nm (o) and of [MeBTPP-OCH$_3$]$^+$ (x) are included for better comparison ($c_L = 1 \times 10^{-6}$ M).*

FEF of 6.5 is observed for its Ag^I complex. Here, the normal ET fluorescent probe behavior becomes evident, i. e., inhibition of ET, indicated by negligible changes in band position of the steady-state spectra, fluorescence enhancement, and an increase in fluorescence lifetime (see below).

Whereas the titration spectra for Hg^{II} suggest that complex formation at the two binding sites is consecutive in the case of Cu^{II} (lower complex stability of AT$_4$15C5⊂Cu^{II} compared to a N,N-5-membered ring chelate of that ion, see Ch. 5.5.3) the different kinetics do not allow for a reliable determination of the single fluorescence quantum yields. Thus, a definite statement on the presence or absence of paramagnetic quenching is not possible.

5.5.1.2 Fluorescence Lifetimes

The different behavior of the three ions is also reflected by the cation-induced changes in fluorescence decay kinetics. Ag^I is bound only to the designated receptor part and engages the lone electron pair completely in coordination, hence, the fluorescence decay being sufficiently well described by a single exponential *(Table 34)*. In the presence of Cu^{II}, two decay components are observed. Their relative amplitudes depend on emission and excitation wavelength in the same way as reported before for the corresponding steady-state emission and fluorescence excitation spectra. Thus, the lifetime of 3.2 ns can be attributed to the "blue" complex with coordination at the crown and the fast decay component (0.7 ns) originates from the "red" chelate (see Ch. 5.5.3 for discussion).[xciii]

For Hg^{II}, the lower FEF compared to Ag^I and the two decay components with time constants comparable to those of the free probe suggest that the "switching off" of the ET process is either less efficient or counterbalanced by another process. With increasing Hg^{II} concentration, the relative amplitudes remain nearly unchanged ($a_{rel}(1) = 0.85$, *Table 34*) but a third decay component, displaying similar features as the fast

xcii) Due to the oxidative character of Cu^{II} in acetonitrile, the studies concerning Cu^{II} were carried out only at $x_{M/L} \le 2$ (cf. Ch. 5.5.3).

xciii) Note that these are the lifetimes of the complex(es) after one day of equilibration.

component in the case of Cu^{II}, appears (a_{rel} increases with increasing excitation and detection wavelength). Moreover, the lifetimes of the two slow decay components (those in the high-energy band) decrease with increasing Hg^{II} concentration (e. g., from 2.88 ns at $x_{M/L}$ = 1 to 2.08 ns at $x_{M/L}$ = 1000) pointing to diffusion-controlled quenching of this "heavy ion". However, the elucidation of a mechansim accounting for the reduced ET activity of Hg^{II} at $x_{M/L}$ = 1 was not possible up to the present stage of investigation. When considering $AT_4$15C5⊂Hg^{II} as a "heavy atom substituent" a possible explanation might arise from the heavy atom quenching effect which has been observed for the 5-*p*-iodo derivative of PPP-H before [283a]. Another possible explanation involves two ground state conformers of the complexes showing different ET blocking efficiencies (cf. Ch. 6.5).

The higher sensitivity of this ET process compared to the ICT process governing the spectroscopic behavior of the D-A-chalcones is exemplified by complexation to Cu^{I}. Whereas for BTAC-$AT_4$15C5 no effects on the photophysical properties of the molecule upon addition of Cu^{I} ions were observable, for BTPP-$AT_4$15C5 a slight but significant fluorescence enhancement is found. As would be expected for the site of complexation, i. e., the $AT_4$15C5 moiety, and their comparable chemical nature, Cu^{I} behaves very much like Ag^{I}.

Moreover, the second evidence for binding of these metal ions to the crown ether moiety can directly be concluded from the decrease of the characteristic absorption band of the aniline moiety at 37 700 cm^{-1}.

5.5.2 Complexation Behavior of BTPP-A15C5

In the presence of alkali and alkaline-earth metal ions, the tetraoxa analogue BTPP-A15C5 displays ET sensing properties with analytically favorable average FEF of *ca.* 25 for the alkali and *ca.* 35 for the alkaline-earth metal ions (maximum FEF = 44 for Ca^{II}). These changes in fluorescence quantum yield are reflected by corresponding changes in fluorescence lifetime with the spectral properties remaining nearly unchanged. The spectroscopic properties of the complexes of BTPP-A15C5 are summarized in *Table 35*.

The "switching on/off" nature of the quenching process is further demonstrated by the small differences in fluorescence quantum yields and lifetimes within a group of mono- or divalent main group metal ions. In the complex (at full complexation), when the lone electron pair of the anilino nitrogen atom is predominantly engaged in cation complexation, the redox properties of the anilino fragment are essentially changed and the ET process is blocked [62]. The best fit of ion into the cavity for Ca^{II} and the high charge density of this ion is demonstrated by identical rate constants for fluorescence and non-radiative deactivation as for BTPP-H.

Another corollary of electron pair abstraction has been mentioned above and is also valid for the complexes discussed here, i. e., the absence of any anilino absorption band for the bound fluorescent probe.

Complete absence of excited-state ET is found in the case of BTPP-A15C5⊂Pb^{II} as well. Although, the Pb^{II} ion does not fit well into the crown ether's cavity, the ion"s "softer" character implies tighter binding to the crown ether nitrogen atom than in the case of the alkaline-earth metal ions.

The results obtained for BTPP-$AT_4$15C5⊂Cu^{II} and Hg^{II} suggested that addition of these ions to a solution of BTPP-A15C5 might as well result in the occurrence of a red-shifted second absorption band at higher concentrations. Accordingly, this was found for BTPP-A15C5 *(Table 35)* and led to a more closer inspection of the nature of the complexes formed.

5.5.3 Nature of the Complexes

Recalling the investigations conducted for the D-A-chalcones in order to elucidate the nature of the second coordination site, *Scheme 14* comprises the possible complexation mechanisms of crowned BTPP derivatives and metal ions. Again, three different complexes are theoretically possible, i. e., the crown inclusion complex, a bidentate N,N-chelate, and a bidentate S,N-chelate (both with a 5-membered ring). Since the absorption band of the CT transition in the 1,3-diaryl-Δ^2-pyrazoline chromophore is red-shifted, complexation in the acceptor part of this subchromophore leading to increased acceptor strength is anticipated and the experiments described in the following paragraphs confirm this assumption.

The experiments described in this chapter include steady-state absorption and emission measurements of various metal ions and BTPP-DMA, BTPP-OCH_3, BTPP-H, PPP-DMA, PPP-H, and [MeBTPP-OCH_3]$^+$ (for chemical structure, see *Scheme 15*, p. 92).

The absorption spectra of various BTPP derivatives in the presence of Hg^{II} are displayed in *Fig. 60*. For all the spectra shown, the same concentration of dye and the same $x_{M/L}$ were used. Thus, the ability for complex formation at the 5-*p*-substituent and at the chelating site directly correlates to the relative intensities of the bands centered at ca. 25 000 cm^{-1} and 21 300 cm^{-1}, respectively.

The ratio $I_{25\,000\,cm^{-1}} / I_{21\,300\,cm^{-1}}$ decreases on the order of BTPP-$AT_4$15C5 > -A15C5 >> -DMA > -H pointing to the fact that only for the tetrathia crown derivative complexation at the macrocyclic moiety occurs and for A15C5 and DMA loose-coordination to the anilino nitrogen N^{DMA} (without appreciable stabilization by the crown in the case of BTPP-A15C5) is operative (note that the anilino band at 37 700 cm^{-1} disappears). BTPP-H, lacking any other coordination site than the chelate, shows the smallest ratio. Another conclusion which can be directly drawn from *Fig. 60* is the photophysical consequence of chelate formation. Comparison of the band positions in the absorption spectra of the Hg^{II} complexes and [MeBTPP-OCH_3]$^+$ indicates that interaction of the positively charged ion with the benzothiazole nitrogen atom N^{BT} and N(2) seems to be responsible for the bathochromic shift.

Moreover, the emission band of [MeBTPP-OCH_3]$^+$ is centered at the same position as the low energy emission band of the Hg^{II} complexes of the BTPP derivatives and the spectroscopic data of the chelate of BTPP-$AT_4$15C5⊂Hg^{II} and [MeBTPP-OCH_3]$^+$ are in good agreement (cf. *Tables 34* and *36*). For a better comparison, all the relevant data are included in *Table 36*. As would be expected for complexation of a positively charged cation to the acceptor of a chromophoric system undergoing an ICT from the donor to the acceptor upon excitation, the "red" complex is stable in the excited state. This is exemplified by similar Stokes shifts for the

Table 35
Spectroscopic properties of the cation complexes of BTPP-A15C5 in acetonitrile (for the concentration range used and further comments, see Table 22, p. 63; cL = 3 x 10^{-6} M). The corresponding radiative and non-radiative rate constants for BTPP-H in acetonitrile are 1.8 x 10^8 s^{-1} (k_f) and 0.7 x 10^8 s^{-1} (k_{nr}), Table 29, p. 80).

	$\tilde{\nu}$ (abs)	$\tilde{\nu}$ (em)	$\Delta\tilde{\nu}_{cp\text{-}fp}$ (abs)	$\Delta\tilde{\nu}_{cp\text{-}fp}$ (em)	ϕ_f	τ_f	logK_S	k_f	k_{nr}	r_M [a]	n^2 / r_M
	10^3 cm^{-1}	10^3 cm^{-1}	cm^{-1}	cm^{-1}		ns	(em.)	10^8 s^{-1}	10^8 s^{-1}	Å	$Z^2Å^{-1}$
BTPP-A15C5 [b]	25.00	19.52	-	-	0.016	0.03 [c]	-	1.5	89	-	-
⊂Li^I	25.06	19.45	60	-70	0.43	2.77	3.00	1.5	2.0	0.76	1.32
⊂Na^I	25.00	19.42	0	-100	0.49	2.88	2.52	1.7	1.8	1.02	0.98
⊂K^I	25.00	19.42	0	-100	(0.21) [d]	2.82	(2.10) [d]	(0.7)	(2.8)	1.46	0.68
⊂Mg^{II}	25.19	19.52	190	0	0.63	4.03	3.16	1.6	0.9	0.72	5.55
⊂Ca^{II}	25.12	19.42	120	-100	0.71	3.99	4.89	1.8	0.7	1.06 (7)	3.77
⊂Sr^{II}	25.06	19.42	60	-100	0.65	3.97	3.87	1.6	0.9	1.21	3.31
⊂Ba^{II}	25.06	19.42	60	-100	0.50	3.98	3.78	1.3	1.3	1.47 (9)	2.72
⊂Pb^{II}	25.19	19.72	190	200	0.54	4.03	5.5	1.3	1.1	1.19	3.36
⊂Hg^{II}, Cu^{II} [e]	21.46	ca. 16.60	-3540	ca. -2920	-	-	n.d.	n.d.	n.d.	1.02, 0.73	3.92, 5.48

[a] All the radii were taken from ref. [249a] and are for six-coordination except where the coordination number is indicated in brackets [250a]. The values given in brackets have been found by *Jonker* in X-ray analyses of related MAP-A15C5 complexes [250a, 254]; cavity size of the aza crown: 1.7-1.8 Å [249b, c].

[b] no effects observed for Zn^{II}, Cd^{II}, Ni^{II}, Co^{II}, Cu^{I}, Ag^{I};

[c] only the main component included;

[d] extrapolated values because full complexation could not be achieved due to solubility problems;

[e] these bands are only observed at a metal ion excess of $x_{M/L} > 2$ (upper µM concentration range);

chelates of the BTPP derivatives and [MeBTPP-OCH_3]$^+$. The behavior is reflected by the effects induced upon addition of other heavy and transition metal ions which are not thiophilic (e. g., Zn^{II}). Whereas for BTPP-H (lacking the aniline nitrogen with a high charge density) addition of Zn^{II} leads to the appearance of the bathochromically shifted band, this band is not observed for BTPP-DMA/Zn^{II} even at $x_{M/L}$ = 100 (a ratio, where for example complexation of BTPP-$AT_4$15C5 to Ag^I is complete). Furthermore, loose coordination to the DMA group is exemplified by fluorescence enhancement of the typical BTPP emission band and a decrease in the aniline absorption at 37700 cm^{-1}. Even for Cu^{II} and BTPP-DMA, up to $x_{M/L} \leq 2$, no red-shifted absorption band is measurable.

The data obtained for the protonation studies fit into the picture as well. Treating acetonitrile solutions of BTPP-H and BTPP-DMA with a solution of 0.01 M $HClO_4$ in acetonitrile leads to the appearance of the intense low-energy absorption band at ca. 21 100 cm^{-1} for both derivatives accompanied by the disappearance of the 37 700 cm^{-1} absorption band

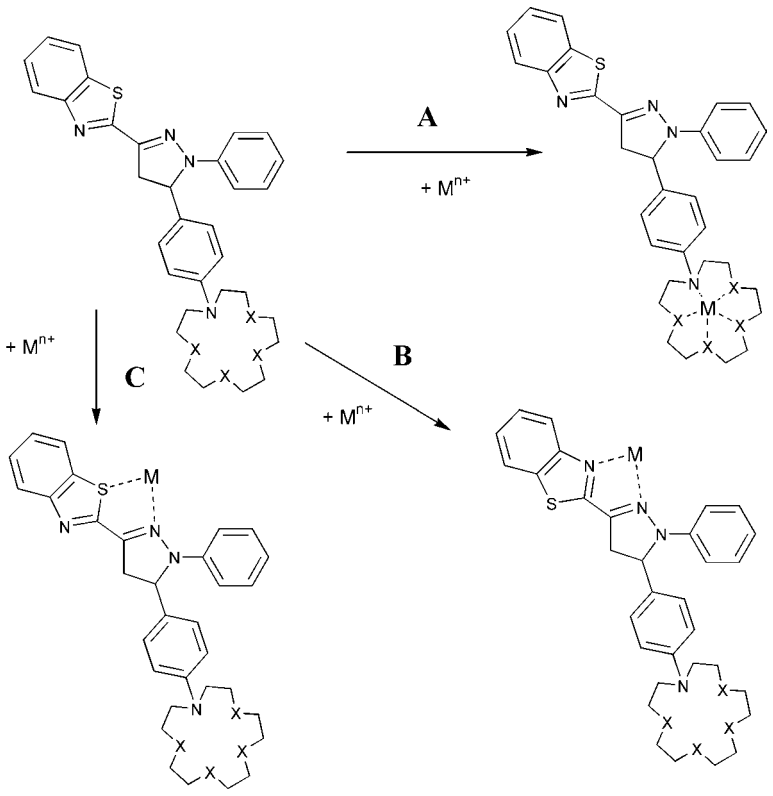

Scheme 14
*Possible coordination sites in triaryl-Δ^2-pyrazolines containing a benzothiazole acceptor and a monoaza crown ether donor. Formation of the ion-macrocycle complex (route **A**), a N,N-chelate (route **B**) and a S,N-chelate (route **C**).*

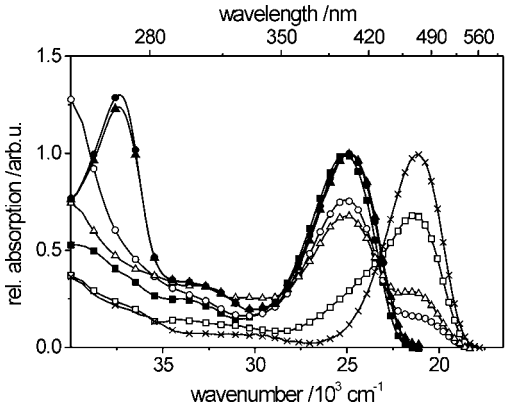

Fig. 60
Steady-state absorption spectra of BTPP-AT$_4$15C5 (o,•) BTPP-A15C5 (Δ , ▲), and BTPP-H (□ , ■) in the absence (solid signs) and presence (open signs) of an excess of Hg^{II} in acetonitrile ($x_{M/L}$ = 10, c_L = 5 x 10^{-6} M). The spectrum of [MeBTPP-OCH$_3$]$^+$ (x) is included for comparison. In the presence of a 10-fold excess of Hg^{II} , BTPP-DMA yields a spectrum very similar to that of BTPP-A15C5 (spectra not shown). All the spectra displayed were corrected for molar absorptivity and dilution and the changes in band intensity are directly proportional to the amount of complex formed (assuming similar molar absorptivities for the latter).

in the case of BTPP-DMA.[xciv] Accordingly, excitation in the "red" band produces an emission band centered at ca. 16 600 cm^{-1}, identical to the emission characteristics of [MeBTPP-OCH$_3$]$^+$.

The resulting extraordinary large bathochromic shift observed upon addition of Cu^{II} to a solution of BTPP-H, i. e., immediate formation of an intense band at 14 000 cm^{-1} (with a shoulder at 15 300 cm^{-1}), will be discussed in a separate paragraph.

PPP derivatives. The experiments carried out with the PPP derivatives, where no N,N-chelate formation is possible, did not reveal further evidence for chelate formation in a straightforward way. At first sight, the absence of a new low-energy band upon addition of Hg^{II}, Cu^{II}, Zn^{II}, or any other ion to PPP-DMA and PPP-H (with the exception of Cu^{II} for the latter, see below) seems to support the above findings. Regarding only charge density, the ions should be (loosely) coordinated preferably to N^{DMA} and/or N(1) (no chelate formation/stabilization is possible with the 3-substituent of the PPP derivatives) in the ground state and thus, at most, a hypso- instead of a bathochromic shift should occur. But instead, no such shifts (besides coordination to N^{DMA} exemplified by a decrease in anilino absorption) are found even at a large excess of Zn^{II}, Pb^{II}, Ni^{II}, and Hg^{II} for both PPP derivatives. Cu^{II} induces a hypsochromic shift accompanied by a decrease in molar absorptivity and fluorescence quenching in the case of PPP-DMA. Whether Cu^{II} coordinates to N(1) (with a higher charge density) or N(2) (sterically more favored) could not be verified. For related heterocycles, i. e., 1-alkylated imidazoles and pyrazoles, the ability of Cu^{II} to bind to the sterically less hindered aromatic nitrogen (without stabilizing chelate formation) is known [267b, c].

Moreover, protonation leads to a similar decrease in the PPP's low energy band accompanied by an increase of a high-energy band and an isosbestic point at 32150 cm^{-1}. These findings are in accordance with results published by *Elguero* and *Jaquier* as well as *Strähle* et al. [289d, 309]. These two research groups found that protonation (and methylation) takes place at N(1) and excludes the 1-phenyl ring from the chromophore leading to a pronounced hypsochromic shift of the absorption band and drastic quenching of the fluorescence (*Table 37*, p. 92 [HPPP-H]$^+$).

Quantum Chemical Calculations. Returning to the quantum chemical calculations the results support these findings (*Table 37*, p. 92). Only protonation or methylation at N^{BT} yields a transition shifted to lower energies with a higher oscillator strength in accordance with the experimental protonation studies (although the trend is less pronounced for a direct comparison of the experimentally determined oscillator strengths of *f* = 0.39 (BTPP-OCH$_3$) and *f* = 0.41 ([MeBTPP-OCH$_3$]$^+$) in acetonitrile according to eqn (37)). For both other possible protonation sites, the calculations predict an anti-auxochromic effect, most pronounced for the nitrogen atom with the highest charge density, N(1). The same tendency is found for the protonated PPP derivatives and here the experiments show indeed a strong hypsochromic shift.[xcv]

Although the highest charge density in the ground state is expected to reside at N(1) (the calculations reveal the order of N^{DMA} > N(1) ≥ N^{BT} >> N(2)), delocalization as depicted in *Scheme 15* is possible in the BTPP derivatives and results in a nearly similar bond order (with pronounced π character for the single bonds) [297] within the chromophore (from N^{BT} to N(1), *Table 31*, p. 83). This is supported by the fact that the pK_a value of alkyl or aryl substituted benzothiazoles is considerably high in acetonitrile [310]. Furthermore, the pyramidalization at N(1) is lost and full orbital interaction of sp^2 hybridized N(1) with the remaining chromophore is gained [311].

Moreover, coordination to N^{BT} and N(2) is confirmed by a comparison of the stability constants of the corresponding Cu^{II} complexes with those obtained for a series of substituted pyridines. Whereas N,N-chelation of Cu^{II} by 2-pyrid-2-yl-1,3-thiazole yields logK_S = 5.65 [312], the same value is much smaller for 5-pyrid-2-yl-1,3-thiazole (logK_S = 1.70)[xcvi] [313a]. In the second derivative, only stabilization via a S,N-chelate is possible and is clearly not favored. Furthermore, when stabilized by a chelate structure, complex formation involving the benzothiazole nitrogen donor atoms is known to occur for transition metal ions [313]. Additionally, the quantum chemical calculations reported above reveal that the charge density is much higher on the benzothiazole nitrogen atom than on the sulfur atom. Hence, N,N-chelation is anticipated for the BTPP acceptor chelates.

Binding of Cu^{II} by the AT$_4$15C5 Moiety. The complications imposed on the interpretation of the absorption spectra by Cu^{II}-thioether photophysics have already been discussed in Ch. 4.5.7 for BTAC-AT$_4$15C5. Similar observations, i. e., partly different absorption spectra for BTPP-AT$_4$15C5⊂Cu^{II} compared to that of corresponding BTPP-AT$_4$15C5⊂Hg^{II} were also made during these studies. Again, the large overlap of electronic transitions centered on the fluorescent probe and on the Cu^{II}-thioether fragment did not allow for any spectral

xciv) Similar proton-induced changes have been qualtitatively reported by *Buryakovskaya* et al. for 3-quinolin-2-yl and 3-pyrid-2-yl derivatives of PPP-H [287b].

xcv) It is interestingly to note that AM1/HyperChem yields results in a generally better agreement with the experimental data than ZINDO/S/HyperChem.

xcvi) logK_S values for M + L → ML. This is stressed by the logK_S values for Cu^{II} complexation with 2-thien-2-yl-pyridine (logK_S = 0.2) [313b] and 4-pyrid-2-yl-imidazole (logK_S = 8.76) [313c].

Table 36
Spectroscopic properties of various cation complexes of triaryl-Δ^2-pyrazolines in acetonitrile ([MeBTPP-OCH_3]$^+$ in MeCN: ϕ_f = 0.07, ε [$\tilde{\nu}$ (abs)] = 33.5 x 10^3 M^{-1} cm^{-1}; (sh) - shoulder).

	$\tilde{\nu}$ (abs)^{blue}	$\tilde{\nu}$ (abs)^{red}	$\tilde{\nu}$ (em)^{blue}	$\tilde{\nu}$ (em)^{red}	$\Delta\tilde{\nu}_{cp\text{-}fp}$ (abs)^{red}	$\Delta\tilde{\nu}_{cp\text{-}fp}$ (em)^{red}	rel. fluo. [a]
	10^3 cm^{-1}	10^3 cm^{-1}	10^3 cm^{-1}	10^3 cm^{-1}	cm^{-1}	cm^{-1}	
BTPP-$AT_4$15C5 [b]	24.94		19.47		-	-	-
⊂Hg^{II}	25.13	21.69	19.61	16.61	-3250	-2860	E
BTPP-DMA [c]	24.94		19.34		-	-	-
⊂Hg^{II} [d]	(24.94)	21.69	(19.34)	16.61	-3250	-2730	(E)
⊂Zn^{II}	(24.94)	-	(19.34)	-	-	-	(E)
H^+ [e]	(24.94)	21.19	(19.34)	16.58	-3750	-2760	(E)
BTPP-H [f]	25.13		19.17		-	-	-
⊂Hg^{II}	-	21.69	-	16.61	-3440	-2560	Q
⊂Cu^{II}	-	14.00, 15.29 (sh)	-	n.d.	-11130	-	Q
⊂Zn^{II}	-	21.74	-	16.61	-3390	-2560	Q
H^+	-	21.05	-	16.58	-4080	-2590	Q
PPP-DMA [g]	27.70		21.34		-	-	-
⊂Cu^{II}	(28.17)	-	(21.34)	-	-	-	(Q)
H^+	39.21	-	-	-	11510	-	Q
PPP-H [g]	28.09		21.50		-	-	-
⊂Cu^{II}	-	15.06, 16.29 (sh)	-	n.d.	-13030	-	Q
H^+	39.21	-	-	-	11120	-	Q
[MeBTPP-OCH_3]$^+$	21.10		16.49		-	-	-

[a] "E" - enhancement, "Q" quenching of the high-energy emission band; letters and values in brackets refer to effects due to loose coordination to N^{DMA};

[b] the effects observed for protons are similar to those of BTPP-DMA;

[c] similar effects observed for BTPP-A15C5;

[d] similar effects for Cu^{II} at $x_{M/L}$ = 2, only quenching;

[e] protonation at N^{DMA} and fluorescence enhancement at low concentrations indicated in brackets;

[f] similar effects observed for BTPP-OCH_3;

[g] no effects observed in the presence of Zn^{II} and Hg^{II} (only a decrease in anilino absorption for PPP-DMA)

separation and a further assignment of single bands. Thus, for a more detailed discussion, the reader is referred to Ch. 4.5.7.

Reaction of BTPP-H and PPP-H with Cu^{II}. Already at $x_{M/L}$ = 1, the presence of Cu^{II} in an acetonitrile solution containing BTPP-H or PPP-H leads to an immediate change in color from yellow (BTPP-H) or colorless (PPP-H) to (deep) blue (14 000 cm^{-1} for BTPP-H, 15 060 cm^{-1} for PPP-H, *Fig. 61*). Both spectra are comparable in shape and display a shoulder at the high-energy side (ca. 1 300 cm^{-1} shifted to higher energies; the shoulder is more pronounced in the case of BTPP-H). Furthermore, both bands are more intense than the lowest-energy absorption bands of the "uncomplexed" dye.

At first sight, these results seem to be surprising but a closer look at the extensive works on the electrochemistry and luminescence behavior of triaryl-Δ^2-pyrazolines by *Pragst* et al. provides an explanation. Having the "*Knorrsche* Pyrazolin-probe" in mind (*Knorr's* pyrazoline test[xcvii]) [314], *Pragst* et al. found an intense absorption band with similar features reported above for PPP-H and Cu^{II} for the dicationic product of the electrochemical oxidation of PPP-H[xcviii] [280a, 315]. In this oxidation reaction, removal of an electron from the triaryl-Δ^2-pyrazoline leads to activation of the carbon atom at the 1-*p*-position and is followed by the formation of a corresponding 4,4'-bis[1-(3,5-diaryl-Δ^2-pyrazolinyl)]-biphenyl derivative. This substituted biphenyl is immediately oxidized (via the corresponding radical cation) to the intensively blue-colored dication. The dication is highly planar and electron delocalization is possible within the whole bis-(1-[3-aryl-Δ^2-pyrazolinyl])-biphenyl chromophore leading to the structured and intensive NIR absorption [280a]. Moreover, the results presented here support other findings by *Pragst* et al., i. e., a sterically more demanding substituent in 3-*p*-position does not prevent oxidation[xcix] but 5-*p*-dimethylamino triphenyl-Δ^2-pyrazoline is only oxidized in acidic acetonitrile [315]. Accordingly, in neu-

xcvii) *Knorr's* pyrazoline test is based on the reaction of triphenyl-Δ^2-pyrazoline with Fe^{III} in acidic solution yielding an intense blue colour.

xcviii) The studies by Pragst et al. were carried out in acetonitrile as well. In the case of PPP-H and Cu^{II}, a (weak) band at 22 400 cm^{-1} being characteristic for the intermediately formed radical cation [280a] was also detected during our studies.

xcix) *Pragst* succeeded in reacting the 3-biphenylyl derivative [280a] and the product formed in the case of BTPP-H indicates that an acceptor in the 3-position does not prevent the reaction.

Table 37
Measured ($\tilde{\nu}$ (abs, exp)) and calculated ($\tilde{\nu}$(abs, theo)) absorption maxima of BTPP-DMA, BTPP-H, PPP-DMA, PPP-H, and their methylated or protonated species (oscillator strength given in brackets).

	-R+ [a]	$\tilde{\nu}$ (abs, exp) [b]	$\tilde{\nu}$ (abs, theo)	$\tilde{\nu}$ (abs, theo)
		10^3 cm^{-1}	10^3 cm^{-1}	10^3 cm^{-1}
		hexane	AM1	ZINDO/S
BTPP-DMA	-	25.13 (0.42)	26.74 (0.57)	29.15 (1.05)
BTPP-H	-	25.32 (0.42)	26.81 (0.53)	29.24 (1.04)
[MeBTPP-OCH$_3$]$^+$	N^{BT}	21.05 (0.41) [c]	21.14 (1.11)	21.55 (1.24)
[HBTPP-OCH$_3$]$^+$	N(2)	-	24.57 (0.08) [d]	22.23 (0.14)
[HBTPP-OCH$_3$]$^+$	N(1)	-	27.47 (0.21)	27.70 (0.81)
PPP-DMA	-	27.70 (0.29)	28.57 (0.71)	33.78 (0.82)
PPP-H	-	28.2 [e]	28.65 (0.70)	33.78 (0.81)
1,3-diph.-pyraz. [f]	-	28.17 (0.33) [g]	28.41 (0.69)	33.56 (0.80)
[HPPP-H]$^+$	N(1)	39.06 [h]	32.36 (0.28)	37.45 (0.05) [i]
[HPPP-H]$^+$	N(2)	-	28.65 (0.58)	32.15 (0.54)

[a] position of protonation or methylation;
[b] *f* calculated according to eqn (37), Appendix B;
[c] in acetonitrile,
[d] next lowest transition at 26 190 cm^{-1} (0.70);
[e] ref. [284a];
[f] 1,3-diphenyl-Δ^2-pyrazoline;
[g] in *i*-octane [289d], oscillator strength taken from ref. [289c];
[h] 1,3-diphenyl-Δ^2-pyrazoline protonated at N(1) in dichloromethane [289d] as well as 1,1-dimethyl-3-phenyl-Δ^2-pyrazolinium chloride in ethanol [309];
[i] next lowest transition at 39 520 cm^{-1} (0.86)

tral acetonitrile, no reaction was observed for PPP-DMA and BTPP-DMA. *Pragst* carried out his studies with Fe^{III} in acetonitrile but the observations made here demonstrate that a similar reaction is induced by redox-active Cu^{II} in acetonitrile as well. The strong oxidation power of Cu^{II} in acetonitrile is manifested in the positive half wave potential $E_{1/2}(Cu^{II}/Cu^{I})$ = 0.96 V vs. SCE [316] (compared to $E_{1/2}(Cu^{II}/Cu^{I})$ = -0.09 V vs. SCE in water) [316]. Particularly in this solvent, the amount of stabilizing solvation of Cu^{I} and destabilizing solvation of Cu^{II} account for this pronounced difference.

For a better comparison, *Fig. 61* combines all the metal ion- or proton-induced absorption changes found for BTPP-H and PPP-H in acetonitrile.

5.5.4 Complex Stability Constants and Spectroscopic Effects

Concerning complex stability constants, the tendencies reported for the D-A-chalcones are similar for the crowned BTPP probes (*Tables 34* and *35*, pp. 86, 89). The preference of small cations (unless they are not too small like, e. g., Mg^{II}) with a high charge density for A15C5 is demonstrated by the order of complex stability constants, i. e., Ca^{II} >> Sr^{II} > Ba^{II} > Mg^{II} > Li^{I} >> Na^{I} > K^{I}, and will not be discussed in detail here (cf. Ch. 4.5.4).

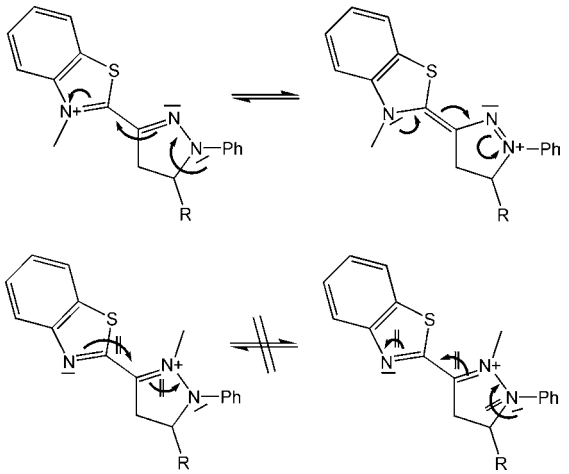

Scheme 15
Possible mesomeric stabilization of a positive charge at N^{BT} (or N(1), upper part, [MeBTPP-OCH$_3$]$^+$: R = Ph-OCH$_3$) and at N(2) (lower part).

Whereas the sensing potential of the BTPP crowns is higher (due to larger FEF), this increase in sensitivity (e. g., complexation of Cu^{I} is detectable) is contrasted by a lack in specifity. For example, in the case of BTPP-A15C5, all the divalent and all the monovalent cations yield similar fluorescence lifetimes and comparable FEF rendering it impossible to discriminate between different mono- or divalent cations on the basis of photophysical changes as a function of charge density, class A or ionic index.

Upon exchanging the macrocyclic receptor, similar ion-binding preferences are found as in the case of the BTAC fluorescent probes and the reader is referred to Ch. 4.5.5 for a more detailed discussion.

5.5.5 Considerations on Improved Sensor Design

The ET sensing properties and complexation behavior of the BTPP crowns described here point to the question of the design of more sophisticated triaryl-Δ^2-pyrazoline systems showing better sensitivity and applicability[c]. Sensitivity is directly connected to the efficiency of the ET process and its inhibition by cation complexation and applicability implies shifting of both absorption and emission bands to longer wavelengths[ci]. With the results and the discussion given so far in mind, both effects cannot be separated from each other.

c) Of course, improved selectivity is a goal of similar importance but the chemistry of specific receptor design will not be deepened here.

ci) And, of course, water solubility. But this question is directed towards further, more synthetically oriented work.

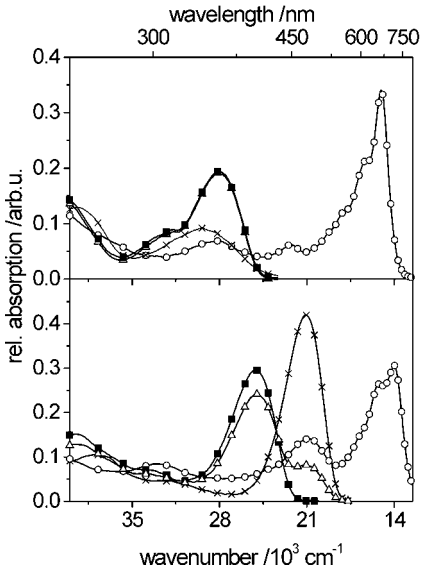

Fig. 61
Steady-state absorption spectra of PPP-H (top) and BTPP-H (bottom) in the absence and presence of Cu^{II}, Zn^{II}, and H^+ in acetonitrile. The spectra displayed were recorded for solutions containing the dye (■) and Zn^{II} (Δ, $x_{M/L}$ = 10), Cu^{II} (o, $x_{M/L}$ = 2), or 0.01 M $HClO_4$ (x) (c_L = 1 x 10^{-5} M).

For a given donor in 5-position, a stronger ICT character of the 1,3-chromophore (Ar-C(3)= N(2)-N(1)-Ar) results in red-shifted spectral band positions and (possibly) higher ET quenching efficiency. Unfortunately, not only the ET process may be enhanced (above all in polar solvents) but the smaller gap between the excited and ground state also increases radiationless deactivation of the excited state [243]. This in turn should lead to a weaker fluorescent "switched on" state.

The "ideal sensor" cannot be proposed at the present stage but some features which have to be kept in mind for long-wavelength and efficient ET sensor design of the triaryl-Δ^2-pyrazoline type will be briefly described and discussed by means of comparing results obtained during this work and reported by other research groups.

The fluorescence quantum yields given in *Table 28*, p. 77, and the data reported on various 1,3-*p*-donor-acceptor substituted PPP-H derivatives give a first hint for alternative donor-acceptor choice. Increasing the CT character and maintaining a reasonable fluorescence quantum yield in the basic fluorophore (i. e., in its "switched on" state) is only possible by the careful choice of the acceptor. As has been mentioned above the substituent in 1-*p*-position does not only influence the strength of the CT process but plays a crucial role in excited-state deactivation as well. For a better illustration, *Table 38* combines the relevant data of some compounds of interest. It is apparent that substitution with heteroatom-free aromatic groups such as *p*-biphenylyl or styryl does not yield a stronger bathochromic shift than 3-BT substitution, even in combination with an electron donating substituent in 1-*p*-position (e. g., -OCH_3). Accordingly, their reduction potentials lie inbetween those of PPP and BTPP derivatives (-2.16 V vs. SCE in MeCN) [280b].

The same accounts for a number of small heterocycles (e. g., 4-pyridyl and 2-thienyl, not included in the table) [287a, b] which absorb at shorter wavelengths than BT and show the complication in terms of transition metal ion sensing, i. e., a second chelating site, in most cases, too. The 3-benzophenonyl ("CO-Ph" in *Table 38*) substituted Δ^2-pyrazoline would be an alternative regarding spectral band position and fluorescence intensity, but here, the question of acceptor chelation would appear again. Furthermore, increasing the donor strength at the 1-*p*-position is even more crucial for the overall fluorescence quantum yield of the unquenched molecule (absence of ET involving any 5-substituent). Both, 1-*p*-methoxy- and 1-*p*-amino-3-*p*-cyano-triphenyl-Δ^2-pyrazoline show reduced emission already in apolar solvents. In polar solvents, their fluorescence is even more quenched resulting in ϕ_f = 0.25 in acetone and 0.06 in MeOH (1-*p*-methoxy-triphenyl-Δ^2-pyrazoline) [289c] as well as < 0.01 in MeOH (1-*p*-amino-triphenyl-Δ^2-pyrazoline [283c]; compared to BTPP-H: ϕ_f = 0.75 in acetone and 0.38 in MeOH).

Due to the lack of spectroscopic data and 1-*p*-substitution pattern for 1-*p*-D-3-A-substituted Δ^2-pyrazolines (especially fluorescence quantum yield data), the role of enhanced twisting of the 1-*p*-D-aryl group in terms of non-radiative deactivation remains obscure (for a discussion of pretwisted, unsubstituted PPP derivatives, see Ch. 5.2.1). But from the data available so far it seems that 1-*p*-substitution does not yield more favorable ET sensors. Unfortunately, no fluorescence quantum yields were reported for 3-naphthoylene-benzimidazolyl-substituted Δ^2-pyrazolines by *Pereyaslova* et al. [287f] but recent results obtained by us for Δ^2-pyrazolines carrying a naphthalimide acceptor in 3-position suggest, that bathochromically absorbing and emitting Δ^2-pyrazolines still maintain a reasonable fluorescence quantum yield in highly polar solvents (s. *Table 39* [317]). Consequently, for Δ^2-pyrazoline sensor design, careful tuning of the 3-*p*-acceptor moiety is a more promising start than (simultaneously) increasing both acceptor and donor strength.

5.6 Analytical Applications

The high FEF observed for the alkali and alkaline-earth metal ions and BTPP-A15C5 suggest that the latter can act as a suitable sensor molecule for these ions in the µM to mM concentration range in solution. Especially valuable is the insensitivity of the main fluorophore towards binding of Pb^{II} to the 5-receptor, i. e., large FEF without pronounced "heavy ion" interaction. Although species-characteristic fluorescence signals (e. g., fluorescence lifetime) are not provided by most ET probes, the lack in spectroscopic selectivity can be overcome by introducing more specific receptors [108g] and thus, discriminating between the ions of interest (as, e. g., with $AT_4$15C5). The excellent correlation observed for a plot of metal ion concentration vs. fluorescence intensity is indicated in *Fig. 62*, respectively and suggests a straightforward applicability in chemical analysis. Moreover, when employing probe concentrations of ca. 1 x 10^{-5} M, the interferences by Cu^{II} or Hg^{II} (N,N-chelation) play no role in most media of environmental sensing due to the low concentration of these trace metal ions.

In the case of Ag^I, application of BTPP-$AT_4$15C5 is very favorable when excluding (masking) the presence of Cu^{II} and Hg^{II}. Chelation of these ions to the acceptor cannot be instrumentally circumvented by employing time-resolved fluorometry and analysis of TRES, because the amplitudes of, e. g., such a Ag^I-crown-Cu^{II}-chelate triple complex cannot be

Table 38
Selected spectroscopic data of substituted triaryl-Δ^2-pyrazolines investigated in this work and by other research groups (Naph-Bzlm: naphthoylene-benzimidazolyl).

1-R	3-R	Solvent	$\tilde{\nu}$ (abs)	$\tilde{\nu}$(em)	$\Delta\tilde{\nu}$(abs-em)	ϕ_f
			10^3 cm^{-1}	10^3 cm^{-1}	cm^{-1}	
Ph	BT	Tol	24.81	20.33	4480	0.84
		Hex	25.32	21.19	4130	0.73
Ph	Ph	Benz [a]	27.55	22.57	4980	0.92 [b]
		CH [c]	28.1	23.4	4730	0.82
Ph	p-biphenyl	Tol [d]	n.r.	21.83	-	n.r.
	p-CN-Ph	CH [c]	25.25	21.41	3840	0.91
	CO-Ph	Benz [a]	24.15	20.00	4150	0.96 [b]
	Naph-Bzlm	Tol [e]	19.80	16.81	2990	n.r.
p-OCH_3-Ph	Ph	Benz [a]	27.03	21.10	5930	0.93 [b]
	p-biphenyl	CH [f]	n.r.	20.92	-	n.r.
	Styryl	CH [f]	n.r.	20.53	-	n.r.
	p-CN-Ph	Benz [g]	24.04	18.69	5350	0.66
p-NH_2-Ph	p-CN-Ph	CH [h]	23.64	18.62	5020	0.36 [b]

[a] ref. [289b];
[b] degassed solution;
[c] ref. [283a];
[d] ref. [279b];
[e] ref. [287f];
[f] ref. [280b];
[g] ref. [289c];
[h] ref. [283c]

simply correlated with a calibration curve for Ag^I or Cu^{II} and the probe.

Similarly, given the absence of Ag^I and Cu^{II}, BTPP-$AT_4$15C5 could be employed for sensing Hg^{II}. But here, the amount of two distinct fluorescence lifetimes in the free probe and three different lifetimes for the ("blue" and "red") complex require high-quality decay data recorded at different emission wavelengths to allow for a reliable determination of the single amplitudes.

In order to improve the sensing possibilities for heavy and transition metal ions, the development of a 1,3-diaryl-Δ^2-pyrazoline chromophore which is more easily reduced than BTPP and does not offer a second chelating site is required. First studies of the naphthalimide derivatives of BTPP point into this direction [317]. The data given in *Table 39* indicate the high sensing potential of these probe molecules accompanied by an analytically very favorable wavelength region of absorption and emission. Furthermore, no interferences by metal ion complexation or protonation to the 1,3-chromophore were found for these dyes.

Considering a reduction in LOD by means of higher excitation power using lasers, photooxidation of the triaryl-Δ^2-pyrazolines has be to taken into account. *Yamamoto* et al. found oxidation products, i. e. the corresponding pyrazoles, when irradiating samples of triaryl-Δ^2-pyrazolines with light of 366 nm[cii] [287c], and *Grimshaw* et al. observed similar phenomena during the clean-up of newly synthesized pyrazolines [284c].

In the case of the derivatives investigated here, only for BTPP-A15C5 the occurance of such a photoreaction could be verified when using comparatively high laser power (> 9 kW pulse peak power) for excitation of a sample. Moreover, the interference of oxidizing metal ions such as Cu^{II} is strongly reduced in H-acidic solvents such as alcohols ($E_{1/2}(Cu^{II}/Cu^{I})$ = 0.26 V vs. SCE in ethanol) [316] and water since Cu^{II} is more stabilized in these solvents.

Compared to other ET fluorescent probes, the FEF obtained for BTPP-A15C5 are promising.[ciii] While gaining a bathochro-

cii) In earlier works, *Nurmukhametov* et al. assigned a weak green phosphorescence to the "independent chromophore" at the 5-position [286a]. However, the spectral characteristics reported for this phosphorescence are very similar to those found by *Yamamoto* for the triphenyl pyrazoles [287c].

ciii) Note that the FEF of 44 for BTPP-A15C5 and Ca^{II} is maintained in the same complex of the naphthalimide A15C5 derivative [317].

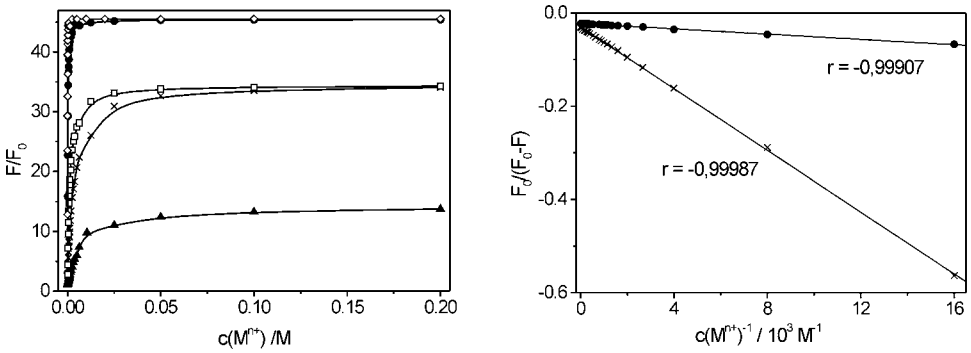

Fig. 62
Left part: Plot of relative fluorescence enhancement vs. metal ion concentration for BTPP-A15C5 and Ca^{II} (◊), Sr^{II} (●), Li^I (□), Na^I (x), and K^I (▲) in acetonitrile (c_L = 1 x 10^{-6} M). Right part: Fit of a $F_0/(F_0-F)$ vs. c_M^{-1} plot for BTPP-A15C5 and titrations with Sr^{II} (●) and Na^I (x) in acetonitrile (c_L = 1 x 10^{-6} M).

Table 39
Spectroscopic data of the 3-[4-(N-phenyl-naphthalimidyl)]-1-phenyl-5-(p-R-phenyl)-Δ^2-pyrazolines in acetonitrile.

5-p-R	$\tilde{\nu}$ (abs)	$\tilde{\nu}$ (em)	$\Delta\tilde{\nu}$ (abs-em)	ϕ_f
	10^3 cm^{-1}	10^3 cm^{-1}	cm^{-1}	
H	20.58	14.72	5860	0.17
H/Hg^{II} [a]	20.58	14.72	5860	0.17
DMA	20.37	14.59	5780	0.002
DMA-H$^+$	20.58	14.72	5860	0.17
A15C5	20.16	14.59	5570	0.004
A15C5⊂Ca^{II}	20.62	14.72	5900	0.17

[a] no effects upon addition of protons as well

mic shift of 30 to 50 nm, the sensing potential should at least be equal to that of other Δ^2-pyrazoline ET probes recently introduced by *de Silva* et al. (their investigations had been carried out in methanol) [108g, 114a, b]. Higher FEF, between a several hundred to a several thousand (cf. Ch. 6.5 and refs [108e], [109a, b], and [112a]) might be possible but the increase in ET efficiency with increasing ICT strength of the 3-acceptor is always counterbalanced by the smaller energy gap between excited and ground state.

5.7 Triaryl-Δ^2-Pyrazolines in Conclusion

The sensible interplay of two intramolecular excited-state processes, an electron and a charge transfer, governs the fluorescence behavior of 5-*p-N,N*-alkylanilino substituted 3-benzothiazol-2-yl-1-phenyl-Δ^2-pyrazolines in polar solvents. Whereas the corresponding triphenyl-Δ^2-pyrazolines are highly fluorescent, the emission of ^{1}CT*, formed in less than 2 ps after excitation, is quenched in acetonitrile by an ET process from the largely isolated 5-substituent to the main chromophore in ca. 30 ps for BTPP-DMA. Accordingly, the crowned derivatives exhibit a similar behavior with the strength of the ET being less pronounced. However, cation complexation in the 5-*p*-crown receptor leads to an increase in both fluorescence quantum yield and lifetime with both effects being equally strong (FEF of 44 at maximum). These analytically valuable cation-induced changes are not only observed for alkali and alkaline-earth metal ions but also for Ag^I, Hg^{II}, and Pb^{II}. Both fluorescent probes BTPP-A15C5 and BTPP-AT$_4$15C5 show the characteristic cation selectivities expected for these receptors but formation of a N,N-chelate with aminophilic metal ions hampers a direct, straightforward application in the latter case.

6 Boron Dipyrromethene Fluorescent Probes

In the last two chapters, the possibilites in metal ion detection with fluorescent probes based on the commonly employed approach of ICT and ET probe design were described and discussed. The design principle developed for the fluorescent probe introduced in this chapter is the same as for ICT probes in terms of the modular sketch used, i. e., directly coupled fluorophore and receptor moiety, but the two parts are combined in a "virtual ET probe setup" showing minimum electronic interaction in a perpendicular arrangement. In its entire spectroscopic behavior, this orthogonal system with a virtual "zero-spacer" between aromatic donor and acceptor fragment combines typical ICT and typical ET characteristics and shows very remarkable sensing properties [106].

6.1 Donor-Acceptor Aromatics - Literature Review

Aromatic amine donor groups are often employed to modify the emission behavior of (larger) aromatic chromophores such as anthracene [318-320], pyrene [304, 320c], phenanthrene [321], acridine/ium [78, 250a, 254, 322], or bis-pyrazolopyridine [323] in order to generate red-shifted CT fluorescence. In contrast to the large number of publications on mechanistic features of these compounds they have only seldomly been used to probe analytes via specific changes in fluorescence. The few examples known until today include the use of ADMA [320a] and D-A-biphenyl [324] as pH probes and the use of MAP-A15C5 [78] for metal ion sensing purposes (for the chemical structures see Appendix D). Moreover, DMABN crowns, related to these D-A-biaryls due to a very similar excited-state CT behavior, have been employed as ion-sensitive fluorescent probes [103] Giving only a very simplified picture in this introduction, a fast charge transfer process in the excited state of the molecule leads to formation of (at least) another excited species and emission can be detected from either state or both states, the initially excited LE^{civ} or the CT state. Since a CT process is involved, the mechanism is strongly influenced by solvent polarity and, depending on the latter and the molecule of interest, e. g., dual fluorescence with well-separated bands can be generated [240]. However, the exact reaction mechanism is still not fully understood and different intramolecular relaxation pathways are discussed for these molecules (e. g., TICT formation) [240, 325].

Sterically restricted derivatives such as, e. g., 3,5-ATMA or DMA-DMPP with interannular twist angles of > ca. 60° already in the ground state as well as related DMPYRBN or 4-DMAP, show dual emission in many solvents [240, 323a, 326]. Often, the dynamic excited-state behavior is complicated. Whereas in some systems, the charge transfer reaction can be sufficiently described with a two-state model (e. g., DMA-DMPP) [323a] for others, a more complex situation involving different transient species and nonexponential fluorescence decay kinetics is observed (e. g., ADMA) [304, 318]. In the sterically restricted derivatives such as 2,6-dimethyl-D-A-biphenyl (78°, calculated) [327] or ADDMA [318c] as well as in charged

civ) In order to avoid misunderstandings (DE is used for the dienol tautomer of BP(OH)$_2$ in this work), no differences concerning the labeling of "localized" (LE) and "delocalized" excited state (DE; relaxed initially excited Franck-Condon state) are made here and only the abbreviation LE is used in the text.

compounds (A-Rh) [328] sometimes an even more complicated behavior involving different twisting motions of the aryl moieties during the lifetime of the excited state is noticed.

In contrast to polarity, in H-acidic solvents, protonation of the amino group totally blocks the CT process and only emission from the LE state is observed [48, 62, 106, 320a, 324].

6.2 Boron Dipyrromethene (BDP) Dyes

1,7-dimethyl-8-aryl-substituted difluorobordiaza-*s*-indacenes (boron dipyrromethene dyes, BDPs) are highly pretwisted molecules with the two aromatic π systems being more or less decoupled. The intense, main absorption band of the BDP chromophore ($\varepsilon > 70\,000$ M^{-1} cm^{-1}) is centered well within the visible range of the spectrum (ca. 20 000 cm^{-1}). Moreover, most BDP dyes show high fluorescence quantum yields (ϕ_f ca. 0.5-0.8) in apolar as well as polar solvents. These properties have led to the development of BDP-based fluorescent probes for many different applications such as local polarity in lipid membranes and proteins [329a], for other biomolecules [329b], and for intramolecularly generated electric fields [329c]. Furthermore, BDP dyes are used in molecular optoelectronic gates [329d], light-harvesting arrays [329e], and as laser dyes [329b]. When introducing a *N,N*-dimethylanilino donor group at the 8-position of the BDP chromophore, fluorescent probes with good pH sensing capabilities are obtained [140, 330].

The spectroscopically advantageous properties along with the high electron affinity of the BDP fluorophore promised to provide a highly efficient sensing mechanism for a fluorescent probe for metal ions and led to the synthesis of BDP-A15C5 *(Scheme 16)* by the group of Prof. *Daub*, University of Regensburg, and the spectroscopic studies described here. In order to get more insight into the photophysical mechanisms being operative in BDP-A15C5, the DMA derivative (BDP-DMA) and the reference compound BDP-H were also investigated by steady-state and time-resolved spectroscopy.

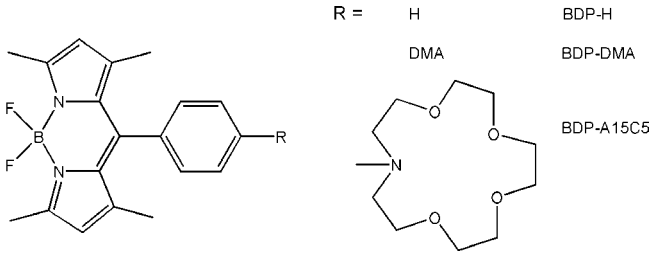

Scheme 16
Chemical structures of the BDP dyes investigated.

6.3 Photophysics

The BDP derivatives investigated here are highly pretwisted already in the ground state and show interannular angles of ca. 75° (78°, X-ray structure of crystalline BDP-DMA) [140] and their photophysical properties are very much governed by this sterical prearrangement.

Keeping in mind the photophysical processes of the D-A-chalcones and the Δ^2-pyrazolines, a short remark on the use of photophysical and mechanistical terms is necessary. Whereas some authors refer to the behavior in D-A-biaryls as a TICT mechanism, others call it an ET mechanism. However, both processes require some kind of geometric rearrangement of the molecule in the excited state involving a separation of charge between a donating and an accepting moiety. Thus, photoelectrochemically speaking, the driving force for both processes is virtually the same. Within the general framework of charge transfer, electron transfer resembles a special case and accordingly, TICT state formation is a further subdivision of ET. However, for the donor-substituted BDP dyes an ICT process governs their photophysical behavior and the features of their metal ion and pH sensing properties resemble those of an ET fluorescent probe.

6.3.1 Steady-State Spectra

The absorption spectra of the three BDP dyes are identical and show the pattern typical for BDP chromophores [329a, 331]. A strong $S_0 \rightarrow S_1$ transition with a maximum at 20 000 cm^{-1} ($\varepsilon = 88\,000$ M^{-1} cm^{-1}) and a blue-shifted shoulder as well as a broader, much weaker transition at 26 300 cm^{-1} ($\varepsilon = 6\,000$ M^{-1} cm^{-1}) are observed in apolar solvents such as hexane. No red-shifted CT absorption is detectable for BDP-A15C5 and BDP-DMA indicating a lack of pronounced donor-acceptor interactions in the ground state. Most favorable, the high steric restriction in these molecules accounts for this fact. Furthermore, for all the three molecules, the absorption spectra are only barely affected by solvent polarity (*Table 40* and *Fig. 63*).

Unlike their absorption properties, the emission behavior of BDP-A15C5 and BDP-DMA is strongly solvent-dependent *(Fig. 63)*. In hexane, emission of mirror shape to the absorption spectrum occurs from the LE state of the BDP fluorophore at ca. 19 700 cm^{-1}. Similar features are found for BDP-H. With increasing solvent polarity this emission is strongly quenched in the amino-substituted derivatives and a red-shifted, broad second emission band is observed. This second emission band shows rather low fluorescence quan-

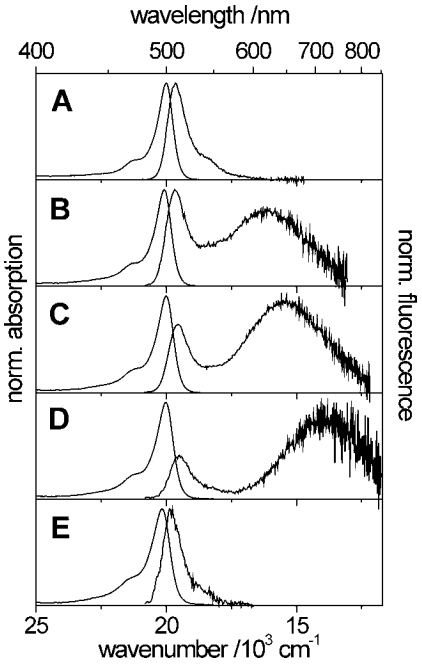

Fig. 63
*Normalized steady-state absorption and emission spectra of BDP-DMA in hexane (**A**), diethylether (**B**), 1,4-dioxane (**C**), tetrahydrofuran (**D**), and acetonitrile (E).*

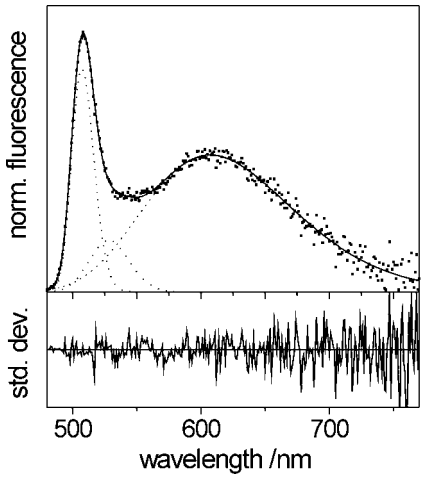

Fig. 64
Fit of the fluorescence spectrum of BDP-DMA in diethylether. The LE band is modeled from the sub- and the main band of BDP-H in the same solvent (measured spectrum (■), fit (—), and single components (·····)).

tum yields and its center is shifted to lower energies with increasing polarity of the solvent. In acetonitrile however, this band could not be detected any more. The fluorescence quantum yields reported for the LE and CT emission in *Table 40* were obtained after spectral separation of the two bands.

The LE band was modeled by fitting the emission spectrum of the reference compound BDP-H in the corresponding solvent to two lognormal functions describing the sub and main band centered at 507 and 529 nm, respectively. In a fit of the spectra showing dual emission, the position, half-width, and skewness of these two components were kept fixed (within a certain interval) and a third lognormal function was included to describe the remaining low-energy band. An example of a fit is given in *Fig. 64* and the calculated fluorescence quantum yields are included in *Table 40*.

Fluorescence excitation spectra of BDP-A15C5 and BDP-DMA recorded with observation wavelengths in both regions, i. e., the LE as well as the CT emission band, have identical shapes and match the UV/Vis absorption spectra. Thus, the low-energy emission can be attributed to a species formed only in the excited state and both, the solvatochromism and the positive solvatokinetic effect suggest its highly dipolar nature, i. e., this species has pronounced CT character.

A similar behavior has been observed for ADMA and related compounds and is consistent with the picture of pretwisted biaryls where charge separation occurs by a fast excited-state reaction [322].

6.3.2 Fluorescence Lifetimes

The fluorescence decay profiles of BDP-H could always be fitted to a single exponential (τ_f = 2.7 to 3.3 ns) in the solvents-investigated *(Table 40)*. In combination with the solvent independent fluorescence quantum yields, similar rate constants for fluorescence deactivation of 0.18 x 10^9 s^{-1} (within experimental errors, *Table 40*) are found for the photophysical behavior of BDP-H regardless of solvent polarity. BDP-A15C5 and BDP-DMA show a comparable dynamic emission behavior in hexane, i. e., monoexponential decay kinetics. As a consequence, the radiative rate constants are very similar to those of BDP-H. However, the non-radiative rate constants are slightly higher than for BDP-H which may be attributed either to the higher conformational flexibility due to the attached dimethylamino and crown substituents or to the interaction with an energetically low-lying local triplet state

Table 40
Spectroscopic properties of BDP-A15C5, BDP-DMA, and BDP-H in different solvents.

	Solvent	$\tilde{\nu}$ (abs)	$\tilde{\nu}$ (em)^{LE}	$\tilde{\nu}$ (em)^{CT}	ϕ_f^{LE}	ϕ_f^{CT}	ϕ_f^{CT} / ϕ_f^{LE}	τ_1	τ_2	τ_3	k_f	k_{nr}
BDP-		**10^3 cm^{-1}**	**10^3 cm^{-1}**	**10^3 cm^{-1}**				**ps**	**ps**	**ns**	**10^9 s^{-1}**	**10^9 s^{-1}**
A15C5	Hex	20.0	19.7	-	0.26	-	-	1590	-	-	0.16	0.46
	Et_2O	20.1	19.6	16.2	0.004	0.050	12	15	405	3.65		
	Diox	20.0	19.5	15.7	0.001	0.033	33	6	150	3.54		
	THF	20.0	19.5	14.3	0.0003	0.014	47	<3	76	2.45		
	MeCN	20.2	19.8	[a]	0.0002	[a]	-	5	-	2.56		
DMA	Hex	20.0	19.5	-	0.31	-	-	1610	-	-	0.19	0.43
	Et_2O	20.1	19.6	16.1	0.012	0.050	4.2	10	-	3.54		
	Diox	20.0	19.6	15.5	0.004	0.029	7.2	6	-	3.50		
	THF	20.0	19.5	13.9	0.001	0.009	9.0	4	-	2.40		
	MeCN	20.2	19.8	[a]	0.0003	[a]	-	3	-	2.79		
H	Hex	20.0	19.6	-	0.50	-	-	2720	-	-	0.18	0.18
	Et_2O	20.1	19.6	-	0.59	-	-	2980	-	-	0.20	0.14
	Diox	20.0	19.6	-	0.58	-	-	3350	-	-	0.17	0.12
	THF	20.0	19.6	-	0.56	-	-	3060	-	-	0.18	0.14
	MeCN	20.1	19.8	-	0.60	-	-	3170	-	-	0.19	0.13

[a] too low to be measured

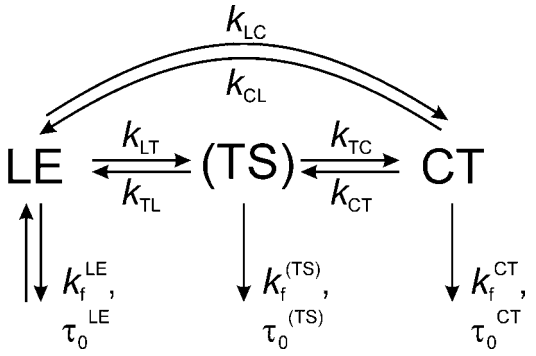

Scheme 17
Generalized kinetic scheme of the photophysical processes governing the excited-state behavior of BDP-A15C5 and BDP-DMA. Three excited species (LE, CT, (TS)) are involved in a possible parallel or consecutive reaction mechanism. For BDP-DMA, only the LE and the CT state are observed and thus $k_{LT} = k_{TL} = k_{TC} = k_{CT} = 0$; (TS) = transient or third species.

(increase of k_{isc}) [302a]. In accordance with the steady-state emission behavior, in the more polar solvents investigated here, the fluorescence decays of both BDP-A15C5 and BDP-DMA could be only fitted to the sum of at least two exponentials. Fluorescence lifetimes of 3-10 ps are found for a fast component and those of 2-3 ns for a slow component *(Table 40)*. Emission wavelength-resolved measurements of the fluorescence decay profiles in the spectral region of 495-690 nm revealed a decrease of the relative amplitude of the fast component with increasing detection wavelength and correspondingly, an increase in a_{rel} of the slow component. Again, this supports a mechanism involving excitation of a single ground state species to a LE state followed by a fast reaction to a CT state *(Scheme 17)*.

In the case of an excited-state reaction with only a single excited precursor species, the occurrence of a rise time for any successor excited species could be expected in the corresponding spectral region of its emission. This (or these) rise time(s) should be similar to the main decay time in the spectral region of the initially observable LE emission. Due to the sterical restriction and fast charge transfer, a contribution from other transient "dark" species leading to a rise time with a longer lifetime in the low energy region of the emission band is not expected for the BDP dyes [318c]. However, the large differences in the two lifetimes and the limitations of the ps-LIF employed made it difficult to detect the rise times (decay times of *ca.* 10 ps expected and a minimum temporal resolution of 5.2 ps chn^{-1} available). The detection of rise times was only possible for BDP-A15C5 in diethylether and for BDP-DMA in both, diethylether and 1,4-dioxane. As expected, the rise times are very similar to the decay times of the fast component. Only in the case of BDP-A15C5, a third decay component with a very low relative amplitude of ≤ 0.05 and lifetimes of τ_f = 405 ps (diethylether), 150 ps (1,4-dioxane), and 76 ps (tetrahydrofuran) was observed in these three solvents. Obviously, a third weakly fluorescing species with CT character is involved in the emission behavior of BDP-A15C5. The appearance of a second transient excited species ((TS) in *Scheme 17*) can most favorably be explained by a double minimum in the potential surface of the excited CT state as a function of the interannular twist angle, a mechanism recently observed in the highly pretwisted 2,6-dimethyl-D-A-biphenyl [327, 332]. However, it was not possible to detect a second rise time and the limiting experimental possibilities, especially in the NIR region, did not allow for global analysis of the wavelength-dependent fluorescence decay data with respect to the verification of such an excited-state reaction mechanism [233]. Thus, the real nature of the transient species and the deactivation process of initially excited BDP-A15C5 remains unclear at present *(Scheme 17)*.

In acetonitrile, CT emission is extremely weak and the relative amplitude of the slow decay component very small (< 0.5 %). The quality of the data obtained at wavenumbers < 18000 cm^{-1} (in acetonitrile, cf. *Fig. 63*, p. 96) was too poor to allow for the detection of the rise times or a global analysis of the time-resolved emission data. Nevertheless, exactly this behavior is very important for the application of BDP-A15C5 as a fluorescent probe.

6.4 Excited-State Reactions of BDP-DMA

Having mentioned the rate constants in apolar solvents above (*Table 40)*, evaluation of steady-state and time-resolved emission data allows at least for BDP-DMA the determination of all the excited-state rate constants in the more polar solvents diethylether and 1,4-dioxane.

A global analysis of the time- and wavelength-resolved emission data in diethylether and 1,4-dioxane was performed. According to eqn (63) given in Appendix B, the temporal evolution of a fluorescence decay corresponding to a two-state model, i. e., emission from the LE and the CT state, can be described by a sum of two exponentials:

$$I_{LE}(t) = a_{11}e^{-t(\tau_1)^{-1}} + a_{12}e^{-t(\tau_2)^{-1}} \quad (19)$$

$$I_{CT}(t) = a_{21}e^{-t(\tau_1)^{-1}} + a_{22}e^{-t(\tau_2)^{-1}} \quad (20)$$

The two decay rates τ_i^{-1} directly observed in the experiment are linked to the species-related fluorescence lifetimes τ_0^X (X = *LE, CT*) through eqns (21) – (25) involving the rate constants of the excited-state reactions, k_{LC} and k_{CL} [333, 334]. Using the decay times τ_i and amplitudes a_{ij} given in the caption of *Fig. 65* and a reasonable estimate for τ_0^{LE}, an analytical solution of eqns (21) – (25) yields the photophysical parameters given in *Table 41*[cv] [333, 334].

$$\frac{a_{12}}{a_{11}} = \frac{X - \tau_1^{-1}}{\tau_2^{-1} - X} \quad (21)$$

$$X = k_{LC} + (\tau_0^{LE})^{-1} \quad (22)$$

cv) τ_0^{LE} and τ_0^{CT} are the fluorescence lifetimes of the LE and CT state, respectively. The calculation of the photophysical parameters is only possible if one of these fluorescence lifetimes is known. However, τ_0^{LE} can only be estimated from the fluorescence lifetime of a model compound which does not show the excited-state reaction investigated. Because of the independence on solvent polarity of the photophysical parameters k_r and k_{nr} of BDP-H and the similarity of these parameters for BDP-A15C5 and BDP-DMA in hexane, the value of τ_f of BDP-H in the corresponding solvent was chosen for τ_0^{LE}. Although in hexane, k_{nr} of BDP-A15C5 and BDP-DMA are somewhat larger than k_{nr} of BDP-H, which is most likely attributed to a low-lying non-polar triplet state, the population of this state should be energetically unfavorable in the polar solvents diethylether and 1,4-dioxane. Thus, k_{nr} should decrease resulting in more similar values of k_{nr} for all the three molecules in the medium polar solvents and τ_f of BDP-H is taken as τ_0^{LE}. However, the calculated values of k_{LC}, k_{CL} and τ_0^{CT} show only minor changes (< 5%) when choosing τ_f of BDP-DMA in hexane instead as value for τ_0^{LE}.

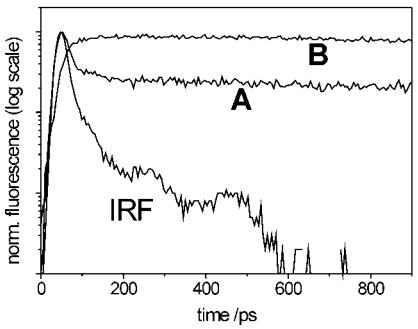

Fig. 65
*Normalized fluorescence decay curves of BDP-DMA in diethylether at 500 nm (curve **A**) and 670 nm (curve **B**), instrumental response function **(IRF)** shown for comparison. Global analysis with τ_1 = 3.42 ns and τ_2 = 11ps yields a_{11} = 1.36 and a_{12} = 24.2 for curve **A** and a_{21} = 5.1 and a_{22} = -4.9 for curve **B**, respectively (excitation at 475 nm, c_L = 1 x 10^{-6} M).*

$$Y = k_{CL} + (\tau_0^{CT})^{-1} \tag{23}$$

$$\tau_{1,2}^{-1} = \frac{1}{2}\left\{(X+Y) \pm \left[(X-Y)^2 + 4k_{LC}k_{CL}\right]^{\frac{1}{2}}\right\} \tag{24}$$

with
$$X + Y = \tau_1^{-1} + \tau_2^{-1} \tag{25}$$

The fast charge transfer reaction results in high rate constants for the formation of the CT state of 8.6 x 10^{10} s^{-1} in diethylether and 1.6 x 10^{11} s^{-1} in 1,4-dioxane. The high efficiency of this process on the ps time scale is also documented by the high ratio of k_{LC} / k_{CL} of 18 in diethylether and 56 in 1,4-dioxane. However, *Scheme 17* and the kinetic parameters given in *Table 41* put forward the question if the backward reaction does really contribute to the excited-state reaction mechanism proposed. Here, construction of the decay- as well as the species-associated spectra *($DAS_i(\lambda)$* and *$SAS_i(\lambda)$)* allows a verification of the kinetic model employed (e. g., *Fig. 66*). The $DAS_i(\lambda)$ and $SAS_i(\lambda)$ are given by eqns (3), (26) – (28), and (47) (p. 33 and Appendix B) [183]. An example of the $DAS_i(\lambda)$ and $SAS_i(\lambda)$ of BDP-DMA in diethylether is given in *Fig. 66*.

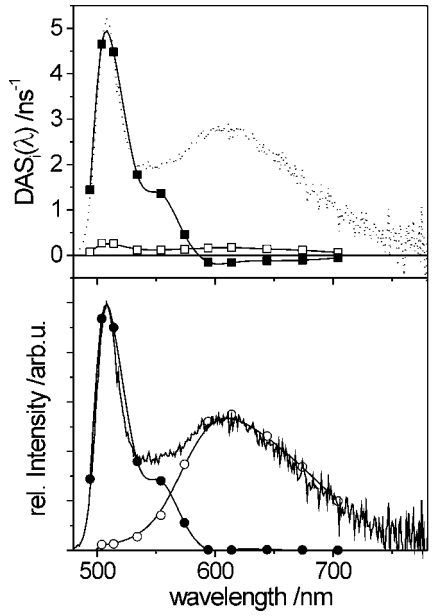

Fig. 66
DASi(λ) (upper part) and spectral contributions $SAS_i(\lambda)$ (lower part) of the two decaying species of BDP-DMA. The solid symbols denote the fast component (■, ●= LE) and the open symbols the slow component (□, o = CT). In the lower part, the full line represents the steady-state emission spectrum of the mixture and the same spectrum (·····) is included in the upper part for better comparison (excitation at 485 nm, explanation see text).

$$SAS_i(\lambda) = F_{SS}^{tot}(\lambda)\int_0^{\infty}\frac{I_i}{I_{tot}}(\lambda,t)dt \quad \text{with i= LE or CT} \tag{26}$$

with i = LE or CT

$$SAS_{LE}(\lambda) = [DAS_1(\lambda) + DAS_2(\lambda)]\tau_1\tau_2 Y \tag{27}$$

$$SAS_{CT}(\lambda) = [(\tau_2^{-1} - Y)DAS_1(\lambda) - Y)DAS_1(\lambda) - (Y - \tau_1^{-1})DAS_2(\lambda)]\tau_1\tau_2 \tag{28}$$

Furthermore, assuming that in the high-energy region of the spectrum only the LE species emits, $SAS_{LE}(\lambda)$ can be substituted by $F_{SS}^{tot}(\lambda)$ in eqn (27). In this (short or "blue" wavelength) spectral region where $I_{CT} \rightarrow 0$, convergence of a plot of $Y(\lambda)$ vs. λ according to eqn (29) (= rearranged eqn (27) with $SAS_{LE}(\lambda) = F_{SS}^{tot}(\lambda)$) yields the true value of Y (for BDP-DMA in diethylether $Y(\lambda \rightarrow \lambda_{blue})$ = 4.99 x 10^9 s^{-1})[cvi]. When no backward reaction occurs, this value must equal the value for Y in an irreversible process, i. e., $Y^{irr} = \tau_1^{-1}$ (in such a case, k_{CL} = 0 in eqn (23)). With τ_1 = 3.42 ns, as indicated in the caption of *Fig. 65*, a value of Y^{irr} = 2.93 x 10^8 s^{-1} is obtained, clearly smaller than that found in the experiment. This corroborates the fact that, although the forward CT process is fast and efficient, the back reaction is not negligible.

$$\lim_{\lambda \rightarrow blue} Y(\lambda) = \frac{F_{SS}^{tot}(\lambda)}{[DAS_1(\lambda) + DAS_2(\lambda)]\tau_1\tau_2} \tag{29}$$

$$\frac{c_{CT}(t)}{c_{LE}(t)} = \frac{k_{LC}(e^{-t(\tau_1)^{-1}} - e^{-t(\tau_2)^{-1}})}{(\tau_2^{-1} - X)e^{-t(\tau_1)^{-1}} + (X - \tau_1^{-1})e^{-t(\tau_2)^{-1}}} \tag{30}$$

$$\frac{\phi_{CT}}{\phi_{LE}} = \frac{k_f^{CT}c_{CT}}{k_f^{LE}c_{LE}} = \frac{k_f^{CT}k_{LC}}{k_f^{LE}[k_{LC} + (\tau_0^{CT})^{-1}]} \tag{31}$$

The rate constants for fluorescence deactivation k_f of both emitting states can be compared when plotting the concentration ratio c_{CT} /c_{LE} as a function of time (eqn (30)) and calculating k_f^{CT}/k_f^{LE} from the ratio of both the fluorescence intensities and concentrations of the species (LE and CT) at equilibrium (t → ∞) according to eqn (31)[cvii]. In both solvents analyzed, this ratio is less than 1 *(Table 41)* pointing to a strongly forbidden transition of the CT state of BDP-DMA.

cvi) Note that the value obtained by graphically analyzing this high-energy part of the spectrum is in good agreement with the value of Y = 5.11 x 10^9 s^{-1} obtained from a single set of amplitudes measured at the blue edge of the spectrum (cf. eqns (21) and (25)).

cvii) The ratio c_{CT} / c_{LE} in eqn (31) is a value obtained for photostationary conditions, i. e., for c_{CT} / c_{LE} (t_{stat}) ≥ 0.99 c_{CT} / c_{LE} (t_∞). This equilibrium is reached after ca. 85 ps in diethylether and 60 ps in 1,4-dioxane, respectively.

Table 41
Calculated photophysical parameters of BDP-DMA

Solvent	k_{LC}	k_{CL}	$(\tau_0^{CT})^{-1}$	k_f^{CT} / k_f^{LE}
	10^9 s^{-1}	10^9 s^{-1}	10^9 s^{-1}	
Et_2O [a]	85.8	4.8	0.29	0.234
Diox [b]	163	2.9	0.32	0.132

[a] see *Fig. 65* for values of a_{ij};

[b] global analysis with τ_1 = 3.09 ns and τ_2 = 6 ps yields a_{11} = 1.32 and a_{12} = 73.8 for a fluorescence decay monitored at 500 nm

The main driving force for the fast formation of the polar, weakly emissive CT state is the high electron affinity of the BDP fluorophore ($E_{1/2}$(A/A-) of BDP-H: -1.26 V vs. SCE [140] compared to, e. g., -2.22 V vs. SCE [335a] for phenylanthracene). For other electron deficient dyes, e. g., some rhodamine derivatives (-0.8 to -0.9V vs. SCE for several rhodamines) [335b] similar fast charge transfer reactions in the excited state have been observed [328].

Radiative deactivation of the CT state of BDP-DMA with its orthogonal conformation is strongly forbidden and the small transition moment can be directly read from a ratio < 1 of k_f^{CT} / k_f^{LE}. A similar tendency has been reported for ADMA and its pretwisted derivative 3,5-ATMA. For example, in the case of ADMA, k_f^{CT} has been determined to 0.41 x 10^8 s^{-1} in *n*-butanol at room temperature [318b]. Accordingly, for an excited-state equilibrium with k_{CL}, $k_{LC} >> k_f^{CT} + k_{nr}^{CT}$, $k_f^{LE} + k_{nr}^{LE}$, the equilibrium constant K_e can be obtained from eqns (30) and (31) and allows the calculation of the rate constant of non-radiative deactivation of the CT species (eqn (32)) [336].

$$k_{nr}^{CT} = \frac{K_e + 1}{K_e \tau_1} - \frac{k_f^{LE} + k_{nr}^{LE}}{K_e} \qquad (32)$$

Here, k_f^{LE} and k_{nr}^{LE} correspond to the unperturbed LE state and are taken from the reference compound BDP-H (cf. footnote cv, *Table 40*). For BDP-DMA in diethylether and 1,4-dioxane[cviii], values of ca. 2.7 x 10^8 s^{-1} are obtained which are comparable, for instance, to k_{nr}^{CT} of DMABN in dichloromethane (2.5 x 10^8 s^{-1}) [336]. On the other hand, for BDP-DMA, the effective rate constant for radiative deactivation, $k_f^{eff}(CT)$ (in the case of a fast excited state equilibrium $k_f^{eff}(CT)$ can be calculated by eqns (40) and (41)) shows considerably lower values already in diethylether (0.14 x 10^8 s^{-1}) and much more pronounced in THF (0.04 x 10^8 s^{-1}) stressing the strongly forbidden character of CT emission. In the case of ADMA in n-butanol and the pretwisted DMABN derivative 3-MMABN (see Appendix D for chemical structure) in acetonitrile, values of 0.41 and 1.12 x 10^8 s^{-1} were found [318b, 336]. Furthermore, the relatively long-lived emissive CT state in the neutral anilino substituted BDP dyes is completely absent in related electron-deficient but charged dyes, e. g., the amino rhodamine dye A-Rh [328]. Here, ultrafast formation of a non-emissive TICT state occurs [328].

Nevertheless, for both type of dyes, CT state formation can be efficiently blocked by protonation [106, 328]. For the BDP dyes in acetonitrile, the effect of protonation on the absorption behavior of BDP-A15C5 and BDP-DMA is small and only a slight bathochromic shift can be observed. In contrast, the emission properties are drastically altered *(Table 42)* and independent of solvent, protonation reestablishes LE emission. Accordingly, time-resolved fluorescence measurements yield monoexponential decay kinetics, the lifetime of the LE state being increased by a factor of ca. 1000 and calculated radiative rate constants similar to that of BDP-H.

6.5 Complexes of BDP-A15C5

The analytically valuable proton-induced effects on the absorption and emission behavior of BDP-A15C5 and BDP-DMA suggested that comparable results should be obtained upon complexation of alkali and alkaline-earth metal ions to the crowned BDP derivative. Thus, the spectroscopic effects of cation coordination were investigated for BDP-A15C5 with steady-state and time-resolved fluorometry. The studies were carried out in acetonitrile and the cations employed included Li^{I}, Na^{I}, Mg^{II}, Ca^{II}, Sr^{II}, and Ba^{II}.

6.5.1 Steady-State Spectra

The complexation-induced effects on the steady-state absorption and emission spectra are only small, and indeed similar to those found in the protonation studies, i. e., quenching of CT and enhancement of LE emission *(Table 43)*. Furthermore, the fluorescence excitation spectra measured at different emission wavelengths always match and resemble the corresponding absorption spectra. No cation-dependent shifts of the fluorescence band were detectable. This leads to the conclusion that binding of a cation to the crown ether receptor only suppresses the charge transfer process. Accordingly, the electrostatic interactions between the positively charged cation and the nitrogen electron donor atom prevent the excited-state reaction. The data in *Table 43* clearly show the extraordinary sensing potential of BDP-

cviii) 4.3 x 10^8 s^{-1} in THF

Table 42
Photophysical properties of protonated BDP-A15C5 and BDP-DMA in acetonitrile. The corresponding data of the unprotonated compounds and those of BDP-H are included for better comparison.

	$\tilde{\nu}$ (abs)	$\tilde{\nu}$ (em)^{LE}	ϕ_f^{LE}	τ_1	k_f	k_{nr}
	10^3 cm^{-1}	10^3 cm^{-1}		ps	10^9 s^{-1}	10^9 s^{-1}
BDP-A15C5	20.2	19.8	0.0002	5	-	-
BDP-A15C5-H$^+$	20.0	19.6	0.68	3800	0.18	0.08
BDP-DMA	20.2	19.8	0.0003	2.6	-	-
BDP-DMA-H$^+$	20.0	19.6	0.49	2900	0.17	0.18
BDP-H	20.1	19.8	0.60	3170	0.19	0.13

Table 43
Photophysical and complex formation data of the alkali and alkaline-earth metal ion complexes of BDP-A15C5 in acetonitrile

	$\tilde{\nu}$ (abs)	$\tilde{\nu}$ (em)	ϕ_f	τ_1	$a_{rel}{}^1$	τ_2	$F_{SS}{}^1 / F_{SS}{}^2$	FEF	log$K_{tot}{}^a$	$r_M{}^b$	n^2 / r_M
BDP-A15C5	**10^3 cm^{-1}**	**10^3 cm^{-1}**		**ps**		**ns**				**Å**	**Z²Å^{-1}**
⊂Li^{I}	20.1	19.7	0.018	45	0.38	0.54	0.05	90	2.55	0.76	1.32
⊂Na^{I}	20.1	19.7	0.097	64	0.45	1.75	0.02	485	2.20	1.02	0.98
⊂Mg^{II}	20.1	19.7	0.45	-	-	2.95	-	2250	2.90	0.72	5.55
⊂Ca^{II}	20.1	19.7	0.34	1050	0.56	3.30	0.41	1700	4.40	1.06 (7)	3.77
⊂Sr^{II}	20.1	19.7	0.25	820	0.71	3.18	0.64	1250	3.34	1.21	3.17
⊂Ba^{II}	20.1	19.7	0.12	430	0.86	2.75	0.92	600	3.10	1.47 (9)	2.72
H^+	20.0	19.6	0.68	-	-	2.90	-	3400	-		

[a] obtained by M. Kollmannsberger in Regensburg;

[b] All radii were taken from ref. [249a] for six-coordination except where the coordination number is indicated in brackets [250a]. The values given in brackets have been found by *Jonker* in X-ray analyses of related MAP-A15C5 complexes [250a, 254]; cavity size of the aza crown: 1.7-1.8 Å [249b, c]

A15C5, i. e., complexation induced FEF of > 1000 are observed for the alkaline-earth metal ions. Like the shifts in absorption observed for the ICT probes in Ch. 4.5 and the FEF observed for the ET probes in Ch. 5.5, the size of the FEF depends on both the charge density and the extent of coordination of the cation to the crown nitrogen *(Table 43)*. In all the cases studied, complexes of a well-defined 1:1-stoichiometry are formed and analysis of the fluorescence titration curves yields the logK_S values included in *Table 43*. Especially the FEF found for the alkaline-earth metal cations and peaking with FEF = 2 250 for Mg^{II} are amongst the highest fluorescence enhancement factors reported in the literature until today.

6.5.2 Fluorescence Lifetimes

In contrast to the steady-state fluorescence measurements which suggest a quite simple complexation behavior of BDP-A15C5, fluorescence decay measurements reveal a more complex situation. As would be expected, the fluorescence lifetime of the LE species increases drastically upon complexation (*Tables 40*, p. 97 and *43*).

However, the fluorescence decay curves of all the complexes measured (with the exception of Mg^{II}⊂BDP-A15C5) can be described only by a biexponential fit in the region of the LE emission. Moreover, the relative amplitudes of the two distinct decay components are always independent of excitation (for wavelengths < 495 nm/wavenumbers > 20 200 cm^{-1}) and observation wavelength and no rise times were found (*Figures 67* and *68*, p. 101).

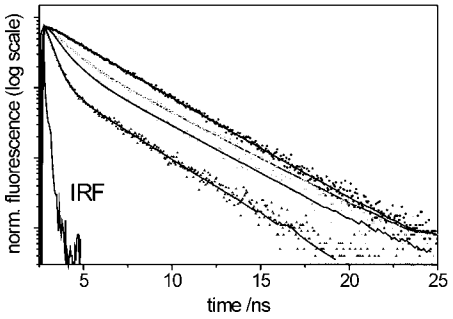

Fig. 67
Fluorescence decay curves (symbols) and fits (—) of the complexes of BDP-A15C5 with Mg^{II}, Ca^{II}, Sr^{II}, and Ba^{II} (from top to bottom). (excitation at 475 nm, observation at 515 nm, c_L = 1 x 10^{-6} M, full complexation).

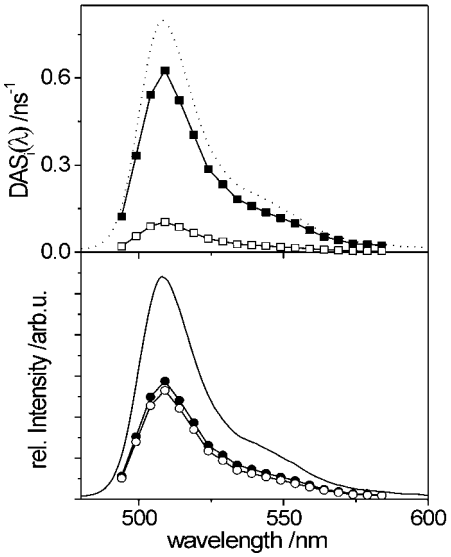

Fig. 68
DAS$_i$(λ) (upper part) and spectral contributions $F_{SS}{}^i$ (lower part) of the two decaying species of the Ba^{2+} complex at $x_{M/L}$ = 400. The species decay with τ_f = 460 ps (■ , ●) and τ_f = 2.54 ns (□ , o). In the lower part, the solid line represents the steady-state emission spectrum of the mixture and the same spectrum (·····) is included in the upper part for better comparison (excitation at 485 nm, explanation see text).

Recalling the circumstances for the appearance of two distinct fluorescence lifetimes they can be caused either by a photoinduced excited-state process, i. e., an intra- or intermolecular photophysical reaction, or by excitation of two different ground state species.

The first mechanism, an excited-state photoreaction, can be excluded since no shifts in the steady-state spectra are observable and no rise times are detectable (*Fig. 68*, p. 101). Hence, a CT reaction and/or a (resulting) photodecoordination of the complex is not likely to happen. The product of such a process should have a more polar CT character, its emission thus appearing at lower energies compared to that of the precursor and a rise time should appear (cf. BTAC probes in Ch. 4.5.1.2 and 4.5.2.2)[cix]. For systems showing

cix) Especially in the case of the alkaline-earth metal cations showing two fluorescence decay times in the ns time range with comparable relative amplitudes, such a rise time should have been detectable with the instrumental setup employed.

Table 44
Fluorescence decay times of the Ba^{2+} complex of BDP-A15C5 as a function of ion-to-ligand ratio.

$x_{M/L}$	τ_1	a_{rel} [1]	τ_2 [a]
	ps		ns
40	488	0.85	2.59
400	460	0.86	2.54
2250	424	0.85	2.52

[a] The value of τ_2 given in *Table 44* is shorter compared to that given in *Table 43*. This is due to a different repetition rate (here: 82 MHz with a time window of 12 ns) used in these time-resolved experiments and the software dependent neglect of the predecessor decay in the fits given in *Table 44*. The value obtained in the 4 MHz experiments *(Table 43)* is correct.

decoordination of the cation in the excited state and fluorescence deactivation on the ns time scale, so far only similar fluorescence lifetimes have been measured for different cations, in sharp contrast to the results obtained here [77d, 96c]. Furthermore, these excited-state decoordination reactions are very fast (ps time scale) and emission is only observed from the decoordinated species, i. e., monoexponential decay kinetics are observed [96c]. On the other hand, the lack of any dependence of the fluorescence excitation spectra on the emission wavelength does not indicate the existence of two different ground state species at first sight. But if these two species have similar absorption and emission spectra[cx] and only differ in their fluorescence quantum yields, it is very difficult to discriminate between them using steady-state spectroscopy.

In order to investigate the mechanism involved more closely, time-resolved fluorescence measurements were carried out for BDP-A15C5 as a function of cation concentration. The Ba^{II} ion was chosen for these experiments because the two decay components of the Ba^{II} complex show fluorescence lifetimes which are both sufficiently long to be well resolved by the ps-LIF and distinctly different, i. e., 430 ps and 2.75 ns, respectively. The measurements included the recording of TRES for mixtures containing Ba^{II} and BDP-A15C5 at $x_{M/L}$ of 2250 (full complexation), 400, and 40 *(Table 44)*. Again, these experiments revealed no dependence of the fluorescence decay times on detection wavelength as well as no dependence of their relative amplitudes on the metal-to-ligand ratios used[cxi]. Accordingly, this excludes any consecutive formation of two species (e. g., complexes of ML and ML_2 or M_2L stoichiometry) and the occurrence of two consecutive complex formation constants in a titration. The two species must be therefore formed simultaneously. The fluorescence decay times of free BDP-A15C5 could not be detected in these solutions because of their very weak contribution to total fluorescence intensity[cxii].

This unusual complexation behavior is tentatively attributed to the existence of two distinct conformers of the complexes in the ground state with very similar absorption and emission spectra but different fluorescence quantum yields and lifetimes.

Thus, the fluorescence quantum yields obtained for the complexes are average values of the two conformers, weighted by their relative concentrations c_r.

$$\phi_f = c_{r1}\phi_1 + c_{r2}\phi_2 \qquad (33)$$

The only exception is found for the Mg^{II} complex which exists in a single stable ground state conformation. The determination of the actual fluorescence quantum yields ϕ_i of the single conformers as well as their concentration ratios according to eqn (33) is not possible. This implies that both radiative and non-radiative rate constants of the single species remain obscure. Nonetheless, the contributions of both conformers to the overall fluorescence quantum yield can be derived from a global analysis of the wavelength-resolved fluorescence decay data.

With the assumption that the equilibrium of conformers in the ground and in the excited state is the same and that any reaction in the excited state is slower than the involved relaxation processes[cxiii], it is possible to construct the decay-associated spectra from the time-resolved fluorescence data according to eqns (3), p. 33, and (63) [183]. Furthermore, assuming ground state heterogeneity as already described for the complexes of $BP(OH)_2$ in Ch. 3.3.2, the $DAS_i(\lambda)$ are identical with the $SAS_i(\lambda)$, i. e., the contribution $F_{SS}^{\ i}$ of the single species to the overall fluorescence intensity *(Table 43)*:

$$F_{SS}^{i} = \int_0^\infty \frac{DAS_i(\lambda)\tau_i^{-1} F_{SS}^{tot}(\lambda)}{\sum_i DAS_i(\lambda)\tau_i^{-1}} \qquad (34)$$

For a better illustration, the $DAS_i(\lambda)$ and corresponding spectral contours $F_{SS}^{\ i}$ of the two excited species of the Ba^{2+} complex are presented in *Fig. 68*.

Regarding the rate constants of fluorescence deactivation, it is impossible to calculate them for the single conformers. But a closer look at *Tables 42* and *43* reveals that k_f of $Mg^{II}\subset$BDP-A15C5, BDP-A15C5-H^+, BDP-DMA-H^+, and BDP-H are very similar and thus it is reasonable to assume, that k_f of the other metal ion complexes are of comparable magnitude.

With this in mind, i. e., k_f ~ const., those conformers of the Ca^{II} and the Sr^{II} complex which show longer fluorescence lifetimes possess a higher fluorescence quantum yield than $Mg^{II}\subset$BDP-A15C5 (see eqns (40) and (41), Appendix B). Because the overall fluorescence quantum yield of $Ca^{II}\subset$BDP-A15C5 and $Sr^{II}\subset$BDP-A15C5 is lower than that of $Mg^{II}\subset$BDP-A15C5, the second conformer must be a weakly emitting one.

Nevertheless, in contrast to the aforementioned, the determination of the complex stability constants is independent

cx) Here, "similar" means that their spectra cannot be resolved with the spectrofluorometer employed in this work.

cxi) The small decrease in τ_f when going from $x_{M/L}$ = 40 to 2250 is attributed to fluorescence quenching due to the heavy atom effect induced by the large excess of Ba^{2+} ions in the solution.

cxii) With $\log K_S$ = 3.10 and $c_L = 2 \times 10^{-6}$ M, eqns (48), (51), (52), (60), and (62) the calculation of the free probe concentration in solution in order to estimate the relative contribution to the overall fluorescence quantum yield is possible. Since this calculation is based only on the steady-state results (ϕ_f and $\log K_{tot}$), the two species of the complex are treated as one, the sum of complexed probe molecules. With ϕ_f given in *Table 43*, $\Phi_{re}^{\ ffp}$ of 0.016 ($x_{M/L}$ = 40), 0.002 ($x_{M/L}$ = 400), and 0.0003 ($x_{M/L}$ = 2250) are obtained.

cxiii) Note that for complexes of "normal" fully conjugated or electronically coupled intrinsic fluorescent probes actual decomplexation, i. e., ejection of the cation from the crown, is a much slower process (see Ch. 4.5.3.1). This should be even more pronounced in these strongly decoupled systems.

of the existence of differently emitting conformers as long as their absorption spectra do not differ and their concentration ratios remain constant during the titration. Since conformers are equilibrated, the latter assumption is always true and the former follows from the steady-state absorption and emission data. Accordingly, the complex stability constants determined by measuring the total fluorescence intensity, which in turn is proportional to the total concentration of complexed probe molecules, yields the overall complex stability constant K_{tot} *(Table 43)*.

6.5.3 Mechanistic Considerations

Considering the molecular structure of the conformers, an exact statement is not possible on the basis of the investigations presented here. However, the steady-state and dynamic spectroscopic behavior suggests that the main conformational differences should reside at the nitrogen atom of the crown. The two conformers could possibly differ in their twist angles between the aromatic donor and acceptor moieties which should vary the amount of CT interaction being operative. As a second possibility, having the *endo-exo* isomerization of *N*-substituted aza crowns in mind [296], an equilibrium of a loose and a strong complex could affect both the pyramidalization and conformational flexibility at the nitrogen atom of the crown. *Scheme 18* illustrates the different equilibria involved in complex formation of substituted aza crown ethers and metal ions in solution. Within this so-called multi-step *Eigen-Winkler* scheme *(Scheme 18)* [337], for a given aza crown ether the ratio of k_2/k_{-2} varies with the metal ion, counter ion, and solvent, mainly depending on the thermodynamic parameters ΔS and ΔH for de/solvation of cation and crown, ion (pair) association, fit of cation into the cavity, and coordination of the cation to the crown's heteroatoms [338]. The influence of both reaction coordinates, pyramidalization and conformational flexibility (e. g., twisting), on the LE and the CT emission is well documented for related donor-acceptor-substituted compounds and was intensively studied for alkylaminobenzonitriles. Nevertheless, the real mechanism is still not clear yet [103a, 241, 334]. However, both coordinates cannot be seen separately and depend on each other for the complexes studied here. As a direct consequence, electronic and conformational differences of the two conformers lead to differences in orbital overlap between the lone electron pair of the nitrogen atom and the aromatic π system resulting in different CT quenching constants. Hence, different fluorescence decay times are observed for the LE emission.[cxiv]

The order of complex stability constants (*Table 43*, p. 101) for the cation complexes of BDP-A15C5 is in good agreement with those observed for the other crown compounds in this thesis. Again, this order of preference ($Ca^{II} > Sr^{II} > Ba^{II} > Mg^{II} > Li^{I} > Na^{I}$) can be explained by the best match of cation size and cavity diameter (*Table 43*, p. 101) as well as the charge density of the cations. The value of $\log K_S$ correlates well with the charge densities[cxv] n^2/r^{n+} as a measure for the electrostatic attraction in the complexes. Moreover, the exceptional behavior of Mg^{II} showing the highest FEF value but only a moderate complex stability constant is found for this series of complexes, too. Mg^{II} is too small to fit well into the cavity but has the strongest affinity to the nitrogen donor atom of the crown. This is further stressed by the fact, that for Mg^{II}, only one emitting conformer is observed, namely the one with strong coordination to the nitrogen atom. Another peculiarity, documented for the other crown ether containing probes as well, is manifested in the properties of the Li^{I} complex, i. e., a small FEF but a relatively high $\log K_S$. The predominant coordination of Li^{I} to the oxygen donor atoms (and one or two solvent molecules) accounts for the weak interaction with the crown ether nitrogen atom. The good correlation of FEF and n^2/r^{n+} for all the cations studied except for Li^{I} confirms this complexation behavior.

A closer examination of the fluorescence lifetimes of the complexes with Ca^{II}, Sr^{II}, Ba^{II}, Li^{I}, and Na^{I} reveals the following tendency, i. e., both fluorescence lifetimes increase with increasing values for FEF. This correlation suggests that the increase in the fluorescence lifetimes of both components seems to be the direct consequence of the complex formation in the ground state and the emission of both excited complex conformers. Ca^{II} forms the most stable complexes in the ground state and these complexes show the longest fluorescence lifetimes and highest fluorescence quantum yields. Assuming comparable rate constants of fluorescence

cxiv) Note that the detection of any CT emission was not possible in acetonitrile.

cxv) Here, the charge density is expressed as n^2 / r^{n+}, the so called "class A" or ionic index [253].

A

$$M^+ + ClO_4^- \rightleftharpoons MClO_4 \qquad k_{ia,-ia}$$

$$M^+ + \mathbf{L} \rightleftharpoons (\mathbf{L}\text{-}M^+) \qquad k_{1,-1,2,-2}$$

$$(\mathbf{L}\text{-}M^+) + ClO_4^- \rightleftharpoons (\mathbf{L}\text{-}M^+ClO_4^-) \qquad k_{cip,-cip}$$

B

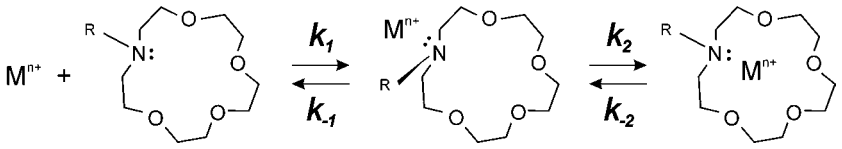

Scheme 18
Generalized kinetic scheme of the processes participating in the complex formation of BDP-A15C5 and metal ion perchlorates in solution. ***A****: Single equilibria describing ion association (ia), complex formation and complex ion pair association (cip).* ***B****: Complex formation of M^{n+} with a substituted aza crown ether involving the formation of a contact pair (loose complex, step 1) and a (strong) complex (step 2).*

deactivation for all the complexes studied[cxvi], the increase in τ_f and ϕ_f suggest a decrease in k_{nr} with increasing complex stability.

Regarding the fluorescence behavior of the complexes and the lack of any detectable CT emission the excited complexes seem to be stable. No photoejection or decoordination of the cation could be observed. Thus, the cation complexation of BDP-A15C5 is much more reminiscent of ET probe sensing than the typical ICT probe behavior.

6.6 Analytical Applications

The main analytical value of BDP-A15C5, a fluorescent probe with a virtual "zero-spacer" and an orthogonal orientation of receptor and signal transducing moiety, is its extremely high FEF for alkali and alkaline-earth metal cations. Along with the considerably high complex stability constants (for this monoaza crown ether and the ions studied), the LODs are lower for this probe compared to those of many other probes. With c_L = 1 x 10^{-6} M, the optimum probe concentration considering S/N ratio of the measurement, experimental time (scan speed for the recording of an emission spectrum or accumulation time in a time-resolved fluorescence experiment), and dynamic metal ion concentration range, the LODs obtained for Ca^{II}, Mg^{II}, and Na^{I} with a typical steady-state setup are determined to *ca.* 45 nM, 1 µM, and 25 µM, respectively (see Ch. 2.12 for a more detailed discussion of LOD). Again, employing laser excitation and photon counting techniques, this LOD can be lowered by 2-3 orders of magnitude.

Unfortunately, the high sensitivity of the probe molecule is a major disadvantage in improving its analytical potential for the discrimination between several metal ions in a liquid mixture or sample. Displaying the typical ET behavior, a spectral discrimination between several cations with steady-state spectroscopy is impossible and the recording of TRES does not leads to any improvement either. But here, not only the formation but mainly the spectroscopic visibility of the two conformers of a single M^{n+}⊂BDP-A15C5 sets limitations for time-resolved fluorometry. The appearance of two distinct fluorescence lifetimes for all the cations investigated (with the exception of Mg^{II}) leads to decay kinetics which have to be described by four exponentials for a mixture of only two cations. Moreover, the variations between the fluorescence lifetimes of the cation complexes are not large enough to allow a reliable separation of the decay components in any mixture of two ions. Only for certain pairs of cations, i. e., a mixture of one alkali and one alkaline-earth metal ion, the fluorescence lifetimes enable a separation of the species.

Nevertheless, the effects observed and the molecular design of the fluorescent probe suggested that this "concept of orthogonality" seems to be very promising in terms of developing fluorescent probes for heavy metal or paramagnetic transition metal ions which do not transduce a signal by fluorescence quenching but rather by fluorescence enhancement.

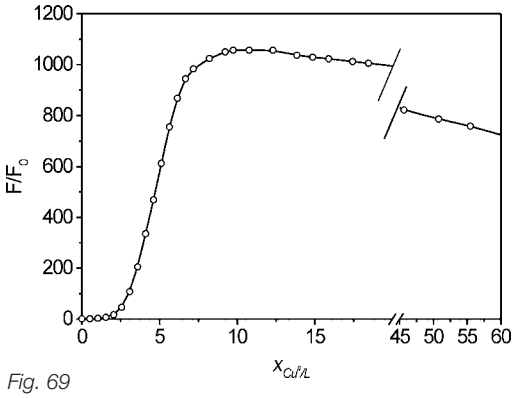

Fig. 69
Fluorometric titration curve of BDP-A15C5 with Cu^{II} in acetonitrile (excitation 480 nm, c_L = 6 x 10^{-7} M). Cu^{II}⊂BDP-A15C5 shows absorption at 20 000 cm^{-1}, emission at 19 600 cm^{-1}, ϕ_f = 0.23, τ_f = 3.5 ns (both obtained for $x_{M/L}$ = 11), and a complex stability constant of logK_S ~ 5.5, respectively.

Although the A15C5 macrocycle is by far the optimum receptor for Cu^{II} ions, it is well known that Cu^{II} coordinates to these monoaza crown ethers similarly as to other tertiary alkyl amines [263, 265a]. Thus, experiments concerning Cu^{II} ion sensing with BDP-A15C5 were carried out under the premise of simply testing this modular design approach.

And indeed, UV/Vis-spectrophotometric and fluorometric titrations revealed, that binding of Cu^{II} to BDP-A15C5 leads to the formation of a fluorescent complex, its properties being very similar to those described for the other ions. From the fluorometric titration curve shown in *Fig. 69* the large fluorescence enhancement upon addition of Cu^{II} up to a ratio $x_{M/L}$ = 10 can be directly seen. When the Cu^{II} concentration is further increased, a plateau (full complexation, i. e., signal saturation) up to $x_{M/L}$ ~ 15 is observed. At higher Cu^{II} concentrations the intensity linearly drops which is ascribed to diffusion controlled (dynamic) quenching. However, since Cu^{II} binds predominantly to the nitrogen donor atom of the crown ether, monoexponential decay kinetics are found. The photophysical and complexation data of the Cu^{II} complex are given in the caption of *Fig. 69*.

Compared to the very few other fluorescent probes which show fluorescent enhancement upon binding to paramagnetic ions [112, 119e, f, 135], this molecular approach is simple, the synthesis of the dye straightforward, and a lot of other receptors could be attached to the BDP chromophore, allowing a tuning of the analytical dynamic range, LOD, and ion discrimination [339].

Recalling the discussion on analytical applicability of the other fluorescent probes, the outstanding features of BDP-A15C5 render this dye a very promising candidate for post-column derivatization in HPLC with fluorescence detection. Excitable in the Vis spectral region, its complexes possess high fluorescence quantum yields and decay with comparably long, cation-specific fluorescence lifetime(s).

And finally, having the dual fluorescence in medium polar solvents in mind, careful tuning of the fluorescent probe's molecular design should be possible in such a way that this phenomenon can be utilized for ion recognition. Especially the

cxvi) The values of k_f given in *Tables 40* and *42* (pp. 97, 100) support the assumption that the rate constants of fluorescence deactivation of the complexes are comparable to those observed for BDP-A15C5, BDP-DMA, and BDP-H under conditions when only the LE emission is present. The measured fluorescence lifetime and quantum yield, τ_f and ϕ_f, and the radiative and non-radiative rate constants are linked by eqns (40) and (41). Thus, with $\phi_f = k_f\tau_f$, not only the values obtained for $F_{SS}^{\ i}$ from the time-resolved measurements (eqns (3), (34), and (63)), but also the actual fluorescence quantum yields ϕ_f of the complex species should increase with increasing complex stability.

occurence of well-separated bands already at room temperature is very rarely found in dual emitting dyes [240, 241]. Accordingly, for another example of this type, DMABN crown, switching between A* (CT) and B* (LE) fluorescence upon coordination to a cation has only recently been reported [103a].

6.7 BDP Dyes in Conclusion

The orthogonal molecular setup of the substituted BDP derivatives carrying an aniline-like donor gives rise to an ultrafast ICT process in the excited state leading to a dual emission behavior as a function of solvent polarity. The ICT process has been characterized here employing time- resolved fluorometry and already in medium polar solvents such as diethylether or 1,4-dioxane, the excited-state reaction is completed within a few ps. Moreover, not only covalent binding of protons to the crown ether (or dimethylamino) nitrogen atom leads to the formation of a stable, protonated, excited dye, but in the case of cations, the (two) complexes were found to be stable in the excited state as well. This effect results in the very high fluorescence enhancement factors reported here and is the basis for potential analytical applications.

7 Final Conclusions on Cation-Sensitive Fluorescent Probes

At first the bad news – unfortunately, the ideal fluorescent probe for metal ions has not been found yet... but now the good news – some very interesting results were obtained which are valuable for the design of improved cation-complexing fluorescent probes and show the potential of time-resolved fluorometry for fluorometric metal ion analysis.

Concerning cation selectivity, the concept of modular fluorescent probes is clearly superior to (simple) fluorescent ligands. For $BP(OH)_2$, the cation selectivity cannot be synthetically controlled without largely altering the molecular structure of the probe itself. Hence, any analytical application of this probe is limited to its present sensing properties. Since only complexation to the closed d-shell transition metal ions Zn^{II} and Cd^{II} leads to fluorescence enhancement accompanied by cation-specific fluorescence lifetimes, the *in situ* sensing potential of this probe is rather poor. Furthermore, the presence of paramagnetic metal ions, which are bound stronger by the fluorescent ligand than Zn^{II} and Cd^{II} and quench its fluorescence, interferes with the detection of those d^{10} metal ions.

In contrast, modular fluorescent probes have clearly the advantage of enabling the choice of an appropriate, i. e., analyte-specific receptor which could be confirmed by the strongly enhanced cation selectivities found for the two probe pairs BTAC-$AT_4$15C5 and -A15C5 and BTPP-$AT_4$15C5 and -A15C5. Whereas the polyoxa monoaza crown provides an emission signal upon binding to the main group metal ions, the probe equipped with the "softer" [143] receptor shows complexation-induced changes in the presence of Hg^{II} and Ag^{I}. No interferences occur for the main group metal ions. Thus, future research should be more focused on the design and use of improved receptors in order to meet the growing need for specific and selective sensor molecules.

The complexation-induced changes of the spectrosopic properties of the probes are generally favorable. Whereas most ICT probes show cation-induced fluorescence quenching and often lack any effects on the fluorescence lifetime, complexation of both BTAC-$AT_4$15C5 and BTAC-A15C5 is accompanied by a cation-induced increase in fluorescence quantum yield and lifetime. Whereas for BTAC-A15C5, without expensive instrumentation, the effects are too small to be analytically exploited for ion discrimination, in the case of BTAC-$AT_4$15C5 this should be possible. Moreover, besides its selectivity for Ag^{I} and Hg^{II} this ICT probe shows the very rare effect of fluorescence enhancement upon binding to the well-known fluorescence quencher Hg^{II}. Furthermore, for both Ag^{I} and Hg^{II}, cation-specific decay times in the range of 0.3 to 1.1 ns are found for the emitting complexes. These very exceptional features of BTAC-$AT_4$15C5 render this probe a potential candidate for ion sensing.

ET fluorescent probes follow a different approach of signal generation, i. e., chelation-induced suppression of an intramolecular ET quenching channel. As a consequence, application of these probes aims at a more sensitive detection of analytes than in the case of the ICT probes but accepts the lack of spectral shifts. The BTPP derivatives studied here show relatively large enhancement factors of up to 44 compared to other systems reported in the literature so far. However, the fluorescence lifetimes are very similar for a group of metal ions (monovalent or divalent) and discrimination between several ions is not possible.

On the other hand, the last type of fluorescent sensor molecule studied, BDP-A15C5, shows the largest fluorescence enhancement factors known so far but unfortunately goes beyond the limits of lifetime-based sensing. For the alkali and alkaline-earth metal ion complexes of this probe, always two decay components with largely different lifetimes are found for a certain ion (with the exception of Mg^{II}). Hence, even a mixture of only two ions generates four decaying species which leads to very complicate data evaluation. However, the outstanding fluorescence enhancement factors of > 1000 in the case of the alkaline-earth metal ions directly reveal the enormous potential of the "virtual spacer" setup employed here.

The remarkable increase in ion discrimination and detection when going from steady-state to time-resolved fluorometry has been demonstrated successfully for the Zn^{II} and Cd^{II} complexes of $BP(OH)_2$. Global analysis of such a two-dimensional emission matrix provides a relatively straightforward tool for metal ion detection and discrimination when only a limited amount of emitting species is present in a certain wavelength region for detection.

In the other main field of fluorescent cation probe application, (time-resolved) fluorescence detection in HPLC or ion exchange chromatography, the use of the ET probes and especially BDP-A15C5 may lead to an increase in sensitivity. For the complexes of BDP-A15C5, besides complexation-induced changes in fluorescence intensity, two cation-specific fluorescence lifetimes should enable the unequivocal assignment of the resulting chromatographic peaks to the corresponding cation complexes and thus the metal ion. In the

case of metal ion analysis with HPLC and fluorometric detection, $BP(OH)_2$ could be also employed as fluorescent probe. However, only in the case of Zn^{II} and Cd^{II} the second analyte-specific detection parameter, the fluorescence lifetime of these complexes, can be used. With other paramagentic cations, unspecific static quenching occurs.

Finally, switching back once more to the mechanistic part of these studies, the complexation-induced processes responsible for spectral shifts and/or fluorescence enhancement have been assigned to a weakening of the donor strength in the ground state and a reduction of the rate constant of internal conversion for the relaxing excited state (BTAC probes), to a blocking of an intramolecular ET process (BTPP probes), and to a "switching off" of a CT process in the highly pretwisted BDP probe. Aiming at an enhancement of the already observed processes, desktop design of probes by careful choice of donor and accpetor might lead to the desired effects.

However, the basic disadvantages, i. e., generally much lower FEF for intrinsic probes compared to ET probes and generally much smaller spectral shifts for the latter compared to the former are the real challenge for future probe design. Here, the interfering effects observed during the studies of the D-A-chalcones and the triaryl-Δ^2-pyrazolines, i. e., formation of a chelate involving the acceptor moiety of the ICT chromophore, open new possibilities. Moreover, considering the dual emission behavior of BDP-A15C5 in medium polar solvents, careful tuning of donor and acceptor in a "virtual spacer" arrangement should give rise to dual emission in polar sovents such as acetonitrile as well (most favorably in the NIR spectral region). Depending on the choice of the receptor, such a two-band system should show comparably large cation-induced shifts in emission accompanied by an increase in fluorescence lifetime.

Accordingly, the present discussion clearly revealed that in the case of fluorometric metal ion analysis, chemistry is much more challenged to provide the "ideal sensor molecule"...

Appendix A

Abbreviations

In the case of most reference compounds taken from the literature, only the trivial names or most common abbreviations are used in this work. These compounds are compiled in Appendix D and systematic names according to IUPAC nomenclature are not given here. In the case of the crown ethers the generally accepted short notation is used (the IUPAC name is included for A12C4).

^{1}XY*	lowest excited singlet state
^{3}XY*	lowest excited triplet state
8-HQ	8-hydroxy-quinoline (see Appendix D for chemical structure)
α	polarizability
A	acceptor
A*	(highly) polar, emissive, single bond-twisted excited state
a_i	amplitude of compound *i*/arb. u.
a_{ij}	amplitude of compound *j* at wave length or analyzed decay *i*/arb. u.
a_O	Onsager cavity radius /Å
a_{rel}	relative amplitude
A_λ, $A(\tilde{\nu})$	absorbance at wavelength λ or wavenumber $\tilde{\nu}$/arb. u.
A-diagram	absorbance diagram
A12C4	trioxa monoaza 12-crown-4 (1,4,7-trioxa-10-aza-cyclopenta decane)
A15C5	tetraoxa monoaza 15-crown-5
A18C6	pentaoxa monoaza 18-crown-6
$A_2$15C5	trioxa diaza 15-crown-5
$A_2$18C6	tetraoxa diaza 18-crown-6
$A_2T_2$14C4	dithia diaza 14-crown-4
AAS	atomic absorption spectroscopy
abs	absorption (as index or in brackets)
ADI	acceptable daily intake (value)
AM1	Austin model 1
AO	atomic orbital
app	apparent (as index or in brackets)
Ar	aromatic group
arb. u.	arbitrary units
ASV	anodic stripping voltammetry
$AT_4$15C5	tetrathia monoaza 15-crown-5
b	bond
B15C5	benzo 15-crown-5
B18C6	benzo 18-crown-6
BAPTA	1,2-bis-(2-aminophenoxy)-ethane-*N,N,N',N'*-tetracetic acid
BDP	boron dipyrromethene (dye), 8-aryl substitued 1,3,5,7-tetramethyl-4-borata-3a-azonia-4a-aza-s-indacene with aryl = phenyl, p-(*N,N*-dimethylamino)phenyl, p-(A15C5)phenyl
BEM	biological effect monitoring
Benz, benz	benzene
BESSY	Berlin Electron Storage Ring for Synchrotron Radiation
bipy	2,2'-bipyridine
BPOH	2,2'-bipyridyl-3-ol
$BP(OH)_2$	2,2'-bipyridyl-3,3'-diol
BT	benzothiazole/yl
$BT_2$18C6	dithia benzo 18-crown-6
BTAC	benzothiazol-2-yl acceptor chalcone
BTPP	benzothiazol-2-yl-diphenyl-Δ^2-pyrazoline
Bu_2O	di-n-butylether
χ_m	electronegativity value
χ_R^2	(reduced) chi-squared
c	concentration/M or s-cis isomer
C (as index)	Coulomb
C*(j)*	autocorrelation function of the residuals
$C_n^{(t)}$	spectral response function
c_{L0}-titrations	titration by adding aliquots of ligand solution

c_{M0}-titrations	titration by adding aliquots of metal ion solution
c_{ri}	relative concentration of the species *i*
CFD	constant fraction discriminator
CH	cyclohexane
CH_2Cl_2	dichloromethane
CI	configuration interaction
cip (as index)	complex ion pair association
CPC	counts in the peak channel
cps	counts per second/cts s^{-1}
CT	charge transfer
δ	NMR chemical shift
Δ, $\Delta\delta$	difference in NMR chemical shifts
ΔE_{00}	energy of 0-0 transition
ΔH	enthalpy
$\Delta G^{\#}$	free energy of activation (activation barrier)
ΔG_{XY}	free energy (of a process XY)
ΔS	entropy
d	optical path length/cm
d_{DA}	charge separation distance/Å
D	donor
D-A-	donor-acceptor (substituted)
$DAS_i(\lambda)$	decay associated spectrum (of decay component *i*)/ns^{-1}
DE	dienol tautomer
Diox	1,4-dioxane
DK	diketo tautomer
DMA	*N,N*-dimethylamino
DMAn	N,N-dimethylanilino
DW	Durbin Watson parameter
ε_r, ε_S	dielectric constant (relative permittivity) of a solvent at 25° (ref. [340a] and references cited therein)
ε, ε ($\tilde{\nu}$)	molar absorption coefficient/M^{-1} cm^{-1}
E	energy or trans isomer
$E_{1/2}$	oxidation or reduction potential
E*	initially excited state
EA	electron affinity
EDTA	ethylene diamine-*N,N,N',N'*-tetraacetic acid
eff (as index or in brackets)	effective
EGTA	ethylene glycol bis-(β-aminoethyl ether)ethane-*N,N,N',N'*-tetraacetic acid
EK	enol-keto tautomer
em (as index or in brackets)	emission (fluorescence emission)
es (as index or in brackets)	excited state
ESIPT	excited-state intramolecular proton transfer
ET	electron transfer
$E_T(N)$, $E_T(30)$	solvent polarity scales
Et_2O	diethylether
EtOH	ethanol
exc (as index or in brackets)	excitation (fluorescence excitation)
exp (as index or in brackets)	experimental (ly obtained)
ϕ_f, ϕ_i	fluorescence quantum yield
Φ_{rel}	relative fluorescence quantum yield
f (as index or in brackets)	fluorescence
f(ε), *f*(n), *f'*(ε), *f'(n)*	solvent polarity function
f	oscillator strength
fm (as index)	free metal
F_{SS}	steady-state emission spectrum
Fc/Fc^+	Ferrocen/Ferrocenium
FEF	fluorescence enhancement factor
F/GFAAS	flame or graphite furnace atomic absorption spectroscopy
fp (as index)	fluorescent probe
fwhm	full width at half maximum/nm or cm^{-1}
γ	asymmetry of a band
g (as index or in brackets)	glass point
gs (as index or in brackets)	ground state
H-bond	hydrogen bond
H_2O	water
Hex	n-hexane
HOMO	highest occupied molecular orbital

HPLC	high performance liquid chromatography
I	intensity/arb.u.
ia (as index)	ion association
ic (as index)	internal conversion
ICP-AES/MS	atomic emission spectroscopy or mass spectrometry with inductively coupled plasma
ICT	intramolecular charge transfer
IEC	ion exchange chromatography
IP	ionization potential
IRF	instrumental response function
irr	irreversible (as index or in brackets)
isc (as index)	intersystem crossing
ISE	ion specific electrode
J	coupling constant (NMR)
Jul	julolidyl
κ_f	reduced k_f (independent of wavenumber)
K*	polar, non-emissive, single bond-twisted excited state
k_f	rate constant for fluorescence deactivation/s^{-1}
k_{nr}	rate constant for non-radiative deactivation/s^{-1}
k_p	rate constant for phosphorescence deactivation/s^{-1}
K_e	equilibrium constant
K_S	complex stability constant
k_{XY}	rate constant for excited- state reactions such as, e. g., proton or charge transfer/s^{-1}
λ	wavelength/nm
$\lambda_{S,0,i}$	reorganization energy (solvent, overall, internal)
l	bond length/Å
L (as index)	ligand
LE	locally excited
LIF	laser impulse fluorometer
LMCT	ligand-to-metal charge transfer
ln	natural logarithm
LOD	limit of detection
log	decadic logarithm
LUMO	lowest unoccupied molecular orbital
μ	dipole moment/D (1 D = 3.335 x 10^{-30} C m)
$M_{gs,es}$	transition dipole moment for a transition from state gs to es/D
MAC	maximal allowable concentration
MCA	multi channel analyzer
MCP (PMT)	micro channel plate (photomultiplier tube)
M (as index)	metal salt or metal ion
ME	monoenol tautomer
MeCN	acetonitrile
MeOH	methanol
MELIMEX	metal limnological experiment
MK	monoketo tautomer
MLCT	metal-to-ligand charge transfer
MO	molecular orbital
mod (as index)	model
MPC	maximal permissible concentration
ν	frequency/cm^{-1}
$\tilde{\nu}$	wavenumber/cm^{-1}
n	refractive index or charge (of a cation)
n. d.	not determined
n. r.	not reported
NAA	neutron activation analysis
NIR	near-infrared
NLO	non-linear optics
NTA	nitrilo triacetic acid
obs (as index or in brackets)	observation wavelength (in a fluorescence excitation experiment)
OEL	occupational exposure limit
oPP	*o*-(2-pyridino)phenol
p (as index)	peak
P, Ph	phenyl
P*	weakly polar, non-emissive, double bond-twisted excited state
PAC	phenyl acceptor chalcone
PET, (P)ET	photoinduced electron transfer
Ph, P	phenyl
Ph-A15C5/-$AT_4$15C5	*N*-phenyl-A15C5/-$AT_4$15C5
pK_a	negative decadic logarithm of acidity constant
PPP	triphenyl-Δ^2-pyrazoline

ps-LIF	picosecond-laser impulse fluorometer
PT	proton transfer
q	reaction coordinate
Q	quinoline/yl
R	substitutent
r_i	radius (of species or fragment *i*)/Å
S	solvent or sulfur
QAC	quinolin-2-yl acceptor chalcone
S/N	signal-to-noise (ratio)
$SAS_i(\lambda)$	species associated spectrum (of species *i*)/arb. u.
SB (as index)	Strickler Berg
SCE	standard calomel electrode
SC(R)F	self consistent (reaction) field
SHG	second harmonic generation
solv (as index)	solvent
SPP^N	solvent polarity scale
stock (as index)	stock solution
τ, τ_f, τ_0^X, $<\tau_f>$	fluorescence lifetime, further explanations see text/ns or ps
τ_l	longitudinal solvent relaxation time/ns or ps
τ_M, $<\tau>$	microscopic or average solvent relaxation time/ns or ps
τ_i^{-1}	decay rates/s^{-1}
Θ	torsion angle/°
t	time or s-trans isomer
T	temperature/K
T_{pH}-curve	titration curve
$T_4$14C4	tetrathia 14-crown-4
TAC	time-to-amplitude converter
TCSPC	time-correlated single photon counting detection
theo (as index)	theoretical (ly obtained)
THF	tetrahydrofuran
TICT	twisted intramolecular charge transfer
TLV	threshold limit value
TMS	tetramethylsilane
Tol	toluene
tot (as index)	overall volume, concentration etc.
TRES	time-resolved emission spectroscopy or spectrum/a
TS	transient state or transient species
T/XRF	(total) X-ray fluorescence
V	volume/cm^3 or electronic coupling matrix element
vac (as index)	vacuum
w	width of a band/nm or cm^{-1}
ζ	spin orbit coupling constant
x_i	molar fraction of species *i*
x_I	intensity (or signal) ratio
$x_{M/L}$	metal-to-ligand ratio
Y_I	difference in measured and calculated absorbance/arb. u.
Z	atomic number or cis isomer
ZINDO/S	Zerner's modified algorithm of intermediate neglect of differential overlap

Constants

taken from ref. [340b]

N_A	Avogadro constant, 6.022×10^{23} mol^{-1}
k_B	Boltzmann constant, 1.381×10^{-23} J K^{-1}
m_e	electron rest mass, 9.109×10^{-31} kg
e	elementary charge, 1.602×10^{-19} C
R	gas constant, 8.314 J mol^{-1} K^{-1}
ε_0	permittivity of vacuum, 8.854×10^{-12} C V^{-1} m^{-1}
h	Planck constant, 6.626×10^{-34} J s ($\cong$ C V s $\cong$ kg m^2 s^{-1})
c_0	speed of light in vacuum, 2.998×10^8 m s^{-1}

Appendix B

Basic Equations in Absorption and Fluorescence Spectroscopy

The absorption spectrum of a compound is given by the correlation between its molar absorption coefficient $\varepsilon(\tilde{\nu})$ and the wavenumber $\tilde{\nu}$. For any absorption measurement in (dilute) solution, the intensity ratio of light entering the sample *(I_0)* to light emerging the sample *(I)* is connected to the concentration *c* of a compound by eqn (35) (*d* = optical path length):

$$\log\frac{I_0}{I} = \varepsilon(\tilde{\nu})cd = A(\tilde{\nu}) \tag{35}$$

The intensity of absorption is a measure for the probability of the transition of an electron from the ground state *gs* to an excited state es and can be quantified by the oscillator strength $f_{gs,es}$. The latter is given by eqn (36) where $/M_{gs,es}/^2$ is the squared transition dipole moment and *G* a correction factor (usually taken equal to unity; the other constants are given in Appendix A)

$$f_{gs,es} = \frac{8\pi^2 mc_0}{3he^2}\tilde{\nu}_{gs,es}G\left|M_{gs,es}\right|^2 \tag{36}$$

The experimental expression for $f_{gs,es}$ is connected with the absorption spectrum according to eqn (37) (*n* = refractive index of the solvent, for other constants see Appendix A)

$$f_{gs,es} = \frac{mc_0{}^2\ln 10}{\pi e^2 N_A n}\int_{band}\varepsilon(\tilde{\nu}_{gs,es})d\tilde{\nu}_{gs,es} \tag{37}$$

Accordingly, the transition dipole moment and the corresponding absorption band are related by eqn (38) [333]

$$\left|M_{gs,es}\right|^2 = \frac{3hc_0\ln 10}{8\pi^3 N_A n}\int_{band}\varepsilon(\tilde{\nu}_{gs,es})d\ln\tilde{\nu}_{gs,es} \tag{38}$$

Correspondingy, the transition dipole moment for fluorescence is related to the spectral and kinetic parameters of a molecule's emitting state in the following way (eqn (39)) [333]

$$\left|M_{es,gs}\right|^2 = \frac{3h}{64\pi^4 n^3}\frac{\phi_f}{\tau_f\tilde{\nu}_{es,gs}{}^3} \tag{39}$$

with

$$\tau_f = \frac{1}{k_f + k_d} \tag{40}$$

$$\phi_f = \frac{k_f}{k_f + k_d} \tag{41}$$

In the following, the transitions gs,es *(gs→es)* and *es,gs (es→gs)* are refered to as absorption and emission and are denoted with the indices *abs* and *em*.

Since fluorescence spectra are recorded by scanning increments of a certain wavelength region, conversion to a linear energy scale involves correction of the intensities according to eqn (42) [341].

$$I_{\tilde{\nu}} = \lambda^2 I_\lambda \tag{42}$$

The energy loss resulting in a difference of the band position of the absorption and fluorescence spectrum is described by Stokes law:

$$\Delta\tilde{\nu}(abs-em) = \tilde{\nu}(abs) - \tilde{\nu}(em) \tag{43}$$

A relationship between the rate constant of fluorescence deactivation k_f and the integral absorption spectrum of a molecule has been developed by *Strickler* and *Berg* (eqn (44)) [342] and allows the estimation of the radiative lifetime $\tau_{f,0}$:

$$k_f^{SB} = \frac{8\pi c_0\ln 10}{N_A}n^2\tilde{\nu}_{em}{}^3\int_{band}\varepsilon(\tilde{\nu}_{abs})d\ln\tilde{\nu}_{abs} = \tau_{f,0}{}^{-1} \tag{44}$$

Besides estimating $\tau_{f,0}$ combination of eqns (38) and (44) provides a straightforward way to compare the rate constant of fluorescence deactivation derived from absorption *(k_f^{SB})* and emission measurements (k_f, eqns (40), (41)). Furthermore, employing the combined eqns (38) and (44) and rearranging eqn (39), the transition dipole moments of absorption and emission can be compared and a conclusion on the similarity of absorbing and emitting states can be drawn.

$$k_f = \frac{64\pi^4}{3h}n^3\tilde{\nu}_{em}{}^3\left|M_{em}\right|^2 \tag{45}$$

$$k_f^{SB} = \frac{64\pi^4}{3h}n^3\tilde{\nu}_{em}{}^3\left|M_{abs}\right|^2 \tag{46}$$

Accordingly, misinterpretations due to the dependence of k_f on the wavenumber of emission are also circumvented by comparing the corrected k_f values κ_f (eqn (47)).

$$\kappa_f = \frac{k_f}{\left\langle n^3\tilde{\nu}_{em}{}^3\right\rangle} \text{ with } \left\langle n^3\tilde{\nu}_{em}{}^3\right\rangle \approx n^3\frac{\sum\tilde{\nu}_{em}{}^3 I_{\tilde{\nu}_{em}}}{\sum I_{\tilde{\nu}_{em}}} \tag{47}$$

Complexation Experiments and Complex Stability Constants

Titrations

Two types of titrations are possible for the determination of complex stability constants in metal ion-ligand systems, i. e., titrating a solution of ligand by adding aliquots of metal ion solution (c_{M0}-titration) or vice versa (c_{L0}-titration). In all the experiments reported in this thesis, c_{M0}-titrations were carried out. Often the solubility of the fluorescent probe is the limiting factor, especially when a high excess towards the end of the titration is required. Moreover, the measurement of spectroscopic quantities such as fluorescence or absorption relies on the intensity of the signal generated by the organic ligand and thus, at low ligand concentrations (very dilute solutions), the errors encountered especially in absorption measurements are large. In most titrations, especially the fluorometric titrations, for each step a new solution was prepared. The concentrations and volumes of the components are then given by eqns (49) and (50). The dilution of the determinand

was either mathematically corrected or an equal amount of determinand was added to the titrant solution prior to the titration. All the complexometric quantities referred to in the text and captions are calculated according to the following equations.

$$x_{M/L} = \frac{c_M}{c_L} \tag{48}$$

$$V_L = \frac{c_L}{c_{stock}^L} V_{tot} \text{ and } V_M = \frac{c_M}{c_{stock}^M} V_{tot} \tag{49}$$

$$V_{solv} = V_{tot} - V_L - V_M \tag{50}$$

$$c_L = c_{fp} + c_{cp} \text{ and } c_M = c_{fm} + c_{cp} \tag{51}$$

Complex Stability Constants

For the fitting of the complexometric titration data, the following equations apply (*X* - absorption or fluorescence intensity; a, b - constants).

$$K = \frac{c_{ML}}{c_L c_M} \tag{52}$$

$$X_0 = ac_{L0},\ X_{\lim} = bc_{L0}, \text{ and } X = ac_L + bc_M \tag{53}$$

$$c_{L0} = c_L + c_{ML} \text{ and } c_{M0} = c_M + c_{ML} \tag{54}$$

Combination allows the graphical determination of *K* according to eqn (55) (or (56)) when X_{lim} is known (or not known).

$$\frac{X_0 - X}{X - X_{\lim}} = Kc_M \tag{55}$$

$$\frac{X_0}{X - X_0} = \frac{a}{b-a}\frac{1}{K}c_M + 1 \tag{56}$$

For efficient complexation, when $c_M \sim c_{M0}$ is not valid anymore, the following equation can be derived from eqns (52) – (54) [86b]:

$$X = X_0 + \frac{X_{\lim} - X_0}{2c_{L0}}\left\{c_{L0} + c_{M0} + \frac{1}{K} - \left[\left(c_{L0} + c_{M0} + \frac{1}{K}\right)^2 - 4c_{L0}c_{M0}\right]^{\frac{1}{2}}\right\} \tag{57}$$

In the case of 1:2 complexation (K_1 and K_2), the set of equations extends for the second complexation step and the data can be fitted according to eqns (58) and (59) [90e]:

$$\frac{X_0 - X}{X_0 - X_{\lim}} = Y \tag{58}$$

$$c_M = \frac{1 + K_1(1-Y)c_{L0} + K_1K_2(1-Y)^2{c_{L0}}^2}{K_1(1-Y)\left[1 + 2K_2(1-Y)c_{L0}\right]}Y \tag{59}$$

Most of the crowned fluorescent probes investigated here form well-defined 1:1 complexes with alkali, alkaline-earth metal ions, Ag^I, and Hg^{II} and logK_S values were determined according to eqn (56) and (57). However, in the case of Hg^{II} and $AT_4$15C5, the complex stability constants are too high to be determined with acceptable accuracy employing optical spectroscopy.

Apparent Complex Stability Constants

The same was found for the complexes of $BP(OH)_2$ with paramagnetic ions, i. e., high complex stability constants and mixed stoichiometries. Fitting the data to 1:1 and 1:2 complexes yielded no K_n of accetable accuracy in many cases. Moreover, due to the spectral similarity of the complexes, it was not possible to analyse consecutive complex formation steps in different spectral regions. Thus, in order to have a measure for all the cations investigated, the apparent stability constant was obtained by carrying out c_{M0}-titrations with similar c_{L0} and fitting the sigmoidal curve of a $\Delta A(\lambda)$ vs. -logc_M plot. In such a c_{M0}-titration K^{app} corresponds best to the process $M + ML_2 \rightarrow 2ML$.

Furthermore, for $BP(OH)_2$, showing complex prototropic and tautomeric equilibria, the determination of K_{MHL} was not employed here. In such an experiment, a pH titration is carried out for different $x_{M/L}$ and in combination with the p*K* data of the free ligand, the characteristic displacement of a metal ion at a certain pH allows to calculate consecutive complex stability constants K_{MHL} for strong complexes [343].

Basic Equations for Fluorometry

$$I_i = c_i\phi_i \tag{60}$$

$$I_{tot} = I_{fp} + I_{cp} \tag{61}$$

$$\Phi_{rel}^{\ i} = \frac{I_i}{I_{tot}} \tag{62}$$

Basic Equations for the Evaluation of Fluorescence Decay Data

The basic equations for obtaining certain quantities in the evaluation of time resolved emission data are given by the following equations:

$$I_{tot}(\lambda, t) = \sum_i a_i(\lambda)e^{-t(\tau_i)^{-1}} \tag{63}$$

$$a_{rel}^i = \frac{a_i}{\sum_i a_i} \tag{64}$$

$$\Phi_{rel}^i = \frac{a_i\tau_i}{\sum_i a_i\tau_i} \tag{65}$$

In some cases, e. g., two or more closely related species decaying with different lifetimes showing no excited-state reaction but a large spectral overlap, the mean fluorescence lifetime $\langle\tau_f\rangle$ is helpful in expressing average or effective rate constants (with the average fluorescence quantum yield measured).

$$\langle\tau_f\rangle = \frac{\sum_i a_i\tau_i}{\sum_i a_i} \tag{66}$$

Solvation Dynamics

The spectral response function for following solvation dynamics, eqn (5), p. 53, is obtained from lognormal fits of TRES and include the peak frequency $\nu_p(t)$ and the average frequency of the spectrum.

$$\bar{\nu}(t) = \nu_p(t) + \left(\frac{w(t)}{2\gamma(t)}\right)\left[\exp\left(\frac{3\gamma(t)^2}{4\ln 2}\right) - 1\right] \quad (67)$$

Here, w is the width and γ the asymmetry of the fitted time trace spectrum. For a more detailed discussion, see refs [228] and [229]. The correlation function $C_\nu(t)$ (eqn (5)) is fitted to a sum of exponentials and the single components are related to $\langle\tau\rangle$ according to eqn (69).

$$C_\nu(t) = \sum_i a_i e^{-t(\tau_i)^{-1}} \quad \text{with } a_i \geq 0 \text{ and } \sum_i a_i = 1 \quad (68)$$

$$\langle\tau\rangle = \sum_i a_i \tau_i \quad (69)$$

Basic Equations for Analysis of Solvatochromic Behavior[cxvii]

Most asymmetric organic dye molecules are characterized by different charge distributions in the ground and first excited singlet state resulting in different dipole moments for both states. In such a case, both states involved in the transition are not stabilized in the same way in a solvent of given polarity (by dipole-dipole interactions between solute and solvent). Hence, the dependence of band position on solvent polarity deviates for absorption (lowest-energy band) and fluorescence. Analysis of this solvatochromic behavior allows to draw a conclusion on the nature of the absorbing and the emitting species to some extent. Various formalisms have been introduced in the literature based on a classical [218] or quantum mechanical approach [344] but here, only the most widely used equations derived by *Lippert* and *Mataga* [218] will be used[cxviii].

$$\Delta\tilde{\nu}(abs-em) = \Delta\tilde{\nu}^{vac}(abs-em) + \frac{2(\mu_{es}-\mu_{gs})^2}{hc_0 a_O^{\,3}}\left(f(\varepsilon_r) - f(n)\right) \quad (70a)$$

cxvii) All dielectric constants and refractive indices taken from ref. [340a] and references cited therein.

cxviii) The formulae developed by *McRae* and *Bakhshiev* take additionally into account the polarizability of the solute (i. e., the solvent-induced changes of the electron distribution in the molecule) [344a-d]. *Bilot* and *Kawski* use a comparable formalism but split the reaction field working on the molecule into an orientational and an inductive part and consider the quadratic *Stark* effect as well (eqn (70b) [344e]).

$$\Delta\tilde{\nu}(abs-em) = \Delta\tilde{\nu}^{vac}(abs-em) + \frac{2(\mu_{es}-\mu_{gs})^2}{hc_0 a_O^{\,3}}\left(\frac{f(\varepsilon_r) - f(n)}{(1-\beta f(n))^2(1-\beta f(\varepsilon_r))}\right) \quad (70b)$$

with $\beta = 2\alpha/a_O^3$ (α = polarizability). However, the results obatined with formulae of McRae, Bakhshiev, and Bilot and Kawski differ only slightly [344f].

where $f(\varepsilon_r)$ and $f(n)$ are given by

$$f(\varepsilon_r) = \frac{\varepsilon_r - 1}{2\varepsilon_r + 1} \text{ and } f(n) = \frac{n^2-1}{2n^2+1} \quad (71)$$

The change in dipole moment when comparing absorbing and emitting species is related to the absorption and emission maximum of a molecule in a solvent (of a certain dielectric constant ε_r and refractive index n) by eqn (70a). Graphical analysis of a plot of the Stokes shift (or emission maximum) vs. the solvent polarity function (last term in eqn (70a)) allows the determination of $(\mu_{es} - \mu_{gs})$ and μ_{es} (if μ_{gs} is known) according to eqns (70a) (or (73)) (for h, c_0, and a_O see Appendix A)[cxix,cxx].

The specific physicochemical implications connected with the different solvent polarity terms (in eqns (70a) and (70b), (72) and (74), and (73) and (75)) have been treated elsewhere in detail and will be only briefly summarized here (cf., e. g., ref. [322]). In the case that plots according to eqn (70a) and (73) yield straight lines with a good correlation and similar values for μ_{es}, the state reached directly after excitation (*Franck-Condon* state) and the emitting state have the same nature, e. g., a CT state. If deviations occur [321, 322, 347] contributions of a solvent-induced dipole moment could account for such a behavior. In order to analyse solvatochromic data for the aforementioned, the polarizability of the solute is taken into account [344a] resulting in modified *Lippert-Mataga* equations (74) and (75).

$$\tilde{\nu}(abs) = \tilde{\nu}^{vac}(abs) + \frac{2\mu_{gs}(\mu_{es}-\mu_{gs})}{hc_0 a_O^{\,3}}\left(f(\varepsilon_r) - \frac{1}{2}f(n)\right) \quad (72)$$

$$\tilde{\nu}(em) = \tilde{\nu}^{vac}(em) + \frac{2\mu_{es}(\mu_{es}-\mu_{gs})}{hc_0 a_O^{\,3}}\left(f(\varepsilon_r) - \frac{1}{2}f(n)\right) \quad (73)$$

$$\tilde{\nu}(abs) = \tilde{\nu}^{vac}(abs) + \frac{2\mu_{gs}(\mu_{es}-\mu_{gs})}{hc_0 a_O^{\,3}}\left(f'(\varepsilon_r) - \frac{1}{2}f'(n)\right) \quad (74)$$

cxix) A crucial point in the determination of $(\mu_{es} - \mu_{gs})$ is the choice of an appropriate Onsager (solvent cavity) radius [345] Different methods have been described in the literature involving X-ray data [224] or molecular modeling geometries [322] and applying further assumptions suggested, e. g., by *Lippert* [218a, b]. If the density of the molecule of interest is known, an alternative approach includes the mass-density relationship [346]. In this work, whenever a_O is used, the basis of estimation is described in the corresponding chapter. Accordingly, applying eqn (70b) leads to generally lower dipole moments than eqn (70a). If both plots yield the same linear correlations (or the same deviations from a linear correlation) the choice of "the right value" is somewhat arbitrary (when no experimental data is at hand) due to the comparatively large error possibly induced by a rough estimate for a_O.

cxx) The solvent-dependent shifts in absorption observed for the D-A-molecules investigated here are much smaller compared to those in emission and a graphical evaluation of μ_{gs} by eqns (70a) and (72) often leads to poor results. In this work, the values used for μ_{gs} were obtained from the optimized geometry in the ground state by semi-empirical calculations (AM1) since no experimentally obtained values were accessable.

$$\tilde{\nu}(em) = \tilde{\nu}^{vac}(em) - \frac{2\mu_{es}(\mu_{es} - \mu_{gs})}{hc_0 a_O^{\,3}}\left(f'(\varepsilon_r) - \frac{1}{2}f'(n)\right) \quad (75)$$

$$\text{with } f'(\varepsilon_r) = \frac{\varepsilon_r - 1}{\varepsilon_r + 2} \text{ and } f'(n) = \frac{n^2 - 1}{n^2 + 2} \quad (76)^{cxxi}$$

Empirical Solvent Polarity Scales

On the basis of solvatochromic shifts measured for the absorption and/or emission band(s) of different dye molecules, various empirical solvent polarity scales have been developed, upon those most often employed are the *Z*-scale [348], E_T(30)-scale [349], and π*-scale [350]. Only recently, a new scale was introduced by *Catalán* et al., the *SPP*-scale [220, 221]. Both types of polarity sensitive molecules have been employed, those of $\mu_{gs} > \mu_{es}$-type and those of the vice versa type, and accordingly, the polarity scales differ markedly in correlating absorption and emission data or their differences, i. e., the Stokes shift. A comprehensive discussion of this topic is found in some recent works of *Maroncelli* et al. and will not be repeated here [228]. The observations reported by this group for the correaltion of solvatochromic data of Coumarin 153 (with $\mu_{es} > \mu_{gs}$) with solvent polarity terms (see above) and empirical solvent polarity scales were made for the D-A-chalcones and Δ^2-pyrazolines during the studies for this work as well. The solvents with a low net dipole moment but significantly polar bonds (e. g. 1,4-dioxane or toluene) cannot be adequately modeled in terms of continuum dielectric descriptions and thus, when included in solvatochromic plots simply correlated to the reation field described as a function of ε_r and *n*, often lead to poor correlations [228c]. In this respect, empirical polarity scales obtained with a certain molecule "do not know" if a solvent is apolar or not. In accordance with *Maroncelli* et al., the best correlations of emission maxima and Stokes shifts including all solvents were obtained in this work with the E_T*(30)*-scale (for the classical scales), the polarity scale which measures the nuclear reorganization energies best and is least sensitive to solvent repolarization [228c]. However, the E_T*(30)*-scale is sensitive to hydrogen-bonding solvents. In contrast, the newly developed *SPP*-scale, being relatively precise in accounting for both dipolar nature and polarizability of solvents, shows a good correlation even when including alcohols [220, 221].

The Solvatokinetic Principle

The solvatokinetic behavior of a fluorescent compound relates to the solvent dependence of the non-radiative rate constant k_{nr} [223]. The solvatokinetic principle has been introduced to described the solvent-dependent excited-state interaction of highly and weakly polar emissive and non-emissive (transient) states in molecules with multiple flexible (single and double) bonds, e. g., stilbenes. Positive solvatokinetics are exemplified by an increase in k_{nr} with increasing solvent polarity (fluorescence quenching) and negative solvatokinetics describe the vice versa trend. When considering two excited transient species, an initially excited, emissive precursor state E* and a non-emissive product state P*, formed in an excited-state reaction, positive solvatokinetic behavior relates to a stronger stabilization of P* with increasing solvent polarity. Depending on the substitution pattern of such stilbenoid systems, either E* or P* has a higher dipole moment and is more stabilized upon increasing solvent polarity. However, if other fluorescent or non-fluorescent transient species are involved, the simple model is not valid anymore. Furthermore, the energy gap rule has to be taken into account. In the present work, the two terms are only used to describe the solvent-induced changes in fluorescence quantum yield and do not imply the classical stilbene model case.

Excited-State Reaction Scheme Involving Three Emitting Species

For a simple excited-state reaction model involving one excited species A* and two successor species B* and C*, all able to fluoresce, either a consecutive (A*→B*→C*) or a parallel (C*←A*→B*) reaction can occur. After construction of the $DAS_i(\lambda)$ (eqns (3), (26), pp. 33, 100) the $SAS_i(\lambda)$ can be obtained for either reaction mechanism involving more or less complicated expressions depending on further assumptions made, i. e., concerning backward or triangle reactions. Moreover, only if a spectral region exists where only one species emits (far blue or red side), the model can be tested by an extrapolation method given below [183b, 233]. Basically, construction of the $SAS_i(\lambda)$ is possible for a consecutive reaction mechanism according to eqns (77) – (79) and for a parallel reaction mechanism according to eqns (77), (80), and (81).

$$SAS_A(\lambda) = \frac{\sum DAS_i(\lambda)}{\tau_1^{-1}} \quad (77)$$

$$SAS_B(\lambda) = \frac{(\tau_1^{-1} - \tau_2^{-1})DAS_2(\lambda) + (\tau_1^{-1} - \tau_3^{-1})DAS_3(\lambda)}{\tau_1^{-1}\tau_2^{-1}} \quad (78)$$

$$SAS_C(\lambda) = \frac{(\tau_1^{-1} - \tau_3^{-1})(\tau_2^{-1} - \tau_3^{-1})DAS_3(\lambda)}{\tau_1^{-1}\tau_2^{-1}\tau_3^{-1}} \quad (79)$$

$$SAS_B(\lambda) = \frac{(\tau_1^{-1} - \tau_2^{-1})DAS_2(\lambda)}{\tau_1^{-1}\tau_2^{-1}} \quad (80)$$

$$SAS_C(\lambda) = \frac{(\tau_1^{-1} - \tau_3^{-1})DAS_3(\lambda)}{\tau_1^{-1}\tau_3^{-1}} \quad (81)$$

The models can be tested by extrapolation of the ratio of experimentally (exp) found $SAS_B(\lambda)$ or $SAS_C(\lambda)$ and the corresponding calculated (mod) $SAS_i(\lambda)$.

$$\lim_{\lambda\to\infty}(blue) = \frac{F_{SS}(\lambda)_{\exp} - SAS_A(\lambda)_{\exp}}{SAS_B(\lambda)_{\mathrm{mod}}} = 1 \quad (82)$$

$$\lim_{\lambda\to\infty}(red) = \frac{F_{SS}(\lambda)_{\exp} - SAS_A(\lambda)_{\exp}}{SAS_C(\lambda)_{\mathrm{mod}}} = 1 \quad (83)$$

cxxi) The polarizabilities of the molecule in ground and excited state are taken to $\alpha_{gs}/\alpha_O^{\,3} = \alpha_{es}/\alpha_O^{\,3} = 0.5$ [344a, e].

Appendix C

Spectrophotometric Determination of pK_a Values

To get more insight into the protolytic equilibria governing the pH-dependent spectroscopic behavior of $BP(OH)_2$ and BPOH pH titrations were carried out. For these experiments, the absorption spectrum was recorded every 0.25 pH units and the 60 spectra obtained allowed an analysis of the different pK_a values (*Fig. 70* and *71*).

For the analysis of the pH titration data, the spectrophotometric titration curves (T_{pH}-curves) and absorbance diagrams (A-diagrams) were constructed *(Fig. 72)* [351]. In the case of clearly resolved equilibria ($\Delta pK_a \sim 3$), combination and graphical evaluation of these diagrams yield the pK_a values in the following way. A plot of $A_{\lambda 1}$ vs. $A_{\lambda 2}$, the absorbances at two carefully chosen wavelengths, is analyzed for linear regions (corresponding to a pH range of interconversion, i. e., protonation or deprotonation).From the center of these regions, two straight lines are drawn into the adjacent plots, the corresponding $A_{\lambda n}$ vs. pH T_{pH}-curves. The pH value at the points of intersection of these lines with the T_{pH}-curves equals the pK_a value. In this way, 5 different A-diagrams and corresponding T_{pH}-curves were analyzed and the mean pK_a values found are included in *Table 2*, p. 22. An example of the graphical treatment of the pH-dependent data is given in *Fig. 72*. However, a direct attribution of the subbands to any tautomeric form is not possible at the present stage of investigation (*Scheme 4*, p. 24).

The pK_a values obtained in this way are only the macroscopic constants, since the different tautomeric equilibria shift as a function of pH as well. Any further attempts to extract microscopic acidity constants or tautomeric equilibrium constants were not made here [352].

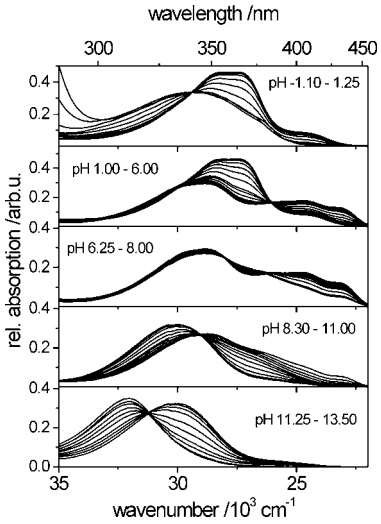

Fig. 70
Spectrophotometric pH titration of $BP(OH)_2$ in water. The pK_a values and band maxima are included in Table 2, p. 23 (c_L = 1 x 10^{-5} M; 50 mm absorption cells).

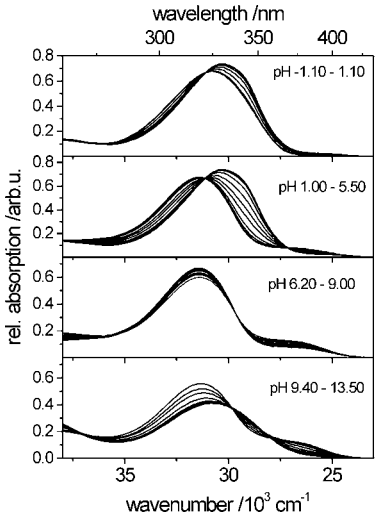

Fig. 71
Spectrophotometric pH titration of BPOH in water. The pK_a values and band maxima are included in Table 4, p. 28 (c_L = 1 x 10^{-5} M; 50 mm absorption cells).

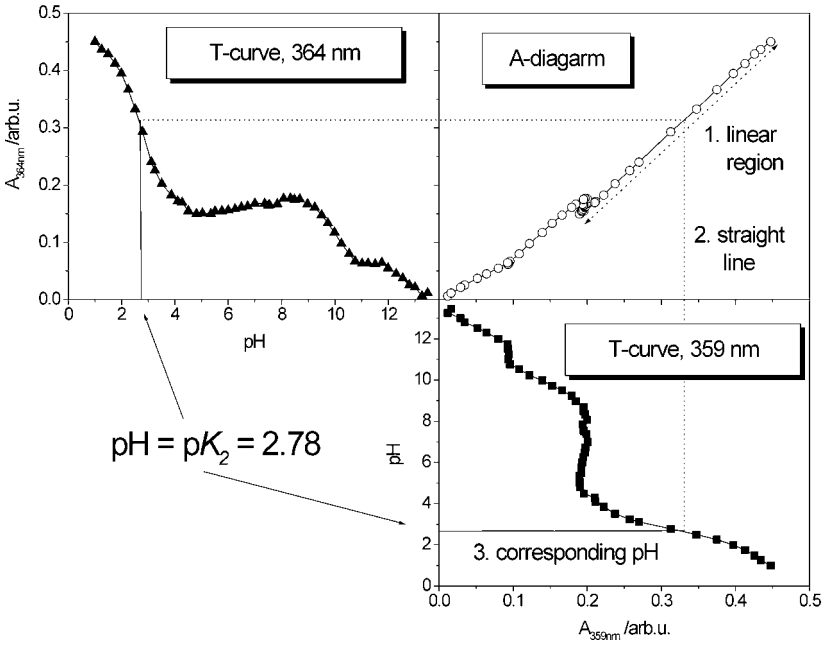

Fig. 72
A-diagram with corresponding T_{pH}-curves for λ_1 = 359 nm and λ_2 = 364 nm. As an example, the graphical estimation of pK_2 of $BP(OH)_2$ is shown (see text for details).

Appendix D

Chemical Structures of Related Compounds

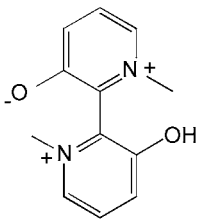

DDB

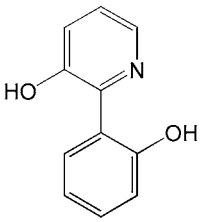

HPP

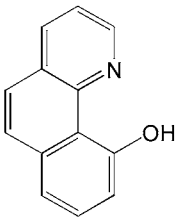

HBQ

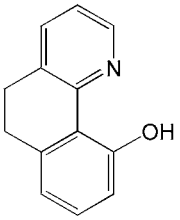

HdihBQ

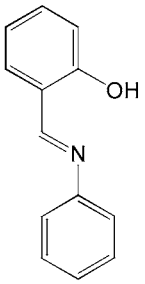

HBA

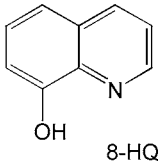

8-HQ

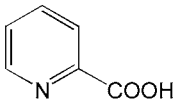

pyridine-2-carboxylic acid

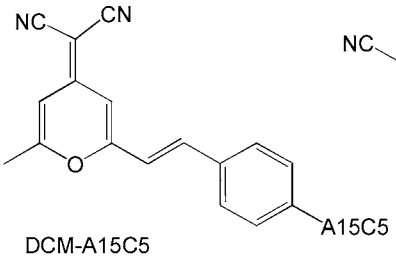

DCM-A15C5

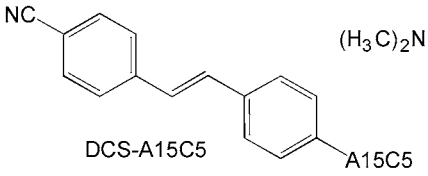

DCS-A15C5

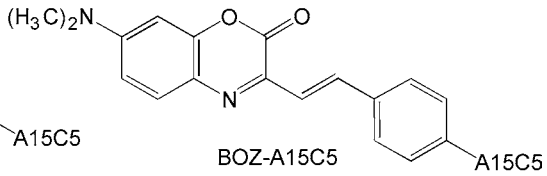

BOZ-A15C5

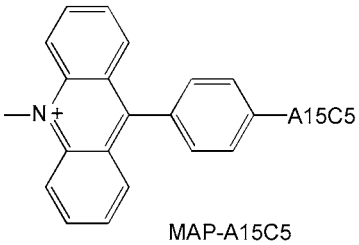

MAP-A15C5

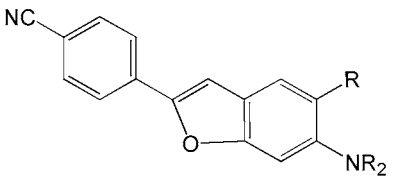

fura derivative

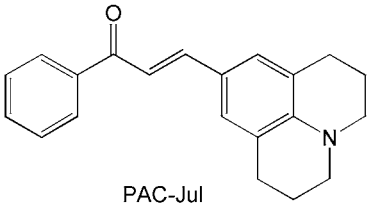

PAC-Jul

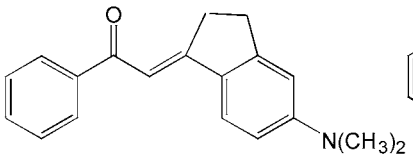

PAC-DMA-b4-5

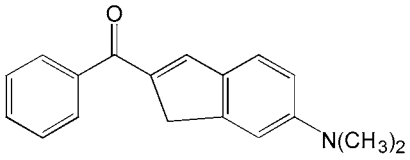

PAC-DMA-b34-5

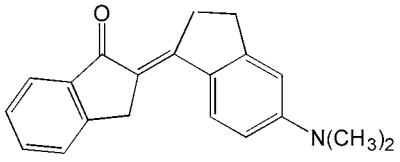

PAC-DMA-b124-5-2

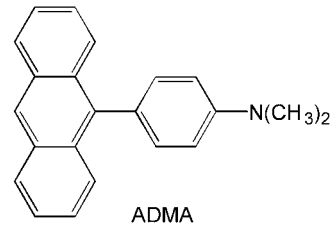

ADMA

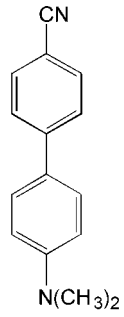

DA-Biphenyl

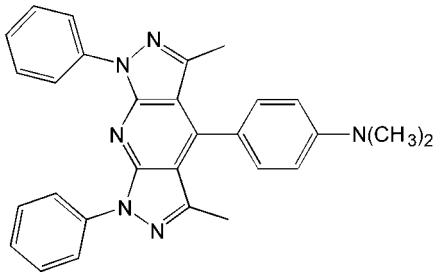

DMA-DMPP

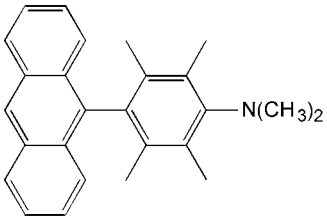

3,5-ATMA

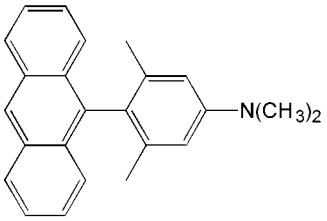

ADDMA

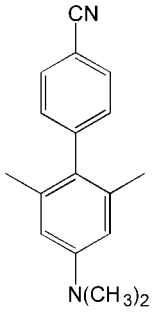

2,6-Dimethyl-
DA-Biphenyl

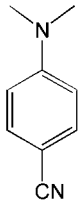

DMABN

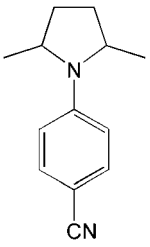

DMPYRBN

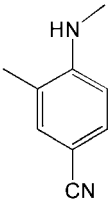

3-MMABN

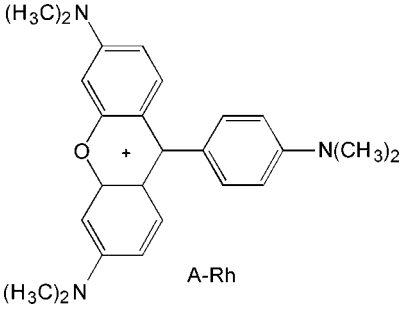

A-Rh

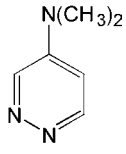

4-DMAP

References

[1] Morgan, J. J.; Stumm, W.
In *Metals and Their Compounds in the Environment;* Merian, E., (Ed.); VCH: Weinheim, 1991, p. 67.

[2] Ewers, U.; Schlipköter, H.-W.
In *Metals and Their Compounds in the Environment*; Merian, E., (Ed.); VCH: Weinheim, 1991, p. 591.

[3] Beyersmann, D.
In *Metals and Their Compounds in the Environment*; Merian, E., (Ed.); VCH: Weinheim, 1991, p. 491.

[4] Guimaraes-Motta, H.; Sande-Lemos, M. P.; de Meis, L.
J. Biol. Chem. **1984**, 259, 8699.

[5] Romani, A.; Scarpa, A.
Arch. Biochem. Biophys. **1992**, 298, 1.

[6] Förstner, U.; Salomons, W.
In *Metals and Their Compounds in the Environment*; Merian, E., (Ed.); VCH: Weinheim, 1991, p. 379.

[7] a) Sager, M.
In *Hazardous Metals in the Environment*; Stoeppler, M., (Ed.); Elsevier Science: Amsterdam, 1992, p. 133;
b) Förstner, U.
Intern. J. Environ. Anal. Chem. **1993**, *51*, 5;
c) Chakrabarti, C. L.; Lu, Y.; Back, M. H.; Schroeder, W. H.
Anal. Chim. Acta **1993**, *267*, 47.

[8] Reuter, J. H.; Perdue, E. M.
Geochim. Cosmochim. Acta **1977**, *41*, 325.

[9] Wennrich, R.; Mattausch, J.; Morgenstern, P.; Brüggemann, L.; Dittrich, B.
Vom Wasser **1996**, *87*, 51.

[10] Daum, K. A.; Newland, L. W.
In *Handbook of Environmental Chemistry - Reactions & Processes*; Hutzinger, O., (Ed.); Springer: Berlin, 1982; Vol. 2 B, p. 129.

[11] Singer, P. C.
In *Fate of Pollutants in the Air and Water Environment*, Suffet, I. H. (Ed.); John Wiley: New York, 1977, Part I, p. 155.

[12] Schmitt, H. W.; Sticher, H.
In *Metals and Their Compounds in the Environment*; Merian, E., (Ed.); VCH: Weinheim, 1991, p. 311.

[13] a) Sigg, L.
Mitteilung der EAWAG **1991**, *32D*, 32;
b) Sigg, L.; Kuhn, A.; Xue, H.; Kiefer, E.; Kistler, D.
In *Aquatic Chemistry: Interfacial and Interspecies Processes*; Huang, C. P.; O'Melia, C. R.; Morgan, J. J., (Eds.); ACS Adv. Chem. Ser.; ACS: Washington, D. C., 1995; Vol. 244, p. 177;
c) Xue, H.; Kistler, D.; Sigg, L .
Limonl. Oceanogr. **1995**, *40*, 1142.

[14] Zielhuis, R. L.
In *Metals and Their Compounds in the Environment*; Merian, E., (Ed.); VCH: Weinheim, 1991, p. 651.

[15] Gächter, R.
Schweiz. Z. Hydrol. **1979**, *41*, 169.

[16] a) Emons, H.
Fresenius J. Anal. Chem. **1996**, *354,* 507;
b) *Specimen Banking;* Rossbach, M.; Schladot, J. D.; Ostapczuk, P., (Eds.), Springer: Berlin, 1992.

[17] a) Ewers, U.
In *Metals and Their Compounds in the Environment*; Merian, E., (Ed.); VCH: Weinheim, 1991, p. 687;
b) Lieser, K. H.
GIT Fachz. Lab. **1992**, 293.

[18] Raspor, B.
In *Metals and Their Compounds in the Environment*; Merian, E., (Ed.); VCH: Weinheim, 1991, p. 233.

[19] Irving, H.; Williams, R. J. P.
Nature **1948**, *162*, 746.

[20] Sigg, L.; Xue, H.
In *Chemistry of Aquatic Systems: Local and Global Perspectives*; Bidoglio, G.; Stumm, W., (Eds.); Kluver Academic: Dordrecht, 1994, p. 153.

[21] Roof, A. A. M.
In *Handbook of Environmental Chemistry - Reactions & Processes*; Hutzinger, O., (Ed.); Springer: Berlin, 1982; Vol. 2 B, p. 43.

[22] Stoeppler, M.
In *Metals and Their Compounds in the Environment*; Merian, E., (Ed.); VCH: Weinheim, 1991, p. 105.

[23] a) Xue, H.; Oestrich, A.; Kistler, D.; Sigg, L.
Aquatic Sci. **1996**, *58*, 69;
b) Xue, H.; Sigg, L.
Limnol. Oceanogr. **1993**, *38*, 1200;
c) *Anal. Chim. Acta* **1994**, *284*, 505.

[24] Bettmer, J.; Buscher, W.; Cammann, K.
Fresenius J. Anal. Chem. **1996**, *354*, 521.

[25] Hiraide, M.
Anal. Sci. **1992**, *8*, 453.

[26] a) Lieberman, S. H.; Inman, S. M.; Theriault, G. A. *Proc. SPIE-Int. Soc. Opt. Eng.* **1989**, *1172*, 94;
b) Carroll, M. K.; Bright, F. V.; Hieftje, G. M. *Anal. Chem.* **1989**, *61*, 1768;
c) Wehry, E. L. *In Practical Fluorescence*; Guilbault, G. G., (Ed.); Marcel Dekker: New York, 1990, p. 367;
d) Cámara, C.; Moreno, M. C.; Orellana, G. In *Biosensors with Fiberoptics*; Wise, D. L.; Wingard, jr., L. B., (Eds.); Humana: Clifton, 1991, p. 29;
e) Resch, U.; Rurack, K.; Senoner, M. *Nachr. Chem. Tech. Lab.* **1994**, *42*, 504;
f) Oehme, I.; Wolfbeis, O. S. *Mikrochim. Acta* **1997**, *126*, 177.

[27] a) Choudhry, G. G. *Toxicol. Environ. Chem.* **1981**, *4*, 261;
b) In *Handbook of Environmental Chemistry – The Natural Environmental and the Biogeochemical Cycles*; Hutzinger, O., (Ed.); Springer: Berlin, 1984; Vol. 1 C, p. 1.

[28] Adhikari, M.; Hazra, G. C. *J. Indian Chem. Soc.* **1976**, *53,* 513.

[29] a) Esteves da Silva, J. C. G.; Machado, A. A. S. C.; Pinto, M. S. S. D. S. *Fresenius J. Anal. Chem.* **1997**, *357*, 950;
b) *J. Environ. Sci. Health, Part B* **1997**, *B32*, 469;
c) Esteves da Silva, J. C. G.; Machado, A. A. S. C. *An. Quim. Int. Ed.* **1996**, *92*, 306;
d) Lombardi, A. T.; Jardim, W. F. *J. Braz. Chem. Soc.* **1997**, *8*, 339;
e) *Chem. Speciation Bioavailability* **1997**, *9*, 27;
f) Butler, G. C.; Ryan, D. K. In *Humic and Fulvic Acids*; Gaffney, J. S.; Marley, N. A.; Clark, S. B., (Eds.); NATO ASI Ser.; ACS: Washington, D. C., 1996; Vol. 651, p. 140.

[30] a) *Applications of Fluorescence in the Biomedical Sciences*; Taylor, D. L.; Waggoner, A. S.; Murphy, R. F., Lanni, F.; Birge, R. R., (Eds.); Alan R. Liss, Inc.: New York, 1986;
b) *Luminescence Techniques in Chemical and Biochemical Analysis*; Baeyens, W. R. G.; De Keukeleire, D.; Korkidis, K., (Eds.); Marcel Dekker: New York, 1991.

[31] Van den Beld, C. M. B.; Lingeman, H. In *Luminescence Techniques in Chemical and Biochemical Analysis*; Baeyens, W. R. G.; De Keukeleire, D.; Korkidis, K., (Eds.); Marcel Dekker: New York, 1991, p. 237.

[32] a) Fleischauer, P. D.; Fleischauer, P. *Chem. Rev.* **1970**, *70*, 199;
b) Lytle, F. E. *Appl. Spectrosc.* **1970**, *24*, 319.

[33] a) McClure, D. S. *J. Chem. Phys.* **1952**, *20*, 682;
b) Robinson, G. W. *J. Chem. Phys.* **1967**, *46*, 572;
c) Kemlo, J. A.; Shepherd, T. M. *Chem. Phys. Lett.* **1977**, *47*, 158;
d) Masuhara, H.; Shioyama, H.; Saito, T.; Hamada,K.; Yasoshima, S.; Mataga, N. *J. Phys. Chem.* **1984**, *88*, 5868.

[34] a) Lytle, F. E.; Storey, D. R.; Juricich, M. E. *Spectrochim. Acta* **1973**, *29A*, 1357;
b) Hiraki, K.; Morishige, K.; Nishikawa, Y. *Anal. Chim. Acta* **1978**, *97*, 121;
c) Craven, T. L.; Lytle, F. E. *Anal. Chim. Acta* **1979**, *107*, 273;
d) Vitense, K. R.; McGown, L. B. *Anal. Chim. Acta* **1987**, *193*, 119;
e) Hoffmann, K.; Stahl, U.; Dähne, S. *Anal. Chim. Acta* **1994**, *286*, 241.

[35] Rurack, K.; Resch, U.; Senoner, M.; Dähne, S. *J. Fluoresc.* **1993**, *3*, 141.

[36] a) Rurack, K.; Resch, U.; Rettig, W. *BESSY Annual Report* **1996**, 459;
b) Rurack, K.; Resch-Genger, U.; Rettig, W. *J. Photochem. Photobiol. A Chem.* **1998**, *118*,143.

[37] Resch, U.; Rurack, K. *Proc. SPIE-Int. Soc. Opt. Eng.* **1997**, *3105*, 96.

[38] Lever, A. B. P. *Inorganic Electronic Spectroscopy*, Elsevier: Amsterdam, 1968.

[39] Crosby, G. A. *Acc. Chem. Res.* **1975**, *8*, 231.

[40] Harriman, A. *J. Chem. Soc. Faraday Trans. 2* **1981**, *77*, 1281.

[41] a) Banfield, T. L.; Husain, D. *Trans. Faraday Soc.* **1969**, *65*, 1985;
b) Varnes, A. W.; Dodson, R. B.; Wehry, E. L. *J. Am. Chem. Soc.* **1972**, *94,* 946.

[42] a) Haddad, P. R. *Talanta* **1977**, *24,* 1;
b) Birch, D. J. S.; Holmes, A. S.; Darbyshire, M. *Meas. Sci. Technol.* **1995**, *6,* 243;
c) Birch, D. J. S.; Rolinski, O. J.; Hatrick, D. *Rev. Sci. Instrum.* **1996**, *67*, 2732;
d) Juskowiak, B. *Anal. Chim. Acta* **1996**, *320*, 115.

[43] a) Warner, I. M.; McGown, L. B. *Anal. Chem.* **1992**, *64*, 343R;
b) Soper, S. A.; McGown, L. B.; Warner, I. M. *Anal. Chem.* **1994**, *66*, 428R;
c) Warner, I. M.; Soper, S. A.; McGown, L. B. *Anal. Chem.* **1996**, *68*, 73R;
d) *Anal. Chem.* **1998**, *70,* 477R.

[44] Czarnik, A. W. *Chem. Biol.* **1995**, *2,* 423.

[45] Diamond, D.; McKervey, M. A. *Chem. Soc. Rev.* **1996**, 15.

[46] Demas, J. N.; DeGraff, B. A.
Anal. Chem. **1991***, 63,* 829A.

[47] Bühlmann, P.; Pretsch, E.; Bakker, E.
Chem. Rev. **1998***, 98*, 1593.

[48] de Silva, A. P.; Gunaratne, H. Q. N.; Gunnlaugsson, T.; Huxley, A. J. M.; McCoy, C. P.; Rademacher, J. T.; Rice, T. E.
Chem. Rev. **1997***, 97*, 1515.

[49] Sousa, L. R.; Larson, J. M.
J. Am. Chem. Soc. **1977**, *99*, 307.

[50] a) Czarnik, A. W.
Trends Org. Chem. **1993***, 4*, 123;
b) In *Fluorescent Chemosensors for Ion and Molecule Recognition*; Czarnik, A. W., (Ed.); ACS Symp. Ser.; ACS: Washington D. C., 1993; Vol. 538, p. 1.

[51] Fernandez-Guiterrez, A.; Munoz de la Pena, A.
In *Molecular Luminescence Spectroscopy*; Schulman, S. G., (Ed.); J. Wiley & Sons: New York, 1985, p. 371.

[52] Golovina, A. P.; Runov, V. K.; Zorov, N. B.
Struct. Bonding **1981***, 47*, 54.

[53] Goppelsröder, F.
J. prakt. Chem. **1867***, 101*, 408.

[54] Castagnetto, J. M.; Canary, J. W.
Chem. Commun. **1998**, 203.

[55] Umland, F.
Theorie und Praktische Anwendung von Komplexbildnern; Akademische Verlagsgesellschaft: Frankfurt/M., 1971, p. 587.

[56] a) Pedersen, C. J.
J. Am. Chem. Soc. **1967***, 89*, 2495;
b) J. Am. Chem. Soc. **1967***, 89*, 7017.

[57] a) Dietrich, B.; Lehn, J. M.; Sauvage, *J. P. Tetrahedron Lett.* **1969**, 2885;
b) J. Chem. Soc. Chem. Commun. **1970**, 1055.

[58] Löhr, H.-G.; Vögtle, F.
Acc. Chem. Res. **1985***, 18,* 65.

[59] a) Valeur, B.; Bourson, J.; Pouget, J.
In *Fluorescent Chemosensors for Ion and Molecule Recognition*; Czarnik, A. W., (Ed.); ACS Symp. Ser.; ACS: Washington D. C., 1993; Vol. 538, p. 25;
b) Valeur, B.
In *Probe Design and Chemical Sensing*; Lakowicz, J. R., (Ed.); Plenum: New York, 1994; p. 21.

[60] Rettig, W.; Lapouyade, R.
In *Probe Design and Chemical Sensing*; Lakowicz, J. R., (Ed.); Plenum: New York, 1994, p. 109.

[61] Bissell, R. A.; de Silva, A. P.; Gunaratne, H. Q. N.; Lynch, P. L. M.; Maguire, G. E. M.; McCoy, C. P.; Sandanayake, K. R. A. S.
Top. Curr. Chem. **1993***, 168*, 223.

[62] Bissell, R. A.; de Silva, A. P.; Gunaratne, H. Q. N.; Lynch, P. L. M.; Maguire, G. E. M.; Sandanayake, K. R. A. S.
Chem. Soc. Rev. **1992**, 187.

[63] a) Czarnik, A. W.
In *Frontiers in Supramolecular Organic Chemistry and Photochemistry*; Schneider, H.-J.; Dürr, H., (Eds.); VCH: Weinheim, 1991, p. 109;
b) *Acc. Chem. Res.* **1994***, 27*, 302.

[64] a) Bouas-Laurent, H.; Castellan, A.; Daney, M.; Desvergne, J.-P.; Guinand, G.; Marsau, P.; Riffaud, M.-H.
J. Am. Chem. Soc. **1986***, 108*, 315;
b) Hinschberger, J.; Desvergne, J.-P.; Bouas-Laurent, H.; Marsau, P.
J. Chem. Soc. Perkin Trans. 2 **1990**, 993;
c) Parker, D.; Williams, J. A. G.
J. Chem. Soc. Perkin Trans. 2 **1995**, 1305;
d) Kubo, K.; Ishige, R.; Kato, N.; Yamamoto, E.; Sakurai, T.
Heterocycles **1997***, 45*, 2365;
e) Bouas-Laurent, H.; Desvergne, J.-P.; Fages, F.; Marsau, P.
In *Fluorescent Chemosensors for Ion and Molecule Recognition*; Czarnik, A. W., (Ed.); ACS Symp. Ser.; ACS: Washington D. C., 1993; Vol. 538, p. 59.

[65] a) Pérez-Jiménez, C.; Harris, S. J.; Diamond, D.
J. Chem. Soc. Chem. Commun. **1993**, 480;
b) Marsella, M. J.; Newland, R. J.; Carroll, P. J.; Swager, T. M.
J. Am. Chem. Soc. **1995***, 117*, 9842;
c) Aoki, I.; Sakaki, T.; Shinkai, S.
J. Chem. Soc. Chem. Commun. **1992**, 730;
d) Lynch, B. M.; Ryan, M. M.; Creaven, B. S.; Barrett, G.; McKervey, M. A.; Harris, S. J.
Anal. Proc. **1993***, 30*, 150.

[66] a) Herrmann, U.; Tümmler, B.; Maass, G.; Tze Mew, P. K.; Vögtle, F.
Biochemistry **1984***, 23*, 4059;
b) Konopelski, J. P.; Kotzyba-Hibert, F.; Lehn, J.-M.; Desvergne, J.-P.; Fages, F.; Castellan, A.; Bouas-Laurent, H.
J. Chem. Soc. Chem. Commun. **1985**, 433;
c) Fages, F.; Desvergne, J.-P.; Bouas-Laurent, H.; Marsau, P.; Lehn, J.-M.; Kotzyba-Hibert, F.; Albrecht-Gary, A.-M.; Al-Joubbeh, M.
J. Am. Chem. Soc. **1989***, 111*, 8672;
d) Desvergne, J.-P.; Fages, F.; Bouas-Laurent, H.; Marsau, P.
Pure Appl. Chem. **1992***, 64*, 1231.

[67] Jacquet, I.; Lehn, J.-M.; Marsau, P.; Andrianatoandro, H.; Barrans, Y.; Desvergne, J.-P.; Bouas-Laurent, H.
Bull. Soc. Chim. Fr. **1996***, 133*, 199.

[68] a) Kakizawa, Y.; Akita, T.; Nakamura, H.
Chem. Lett. **1993**, 1671;
b) Kubo, K.; Sakurai, T.
Chem. Lett. **1996**, 959;
c) Sasaki, D. Y.; Padilla, B. E.
Chem. Commun. **1998**, 1581.

[69] a) Valeur, B.; Pouget, J.; Bourson, J.; Kaschke, M.; Ernsting, N. P.
J. Phys. Chem. **1992**, *96,* 6545;
b) Bourson, J.; Badaoui, F.; Valeur, B.
J. Fluoresc. **1994**, *4,* 275.

[70] Crawford, K. B.; Goldfinger, M. B.; Swager, T. M.
J. Am. Chem. Soc. **1998**, *120*, 5187.

[71] a) Dix, J. P.; Vögtle, F.
Angew. Chem. Int. Ed. Engl. **1978**, *17*, 857;
b) Vögtle, F.
Pure Appl. Chem. **1980**, *52*, 2405;
c) Dix, J. P.; Vögtle, F.
Chem. Ber. **1980**, *113,* 457;
d) Chem. Ber. **1981**, *114*, 638;
e) Löhr, H.-G.; Vögtle, F.
Chem. Ber. **1985**, *118*, 914.

[72] a) Grynkiewicz, G.; Poenie, M.; Tsien, R. Y.
J. Biol. Chem. **1985**, *260*, 3440;
b) Adams, S. R.; Kao, J. P. Y.; Grynkiewicz, G.; Minta, A.; Tsien, R. Y.
J. Am. Chem. Soc. **1988**, *110*, 3212;
c) Minta, A.; Tsien, R. Y.
J. Biol. Chem. **1989**, *264*, 19449;
d) Tsien, R. Y.
Ann. Rev. Neurosci. **1989**, *12*, 227.

[73] Street, jr., K. W.; Krause, S. A.
Anal. Lett. **1986**, *19,* 735.

[74] Stinson, S.
Chem. Eng. News **1987**, 26.

[75] Cobbold, P. H.; Rink, T. J.
Biochem. J. **1987**, *248,* 313.

[76] Fery-Forgues, S.; Le Bris, M.-T.; Guetté, J.-P.; Valeur, B.
J. Phys. Chem. **1988**, *92*, 6233.

[77] a) Bourson, J.; Valeur, B.
J. Phys. Chem. **1989**, *93*, 3871;
b) Martin, M. M.; Plaza, P.; Dai Hung, N.; Meyer, Y. H.; Bourson, J.; Valeur, B.
Chem. Phys. Lett. **1993**, *202*, 425;
c) Martin, M. M.; Plaza, P.; Meyer, Y. H.; Begin, L.; Bourson, J.; Valeur, B.
J. Fluoresc. **1994**, *4*, 271;
d) Martin, M. M.; Plaza, P.; Meyer, Y. H.; Badaoui, F.; Bourson, J.; Lefevre, J.-P.; Valeur, B.
J. Phys. Chem. **1996**, *100*, 6879.

[78] a) Jonker, S. A.; Ariese, F.; Verhoeven, J. W. Recl.
Trav. Chim. Pays-Bas **1989**, *108*, 109;
b) Jonker, S. A.; van Dijk, S. I.; Goubitz, K.; Reiss, C. A.; Schuddeboom, W.; Verhoeven, J. W.
Mol. Cryst. Liq. Cryst. **1990**, *183*, 273.

[79] a) Meuwis, K.; Boens, N.; De Schryver, F. C.; Ameloot, M.; Gallay, J.; Vincent, M.
J. Phys. Chem. B **1998**, *102*, 641;
b) Meuwis, K.; Boens, N.; Gally, J.; Vincent, M.
Chem. Phys. Lett. **1998**, *287*, 412.

[80] Vo-Dinh, T.; Viallet, P.; Ramirez, L.; Pal, A.; Vigo,
J. Anal. Chim. Acta **1994**, *295*, 67.

[81] a) Lakowicz, J. R.; Szmacinski, H.; Berndt, K. W.
Proc. SPIE-Int. Soc. Opt. Eng. **1992**, *1648*, 150;
b) Lakowicz, J. R.; Szmacinski, H.; Johnson, M. L.
J. Fluoresc. **1992**, *2*, 47.

[82] a) Kuhn, M. A.; Hoyland, B.; Carter, S.; Zhang, C.; Haugland, R. P.
Proc. SPIE-Int. Soc. Opt. Eng. **1995**, *2388,* 238;
b) Shortreed, M.; Kopelman, R.; Kuhn, M.; Hoyland, B.
Anal. Chem. **1996**, *68*, 1414.

[83] Viallet, P.; Vigo, J.; Morelle, B.; Salmon, J.-M.
Proc. SPIE-Int. Soc. Opt. Eng. **1994**, *2324*, 223.

[84] Cazaux, L.; Faher, M.; Lopez, A.; Picard, C.; Tisnes, P.
J. Photochem. Photobiol. A Chem. **1994**, *77*, 217.

[85] a) Rurack, K.; Bricks, J. L.; Kachkovskii, A. D.; Resch, U.
J. Fluoresc. **1997**, *7*, 63S;
b) Rurack, K.; Bricks, J. L.; Reck, G.; Radeglia, R.; Resch-Genger, U.
J. Phys. Chem. A **2000**, *104,* 3087.

[86] a) Bourson, J.; Borrel, M.-N.; Valeur, B.
Anal. Chim. Acta **1992**, *257*, 189;
b) Bourson, J.; Pouget, J.; Valeur, B.
J. Phys. Chem. **1993**, *97*, 4552;
c) Bourson, J.; Badaoui, F.; Valeur, B.
J. Fluoresc. **1994**, *4,* 275;
d) Habib Jiwan, J.-L.; Branger, C.; Soumillion, J.-P.; Valeur, B.
J. Photochem. Photobiol. A Chem. **1998**, *116*,127.

[87] a) Crossley, R.; Goolamali, Z.; Gosper, J. J.; Sammes, P. G.
J. Chem. Soc. Perkin Trans. 2 **1994**, 513;
b) Crossley, R.; Goolamali, Z.; Sammes, P. G.
J. Chem. Soc. Perkin Trans. 2 **1994**, 1615.

[88] a) Kastenholz, F.; Grell, E.; Bats, J. W.; Quinkert, G.; Brand, K.; Lanig, H.; Schneider, F. W.
J. Fluoresc. **1994**, *4*, 243;
b) Doludda, M.; Kastenholz, F.; Lewitzki, E.; Grell, E.
J. Fluoresc. **1996**, *6,* 159.

[89] a) Golchini, K.; Mackovic-Basic, M.; Gharib, S. A.; Masilamani, D.; Lucas, M. E.; Kurtz, I. *Am. J. Physiol. (Renal Fluid Electrolyte Physiol.)* **1990**, *27*, F438; b) Alonso, M. T.; Brunet, E.; Hernandez, C.; Rodríguez-Ubis, J. C. *Tetrahedron Lett.* **1993**, *34*, 7465; c) Blackburn, C.; Bai, M.; LeCompte, K. A.; Langmuir, M. E. *Tetrahedron Lett.* **1994**, *35*, 7915; d) Masilamani, D.; Lucas, M. E. In *Fluorescent Chemosensors for Ion and Molecule Recognition*; Czarnik, A. W., (Ed.); ACS Symp. Ser.; ACS: Washington D. C., 1993; Vol. 538, p. 162; e) Akyuz, S.; Bulut, M.; Gocmen, A.; Erk, C. *Spectrosc. Lett.* **1995**, *28*, 603.

[90] a) Barzykin, A. V.; Fox, M. A.; Ushakov, E. N.; Stanislavsky, O. B.; Gromov, S. P.; Fedorova, O. A.; Alfimov, M. V. *J. Am. Chem. Soc.* **1992**, *114*, 6381; b) Alfimov, M. V.; Gromov, S. P. *Supramol. Chem.* **1992**, 343; c) Druzhinin, S. I.; Rusalov, M. V.; Uzhinov, B. M.; Alfimov, M. V.; Gromov, S. P.; Fedorova, O. A. *Proc. Indian Acad. Sci. (Chem. Sci.)* **1995**, *107*, 721; d) Alfimov, M. V.; Fedorov, Y. V.; Fedorova, O. A.; Gromov, S. S.; Hester, R. E.; Lednev, I. K.; Moore, J. N.; Oleshko, V. P.; Vedernikov, A. I. *J. Chem. Soc. Perkin Trans. 2* **1996**, 1441; e) Alfimov, M. V.; Churakov, A. V.; Fedorov, Y. V.; Fedorova, O. A.; Gromov, S. P.; Hester, R. E.; Howard, J. A. K.; Kuz'mina, L. G.; Lednev, I. K.; Moore, J. N. *J. Chem. Soc. Perkin Trans. 2* **1997**, 2249; f) Gromov, S. P.; Levin, D. E.; Burshtein, K. Ya.; Krasnovskii, V. E.; Dmitrieva, S. N.; Golosov, A. A.; Alfimov, M. V. *Russ. Chem. Bull. (Transl. of Izv. Akad. Nauk, Ser. Khim.)* **1997**, *46*, 959.

[91] a) Mateeva, N.; Deligeorgiev, T.; Mitewa, M.; Simova, S.; Dimov, I. *J. Inclusion Phenom. Mol. Recognit. Chem.* **1994**, *17,* 81; b) Mateeva, N.; Enchev, V.; Antonov, L.; Deligeorgiev, T.; Mitewa, M. *J. Inclusion Phenom. Mol. Recognit. Chem.* **1995**, *20,* 323.

[92] Rurack, K.; Bricks, J. L.; Slominskii, J. L.; Resch-Genger, U. In *Near-Infrared Dyes for High Technology Applications;* Dähne, S.; Resch-Genger, U.; Wolfbeis, O. S., (Eds.); NATO ASI Ser., Ser. 3; Kluwer Academic: Dordrecht, 1998; Vol. 52, p. 191.

[93] a) Lednev, I. K.; Hester, R. E.; Moore, J. N. *J. Chem. Soc. Faraday Trans.* **1997**, *93*, 1551; b) *J. Am. Chem. Soc.* **1997**, *119*, 3456; c) *J. Phys. Chem.* **1997**, *101*, 7371; d) Lednev, I. K.; Ye, T.-Q.; Hester, R. E.; Moore, J. N. *J. Phys. Chem.* **1997**, *101*, 4966.

[94] Thomas, K. J.; Thomas, K. G.; Manojkumar, T. K.; Das, S.; George, M. V. *Proc. Indian Acad. Sci. (Chem. Sci.)* **1994**, *106*, 1375.

[95] Patonay, G.; Tarazi, L. A.; George, A.; Van Aken, K.; Gorecki, T.; Strekowski, L. *Proc. SPIE-Int. Soc. Opt. Eng.* **1997**, *2980*, 68.

[96] a) Létard, J.-F.; Lapouyade, R.; Rettig, W. *Pure Appl. Chem.* **1993**, *65*, 1705; b) Dumon, P.; Jonusauskas, G.; Dupuy, F.; Pée, P.; Rullière, C.; Létard, J.-F.; Lapouyade, R. *J. Phys. Chem.* **1994**, *98*, 10391; c) Mathevet, R.; Jonusauskas, G.; Rullière, C.; Létard, J.-F.; Lapouyade, R. *J. Phys. Chem.* **1995**, *99*, 15709; d) Delmond, S.; Létard, J.-F.; Lapouyade, R.; Mathevet, R.; Jonusauskas, G.; Rullière, C. *New J. Chem.* **1996**, *20*, 861; e) Jonusauskas, G.; Lapouyade, R.; Delmond, S.; Létard, J. F.; Rullière, C. *J. Chim. Phys. Phys.-Chim. Biol.* **1996**, *93*, 1670; f) Mathevet, R.; Jonusauskas, G.; Lapouyade, R.; Létard, J.-F.; Rullière, C. *AIP Conf. Proc.* **1996**, *364*, 358.

[97] a) Das, S.; Thomas, K. G.; Thomas, K. J.; Kamat, P. V.; George, M. V. *J. Phys. Chem.* **1994**, *98,* 9291; b) Das, S.; Thomas, K. G.; Thomas, K. J.; George, M. V.; Bedja, I; Kamat, P. V. *Anal. Proc.* **1995**, *32*, 213.

[98] a) Akkaya, E. U. In *Chemosensors of Ion and Molecule Recognition*; Desvergne, J. P.; Czarnik, A. W., (Eds.); NATO ASI Ser., Ser. C; Kluwer Academic: Dordrecht, 1997; Vol. 492, p. 177; b) Oguz, U.; Akkaya, E. U. *Tetrahedron Lett.* **1997**, *38*, 4509; c) Akkaya, E. U.; Turkyilmaz, S. *Tetrahedron Lett.* **1997**, *38*, 4513.

[99] Cornelissen-Gude, C.; Rettig, W.; Lapouyade, R. *J. Phys. Chem. A* **1997**, *101*, 9673.

[100] Wolfbeis, O. S.; Offenbacher, H. *Monatsh. Chem.* **1984**, *115*, 647.

[101] a) Shirai, M.; Murakami, H.; Tsunooka, M. *Macromol. Rapid Commun.* **1994**, *15*, 807; b) *J. Fluoresc.* **1996**, *6,* 237.

[102] Ahmad, A. R.; Mehta, L. K.; Parrick, J. *Tetrahedron* **1995**, *51*, 12899.

[103] a) Létard, J.-F.; Delmond, S.; Lapouyade, R.; Braun, D.; Rettig, W.; Kreissler, M. *Recl. Trav. Chim. Pays-Bas* **1995**, *114*, 517; b) Poteau, X.; Ameer-Beg, S.; LeGourrierec, D.; Brown, R. G., Holmes, C.; Matthew, D.; Rettig, W. *BESSY Annual Report* **1996**, 456; c) Delmond, S.; Létard, J.-F.; Lapouyade, R.; Rettig, W. *BESSY Annual Report* **1996**, 461.

[104] a) Shen, Y.; Sullivan, B. P.
Inorg. Chem. **1995**, *34*, 6235;
b) Collins, G. E.; Choi, L.-S.
Chem. Commun. **1997**, 1135;
c) Kasa, I.; Agai, B.; Kubinyi, M.; Grofcsik, A.
J. Mol. Struct. **1997**, *408-409*, 547;
d) Prodi, L.; Bolletta, F.; Zaccheroni, N.;
Watt, C. I. F.; Mooney, N. J.
Chem. Eur. J. **1998**, *4,* 1090;
e) Roshal, A. D.; Grigorovich, A. V.;
Doroshenko, A. O.; Pivovarenko, V. G.;
Demchenko, A. P.
J. Phys. Chem. A **1998**, *102*, 5907.

[105] a) Resch, U.; Rurack, K.; Bricks, J. L.;
Slominskii, J. L.
J. Fluoresc. **1997**, *7*, 231S;
b) Rurack, K.; Bricks, J. L.; Slominskii, J. L.;
Resch, U.
Dyes Pigm. **1998**, *36*, 121.

[106] Kollmannsberger, M.; Rurack, K.; Resch-Genger, U.;
Daub, J.
J. Phys. Chem. A **1998**, *102*, 10211.

[107] Ghosh, S.; Petrin, M.; Maki, A. H.; Sousa, L. R.
J. Chem. Phys. **1987**, *87*, 4315.

[108] a) de Silva, A. P.; de Silva, S. A.
J. Chem. Soc. Chem. Commun. **1986**, 1709;
b) de Silva, A. P.; Sandanayake, K. R. A. S.
J. Chem. Soc. Chem. Commun. **1989**, 1183;
c) Bryan, A. J.; de Silva, A. P.; de Silva, S. A.;
Rupasinghe, R. A. D. D.; Sandanayake, K. R. A. S.
Biosensors **1989**, *4*, 169;
d) de Silva, A. P.; Gunaratne, H. Q. N.;
Sandanayake, K. R. A. S.
Tetrahedron Lett. **1990**, *31*, 5193;
e) de Silva, A. P.; Gunaratne, H. Q. N.
J. Chem. Soc. Chem. Commun. **1990**, 186;
f) de Silva, A. P.; Sandanayake, K. R. A. S.
Tetrahedron Lett. **1991**, *32,* 421;
g) de Silva, A. P.; Gunaratne, H. Q. N.;
Kane, A. T. M.; Maguire, G. E. M.
Chem. Lett. **1995**, 125;
h) de Silva, A. P.; Gunaratne, H. Q. N.; McCoy, C. P.
J. Am. Chem. Soc. **1997**, *119*, 7891.

[109] a) Huston, M. E.; Haider, K. W.; Czarnik, A. W.
J. Am. Chem. Soc. **1988**, *110*, 4460;
b) Akkaya, E. U.; Huston, M. E.; Czarnik, A. W.
J. Am. Chem. Soc. **1990**, *112*, 3590,
c) Huston, M. E.; Engleman, C.; Czarnik, A. W.
J. Am. Chem. Soc. **1990**, *112*, 7054;
d) Chae, M.-Y.; Cherian, X. M.; Czarnik, A. W.
J. Org. Chem. **1993**, *58*, 5797;
e) Yoon, J.; Ohler, N. E.; Vance, D. H.;
Aumiller, W. D.; Czarnik, A. W.
In *Chemosensors of Ion and Molecule Recognition*; Desvergne, J. P.; Czarnik, A. W.,
(Eds.); NATO ASI Ser., Ser. C; Kluwer Academic:
Dordrecht, 1997; Vol. 492, p. 189.

[110] a) Fabbrizzi, L.; Licchelli, M.; Pallavicini, P.;
Perotti, A.; Sacchi, D.
Angew. Chem. Int. Ed. Engl. **1994**, *33*, 1975;
b) Fabbrizzi, L.; Licchelli, M.; Pallavicini, P.;
Perotti, A.; Taglietti, A.; Sacchi, D.
Chem. Eur. J. **1996**, *2*, 75;
c) De Santis, G.; Fabbrizzi, L.; Licchelli, M.;
Poggi, A.; Taglietti, A.
Angew. Chem. Int. Ed. Engl. **1996**, *35*, 202;
d) Fabbrizzi, L.; Licchelli, M.; Pallavicini, P.;
Tagliette, A.
Inorg. Chem. **1996**, *35*, 1733;
e) De Santis, G.; Fabbrizzi, L.; Licchelli, M.;
Sardone, N.; Velders, A. H.
Chem. Eur. J. **1996**, *2*, 1243;
f) De Santis, G.; Fabbrizzi, L.; Licchelli, M.;
Mangano, C.; Sacchi, D.; Sardone, N.
Inorg. Chim. Acta **1997**, *257*, 69;
g) Fabbrizzi, L.; Licchelli, M.; Pallavicini, P.; Parodi, L.
Angew. Chem. Int. Ed. Engl. **1998**, *37*, 800.

[111] a) Klok, H.-A.; Möller, M.
Macromol. Symp. **1996**, *102*, 363;
b) *Macromol. Chem. Phys.* **1996**, *197*, 1395.

[112] a) Ghosh, P.; Bharadwaj, P. K.; Mandal, S.;
Ghosh, S.
J. Am. Chem. Soc. **1996**, *118*, 1553;
b) Ghosh, P.; Bharadwaj, P. K.; Roy, J.; Ghosh, S.
J. Am. Chem. Soc. **1997**, *119*, 11903.

[113] a) Otoda, K.; Kimra, S.; Imanishi, Y.
J. Chem. Soc. Perkin Trans. 1 **1993**, 3011;
b) James, T. D.; Shinkai, S.
J. Chem. Soc. Chem. Commun. **1995**, 1483;
c) Sclafani, J. A.; Maranto, M. T.; Sisk, T. M.;
Van Arman, S. A.
Tetrahedron Lett. **1996**, *37*, 2193;
d) Iwata, S.; Matsuoka, H.; Tanaka, K.
J. Chem. Soc. Perkin Trans. 1 **1997**, 1357.

[114] a) de Silva, A. P.; Gunaratne, H. Q. N.;
Maguire, G. E. M.
J. Chem. Soc. Chem. Commun. **1994**, 1213;
b) de Silva, A. P.; Gunaratne, H. Q. N.;
Gunnlaugsson, T.; Nieuwenhuizen, M.
Chem. Commun. **1996**, 1967.

[115] Iwata, S.; Tanaka, K.
J. Chem. Soc. Chem. Commun. **1995**, 1491.

[116] Rurack, K.; Bricks, J. L.; Schulz, B;
Maus, M., Reck, G.; Resch-Genger, U.
J. Phys. Chem. A **2000**, *104*, 6171.

[117] Blair, T. L.; Desai, J.; Bachas, L. G.
Anal. Lett. **1992**, *25*, 1823;
Blair, T. L.; Cynkowski, T.; Bachas, L. G.
Anal. Chem. **1993**, *65*, 945.

[118] Nishida, H.; Katayama, Y.; Katsuki, H.;
Nakamura, H.; Takagi, M.; Ueno, K.
Chem. Lett. **1982**, 1853.

[119] a) Alihodzic, S.; Zinic, M.; Klaic, B.; Kiralj, R.; Kojic-Prodic, B.; Herceg, M.; Cimerman, Z. *Tetrahedron Lett.* **1993**, *34*, 8345; b) Petrov, N. K.; Kuehnle, W.; Fiebig, T.; Staerk, H. *J. Phys. Chem. A* **1997**, *101*, 7043; c) Shirai, M.; Matoba, Y.; Tsunooka, M. *J. Fluoresc.* **1997**, *7*, 245; d) Klonkowski, A. M.; Kledzik, K.; Ossowski, T.; Jankowska-frydel, A. *J. Mater. Chem.* **1998**, *8,* 1245; e) Ramachandram, B.; Samanta, A. *Chem. Phys. Lett.* **1998**, *290*, 9; *f) Chem. Commun.* **1997**, 1037.

[120] Rurack, K.; Bricks, J. L. unpublished results.

[121] Valeur, B.; Pouget, J.; Bourson, J. *J. Lumin.* **1992**, *52*, 345.

[122] a) Bruening, R. L.; Izatt, R. M.; Bradshaw, J. S. In *Cation Binding by Macrocycles*; Inoue, Y.; Gokel, G. W., (Eds.); Marcel Dekker: New York, 1990, p. 111; b) Izatt, R. M.; Bradshaw, J. S.; Pawlak, K.; Bruening, R. L.; Tarbet, B. J. *Chem. Rev.* **1992**, *92*, 1261; c) Bradshaw, J. S.; Krakowiak, K. E.; Izatt, R. M. *Aza-Crown Macrocycles*; John Wiley & Sons: New York, 1993; d) Bradshaw, J. S.; Izatt, R. M. *Acc. Chem. Res.* **1997**, *30*, 338.

[123] a) Shinkai, S.; Manabe, O. *Top. Curr. Chem.* **1984**, *121*, 67; b) Lindoy, L. F. In *Synthesis of Macrocycles*; Izatt, R. M.; Christensen, J. J., (Eds.); John Wiley & Sons: New York, 1987, p. 53; c) Dietrich, B.; Viout, B.; Lehn, J.-M. *Macrocyclic Chemistry*; VCH: Weinheim, 1993, p. 3.

[124] a) Lehn, J.-M. *Struct. Bonding* **1973**, *16*, 1; b) *Pure Appl. Chem.* **1980**, *52*, 2441.

[125] a) Mason, W. T.; Hoyland, J.; Davison, I.; Carew, M. A.; Jonassen, J.; Zorec, R.; Lledo, P. M.; Shankar, G.; Horton, M. *Mol. Imaging Neurosci.* **1993**; *130*, 171; b) Ferreira, S. T.; Coelho-Sampaio, T. *Biosci. Rep.* **1996**, *16*, 87; c) Jung, D. W.; Champan, C. J.; Baysal, K.; Pfeiffer, D. R.; Brierley, G. P. *Arch. Biochem. Biophys.* **1996**, *332*, 19.

[126] Clarke, R. J.; Coates, J. H.; Lincoln, S. E. *Inorg. Chim. Acta* **1988**, *153,* 21.

[127] a) Zhou, J.; Zhao, F.; Li, Y.; Zhang, F.; Song, X. *J. Photochem. Photobiol. A Chem.* **1995**, *92*, 193; b) Preigh, M. J.; Lin, F.-T.; Ismail, K. Z.; Weber, S. G. *J. Chem. Soc. Chem. Commun.* **1995**, 2091; c) Atabekyan, L. S.; Chibisov, A. K. *High Energy Chem. (Transl. of Khim. Vys. Energ.)* **1996**, *30*, 261; d) Inouye, M. *Coord. Chem. Rev.* **1996**, *148*, 265; e) Dujols, V.; Ford, F.; Czarnik, A. W. *J. Am. Chem. Soc.* **1997**, *119*, 7386; f) Kimura, K.; Utsumi, T.; Teranishi, T.; Yokoyama, M.; Sakamoto, H.; Okamoto, M.; Arakawa, R.; Moriguchi, H.; Miyaji, Y. *Angew. Chem. Int. Ed. Engl.* **1997**, *36*, 2452.

[128] a) Fabbrizzi, L.; Poggi, A. *Chem. Soc. Rev.* **1995**, 197; b) Krämer, R. *Angew. Chem. Int. Ed. Engl.* **1998**, *37*, 772.

[129] Zabin, S. A.; Jejurkar, C. R. *J. Polym. Mater.* **1997**, *14*, 239.

[130] Maloney, K. M.; Shnek, D. R.; Sasaki, D. Y.; Arnold, F. H. *Chem. Biol.* **1996**, *3*, 185.

[131] Rasmussen, J. C.; Toftlund, H.; Nivorzhkin, A. N.; Bourassa, J.; Ford, P. C. *Inorg. Chim. Acta* **1996**, *251*, 291.

[132] a) Kovtun, J. P.; Shandura, N. P.; Tolmachev, A. I. *Zh. nauchn. prikl. phot.* **1997**, *42*, 63; *b) Zh. org. khim.* **1997**, *33*, 1752; *c) Sci. Appl. Photo.* **1997**, *39*, 295.

[133] Preininger, C.; Wolfbeis, O. S. *Biosens. Bioelectron.* **1996**, *11*, 981.

[134] a) Nakamura, M.; Ikeda, A.; Ise, N.; Ikeda, T.; Ikeda, H.; Toda, F.; Ueno, A. *J. Chem. Soc. Chem. Commun*. **1995**, 721; b) Corradini, R.; Dossena, A.; Marchelli, R.; Panagia, A.; Sartor, G.; Saviano, M.; Lombardi, A.; Pavone, V. *Chem. Eur. J.* **1996**, *2*, 373; c) Corradini, R.; Dossena, A.; Galaverna, G.; Marchelli, R.; Panagia, A.; Sartor, G. *J. Org. Chem.* **1997**, *62*, 6283.

[135] a) Schuster, M.; Unterreitmaier, E. *Fresenius Z. Anal. Chem.* **1993**, *346*, 630; b) Unterreitmaier, E.; Schuster, M. *Anal. Chim. Acta* **1995**, *309,* 339.

[136] a) Naumann, C.; Langhals, H. *Synthesis* **1990**, 279; b) Langhals, H.; Pust, S. *Chem. Ber.* **1985**, *118*, 4674.

[137] a) Zubarovskii, V. M. *Zh. Org. Khim.* **1951**, *21*, 2199; b) Zubarovskii, V. M.; Bricks, J. L. *Ukr. Khim. Zh.* **1982**, *48*, 761; c) *Khim. Heterocycl. Soed.* **1982**, *N5*, 644.

[138] a) Bradshaw, J. S.; Hui, J. Y.; Chan, Y.; Haymore, B. L.; Izatt, R. M.; Christensen, J. J. *J. Heterocycl. Chem.* **1974**, *2*, 45; b) Ross, W. C. J. *J. Chem. Soc.* **1949**, 183; c) Buter, J.; Kellogg, R. M. *J. Org. Chem.* **1981**, *46*, 4481.

[139] Rurack, K.; Dekhtyar, M. L.; Bricks, J. L.; Resch-Genger, U.; Rettig, W. *J. Phys. Chem A* **1999**, *103*, 9626

[140] Kollmannsberger, M.; Gareis, T.; Heinl, S.; Breu, J.; Daub, J. *Angew. Chem. Int. Ed. Engl.* **1997**, *36*, 1333.

[141] *Gmelins Handbuch der Anorganischen Chemie.* Chlor, 8th Edn., VCH: Berlin, 1927.

[142] Riddick, J. A.; Toops, jr., E. E. *Organic Solvents*; 2nd Edn., Interscience: New York, 1967, p. 297.

[143] a) Pearson, R. G. *J. Am. Chem. Soc.* **1963**, *85*, 3533; *b) Inorg. Chem.* **1988**, *27*, 734.

[144] a) Velapoldi, R. A. In *Advances in Standards and Methodology in Spectorphotometry*; Burgess, C.; Mielenz, K. D., (Eds.); Elsevier Science: Amsterdam, 1987, p. 175; b) *J. Res. Natl. Bur. Stand.* **1972**, *76A*, 641; c) Velapoldi, R.A.; Epstein, M.S. *ACS Symp. Ser.,* **1989**, *383*, 98.

[145] a) Eaton, D. F. *J. Photochem. Photobiol. B Biol.* **1988**, *2*, 523; b) *Pure Appl. Chem.* **1988**, *60*, 1107; c) Chen, R. F. *Accuracy in Spectrophotometry and Luminescence Measurements*; Mavrodineanu, R.; Schultz, J. I.; Menis, O., (Eds.); NBS Special Publication No. 260-64, Washington D. C., 1980.

[146] Demas, J. N. *In Optical Radiation Measurements*; Mielenz, K. D., (Ed.); Academic: New York, 1982; Vol. 3, p. 195.

[147] Drexhage, K. H. *J. Res. Natl. Bur. Stand.* **1976**, *80A*, 421.

[148] Olmsted, III, J. *J. Phys. Chem.* **1979**, *83*, 2581.

[149] Drake, J. M.; Lesiecki, M. L.; Camaioni, D. M. *Chem. Phys. Lett.* **1985**, *113*, 530.

[150] Vogel, M.; Rettig, W. *Ber. Bunsenges. Phys. Chem.* **1987**, *91*, 1241.

[151] Boens, N.; Tamai, N.; Yamazaki, I.; Yamazaki, T. *Photochem. Photobiol.* **1990**, *52*, 911.

[152] Sway, M. I.; Ambushamleh, A. S. *J. Chem. Soc. Faraday Trans. 1* **1995**, *91,* 1607.

[153] Dewar, M. J. S.; Zoeblich, E. G.; Healy, E. F.; Stewart, J. P. P. *J. Am. Chem. Soc.* **1985**, *107*, 3202.

[154] Zerner, M. C.; Karelson, M. M. *J. Phys. Chem.* **1992**, *96*, 6949.

[155] Stahl, U.; Rurack, K. In *Analytische Grundlagenuntersuchungen zur Laserimpulsfluorometire im ultravioletten Spektralbereich*; Dähne, S (Ed.); BAM-Forschungsbericht No. 223; BAM, Berlin, 1995, p.30.

[156] a) Soper, S. A.; Davis, L. M.; Brooks Shera, E. *J. Opt. Soc. Am.* **1992**, *9*, 1761; b) Soper, S. A.; Nutter, H. L.; Keller, R. A.; Davis, L. M.; Brooks Shera, E. *Photochem. Photobiol.* **1993**, *57*, 972; c) Keller, R. A.; Ambrose, W. P.; Goodwin, P. M.; Jett, J. H.; Martin, J. C.; Wu, M. *Appl. Spectrosc.* **1996**, *50*, 12A.

[157] Siemanowski, W.; Witzel, H. *Liebigs Ann. Chem.* **1984**, 1731.

[158] a) Irving, H.; Mellor, D. H. *J. Chem. Soc.* **1962**, 5222; b) Kotlicka, J.; Grabowski, Z. R. *J. Photochem.* **1979**, *11*, 413; c) Yagi, M.; Torii, M.; Yamauchi, N.; Kaneshima, T.; Higuchi, J. *Chem. Phys. Lett.* **1991**, *187*, 604; d) Dhanya, S.; Bhattacharyya, P. K. *J. Photochem. Photobiol. A Chem.* **1992**, *63*, 179.

[159] a) Bulska, H. *Chem. Phys. Lett.* **1983**, *98,* 398; b) Bulska, H.; Grabowska, A.; Grabowski, Z. R. *J. Lumin.* **1986**, *35,* 189; c) Sepiol, J.; Bulska, H.; Grabowska, A. *Chem. Phys. Lett.* **1987**, *140,* 607; d) Bulska, H. *J. Lumin.* **1988**, *39,* 293; e) Sepiol, J.; Grabowska, A.; Bulska, H.; Mordzinski, A.; Perez Salgado, F.; Rettschnick, R. P. H. *Chem. Phys. Lett.* **1989**, *163,* 443; f) Grabowska, A.; Borowicz, P.; Mártire, D. O.; Braslavsky, S. E. *Chem. Phys. Lett.* **1991**, *185*, 206; g) Kaczmarek, L.; Nowak, B.; Zukowski, J.; Borowicz, P.; Sepiol, J.; Grabowska, A. *J. Mol. Struct.* **1991**, *248,* 189; h) Eyal, M.; Reisfeld, R.; Chernyak, V.; Kaczmarek, L.; Grabowska, A. *Chem. Phys. Lett.* **1991**, *176*, 531; i) Grabowska, A.; Kaczmarek, L. *Pol. J. Chem.* **1992**, *66*, 715; j) Lipkowski, J.; Grabowska, A.; Waluk, J.; Calestani, G.; Hess, jr., B. A. *J. Crystallogr. Spectrosc. Res.* **1992**, *22,* 563; k) Borowicz, P.; Grabowska, A.; Wortmann, R.; Liptay, W. *J. Lumin.* **1992**, *52,* 265; l) Wortmann, R.; Elich, K.; Lebus, S.; Liptay, W.; Borowicz, P.; Grabowska, A. *J. Phys. Chem.* **1992**, *96,* 9724;

m) Borowicz, P.; Grabowska, A.; Kaczmarek, L.; Lés, A.; Adamowicz, L.
Chem. Phys. Lett. **1995**, *239*, 282;
n) Sitkowski, J.; Stefaniak, L.; Kaczmarek, L.; Webb, G. A.
J. Mol. Struct. **1996**, *385*, 65.

[160] Waluk, J.; Bulska, H.; Grabowska, A.; Mordzinski, A.
New J. Chem. **1986**, *10*, 413.

[161] a) Barone, V.; Adamo, C.
Chem. Phys. Lett. **1995**, *241*, 1;
b) Barone, V.; Milano, G.; Orlandini, L.; Adamo, C.
J. Chem. Soc. Perkin Trans. 2 **1995**, 1141.

[162] a) Sobolewski, A. L.; Adamowicz, L.
Chem. Phys. Lett. **1996**, *252*, 33;
b) Enchev, V.
Int. J. Quantum Chem. **1996**, *57*, 721;
c) Carballeira, L.; Perez-Juste, I.
J. Mol. Struct. THEOCHEM **1996**, *368*, 17.

[163] a) Zhang, H.; van der Meulen, P.; Glasbeek, M.
Chem. Phys. Lett. **1996**, *253*, 97;
b) Marks, D.; Zhang, H.; Glasbeek, M.; Borowicz, P.; Grabowska, A.
Chem. Phys. Lett. **1997**, *275*, 370;
c) Glasbeek, M.; Marks, D.; Zhang, H.
J. Lumin. **1997**, *72-74*, 832;
d) Marks, D.; Prosposito, P.; Zhang, H.; Glasbeek, M.
Chem. Phys. Lett. **1998**, *289*, 535.

[164] Kaschke, M.; Rentsch, S.; Opfermann, J.
Laser Chem. **1988**, *8*, 377.

[165] Johansson, L. B.-Å.; Persson, L.; Langhals, H.
J. Chem. Soc. Faraday Trans. **1996**, *92*, 4909.

[166] Vollmer, F.; Rettig, W.
J. Photochem. Photobiol. A Chem. **1996**, *95*, 143.

[167] Rurack, K.; Senoner, M.; Resch, U.; Dähne, S.
J. Inf. Rec. Mater. **1994**, *21*, 683.

[168] a) LeGourrierec, D.; Ormson, S. M.; Brown, R. G.; Rettig, W.
BESSY Annual Report **1995**, 473;
b) Tokumura, K.; Oyama, O.; Mukaihata, H.; Itoh, M.
J. Phys. Chem. A **1997**, *101*, 1419.

[169] Kaczmarek, L.; Balicki, R.; Lipkowski, J.; Borowicz, P.; Grabowska, A.
J. Chem. Soc. Perkin Trans. 2 **1994**, 1603.

[170] a) Fujii, T.; Murakami, T.; Mabuchi, T.; Tsuchida, T.; Yokoya, Y.; Nakamura, N.; Wakabayashi, S.; Yamazaki, T.; Yamazaki, I.
J. Fac. Eng. Shinshu Univ. **1993**, *73*, 39;
b) Martinez, M. L.; Cooper, W. C.; Chou, P.-T.
Chem. Phys. Lett. **1992**, *193*, 151.

[171] a) Henry, M. S.; Hoffman, M. Z.
J. Am. Chem. Soc. **1977**, *99*, 5201;
b) *J. Phys. Chem.* **1979**, *83*, 618.

[172] Rurack, K.; Radeglia, R.
Eur. J. Inorg. Chem. **2000**, 2271

[173] Holligan, B. M.; Jeffery, J. C.; Norgett, M. K.; Schatz, E.; Ward, M. D.
J. Chem. Soc. Dalton Trans. **1992**, 3345.

[174] Knyazhansky, M. I.; Makarova, N. I.; Metelitsa, A. V.; Kharlanov, V. A.; Pichko, V. A.; Olehnovich, E. P.
Book of Abstracts, XVI IUPAC Symposium on Photochemistry, Helsinki; IUPAC, 1996.

[175] a) Johnston, W. D.; Freiser, H.
Anal. Chim. Acta **1954**, *11*, 301;
b) Kábrt, L.; Holzbecher, Z.
Collect. Czech. Chem. Commun. **1976**, *41*, 540.

[176] a) Das, K.; Sarkar, N.; Ghosh, A. K.; Majumdar, D.; Nath, D. N.; Bhattacharyya, K.
J. Phys. Chem. **1994**, *98*, 9126;
b) Potter, C. A. S.; Brown, R. G.; Vollmer, F.; Rettig, W.
J. Chem. Soc. Faraday Trans. **1994**, *90*, 59;
c) Douhal, A.; Amat-Guerri, F.; Acuña, A. U.
J. Phys. Chem. **1995**, *99*, 76.

[177] a) Itoh, M.; Adachi, T.; Tokumura, K.
J. Am. Chem. Soc. ***1984***, *106*, 850;
b) Konijnenberg, J.; Ekelmans, G. B.; Huizer, A. H.; Varma, C. A. G. O.
J. Chem. Soc. Faraday Trans. 2 **1989**, *85*, 39;
c) McMorrow, D.; Kasha, M.
J. Phys. Chem. **1984**, *88*, 2235.

[178] a) Umland, F.; Poddar, B. K.; Stegemeyer, H.
Z. analyt. Chem. **1966**, *216*, 125;
b) Umland, F.; Hohaus, E.
Angew. Chem. Int. Ed. Engl. **1967**, *6*, 1082.

[179] Cargill Thompson, A. M. W.; Jeffrey, J. C.; Liard, D. J.; Ward, M. D.
J. Chem. Soc. Dalton Trans. **1996**, 879.

[180] Umland, F.
Theorie und Praktische Anwendung von Komplexbildnern; Akademie: Frankfurt/M., 1971, p. 173.

[181] Vosburgh, W. C.; Cooper, G. R.
J. Am. Chem. Soc. **1941**, *63,* 437.

[182] a) Umland, F.
Theorie und Praktische Anwendung von Komplexbildnern; Akademie: Frankfurt/M., 1971, p. 45;
b) Császár, J.
Acta Phys. Chem., Szeged **1982**, *28*, 45;
c) *Acta Phys. Chem., Szeged* **1982**, *28*, 59.

[183] a) Löfroth, J.-E.
Anal. Instrum. **1985**, *14*, 403;
b) *J. Phys. Chem.* **1986**, *90*, 1160;
c) Beechem, J. M.
Methods Enzymol. **1992**, *210*, 37.

[184] a) Bayer, E.
Ber. **1957**, *90*, 2325;
b) Jungreis, E.; Thabet, S.
In *Chelates in Analytical Chemistry*; Flaschka, H. A.; Barnard, jr., A. J., (Eds.);
Marcel Dekker: New York, 1969, p. 149;
c) Braithwaite, A. C.; Waters, N. T.
J. Inorg. Nucl. Chem. **1973**, *35*, 3223;
d) Braithwaite, A. C.; Wrigth, P. E.; Waters, N. T.
J. Inorg. Nucl. Chem. **1975**, *37*, 1669.

[185] a) Schwarzenbach, G.
Adv. Inorg. Radiochem. **1961**, *3*, 257;
b) Parry, R. W.
In *The Chemistry of the Coordination Compounds*; Bailar, jr., J. C.; Busch, D. H., (Eds.);
Reinhold: New York, 1956, p. 221.

[186] a) Ohno, T.; Kato, S.
Bull. Chem. Soc. Jpn. **1974**, *47*, 2953;
b) Castellucci, E.; Angeloni, L.; Marconi, G.; Venuti, E.; Baraldi, I.
J. Phys. Chem. **1990**, *94*, 1740.

[187] Schläfer, H. L.
Z. Phys. Chem., Neue Folge **1956**, *8*, 373.

[188] Ganis, P.; Saporito, A.; Vitagliano, A.; Valle, G.
Inorg. Chim. Acta **1988**, *142*, 75.

[189] a) Pretsch, E.; Clerc, T.; Seibl, J.; Simon, W.
Tables of Spectral Data for Structure Determination of Organic Compounds; Springer: Berlin, 1989, pp. H275, H315;
b) *ibid*. pp. H330, H335.

[190] a) Vögtle, F.
Supramolekulare Chemie; B. G. Teubner: Stuttgart, 2nd edn., 1992; p.36;
b) Castellano, S.; Günther, H.; Ebersole, S.
J. Phys. Chem. **1965**, *69*, 4166.

[191] Jeffery, J. C.; Schatz, E.; Ward, M. D.
J. Chem. Soc. Dalton Trans. **1992**, 1921.

[192] Umland, F.; Poddar, B. K.; Stegemeyer, H.
Z. analyt. Chem. **1966**, *216*, 125.

[193] Sommer, L., cited In Umland, F.
Theorie und Praktische Anwendung von Komplexbildnern; Akademie: Frankfurt/M., 1971, p. 45. (Note that the original reference could not be traced.)

[194] Nakamaru, K.
Bull. Chem. Soc. Jpn. **1982,** *55*, 2697.

[195] Kostanecki, S. V.; Tambor, J.
Ber. **1899**, *32*, 1921.

[196] a) Saitoh, T.; Shibata, S.
Tetrahedron Lett. **1975**, 4461;
b) Nagarajan, G. R.; Parmer, V. S.
Phytochemistry **1977**, *16*, 1317;
c) Woolenweber, E.; Jay, M.; Favre-Bonvin, J.
Phytochemistry **1974**, *13*, 2618;
d) Malterud, K. E.; Anthonsen, T.; Lorentzen, G. B.
Phytochemistry **1977**, *16*, 1805.

[197] a) Dhar, D. N.
The Chemistry of Chalcones and Related Compounds; John Wiley & Sons: New York; 1981;
b) Stecher, H.
Adhaesion **1958**, *2*, 243;
c) Su, G.-B.; He, Y.-P.; Li, Z.-D.
Jiegou Huaxue **1997**, *16*, 263;
d) Mager, L.; Melzer, C.; Barzoukas, M.; Fort, A.; Mery, S.; Nicoud, J.-F.
Appl. Phys. Lett. **1997**, *71*, 2248;
e) Schellenberg, W. D.; Heinz, J.
Farbenfabriken Bayer Akt. Ges. German Patent 1,039,835 (1959),
Chem. Abstr. **1961**, 55, 7119f;
f) Adams, J. H.
British Patent 1,250,388 (1971),
Chem. Abstr. **1972**, *76*, 46956p;
g) Simpson, T. H.; Uri, N.
British Patent 875,164 (1956),
Chem. Abstr. **1962**, *56*, 3582b;
h) Linke, H. A. B.; Eveleigh, D. E.
Z. Naturforsch. **1975**, *30b*, 740;
i) Horowitz, R. M.; Gentili, B.
U.S. Patent 3,890,298 (1975),
Chem. Abstr. **1975**, *83*, 147706g;
j) Monroe, B.; Smothers, W. K.; Keys, D. E.; Krebs, R. R.; Mickish, D. J.; Harrington, A. F.; Schicker, S. R.; Armstrong, M. K.; Chan, D. M. T.; Weathers, C. I.
J. Imaging Sci. **1991**, *35*, 19.

[198] a) Geiger, W. B.; Conn, J. E.
J. Am. Chem. Soc. **1945**, *67*, 112;
b) Schraufstätter, E.; Deutsch, S.
Z. Naturforsch. **1949**, *4b*, 276;
c) Stenlid, G.
Physiol. Plant. **1968**, *21*, 882;
d) Pachmann, A. N.; Rublin, N.
Am. J. Pharm. **1962**, *134*, 45.

[199] a) Lindoy, L. F.
In *Cation Binding by Macrocycles*; Inoue, Y.; Gokel, G. W., (Eds.); Marcel Dekker: New York, 1990, p. 599;
b) Anderegg, G.
Helv. Chim. Acta **1981**, *64*, 1790;
c) Arnaud-Neu, F.; Spiess, B.; Schwing-Weill, M.-J.
Helv. Chim. Acta **1977**, *60*, 2633;
d) Arnaud-Neu, F.; Yahya, R.; Schwing-Weill, M.-J.
J. Chim. Phys. Phys.-Chim. Biol. **1986**, *83,* 403;
e) Luboch, E.; Cygan, A.; Biernat, J. F.
Inorg. Chim. Acta **1983**, *68*, 201.

[200] a) Sakamoto, H.; Ishikawa, J.; Mizuno, T.; Doi, K.; Otomo, M.
Chem. Lett. **1993**, 609;
b) Sakamoto, H.; Ishikawa, J.; Otomo, M.
Bull. Chem. Soc. Jpn. **1995**, *68*, 2831.

[201] a) Saito, K.; Masuda, Y.; Sekido, E.
Anal. Chim. Acta **1983**, *151*, 447;
b) Kodama, M.; Koike, T.; Hoshiga, N.; Machida, R.; Kimura, E.
J. Chem. Soc. Dalton Trans. **1984**, 673.

[202] Nudelman, N. S.; Furlong, J. J. P.
Can. J. Chem. **1991**, *69*, 865.

[203] a) Matsushima, R.; Suzuki, M.
Bull. Chem. Soc. Jpn. **1992**, *65*, 39;
b) Matsushima, R.; Mizuno, H.; Itoh, H.
J. Photochem. Photobiol. A Chem. **1995**, *89*, 251;
c) Matsushima, R.; Suzuki, N.; Murakami, T.; Morioka, M.
J. Photochem. Photobiol. A Chem. **1997**, *109*, 91.

[204] a) Pina, F.; Melo, M. J.; Maestri, M.; Ballardini, R.; Balzani, V.
J. Am. Chem. Soc. **1997**, *119*, 5556;
b) Pina, F.; Melo, M. J.; Ballardini, R.; Flamigni, L.; Maestri, M.
New J. Chem. **1997**, *21*, 969;
c) Pina, F.; Benedito, L.; Melo, M. J.; Parola, A. J.; Lima, J. C.; Macanita, A. L.
An. Quim. Int. Ed. **1997**, *93*, 111.

[205] Stobbe, H.; Bremer, K.
J. prakt. Chem. **1929**, *123*, 1.

[206] Szmant, H. H.; Basso, A. J.
J. Am. Chem. Soc. **1952**, *74*, 4397.

[207] a) Tsukerman, S. V.; Maslennikova, V. P.; Lavruskin, V. F.
Opt. Spectrosc. **1967**, *23*, 213;
b) Nikitina, A. N.; Fedyunina, G. M.; Umirzakov, B.; Yanovskaya, L. A.; Kucherov, V. F.
Opt. Spectrosc. **1973**, *34*, 163.

[208] a) Dhar, D. N.; Singhal, D. V.
Spectrochim. Acta **1970**, *26A*, 1171;
b) Dhar, D. N.; Singh, R. K.
J. Indian Chem. Soc. **1972**, *49*, 241;
c) *J. Indian Chem. Soc.* **1973**, *50*, 129.

[209] a) Nicodem, D. E.; de M. G. Matos, J. A.
J. Photochem. **1981**, *15*, 193;
b) Caldwell, R. A.; Singh, M.
J. Am. Chem. Soc. **1983**, *105,* 5139;
c) Eisenhart, J. M.; Ellis, A. B.
J. Org. Chem. **1985**, *50*, 4108;
d) Ramakrishnaiah, C.; Naidu, R. S.; Naidu, R. R.
J. Indian Chem. Soc. **1986**, *63*, 573;
e) Gustav, K.; Bartsch, U.; Karnizschky, K.
Z. Chem. **1989,** *29*, 213;
f) DeVoe, R. J.; Sahyun, M. R. V.; Schmidt, E.; Sadrai, M.; Serpone, N.; Sharma, D. K.
Can. J. Chem. **1989**, *67*, 1565

[210] Wang, Y.
J. Phys. Chem. **1985**, *89*, 3799.

[211] a) Ebied, E.-Z. M.; Abdel-Kader, M. H.; Issa, R. M.; El-Daly, S. A.
Chem. Phys. Lett. **1988**, *146*, 331;
b) El-Daly, S. A.; Ebied, E.-Z. M.
Spectrochim. Acta **1994**, *50A*, 1227.

[212] a) Wang, P.-F.; Du, W.-Q.; Wu, S.-K.
Acta Chim. Sin. **1992**, *50*, 1140;
b) Wang, P.-F.; Wu, S.-K.
Acta Phys.-Chim. Sin. **1992**, *8*, 405;
c) *Photogr. Sci. Photochem.* **1993**, *11*, 28;
d) *J. Photochem. Photobiol. A Chem.* **1994**, *77*, 127;
e) *Acta Chim. Sin.* **1994**, *52,* 341;
f) *J. Photochem. Photobiol. A Chem.* **1995**, *86*, 109.

[213] a) Jiang, Y.-B.; Wang, X.-J.; Lin, L.
J. Phys. Chem. **1994**, *98*, 12367;
b) Jiang, Y.-B.; Wang, X.-J.
J. Photochem. Photobiol. A Chem. **1994**, *81*, 205.

[214] a) Bangal, P. R.; Lahiri, S.; Kar, S.; Chakravorti, S.
J. Lumin. **1996**, *69*, 49;
b) Akuskar, S. K.; Chondhekar, T. K.; Dhuley, D. G.
U. Scientist Phyl. Sciences **1996**, *8*, 229;
c) Itoh, H.; Takada, A.; Kudo, H.; Yokoyama, H.; Senda, Y.; Urano, T.; Nagasaka, H.
Bull. Chem. Soc. Jpn. **1997**, *70*, 2221;
d) Iwata, S.; Nishino, T.; Inoue, H.; Nagata, N.; Satomi, Y.; Nishino, H.; Shibata, S.
Biol. Pharm. Bull. **1997**, *20,* 1266.

[215] Gularyan, S. K.; Svetlichnyi, V. Y.; Dobretsov, G. E.
Biol. Membr. **1997**, *14,* 324.

[216] Ishikawa, J.; Sakamoto, H.; Mizuno, T.; Otomo, *M.*
Bull. Chem. Soc. Jpn. **1995**, *68*, 3071.

[217] Reichardt, C.
Angew. Chem. Int. Ed. Engl. **1979**, *18,* 98.

[218] a) Lippert, E.
Z. Naturforsch. **1955**, *10a*, 541;
b) *Z. Elektrochem.* **1957**, *61*, 962;
c) Mataga, N.; Kaifu, Y.; Koizumi, M.
Bull. Chem. Soc. Jpn. **1956**, *29*, 465.

[219] Létard, J.-F.; Lapouyade, R.; Rettig, W.
J. Am. Chem. Soc. **1993**, *115*, 2441.

[220] Catalán, J.; López, V.; Pérez, P.; Martín-Villamil, R.; Rodríguez, J.-G.
Liebigs Ann. **1995**, 241;

[221] Catalán, J.
J. Org. Chem. **1995**, *60*, 8315

[222] Fery-Forgues, S.; Le Bris, M. T.; Pouget, J.; Rettig, W.; Valeur, B.
J. Phys. Chem. **1992**, *96*, 701.

[223] a) Kosower, E. M.
Acc. Chem. Res. **1982**, *15*, 259;
b) Rettig, W.
Top. Curr. Chem. **1994**, *169*, 253.

[224] Edward, J. T.
Chem. Ind. **1956**, 774.

[225] Varma, C. A. G. O.; Groenen, E. J. J.
Recl. Trav. Chim. Pays-Bas **1972**, *91*, 296.

[226] Rurack, K.; Resch-Genger, U.; Rettig, W.
to be submitted.

[227] Braun, D.; Rettig, W.
Chem. Phys. Lett. **1997**, *268,* 110.

[228] a) Fee, R. S.; Maroncelli, M.
Chem. Phys. **1994**, *183*, 235;
b) Horng, M. L.; Gardecki, J. A.; Papazyan, A.; Maroncelli, M.
J. Phys. Chem. **1995**, *99*, 17311;
c) Reynolds, L.; Gardecki, J. A.; Frankland, S. J. V.; Horng, M. L.; Maroncelli, M.
J. Phys. Chem. **1996**, *100*, 10337.

[229] Maroncelli, M.; Fleming, G. R.
J. Chem. Phys. **1987**, *86*, 6221.

[230] a) Su, S.-G.; Simon, J. D.
J. Phys. Chem. **1987**, *91*, 2693;
b) Simon, J. D.
Acc. Chem. Res. **1988**, *21*, 128.

[231] Declémy, A.; Rullière, C.; Kottis, P.
Laser Chem. **1990**, *10,* 413.

[232] Gustavsson, T.; Cassara, L.; Gulbinas, V.; Gurzadyan, G.; Mialocq, J.-C.; Pommeret, S.; Sorgius, M.; van der Meulen, P.
J. Phys. Chem. A **1998**, *102*, 4229.

[233] Strehmel, B.; Seifert, H.; Rettig, W.
J. Phys. Chem. B **1997**, *101*, 2232.

[234] a) Kahlow, M. A.; Kang, T. J.; Barbara, P. F.
J. Phys. Chem. **1987**, *91*, 6452;
b) Pöllinger, F.; Heitele, H.; Michel-Beyerle, M. E., Anders, C.; Futscher, M.; Staab, H. A.
Chem. Phys. Lett. **1992**, *198*, 645;
c) Rossky, P. J.; Simon, J. D.
Nature **1994**, *370*, 263.

[235] a) Rabinovich, D.
J. Chem. Soc. B **1970**, 11;
b) Rabinovich, D.; Schmidt, G. M. J., Shakked, Z.
J. Chem. Soc. Perkin Trans. 2 **1973**, 33.

[236] Jungk, A. E.; Schmidt, G. M. J.
J. Chem. Soc. B **1970**, 1427.

[237] a) Orlov, V. D.; Tsukerman, S. V.; Lavrushin, V. F.
Vop. Stereokhim. **1971**, 1, 89;
b) Tsukerman, S. V.; Orlov, V. D.; Lam, N. T.; Lavrushin, V. F.
Khim. Geterotsikl. Soedin. **1969**, *6*, 974;
c) Tsukerman, S. V.; Izvekov, V. P.; Lavrushin, V. F.
Zh. Fiz. Khim. **1968**, *42*, 2159.

[238] Saltiel, J.; Sun, Y.-P.
In *Photochromism;* Dürr, H.; Bouas-Laurent, H., (Eds.); Elsevier: Amsterdam, 1990, p. 64.

[239] a) Wassam, jr., W. A.; Lim, E. C.
J. Chem. Phys. **1978**, *68*, 433;
b) Lai, T.-i.; Lim, B. T.; Lim, E. C.
J. Am. Chem. Soc. **1982**, *104*, 7631.

[240] Rettig, W.
Angew. Chem. Int. Ed. Engl. **1986**, *25*, 971.

[241] Rettig, W.; Majenz, W.; Herter, R.; Létard, J.-F.; Lapouyade, R.
Pure Appl. Chem. **1993**, *65*, 1699.

[242] a) Caldwell, R. A.; Cao, C. V.
J. Am. Chem. Soc. **1982**, *104*, 6174;
b) Görner, H.; Schulte-Frohlinde, D
J. Phys. Chem. **1981**, *85*, 1835;
c) Bonneau, R.
J. Am. Chem. Soc. **1980**, *102*, 3816.

[243] a) Siebrand, W.
J. Chem. Phys. **1967**, *46*, 440;
b) *J. Phys. Chem.* **1967**, *47*, 2441.

[244] Jensen, F. R.; Bushweller, C. H.
J. Am. Chem. Soc. **1969**, *91*, 5774.

[245] a) Vroegop, P. J.; Lugtenburg, J.; Havinga, E.
Tetrahedron **1973**, *29*, 1393;
b) Havinga, E.
Chimia **1976**, *30*, 27;
c) Minnaard, N. G.; Havinga, E.
Recl. Trav. Chim. Pays-Bas **1973**, *92*, 1179.

[246] a) Ameloot, M.; Boens, N.; Andriessen, R.; Van den Bergh, V.; De Schryver, F. C.
J. Phys. Chem. **1991**, *95*, 2041;
b) Andriessen, R.; Boens, N.; Ameloot, M.; De Schryver, F. C.
J. Phys. Chem. **1991**, *95*, 2047;
c) Ameloot, M.; Boens, N.; Andriessen, R.; Van den Bergh, V.; De Schryver, F. C.
Methods Enzymol. **1992**, *210*, 314;
d) Hermans, B.; De Schryver, F. C.; Boens, N.; Ameloot, M.; Jerome, R.; Teyssie, P.; Goethals, E.; Schacht, E.
J. Phys. Chem. **1994**, *98*, 13583.

[247] Vollmer, F.
Ph. D. Thesis, Technische Universität, Berlin, **1995**.

[248] Martin, M. M.; Ikeda, N.; Okada, T.; Mataga, N.
J. Phys. Chem. **1982**, *86*, 4148.

[249] a) Shannon, R. D.
Acta Cryst. **1976**, *32A*, 751;
b) Frensdorff, H. K.
J. Am. Chem. Soc. **1971**, *93*, 600;
c) Dalley, N. K.
In *Synthetic Multidentate Macrocyclic Compounds;* Izatt, R. M.; Christensen, J. J., (Eds.); Academic: New York, 1978, p. 207.

[250] a) Jonker, S. A.; Verhoeven, J. W.; Reiss, C. A.; Goubitz, K.; Heijdenrijk, D.
Recl. Trav. Chim. Pays-Bas **1990**, *109*, 154;
b) Pauling, L.
J. Am. Chem. Soc. **1927**, *49*, 765.

[251] Rorabacher, D. B.; Martin, M. J.; Koenigbauer, M. J.; Malik, M.; Schroeder, R. R.; Endicott, J. F.; Ochrymowycz, L. A.
In *Copper Coordination Chemistry: Biochemical and Inorganic Perspectives*; Karlin, K. D.; Zubieta, J., (Eds.); Adenine: New York, 1983, p. 167.

[252] a) Hinze, J.
Fortschr. Chem. Forsch. **1968**, *9*, 448;
b) Allred, A. L.
J. Inorg. Nucl. Chem. **1961**, *17*, 215;
c) Allred, A. L.; Rochow, E. G.
J. Inorg. Nucl. Chem. **1958**, *5*, 264.

[253] Nieboer, E.; Richardson, D. H. S.
Environ. Pollut. Ser. B **1980**, *1*, 3.

[254] Jonker, S. A.
Ph. D. Thesis, University of Amsterdam, Amsterdam, **1989**.

[255] a) Dähne, S.
Science **1978**, *199*, 1163;
b) *Chimia* **1994**, *45*, 104;
c) Kachkovskii, A. D.; Dyadyusha, G. G.; Dekhtyar, M. L.
Dyes Pigm. **1991**, *15*, 191.

[256] a) Lamb, J. D.; Izatt, R. M.; Swain, C. S.; Christensen, J. J.
J. Am. Chem. Soc. **1980**, *102*, 475;
b) Poonia, N. S.; Bajaj, A. V.
Chem. Rev. **1979**, *79*, 389.

[257] Iwachido, T.; Minami, M.; Kimura, M.; Sadakane, A.; Kawasaki, M.; Toei, K.
Bull. Chem. Soc. Jpn. **1980**, *53*, 703.

[258] Fery-Forgues, S.; Bourson, J.; Dallery, L.; Valeur, B.
New J. Chem. **1990**, *14*, 617.

[259] Riesen, P. C.; Kaden, T. A.
Helv. Chim. Acta **1995**, *78*, 1325.

[260] Gustowski, D. A.; Gatto, V. J.; Mallen, J.; Echegoyen, L.; Gokel, G. W.
J. Org. Chem. **1987**, *52*, 5172.

[261] a) Buschmann, H.-J.
J. Solut. Chem. **1988**, *17*, 277;
b) Burchard, T.; Cox, B. G.; Firman, P.; Schneider, H.
Ber. Bunsenges. Phys. Chem. **1994**, *98*, 1526.

[262] Soroka, K.; Vithanage, R. S.; Phillips, D. A.; Walker, B.; Dasgupta, P. K.
Anal. Chem. **1987**, *59*, 629.

[263] Hancock, R. D.; Martell, A. E.
Chem. Rev. **1989**, *89*, 1875.

[264] Smith, R. M.; Martell, A. E.
Critical Stability Constants Volume 2: Amines; Plenum: New York, 1975; Vol. 2, p. 36.

[265] a) Westerby, B. C.; Juntunen, K. L.; Leggett, G.H.; Pett, V. B.; Koenigbauer, M. J.; Purgett, M. D.; Taschner, M. J.; Ochrymowycz, L. A.; Rorabacher, D. B.
Inorg. Chem. **1991**, *30*, 2109;
b) Jones, T. E.; Rorabacher, D. B.; Ochrymowycz, L. A.
J. Am. Chem. Soc. **1975**, *97*, 7485;
c) Corfield, P. W. R.; Ceccarelli, C.; Glick, M. D.; Moy, I. W.-Y.; Ochrymowycz, L. A.; Rorabacher, D. B.
J. Am. Chem. Soc. **1985**, *107*, 2399.

[266] Atkinson, N.; Blake, A. J.; Drew, M. G. B.; Forsyth, G.; Gould, R. O.; Lavery, A. J.; Reid, G.; Schröder, M.
J. Chem. Soc. Dalton Trans. **1992**, 2993.

[267] a) Nikles, D. E.; Anderson, A. B.; Urbach, F. L.
In *Copper Coordination Chemistry: Biochemical and Inorganic Perspectives*; Karlin, K. D.; Zubieta, J., (Eds.); Adenine: New York, 1983, p. 203;
b) Schugar, H. J.
ibid., p. 43;
c) Amundsen, A. R.; Whelan, J.; Bosnich, B.
J. Am. Chem. Soc. **1977**, *99*, 6730.

[268] Miskowski, V. M.; Thich, J. A; Solomon, R.; Schugar, H. J.
J. Am. Chem. Soc. **1976**, *98*, 8344.

[269] a) Siegfried, L.; Kaden, T. A.
Helv. Chim. Acta **1984**, *67*, 29;
b) Hörmann, E.; Riesen, P. C.; Neuburger, M.; Zehnder, M.; Kaden, T. A.
Helv. Chim. Acta **1996**, *79*, 235;
c) Kaden, T. A.; Kaderli, S.; Sager, W.; Siegfried-Hertli, L. C.; Zuberbühler, A. D.
Helv. Chim. Acta **1986**, *69*, 1216.

[270] Fujisawa, K.; Imai, S.; Kitajima, N.; Moro-oka, Y.
Inorg. Chem. **1998**, *37*, 168.

[271] Lindoy, L. F.; Lip, H. C.; Rea, J. H.; Smith, R. J.; Henrick, K.; McPartlin, M.; Tasker, P. A.
Inorg. Chem. **1980**, *19*, 3360.

[272] Cabbiness, D. K.; Margerum, D. W.
J. Am. Chem. Soc. **1967**, *91*, 6540.

[273] Izatt, R. M.; Terry, R. E.; Hansen, L. D.; Avondet, A. G.; Bradshaw, J. S.; Dalley, N. K.; Jensen, T. E.; Christensen, J. J.; Haymore, B. L.
Inorg. Chim. Acta **1978**, *30*, 1.

[274] Adam, K. R.; Baldwin, D. S.; Bashall, A.; Lindoy, L. F.; McPartlin, M.; Powell, H. R.
J. Chem. Soc. Dalton Trans. **1994**, 237.

[275] Roshal, A. D.; Grigorovich, A. V.; Doroshenko, A. O.; Pivovarenko, V. G.; Demchenko, A. P.
J. Phys. Chem. A **1998**, *102,* 5907.

[276] Cox, B. G.; Garcia-Rosas, J.; Schneider, H.
J. Am. Chem. Soc. **1981**, *103*, 1384.

[277] a) Wagner, A.; Schellhammer, C. W.; Petersen, S.
Angew. Chem. Int. Ed. Engl **1966**, *5*, 699;
b) Krasovitskii, B. M.; Bolotin, B. M.
Organic Luminescent Materials; VCH: Weinheim, 1988, p. 197.

[278] a) Kelly, G. P.; Leicester, P. A.; Wilkinson, F.; Worrall, D. R.
Spectrochim. Acta **1990**, *46A,* 975;
b) Wilkinson, F.; Kelly, G. P.; Michael, C.; Oelkrug, D.
J. Photochem. Photobiol. A Chem. **1990**, *52,* 309.

[279] a) Krasovitskii, B. M.; Bolotin, B. M.
Organic Luminescent Materials; VCH: Weinheim, 1988, p. 200;
b) Wiley, R. H.; Jarboe, C. H.; Hayes, F. N.; Hansbury, E.; Nielsen, J. T.; Callahan, P. X.; Sellars, M. C.
J. Org. Chem. **1958***, 23*, 732;
c) Sandler, S. R.; Loshaek, S.; Broderick, E.; Tsou, K. C.
J. Phys. Chem ***1962****, 66*, 404.

[280] a) Pragst, F.
J. prakt. Chem. **1973***, 315*, 549;
b) Pragst, F.; Weber, F. G.
J. prakt. Chem. **1976***, 318*, 51.

[281] a) Ando, W.; Sato, R.; Yamashita, M.; Akasaka, T.; Miyazaki, H.
J. Org. Chem. **1983***, 48,* 542;
b) Akasaka, T.; Nakagawa, M.; Nomura, Y.; Sato, R.; Someno, K.; Ando, W.
Tetrahedron **1986**, *42,* 3807.

[282] Reddy, G. L.; Santhamma, C.; Lakshmi, G. S. P. B.; Dhananjava, N.; Murthy, Y. L. N.; Anjaneyulu, A. S. R.; Mago, V. K.; Ray, A. K.; Lal, B.
Spectrochim. Acta **1994***, 50A,* 2311.

[283] a) Rivett, D. E.; Rosevear, J.; Wilshire, J. F. K.
Aust. J. Chem. **1979***, 32*, 1601;
b) Leaver, I. H.; Rivett, D. E.
Mol. Photochem. **1974***, 6*, 113;
c) Rivett, D. E.; Rosevear, J.; Wilshire, J. F. K.
Aust. J. Chem. **1983***, 36*, 1649.

[284] a) de Costa, M. D. P.; de Silva, A. P.; Pathirana, S. T.
Can. J. Chem. **1987***, 65*, 1416;
b) de Silva, A. P.; Gunaratne, H. Q. N.; Lynch, P. L. M.
J. Chem. Soc. Perkin Trans. 2 **1995**, 685;
c) Grimshaw, J.; de Silva, A. P.
J. Chem. Soc. Perkin Trans. 2 **1983**, 1679;
d) de Silva, A. P.; Gunaratne, H. Q. N.; Jayasekera, K. R.; O'Callaghan, S.; Sandanayake, K. R. A. S.
Chem. Lett. **1995**, 123.

[285] a) Yan, Z.-l.; Wu, S.-k.
Ganguang Kexue Yu Kuang Huaxue **1994***, 12*, 80;
b) *J. Lumin.* **1993***, 54*, 303;
c) *Wuli Huaxue Xuebao* **1993***, 9*, 556;
d) *Ganguang Kexue Yu Kuang Huaxue* **1993***, 11,* 14.

[286] a) Nurmukhametov, R. N.; Tishchenko, V. B.
Opt. Spectrosc. **1967***, 23*, 43;
b) Kutsyna, L. M.; Voevoda, L. V.; Tishchenko, V. G.; Shepel, A. V.
Opt. Spectrosc. **1969***, 26*, 91.

[287] a) Szücs, L.
Chem. Zvesti **1969***, 23*, 677;
b) Buryakovskaya, E. G.; Tsukerman, S. V.; Lavrushin, V. F.
Russ. J. Phys. Chem. (Engl. Transl.) **1975***, 49*, 532;
c) Yamamoto, H.; Sano, Y.; Shirota, Y.; Seki, H.; Mikawa, H.
Bull. Chem. Soc. Jpn. **1979***, 52*, 1533
d) Zhmurova, I. N.; Yurchenko, R. I.; Voitsekhovskaya, O. M.; Vizir, T. A.; Rykov, A. A.
J. Org. Chem. USSR (Engl. Transl.) **1980**, *16*, 530;
e) Tokmakov, G. P.; Udachin, Y. M.; Patalakha, N. S.; Denisov, L. K.; Lantsov, A. M.; Grandberg, I. I.
Chem. Heterocycl. Compd. (Engl. Transl.) **1980***, 16,* 66;
f) Pereyaslova, D. g.; Skripkina, V. T.; Yagupolskii, L.M.; Vinetskaya, Y. M.; Andreeva, L. P.
Chem. Heterocycl. Compd. (Engl. Transl.) **1982***, 18,* 961
g) Oparin, D. A.; Gella, I. M.; Maskevich, S. A.; Vakula, V. N.; Shul'ga, N. N.
J. Org. Chem. USSR (Engl. Transl.) **1992***, 28*, 445
h) Doroshenko, A. O.; Skripkina, V. T.; Schershukov, V. M.; Ponomaryov, O. A.
J. Fluoresc. **1997***, 7*, 131.

[288] a) Sahyun, M. R. V.; Crooks, G. P.; Sharma, D. K.
Proc. SPIE-Int. Soc. Opt. Eng. **1991***, 1436*, 125;
b) Blair, J. T.; Sahyun, M. R. V.; Sharma, D. K.
J. Photochem. Photobiol. A Chem. **1994***, 77*, 133.

[289] a) Güsten, H.; Meisner, R.
J. Photochem. **1983***, 21*, 53;
b) Strähle, H.; Seitz, W.; Güsten, H.
Z. Naturforsch. **1976***, 31b*, 1248;
c) Güsten, H.; Heinrich, G.; Frühbeis, H.
Ber. Bunsenges. Phys. Chem. **1977***, 81*, 810;
d) Strähle, H.; Seitz, W.; Güsten, H.
Ber. Bunsenges. Phys. Chem. **1976***, 80,* 288;
e) Güsten, H.; Schuster, P.; Seitz, W.
J. Phys. Chem. **1978***, 82*, 459.

[290] Yang, G.; Wu, S.
J. Photochem. Photobiol. A Chem. **1992***, 66*, 69.

[291] a) Herbich, J.; Grabowski, Z. R.; Wójtowicz, H.; Golankiewicz, K.
J. Phys. Chem. **1989***, 93*, 3439;
b) Herbich, J.; Waluk, J.
Chem. Phys. **1994***, 188*, 247.

[292] Shizuka, H.
Acc. Chem. Res. **1985***, 18*, 141.

[293] Maus, M.; Rettig, W.; Bonafoux, D.; Lapouyade, R.
J. Phys. Chem. A **1999**, *103*, 3388

[294] Duffin, B.
Acta Cryst. **1968***, B24*, 1256.

[295] Kavarnos, G. J.; Turro, N. J.
Chem. Rev. **1986***, 86*, 401.

[296] Buschmann, H.-J.
In *Stereochemical and Stereophysical Behavior of Macrocycles*; Bernal, I., (Ed.); Elsevier: Amsterdam, 1987, p. 103.

[297] Wheatley, P. J.
Acta Cryst. **1955**, *8*, 224.

[298] Weber, G.; Sheldrick, G. M.; Dix, J. P.; Vögtle, F.
Cryst. Struct. Comm. **1980**, *9,* 1157.

[299] a) Hush, N. S.
Trans. Faraday Soc. **1961**, *57*, 557;
b) Marcus, R. A.
Annu. Rev. Phys. Chem. **1964**, *15*, 155.

[300] Kavarnos, G. J.
Top. Curr. Chem. **1990**, *156*, 21.

[301] a) Cortés, J.; Heitele, H.; Jortner, J.
J. Phys. Chem. **1994**, *98*, 2527;
b) Barbara, P. F.; Meyer, T. J.; Ratner, M. A.
J. Phys. Chem. **1996**, *100*, 13148.

[302] a) Schütz, M.; Schmidt, R.
J. Phys. Chem. **1996**, *100*, 2012;
b) Maus, M.; Rettig, W.; Jonusauskas, G.; Lapouyade, R.; Rullière, C.
J. Phys. Chem. A **1998**, *102*, 7393.

[303] Weller, A.
Z. Phys. Chem., Neue Folge **1982**, *133*, 93.

[304] Herbich, J.; Kapturkiewicz, A.
Chem. Phys. **1993**, *170*, 221.

[305] Zweig, A.; Hodgson, W. G.; Jura, W. H.
J. Am. Chem. Soc. **1964**, *86*, 4124.

[306] Marcus, R. A.
J. Chem. Phys. **1965**, *43*, 679.

[307] Simmons, H. E.; Fukunaga, T.
J. Am. Chem. Soc. **1967**, *89*, 5208.

[308] a) Anderson, C. P.; Salmon, D. J.; Meyer, T. J.; Young, R. C.
J. Am. Chem. Soc. **1977**, *99*, 1980;
b) Bock, C. R. Connor, J. A.; Gutierrez, A. R.; Meyer, T. J.; Whitten, D. G.; Sullivan, B. P.; Nagle, J. K.
J. Am. Chem. Soc. **1979**, *101*, 4815.

[309] Elguero, J.; Jaquier, R.
Tetrahedron Lett. **1965**, *17*, 1175.

[310] Notario, R.; Herreros, M.; Ballesteros, E.; Essefar, M.; Abboud, J.-L. M.; Sadekov, I. D.; Minkin, V. I.; Elguero, J.
J. Chem. Soc. Perkin Trans. 2 **1994**, 2341.

[311] Dewar, M. J. S.; Dougherty, R. C.
The PMO Theory of Organic Chemistry; Plenum: New York, 1975, p. 120.

[312] a) Kahmann, K.; Sigel, H.; Erlenmeyer, H.
Helv. Chim. Acta **1965**, *48*, 295.
b) Sigel, H.; Wynberg, H.; van Bergen, T. J.; Kahmann, K.
Helv. Chim. Acta **1972**, *55*, 610;
c) Eilbeck, W. J.; Holmes, F-; Phillips, G. C.; Underhill, A. E.
J. Chem. Soc. A **1967**, 1161.

[313] a) Thompson, L. K.; Rendell, J. C. T.; Wellon, G.
C. Can. J. Chem. **1982**, *60*, 514;
b) Matthews, C. J.; Clegg, W.; Elsegood, M. R. J.; Leese, T. A.; Thorp, D.; Thornton, P.; Lockhart, J. C.
J. Chem. Soc. Dalton Trans. **1996**, 1531.

[314] Knorr, L.; Laubmann, H.
Ber. **1888**, *21*, 1205.

[315] Pragst, F.; Siefke, B.
J. prakt. Chem. **1974**, *316*, 267.

[316] Farha, jr., F.; Iwamoto, R. T.
J. Electroanal. Chem. **1964**, *8*, 55.

[317] Rurack, K.; Resch-Genger, U.; Bricks, J. L.; Spieles, M.
Chem. Commun. **2000**, 2103.

[318] a) Siemiarczuk, A.; Grabowski, Z. R.; Krówczynski, A.; Asher, M.; Ottolenghi, M.
Chem. Phys. Lett. **1977**, *51*, 315;
b) Siemiarczuk, A.; Koput, J.; Pohorille, A.
Z. Naturforsch. **1982**, *37a*, 598;
c) Siemiarczuk, A.; Ware, W. R.
J. Phys. Chem. **1987**, *91*, 3677.

[319] a) Okada, T.; Mataga, N.; Baumann, W.; Siemiarczuk, A.
J. Phys. Chem. **1987**, *91*, 4490;
b) Mataga, N.; Nishikawa, S.; Asahi, T.; Okada, T.
J. Phys. Chem. **1990**, *94*, 1443.

[320] a) Shiguza, H.; Ogiwara, T.; Kimura, E.
J. Phys. Chem. **1985**, *89*, 4302;
b) Lee, S.; Arita, K.; Kajimoto, O.; Tamao, K.
J. Phys. Chem. A **1997**, *101*, 5228;
c) Wiessner, A.; Hüttmann, G.; Kühnle, W.; Staerk, H.
J. Phys. Chem. **1995**, *99*, 14923.

[321] a) Onkelinx, A.; De Schryver, F. C.; Viaene, L.; Van der Auweraer, M.; Iwai, K.; Yamamoto, M.; Ichikawa, M.; Masuhara, H.; Maus, M.; Rettig, W.
J. Am. Chem. Soc. **1996**, *118*, 2892;
b) Maus, M.; Rettig, W.; Depaemelaere, S.; Onkelinx, A.; De Schryver, F. C.; Iwai, K.
Chem. Phys. Lett. **1998**, *292*, 115.

[322] Herbich, J.; Kapturkiewicz, A.
J. Am. Chem. Soc. **1998**, *120*, 1014.

[323] a) Rotkiewicz, K.; Rechthaler, K.; Puchala, A.; Rasala, D.; Styrcz, S.; Köhler, G. *J. Photochem. Photobiol. A Chem.* **1996**, *98*, 15; b) Parusel, A. B. J.; Schamschule, R.; Piorun, D.; Rechthaler, K.; Puchala, A.; Rasala, D.; Rotkiewicz, K.; Köhler, G. *J. Mol. Struct. THEOCHEM* **1997**, *419*, 63; c) Parusel, A. B. J.; Schamschule, R.; Köhler, G. *Ber. Bunsenges. Phys. Chem.* **1997**, *101*, 1836.

[324] Maus, M.; Rurack, K. *New J. Chem.* **2000**, *24*, 677.

[325] a) Grabowski, Z. R.; Rotkiewicz, K.; Siemiarczuk, A.; Cowley, D. J.; Baumann, W. *Nouv. J. Chim.* **1979**, *3*, 443; b) Herbich, J.; Grabowski, Z. R.; Wójtowicz, H.; Golankiewicz, K. *J. Phys. Chem.* **1989**, *93*, 3439.

[326] Detzer, N.; Baumann, W.; Schwager, B.; Fröhling, J.-C.; Brittinger, C. *Z. Naturforsch.* **1986**, *42a*, 395.

[327] Rettig, W.; Maus, M.; Lapouyade, R. *Ber. Bunsenges. Phys. Chem.* **1996**, *100*, 2091.

[328] Plaza, P.; Hung, N. D.; Martin, M. M.; Meyer, Y. H.; Vogel, M.; Rettig, W. *Chem. Phys.* **1992**, *168*, 365.

[329] a) Karolin, J.; Johansson, L. B.-A.; Strandberg, L.; Ny, T. *J. Am. Chem. Soc.* **1994**, *116,* 7801; b) Molecular Probes Inc., Eugene, Oregon; URL: http://www.probes.com; c) Debreczeny, M. P.; Svec, W. A.; Wasielewski, M. R. *New J. Chem.* **1996**, *20*, 815; d) Wagner, R. W.; Lindsey, J. S.; Seth, J.; Palaniappan, V.; Bocian, D. F. *J. Am. Chem. Soc.* **1996**, *118*, 3996; e) Li, F.; Yang, S. I.; Ciringh, Y.; Seth, J.; Martin, III, C. H.; Singh, D. L.; Kim, D.; Birge, R.R.; Bocian, D. F.; Holten, D.; Lindsey, J. S. *J. Am. Chem. Soc.* **1998**, *120*, 10001.

[330] a) Gareis, T.; Huber, C.; Wolfbeis, O. S.; Daub, J. *Chem Commun.* **1997**, 1717; b) Werner, T.; Huber, C.; Heinl, S.; Kollmannsberger, M.; Daub, J.; Wolfbeis, O. S. *Fresenius J. Anal. Chem.* **1997**, *359*, 150.

[331] a) Vos de Wal, E.; Pardoen, J.; van Koeveringe, J. A.; Lugtenburg, J. *Recl. Trav. Chim. Pays-Bas* **1977**, *96*, 306; b) Pardoen, J. A.; Lugtenburg, J.; Canters, G. W. *J. Phys. Chem.* **1985**, *89*, 4272.

[332] Maus, M.; Rettig, W.; Lapouyade, R. *J. Inf. Rec.* **1996**, *22*, 451.

[333] Birks, J. B. *Photophysics of Aromatic Molecules;* Wiley-Interscience: New York, 1970.

[334] a) Leinhos, U.; Kühnle, W.; Zachariasse, K. A. *J. Phys. Chem.* **1991**, *95*, 2013; b) Schuddeboom, W.; Jonker, S. A.; Warman, J. M.; Leinhos, U.; Kühnle, W.; Zachariasse, K. A. *J. Phys. Chem.* **1992**, *96*, 10809.

[335] a) Svaan, M.; Parker, V. D. *Acta Chem. Scand. B* **1982**, *35* 559; b) Piechowski, A. P. *J. Electroanal. Chem.* **1983**, *145*, 67.

[336] Rotkiewicz, K.; Rettig, W. *J. Lumin.* **1992**, *54*, 221.

[337] Eigen, M.; Winkler, R. M. In *Neurosciences Second Study* Program, Schmitt, F. O., (Ed.); Rockefeller University: New York, 1970, p. 685.

[338] a) Gokel, G. W.; Echegoyen, L.; Kim, M. S.; Eyring, E. M.; Petrucci, S. *Biophys. Chem.* **1987**, *26,* 225; b) Echegoyen, L.; Gokel, G. W.; Kim, M. S.; Eyring, E. M.; Petrucci, S. *J. Phys. Chem.* **1987**, *91*, 3854.

[339] a) Rurack, K.; Kollmannsberger, M.; Resch-Genger, U.; Daub, J. *J. Am. Chem. Soc.* **2000**, *122*, 968; b) Kollmannsberger, M.; Rurack, K.; Resch-Genger, U.; Rettig, W.; Daub, J. *Chem. Phys. Lett.* **2000**, *329*, 363.

[340] a) Reichardt, C. *Solvents and Solvent Effects in Organic Chemistry*; VCH: Weinheim, 1988, 2nd Edn.. b) Murov, S. L.; Carmichael, I.; Hug, G. L. *Handbook of Photochemistry*; Marcel Dekker: New York, 1993, 2nd Edn..

[341] Lakowicz, J. R. *Principles of Fluorescence Spectroscopy*; Plenum: New York, 1983.

[342] Strickler, S. J.; Berg, R. A. *J. Chem. Phys.* **1962**, *37*, 814.

[343] Riesen, P. C.; Kaden, T. A. *Helv. Chim. Acta* **1995**, *78*, 1325.

[344] a) McRae, E. G. *J. Phys. Chem.* **1957**, *61*, 562; b) Bakhshiev, N. G. *Opt. Spectrosc.* **1961**, *10*, 279; c) *Opt. Spectrosc.* **1962**, *13*, 24; d) *Opt. Spectrosc.* **1962**, *13*, 104; e) Bilot, L.; Kawski, A. Z. *Naturforsch.* **1962**, *17a*, 621; f) Kawski, A. *Acta Phys. Polon.* **1966**, *29*, 507.

[345] Onsager, L. *J. Am. Chem. Soc.* **1936**, *58*, 1486.

[346] Karelson, M.; Zerner, M. C. *J. Am. Chem. Soc.* **1990**, *112*, 9405.

[347] a) Okada, T.; Fujita, T.; Kubota, M.; Masaki, S.; Mataga, N.
Chem. Phys. Lett. **1972**, *14,* 563;
b) Okada, T.; Fujita, T.; Mataga, N.
Z. Phys. Chem., Neue Folge **1976***, 101*, 57.

[348] Kosower, E. M.
J. Am. Chem. Soc. **1958***, 80*, 3253.

[349] Dimroth, K.; Reichardt, C.; Siepmann, T.; Bohlmann, F.
Justsus Liebigs Ann. Chem. **1963***, 661*, 1.

[350] a) Kamlet, M. J.; Abboud, J. L.; Taft, R. W.
J. Am. Chem. Soc. **1977***, 99*, 6027;
b) Kamlet, M. J.; Taft, R. W.
J. *Chem. Soc. Perkin Trans. 2* **1979**, 349.

[351] a) Polster, J.
Z. Phys. Chem., Neue Folge **1975***, 97*, 55;
b) Lachmann, H.
Habilitation, Universität Würzburg, Würzburg, **1982**;
c) Polster, J.; Lachmann, H.
Spectrometric Titrations; VCH: Weinheim, 1989.

[352] a) Benesch, R. E.; Benesch, R.
J. Am. Chem. Soc. **1955***, 77*, 5877;
b) Johnson, J. J.; Metzler, D. E.
Methods Enzymol. **1970***, 18A*, 433;
c) Novo, M.; Mosquera, M.; Prieto, F. R.
J. Phys. Chem. **1995***, 99*, 14726.

Publications

Rurack, K.; Resch, U.; Senoner, M.; Dähne, S.,
„A New Fluorescence Probe for Trace Metal Ions: Cation Dependent Spectroscopic Properties“,
J. Fluoresc. **1993**, *3*, 141-143.

Resch, U.; Rurack, K.; Senoner, M.,
„Zeitaufgelöste Fluorometrie in der Wasseranalytik“,
Nachr. Chem. Tech. Lab. **1994**, *42*, 504-506.

Rurack, K.; Senoner, M.; Resch, U.; Dähne, S.,
„Heavy Metal Complexes of 2,2‘-Bipyridyl-3,3‘-diol“,
J. Inf. Rec. Mater. **1994**, *21*, 683-684.

Resch, U.; Rurack, K.; Bricks, J. L.; Slominskii, J. L.,
„New Fluorophore Receptor Systems for Heavy Metal Ions: A Spectroscopic Study“,
J. Fluoresc. **1997**, *7*, 231S-233S.

Rurack, K.; Bricks, J. L.; Kachkovskii, A. D.; Resch, U.,
„Complexing Fluorescence Probes Consisting of Various Fluorophores Linked to 1-Aza-15-Crown-5“,
J. Fluoresc. **1997**, *7*, 63S-66S.

Rurack, K.; Bricks, J. L.; Slominskii, J. L.; Resch, U., „Cation Complexing Fluorescence Probes Containing the Benz[c,d]indole Fluorophore“,
Dyes Pigm. **1998**, *36*, 121-138.

Rurack, K.; Resch, U.; Rettig, W.,
„Zn^{II} and Cd^{II} Complexes of 2,2’-Bipyridyl-3,3’-diol: Discrimination with Time Resolved Fluorometry“,
BESSY Ann. Rep. **1996**, 459-460.

Resch, U.; Rurack, K.,
„Steady-State and Time Resolved Fluorometry of Fluorescent Pollutants and Heavy Metal Complexes“, Proc. *SPIE-Int. Soc. Opt. Eng.* **1997**, *3105*, 96-103.

Rurack, K.; Resch, U.,
„Design, Synthese und Charakterisierung von Neuen Fluoreszenzstandards und Fluoreszenzmarkern für die Zeitaufgelöste Fluorometrie“,
BAM-Forschungsbericht 223,
Verlag für neue Wissenschaft GmbH, Bremerhaven 1998.

Rurack, K.; Bricks, J. L.; Slominskii, J. L.; Resch-Genger, U.,
„Long Wavelength Emitting Fluorescence Probes for Metal Ions“,
in *Near-Infrared Dyes for High Technology Applications*,

Dähne, S.; Resch-Genger, U.; Wolfbeis, O. S. (Eds.); NATO ASI Series 3, Vol. 52, Kluwer Academic:
Dordrecht, 1998, 191-200.

Rurack, K.; Resch-Genger, U.; Rettig, W.,
„Global Analysis of Time Resolved Emission – A Powerful Tool for the Analytical Discrimination of Chemically Similar Zn^{II} and Cd^{II} Complexes“,
J. Photochem. Photobiol. A: Chem. **1998***, 118*, 143-149.

Kollmannsberger, M.; Rurack, K.; Resch-Genger, U.; Daub, J.,
„Ultrafast Charge Transfer in Amino Substituted Boron Dipyrromethene Dyes and its Inhibition by Cation Complexation: A New Design Concept for Highly Sensitive Fluorescent Probes“,
J. Phys. Chem. A **1998***, 102*, 10211-10220.

Oral Presentations

„Applications of Laserimpulsfluorometry in Analytical Chemistry“,
Polish Academy of Science, Warsaw, PL, **03.11.1993**.

„Spectroscopic Investigations of Fluoroionophores Based on Chalcone and Pyrazoline Dyes“,
Institute of Physics, University of Kiev - Mohyla Academy, Kiev, UKR, **02.10.1996**.

„Fluorescent Probes for Metal Ion Analysis“,
Institute of Organic Chemistry, Ukrainian Academy of Science, Kiev, UKR, **03.10.1996**.

„Steady-State and Time Resolved Fluorometry of Fluorescent Pollutants and Heavy Metal Complexes“,
EnviroSense ‘97, Munich, D, **16.06.-20.06.1997**.

Poster Presentations

„A New Fluorescence Probe for Trace Metal Ions: Cation and pH Dependent Spectroscopical Properties“,
3rd Conference on Methods and Applications of Fluorescence Spectroscopy, Prague, CZ, **18.-21.10.1993**.

„Neue Fluorophor-Rezeptor-Systeme für Schwer- und Übergangsmetallionen“,
4. Berliner Optiktage „Optik 1994“, Berlin, D,
20.-22.09.1994.

„New Fluorophore-Receptor-Systems for the Fluorometric Detection of Transition and Heavy Metal Ions in Analytical Chemistry“, Joint Meeting of the French and German Groups of Photochemistry, Strasbourg, F,
17.-18.11.1994.

„Analytical Applications of Time Resolved Fluorometry“,
Laser ‘95, Munich, D,
19.06.-23.06.1995.

„Spectroscopic Characterization of New Macrocyclic Fluorescence Probes for Metal Ions“,
25. GDCh-Hauptversammlung, Münster, D,
10.-13.09.1995.

„Complexing Fluorescence Probes Consisting of Various Fluorophores Linked to 1-Aza-15-Crown-5“,
4th International Conference on Methods and Applications of Fluorescence Spectroscopy, Cambridge, UK,
24.-27.09.1995.

„Modular Fluorescence Probes for Time Resolved Fluorometry“, Analytica 96, Munich, D,
23.04.-26.04.1996.

„Modular Fluorescence Probes for Time Resolved Fluorometry“, Chemie in Berlin und Potsdam, Potsdam, D,
04.12.1996.

„Unsymmetric Cyanine and Styryl Dyes: Part II. Cation Complexation Behaviour of Styryl Dye Based Fluorescence Probes with Different Receptors“,
V. International Conference on Methods and Applications of Fluorescence Spectroscopy, Berlin, D,
21.09.-24.09.1997.

„Cation Complexation Behaviour of NIR Fluorescence Probes with Different Receptors“,
NATO Advanced Research Workshop on Syntheses, Optical Properties, and Applications of Near-Infrared (NIR) Dyes in High Technology Fields, Trest, CZ,
24.09.-27.09.1997.

„Time Resolved Emission Spectra - A Powerful Tool for the Analytical Discrimination of Chemically Similar Zn(II) and Cd(II) Complexes“,
BESSY User Meeting, Berlin, D,
04.-05.12.1997.

„Photophysics of Donor-Acceptor Substituted Chalcones: Positive versus Negative Solvatokinetic Behaviour“,
Jablonski Centennial Conference on Luminescence and Photophysics, Torun, PL,
23.-27.07.1998.

Coautorship

Oral Presentations

„Anwendungen der Laserimpulsfluorometrie in der Analytischen Chemie“,
Laserverbund Berlin-Brandenburg, Berlin, D, **30.09.1993**.

„Anwendungen der Zeitaufgelösten Laserimpulsfluorometrie in der Wasseranalytik“,
BASF AG, Ludwigshafen, D, **30.11.1993**.

„Anwendungen der Zeitaufgelösten Laserimpulsfluorometrie in der Wasseranalytik“,
BAYER AG, Leverkusen, D, **08.03.1994.**

„Design and Spectroscopic Study of New Fluorescence Probes for Transition and Heavy Metal Ions“,
Institute of Organic Chemistry, Ukrainian Academy of Science, Kiev, UKR, **30.09.1994**.

„Spektroskopische Charakterisierung von Fluorophor-Rezeptor-Systemen“,
Institut für Angewandte Chemie Adlershof, Berlin, D,
04.10.1995.

„Fluoreszenzmarker für die Kationen-Analytik“, Interessengemeinschaft Optische Molekülspektroskopie,
Berlin, D, **15.11.1995**.

Poster Presentations

„Spectroscopic Characterization of New Fluorescence Probes for Heavy and Transition Metal Ions“,
3rd International Symposium on Functional Dyes,
Santa Cruz, USA, **16.-21.07.1995**.

„New Fluorescence Probes for the Fluorometric Detection of Heavy and Transition Metal Ions“,
Colloquium Spectroscopicum Internationale XXIX,
Post Symposium: Lasers, Berlin, D, **01.-03.09.1995**.

„New Fluorophore Receptor Systems for Heavy Metal Ions: a Spectroscopic Study“,
4th International Conference on Methods and Applications of Fluorescence Spectroscopy, Cambridge, UK,
24.-27.09.1995.

„Modular Fluorescence Probes for Heavy and Transition Metal Ions“,
Europt(r)ode III, Zurich, CH, **31.03.-03.04.1996**.

„New Redoxactive Fluorophore Receptor Systems“,
Europt(r)ode III, Zurich, CH, **31.03.-03.04.1996**.

„Modular Fluorescence Probes for Heavy and Transition Metal Ions“,
Analytica 96, Munich, D, **23.04.-26.04.1996**.

„Modular Fluorescence Probes for Heavy and Transition Metal Ions“,
Chemie in Berlin und Potsdam, Potsdam, D, **04.12.1996**.

„Unsymmetric Cyanine and Styryl Dyes: Part I. Sythesis and Spectral Properties of Styryl Dye Based Fluorescence Probes with Different Receptors“,
V. International Conference on Methods and Applications of Fluorescence Spectroscopy, Berlin, D,
21.09.-24.09.1997.

„Unsymmetric Cyanine and Styryl Dyes: Part III. Fluorescence Properties and Cation Complexation Ability“,
V. International Conference on Methods and Applications of Fluorescence Spectroscopy, Berlin, D,
21.09.-24.09.1997.

„Synthesis and Spectral Properties of NIR Fluorescence Probes with Different Receptors“,
NATO Advanced Research Workshop on Syntheses, Optical Properties, and Applications of Near-Infrared (NIR) Dyes in High Technology Fields, Trest, CZ,
24.09.-27.09.1997.

„New Fluorescence Probes Based on Benz[c,d]indole for the Determination of Heavy Metal Cations“,
Ukrainian Conference on Nitrogen Containing Heterocycles, Charkov, UKR, **01.-04.10.1997**.